Summer 8-16-2013

Controlling Surface Chemistry on the Microscopic and Nanoscopic Scale through Photopatterned Self-Assembled Monolayers

Matthew J. Hynes
Washington University in St. Louis

Follow this and additional works at: https://openscholarship.wustl.edu/etd

WASHINGTON UNIVERSITY IN ST. LOUIS

Department of Chemistry

Dissertation Examination Committee:

Joshua A. Maurer, Chair

William E. Buhro

Donald L. Elbert

Erik D. Herzog

Kevin D. Moeller

John-Stephen A. Taylor

Controlling Surface Chemistry on the Microscopic and Nanoscopic Scale through
Photopatterned Self-Assembled Monolayers

by

Matthew J. Hynes

A dissertation presented to the
Graduate School of Arts and Sciences
of Washington University in
partial fulfillment of the
requirements for the degree
of Doctor of Philosophy

August 2013

St. Louis, Missouri

Table of Contents

List of Figures

List of Schemes

List of Abbreviations and Symbols

Å   Angstrom (10^{-10} meters)

AFM   Atomic force microscopy

CHO-K1   Chinese hamster ovary cells

cm^{-1} wave number (IR)

DCC   Dicyclohexylcarbodiimide

DEAD   Diethyl azodicarboxylate

DMAP   Dimethylamino pyridine

DMF   Dimethylformamide

DMSO   Dimethyl sulfoxide

EBL   Electron beam lithography

EDC   N-(3-Dimethylaminopropyl)-N'-ethylcarbodiimide

ESI   Electrospray ionization

g   Grams

HBTU   O-(benzotriazol-1-yl)-N,N,N',N'-tetramethyluronium

                     Hexafluorophosphate

IR   Infrared spectroscopy

ITO   Indium tin oxide

LLM   Lateral force microscopy

LSL   Laser scanning lithography

KPFM   Kelvin probe force microscopy

m   multiplet (NMR)

MALDI   Matrix-Assisted Laser/Desorption Ionization

m/z	mass to charge ratio
NMR	Nuclear magnetic resonance
PDMS	Polydimethyl siloxane
QNM	Quantitative nanomechanical mapping
ROI	Region of interest
s	singlet (NMR)
SAMs	Self-assembled monolayers
SNP	Scanning near-field lithography
SPM	Scanning probe microscopy
SPRi	Surface plasmon resonance imaging
t	triplet (NMR)
THF	Tetrahydrofuran
TMS	Trimethyl silane

Acknowledgements

First and foremost, I would like to thank Joshua Ahab Maurer for his guidance over the past 6 years. I truly enjoyed the freedom he allowed when I wanted to pursue additional research interests.

I would also like to thank Profs. Kevin Moeller and John-Stephen Taylor for the guidance they have provided over the past 5 years serving on my committee. I would also like to thank Kevin for adopting me every Missouri Organic day so I was not an orphaned graduate student. I would like to thank Dr. Taylor for the impromptu hallway discussions especially during this transition phase. I truly appreciate the career advice they have provided.

I would like to thank Profs. William Buhro, Erik Herzog, and Donald Elbert, for serving on my thesis committee. I am looking forward to discussing my science with them. A special thanks to Prof. Herzog for all the Picrotoxin and Picrotoxinin samples. I wish we had been able to get this project further down the pipeline.

I would also like to thank the members of the Washington University Chemistry Department, particularly Ed and Rachel for always being able to find an answer to my question. Thank you to Nancy and Gerry for always being willing to help me locate lost items. Thank you to Greg and Jason for always being able to get the instruments to talk to one another. This process was by far no easy feat. Thank you to Norma and Jessica for all our help over the past 6 years. I would also like to thank Andre and Jeff for helping me troubleshoot the NMR. I need to thank Henry Rohrs for all his help and guidance throughout these years whenever I encountered

an issue with any MS instrument regardless of whose lab it belonged to. Thanks to Jim for the quick turnaround fabricating my gas chamber, since chapter 4 of this dissertation would not have been possible without it.

Next I would like to thank the senior members of the Maurer lab. I could not think of a better way to walk into the office than to have Dawn say hello. I am sorry that all the "prishing" did not payoff for the phosphonate work. Hannah, thanks for the fun lunchtime conversations. Strulson, thanks for all the dance parties and for sometimes doing that outside lab.

To my classmates, Xing, Bo Bi, and Richard, thank you for being a sounding board whenever I had a question or needed help with something, which happened more often than I care to count.

Thank you to 6823 for being the cleanest roommates I have ever had. But seriously, overall those 2 years were great.

To 369 Central, thank you for listening to a six year old. Who would have guessed he would be such a smarty pants.

To 48 Raymond, 9941 Acorn, and 10527 Willow Creek, your support and guidance over these different stages has been critical. To 13 Huron, thanks for all the phone calls and visits. It made living 1100 miles away not seem that far. To 2 Harvard, it is Thursday here. What day is it there?

Last but not least, thank you to Willis for being as close to perfect as a doctor could be, even if the food was far from it.

ABSTRACT OF DISSERTATION

Controlling Surface Chemistry on the Microscopic and Nanoscopic Scale through

Photopatterned Self-Assembled Monolayers

By

Matthew J. Hynes

Doctor of Philosophy in Chemistry

Washington University in St. Louis, 2013

Professor Joshua A. Maurer, Chair

The development of new patterning strategies for self-assembled monolayers (SAMs) using photolithography described here allows for the production of highly functional substrates for biological applications. Photolithography methods have been developed that utilize either high or low irradiation doses of 325 nm ultraviolet light. Utilizing high power led to the development of photo-induced monolayer desorption in which patterns were generated by thermally ablating glycol-terminated thiol monomers from gold substrates. A direct relationship between laser intensity and surface modulus was observed using scanning probe microscopy (SPM), which was expected since higher laser intensities should remove more glycol monomers from the surface exposing a greater percentage of the bare gold substrate. Conversely, an inverse relationship was determined between laser intensity and surface adhesion. Utilizing direct-write photolithography provided a facile means to generate complex protein patterns containing both gradients and punctate regions. Proteins adsorption to patterned substrates was quantified by surface plasmon

resonance imaging (SPRi) and fit to a Boltzmann function, which allowed us to correlate laser intensity with protein adsorption. Thus, the concentration of the protein could be precisely controlled by adjusting the gray scale level in the 8-bit image, since this file is used to modulate the laser intensity during patterning. Moreover, adsorbed neutravidin was detected using a commercial biotin labeled anti-avidin antibody, which allowed for significant signal enhancement over background. The ability to produce complex protein patterns will contribute greatly to creating *in vitro* models that more accurately mimic an *in vivo* environment.

In order to utilize low irradiation doses, two unique photoprotected thiol monomers were designed and synthesized. A nitroveratryl-protected carboxylic acid thiol monomer was synthesized, which when irradiated at 325 nm, resulted in cleavage of the nitroveratryl groups to produce free carboxylic acids on the surface. Direct-write photolithography provided a means to create complex patterns containing functional group gradients, which were observed directly using SPM. In addition, two different amine molecules were sequentially coupled on to a single substrate with spatial control. Coupling was visualized using Matrix-Assisted Laser Desorption/Ionization Mass Spectrometry (MALDI TOF) imaging, which demonstrated the utility of this method for generating complex multi-molecule patterns.

A new cyclopropenone monomer was also developed, which was used to site-selectively pattern azide terminated molecules. Exposure of the monomer to UV light under an argon atmosphere generated a strained cyclooctyne, which was used for Cu-free [3+2] cycloadditions with azide terminated molecules. Using direct-write photolithography, neutravidin gradients were produced by coupling an azido-biotin monomer to the patterned surfaces and a linear relationship, with an R^2 value of 0.993, between laser intensity and protein coupling was found. These patterned surfaces were also visualized using traditional immunohistochemistry by

coupling an azido-cRGD peptide to the surface and probing with a primary anti-RGD antibody followed by a fluorescently labeled secondary antibody. Moreover, patterned surfaces with cRGD could be used to control NIH/3T3 cell growth at various concentrations of functional monomer.

Chapter 1

1.1 Introduction

Self-assembled monolayers (SAMs) are facile method to functionalize a variety of substrates from noble metals to oxide surfaces. The monomers used to construct these monolayers can be divided into three main classes; thiols, silanes, and phosphonates. These three groups are defined by the chemistry used to covalently bind the monomer to the substrate, which is also termed the head group. However, the head group is just one portion of a monomer. Monomers are also comprised of two additional regions; a long alkane chain and a tail group. The long alkane chain provides monolayer stability through van der Waals forces. The longer the alkane chain, the greater the van der Waals forces between the
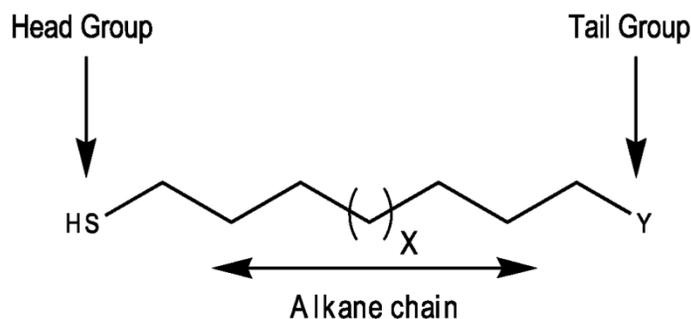
Figure 1.1. Generic thiol monomer

monomers, which results in a more ordered/crystalline like structure.[1] The tail group of the monomer is the portion that will be exposed to the surface and will ultimately define the resulting surface chemistry. A generic thiol monomer comprised of these three regions can be seen in Figure 1.1.

One of the most important classes of tail groups developed to date for biological applications are glycol moieties. This tail functionality has been shown to resist non-specific protein adsorption,[2] which allowed for the creation of protein patterned substrates. SAMs

composed of glycol terminated monomers have been used in a variety of biological applications including cell growth assays, biosensors, and supported lipid bilayers.[3-6] The work discussed in this thesis utilizes glycol-terminated SAMs as a platform to develop complex patterns for use in biological applications.

1.2 Monomers

Thiols are the most studied and best characterized monolayer system, due in part to the ease of substrate fabrication. Surfaces constructed from thiols are most commonly formed on gold, but they have also been reported on silver,[7] copper,[8] platinum,[9] and mercury.[10] These other substrates are less common because the underlying metal readily oxidizes when exposed to air, whereas gold is relatively inert. Thus, thiol-gold monolayers have a wider applicability.
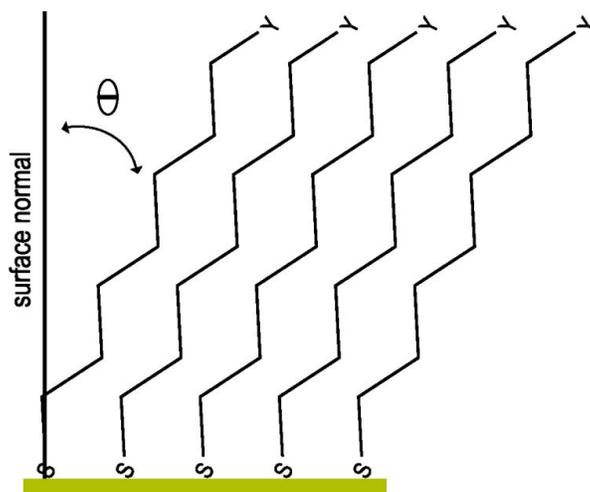
Figure 1.2 A thiol monolayer

Thiol monolayers are typically formed by soaking a substrate in a thiol monomer solution for 12-14 hours, followed by rinsing with ethanol, and drying under a stream of nitrogen. This process results in a "well-ordered" monolayer with a tilt angle between 26-28° from surface normal as shown in Figure 1.2.[11, 12] As the monolayer forms, the C-H

stretching frequencies in the IR will shift from a higher wavenumber that can be attributed to a more liquid state to a lower wavenumber attributed to a more crystalline form. A monolayer is considered "well ordered" when the alkane chains reach an IR symmetric stretching frequency of ≤ 2850 cm^{-1} and an asymmetric stretching frequency of ≤ 2920 cm^{-1}, which correspond to the frequencies observed in crystalline long chain alkanes.[13, 14] Additionally, a thiol head group will occupy a surface area of 21.4 Å^2 in a "well-ordered" monolayer on gold.[15, 16]
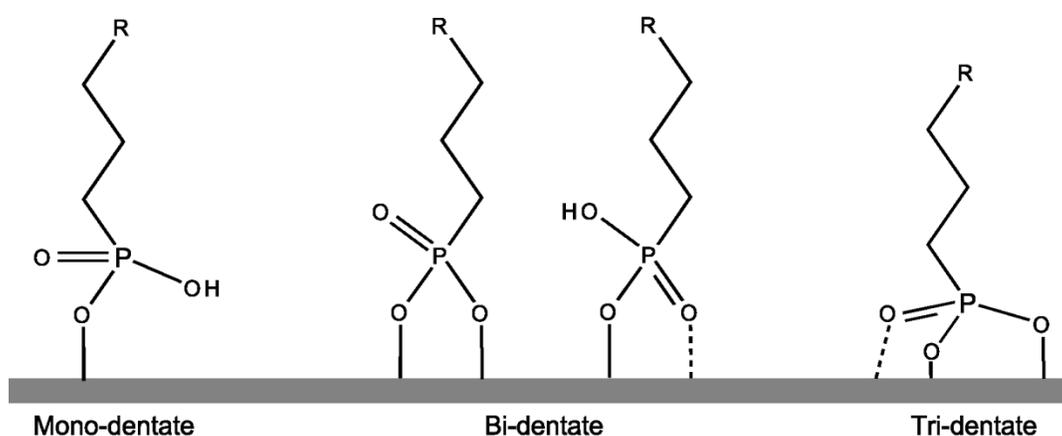
Figure 1.3. Phosphonate binding motifs on metal oxides after annealing the slide to drive the reaction to completion.[17] Both produce well ordered monolayers by surface infrared spectroscopy (IR).

The other major class of monomers used in this work takes advantage of a phosphonate head group. The use of phosphonate head groups allows for functionalization of a variety of oxide substrates including silicon oxide,[18] titanium dioxide,[19] indium-tin oxide,[20] and aluminium oxide[21]. Unlike thiols on gold, phosphonates on oxide surfaces can take on many binding motifs from mono-dentate to bi-dentate, and tridentate as shown in Figure 1.3. The binding mode is dependent on the metal surface being functionalized and the preparation method employed.[22] The phosphonate work presented here primarily focused on functionalizing titanium dioxide (TiO_2). For TiO_2 surfaces, the average tilt angle for a

phosphonate SAM ranges between 37-45° from the surface normal.[23]   Many methods have

been developed to produce phosphonate monolayers including solution deposition and

tethering by aggregation and growth (T-BAG), both of which have been employed here.

Solution deposition involves soaking an oxide substrate in an anhydrous solution of the

phosphonate monomer while heating for 48 hours.   T-BAG consists of dipping an oxide

surface into a solution of a phosphonate monomer, removing the substrate vertically, and

1.3 Patterning Methods

The ability to pattern biologically relevant molecules is central to many fields of study,

including but not limited to cell growth assays, biosensors, bioelectronics, drug screening,

cell biology, and tissue engineering.[24-27] Over the years, many patterning techniques have

been developed to meet the increasing demands of these fields.   The most common

techniques utilized for biological patterning applications are photolithography,[28, 29]

microcontact printing,[30-32] dip-pen nanolithography,[33, 34] microfluidic devices,[35-37] and

electron beam lithography.[38, 39] Recently, photolithographic techniques have evolved as

robust methods for rapidly fabricating complex patterned substrates.   The main focus of the

research presented here is the development of new photolithography techniques for

biological applications.   As a result, we begin by highlighting the recent developments in

lithographic patterning methods for biological applications with particular emphasis on self-

assembled monolayers (SAMs).   Additionally, the fabrication process involved with

microcontact printing and present some relevant examples will be discussed, since

microcontact printing was also utilized in this research.

The main photolithography methods are divided into four general strategies based upon bond cleavage and/or subsequent bond formation during the patterning process, which are depicted in Scheme 1.1. Here, we present an overview of recent work in this area using a bottom up approach (closest to the substrate to furthest from the substrate). First, we examine complete removal of protein-resistant surface coatings, which involves cleavage of protein-resistant monomers from the substrate. Second, we describe strategies that employ partial cleavage of the monomer chain and result in removal of the tail portion of the molecule. Third, we discuss methods for degrading the tail group. The final general strategy presented is photochemical alteration of the tail group to allow for subsequent covalent ligand attachment. These methods highlight the numerous ways substrates can be tailored to meet the demands of different biological applications.
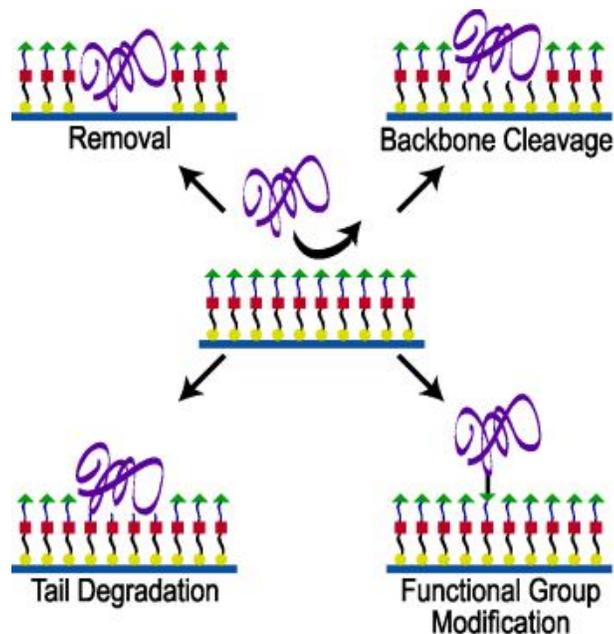
Scheme 1.1 Schematic overview of the four general patterning strategies.

5

1.3.1 Clean Sweep

The use of photochemistry to pattern SAMs has been around since the early 1990s.[40, 41] One of the earliest photolithography methods for patterning SAMs was reported by McIver, Hemminger, and co-workers.[42] In this work, they showed that thiols could be cleanly removed from a gold substrate, which became the foundation for laser desorption Fourier transform mass spectrometry. Hemminger also noted that the thiolate was detected in its oxidized form as a sulfonate. More recently, Leggett and coworkers have used photooxidation of glycol-terminated SAMs to immobilize proteins on the surface as depicted in Figure 1.4A.[43] After oxidation, the glycol regions no longer resisted non-specific protein adsorption, which they demonstrated by adsorbing streptavidin to a patterned surface as shown in Figure 1.4B. Additionally, oxidation of the thiol head group to a sulfonate has been employed by Sun and co-workers in combination with scanning near-field photolithography (SNP).[44] Sun began with an oligo(ethylene glycol) terminated alkylthiolate SAM and selectively ablated regions of the substrate, which allowed them to subsequently bind a different thiol monomer to the patterned regions. In this study, an amine terminated thiol monomer was reacted with the substrate following ablation and, through a series of surface reactions, 200 nm wide lines of ssDNA coated gold and silver nanoparticles were hybridized to the surface.
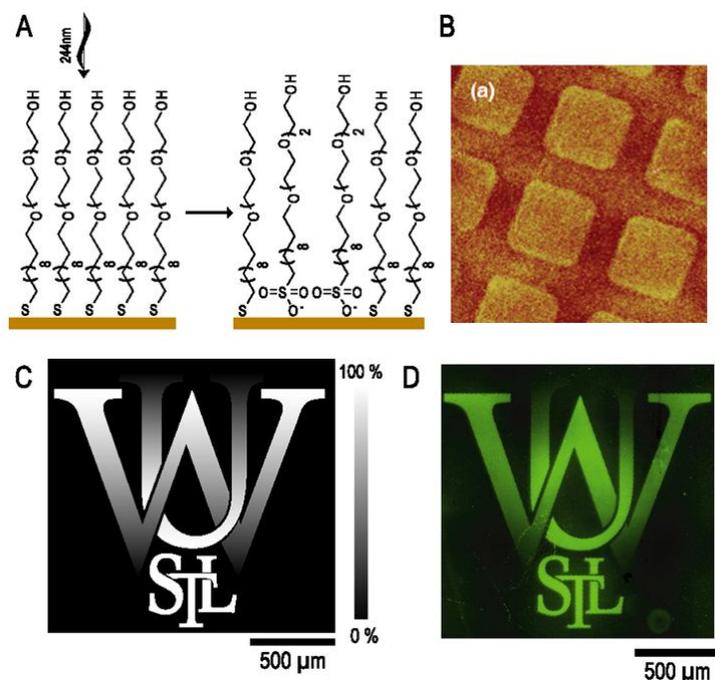
Figure 1.4. Photopatterning through removal of the underlying monolayer. A) Photooxidation of the thiol head group to a sulfonate with 250 nm light, adopted from ref. 43 B) Streptavidin was immobilized on a gold substrate, 40 μm x 40 μm, reproduced from ref. 43 C) 8-bit gray-scale image used to generate pattern by the direct-write photolithography system, reproduced from Chapter 2. D) Fluorescent image of fluorescently labelled neutravidin adsorbed to an ablated substrate, reproduced from Chapter 2.

Besides oxidation, thiol monomers have also been removed from gold substrates by thermal desorption.[45] This method typically involves adsorption into the surface plasmon band of the underlying gold layer, which results in thermal relaxation and localized heating. Local heating cleaves the thiol gold bond leading to thermal desorption. Since this method requires adsorption into the plasmon band, the localized heating generated by a particular excitation wavelength is extremely sensitive to the thickness of the underlying gold layer.[46] Recently, West and co-workers employed thermal desorption in the development of laser scanning lithography (LSL).[47] This method is a "maskless" technique, which provides improved versatility compared to traditional photolithography methods by eliminating the

need for the fabrication of a photomask prior to substrate patterning. West was able to produce micrometer-scale gradients of streptavidin by either controlling the number of iterations from a pulsed femtosecond laser at a given location or by tipping the substrate, which consequently shifted the substrate out of focus of the laser beam. By utilizing LSL, they were able to pattern the GRGDS peptide, a cell adhesive ligand, on the tail of a thiol monomer in regions perpendicular to human plasma fibronectin. This substrate was then used to monitor the growth of human umbilical vein endothelial cells. Thus, LSL provides a means to pattern two cell adhesive ligands on the same substrate.

We have also recently demonstrated that thermal desorption of amide-linked glycol-terminated thiol monomers can be achieved at 325 nm using a continuous wave (CW) He-Cd laser, which is described in detail in Chapter 2.[48] Additionally, we have shown monolayers formed from these monomers are stable under cell culture conditions for up to five weeks.[49] Utilizing a 325 nm CW He-Cd laser provides several advantages over previous thermal desorption techniques. By shifting to a lower wavelength, we absorb into the primary adsorption band of gold and not into the surface plasmon band, which eliminates the sensitivity to thickness. This advantage allows the gold substrate to be either thin, as required for optical microscopy applications, or thick, as required by surface plasmon resonance imaging (SPRi) applications. Additionally, the He-Cd laser was incorporated into a direct-write photolithography system,[50] which generates patterns based on an 8-bit gray-scale image. This variant of direct-write "maskless" photolithography has the advantage that gradients can be easily control by adjusting the gray-scale level in the image file, as shown in Figure 1.4C.[44] Patterns generated by this technique have been visualized using both SPRi and fluorescent microscopy through the adsorption of fluorescently labelled proteins, Figure

1.4D. We have also demonstrated that neutravidin, adsorbed to a glycol ablated substrate, remains active by showing anti-avidin selectively binds to adsorbed neutravidin. This patterning methodology provides a facile way to create gradient protein patterns on a variety of gold substrates independent of their thickness.

1.3.2 Backbone Cleavage

Another popular photopatterning technique for monolayers involved placing a nitrobenzyl group in the backbone of the monomer, which when irradiated will cause the monomer to split into two pieces. Typically, the nitrobenzyl group is used in the backbone to connect a protein resistant tail to an alkane chain covalently bound to a substrate via a thiol or silane head group. Nitrobenzyl is a popular photoprotecting group for these studies because it has reasonable quantum yields for bond cleavage and an ultraviolet adsorption above the absorption wavelength at which triplet oxygen is generated, thus allowing for patterning in air. Additionally, the adsorption maximum for nitrobenzyl allows it to be easily patterned using conventional I-line (365 nm) photolithography equipment. Recently, Nakanishi and co-workers created a mixed monolayer consisting of three unique thiol monomers: a poly(ethylene glycol, PEG) terminated tail with a nitrobenzyl in the backbone, a hepta(ethylene glycol, EG7) terminated tail, and a nitrilotriacetic acid (NTA) functionalized tail.[51] Before irradiation, the PEG monomer sterically blocked the NTA monomer from binding to a His tag, however after the surface was irradiated, the PEG portion of the monomer was cleaved exposing the NTA functionality. Background binding was minimized by the presence of the EG7 monomer.   This mixed monolayer patterning method provided a means to site-selectively pattern fibronectin fragment FNIII$_{7-10}$ and support NIH 3T3 cell growth.

Nakanishi and co-workers incorporated a nitrobenzyl group into the backbone of a silane monomer with a PEG tail.[52] Upon exposure to UV irradiation, the PEG tail of the monomer was cleaved to produce a free amine on the surface. Unlike most patterning techniques, which are done prior to cell culture, in their system, tail group removal could be achieved in cell culture, resulting in a surface that was no longer protein resistant. Thus, patterned cells were able to migrate from their initial location into newly patterned regions on the substrate. In a subsequent report,[53] Kemkemer, Nakanishi, and co-workers demonstrated cleavage of the nitrobenzyl group and removal of the PEG tail to produce an aldehyde functionality on the surface, Figure 1.5A. This strategy was then used to site-selectively pattern epithelial cells into a variety of geometric patterns in order to investigate how boundary curvature affected cell development. They observed that cells on the convex portion of a ring pattern contained more lamellar protrusions than cells on the concave side, as shown in Figure 1.5B. As a result, when the entire surface was irradiated, to remove all the PEG tails, cells on the convex portion of the pattern grew out more rapidly than cells on the concave region. This sequential patterning, in the presence of live cells, demonstrates the versatility photolithography offers for the generation of dynamically modulated substrates.

Besides PEG, Pluronic F108 has also been shown to resist non-specific adsorption of biomolecules on substrates.[54] Recently, Nakanishi, Takarada, and co-workers[55] and Takeda and co-workers[56] have taken advantage of Pluronic F108 resistivity in combination with a nitrobenzyl functionalized slide. Nakanishi, Takarada, and co-workers functionalized a glass coverslip with a nitrobenzyl terminated silane monomer. After silination, Pluronc F108 was coated onto the substrate making it cell repulsive; however, when the surface was irradiated, the nitrobenzyl group was cleaved from the substrate. Consequently, Pluronic F108 was

removed in the patterned regions rendering the irradiated sections cell permissive. Takeda and co-workers took this methodology one step further by creating an initial pattern for PC12 cells to adhere followed by sequentially deprotecting regions around the cell, Figure 1.5C. The PC12 cells then migrated into the newly patterned regions, as shown in Figure 1.5D. Thus, this technique of spin coating a bio-resistant moiety on a photosensitive slide allows for spatial control over cell growth.
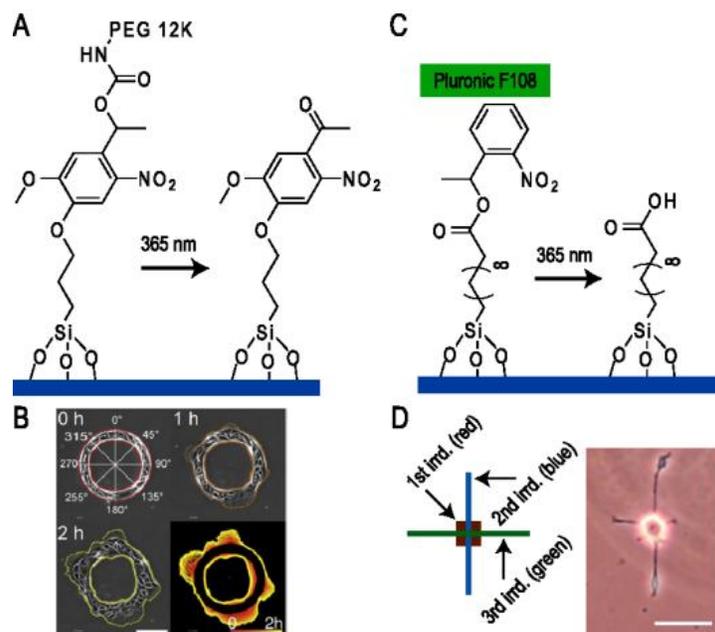
Figure 1.5. Photopatterning through backbone cleavage. A) Nitrobenzyl cleavage releasing the PEG moiety from the substrate, adopted from ref 53. B) Phase-contrast image depicting cell behavior on ring pattern over time. Scale bar, 100 μm, reproduced from ref 53. C) Nitrobenzyl cleavage releasing Pluronic F108, adopted from ref 56. D) Phase contrast image of neurite outgrowth after stepwise photopatterning. Scale bar = 50 μm, reproduced from ref 56.

Contrary to the aforementioned examples, where the patterned region of the substrate became cell permissive, work by Yamaguchi, Nagamune and co-workers has demonstrated the reverse can also be achieved.[57] A plastic substrate was coated with BSA and a photocleavable PEG-lipid was coupled to the free amines of BSA. The PEG-lipid was

oriented with the glycol region being attached to the adsorbed BSA and the alkane chain exposed to the surface with a nitrobenzyl group connecting to two portions. When cells were seeded on the substrate, they became immobilized on the alkane chain. The substrate was then irradiated, which cleaved the nitrobenzyl group and released the alkane chain. This release allowed the cells in the patterned region to be removed from the substrate. Cells in the nonpatterned region did not subsequently migrate into the patterned region due to the presence of the PEG group being exposed after irradiation. This strategy provides a method of "caging" the PEG moiety until irradiation, which results in a reverse patterning strategy compared to typical approaches.

1.3.3 Tail Group Degradation

Interferometric lithography (IL) has been applied by Lopez, Leggett, and co-workers to generate extremely small features on SAMs, Figure 1.6A.[58] This methodology can be applied to thiol,[58] silane,[59] and phosphonate[60] terminated monolayers and produces features as small as 30 nm for silanes and 35 nm for phosphonates. The mechanism of action deals with oxidation of the underlying monolayer from the tail group down to the head group through the creation of excited-state triplet oxygen. They have reported that by controlling the extent of oxidation, they can photochemically oxidize a glycol terminated monomer into an aldehyde while not disturbing the head group covalently bound to the substrate. Once the glycol group has been oxidized, it no longer resists nonspecific protein adsorption. Lopez, Leggett, and co-workers were able to adsorb both BSA and streptavidin to photopatterned glycol-terminated monolayers with a resolution of 100 nm, Figure 1.6B.[58] Thus, IL provides a method for producing nanometer size features on a variety of monolayer substrates.
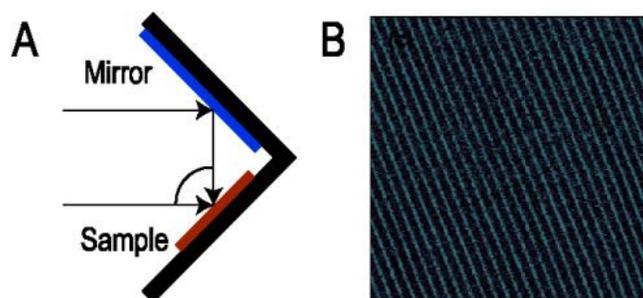
Figure 1.6. Photopatterning by tail degradation. A) Schematic diagram of IL, adopted from ref. 58. B) Phase image from AFM Tapping Mode scan of a glycol-terminated monolayer patterned by IL, 7.4 μm x 7.4 μm, z-contrast range 0-120 dark to bright, reproduced from ref. 58.

1.3.4 Ligand Attachment

The patterning methods described in the previous sections had one aspect in common, photoirradiation resulted in bond cleavage to either remove or expose a protein resistant moiety. Leggett, Chilkoti, and co-workers[61] have developed an alternative strategy in which they functionalized a glass slides with a halogen containing silane monomer on silicon dioxide. Utilizing IL as the photopatterning technique, dehalogenation occurred in the patterned regions and atom transfer radical polymerization (ATRP) was used to grow protein resistant poly[oligo(ethylene glycol)methacrylate] brushes in the nonpatterned regions. These surfaces were exposed to nanoparticles coated with neutravidin to demonstrate that the newly formed polymer brushes resisted nonspecific protein adsorption. Alternatively, work by Klok and coworkers have shown that they can increase protein binding by grafting polymer brushes of poly(glycidyl methacrylate) onto silicon oxide and tantalum pentoxide substrates also utilizing ATRP.[62] Although polymer brushes extend significantly further than SAMs above a substrate, recent work by Hartmann and coworkers has shown that their 3D morphology can be controlled.[63] Overall, grafting polymer brushes provides an alternative strategy that makes use of bond formation after photoirradiation, in place of bond cleavage.

13

Besides the protein-resistant polymer brushes produced by ATRP, other ligands have been attached to substrates after photoirradation in order to control protein adsorption. One popular method for substrate functionalization has been to photoprotect an amine on the surface. Leggett, Micklefield, and co-workers functionalized silicon oxide surfaces with a silane monomer that contained a PEG chain attached to the nitrobenzyl group.[64] Upon UV irradiation with SNP, the nitrobenzyl group was cleaved from the surface, which removed the PEG moiety, and produced a free amine. The free amine was then exposed to NHS-biotin to functionalize the patterned region. Fluorescently labelled neutravidin coated particles were then coupled to the surface and the pattern was visualized by fluorescence microscopy. A similar protein immobilization strategy was employed by del Campo and co-workers to couple streptavidin to a surface.[65] Two major differences exist between the strategies presented by Leggett, Micklefield, and co-workers and del Campo and co-workers. The first difference was the location of the nitrobenzyl group in the silane monomer. del Campo installed the nitrobenzyl group on the tail end of the PEG chain as opposed to in the backbone. The advantage of this strategy is that during the NHS coupling step the amine is not sterically hindered by the adjacent monomers. del Campo also generated gradient patterns by controlling the irradiation dose. Functionalizing a substrate with a photoprotected amine provides a functional handle for additional reactions to occur, which can be utilized to attach ligands for protein immobilization.

We have recently reported a strategy to form amide bonds between photodeprotected carboxylic acids on a surface and free amines in solution, which will be described in detail in Chapter 3.[66] In our system, photoprotected carboxylic acids are deprotected using direct-write photolithography, which provides a facile means to produce gradients. These gradients

were easily visualized by scanning probe microscopy (SPM) using both Kelvin probe force microscopy (KPFM) and quantitative nanomechanical mapping (QNM). After deprotection, site-selective coupling of the acid moiety to two unique amines was achieved resulting in a circle and box pattern. This pattern was visualized by imaging matrix-assisted laser desorption ionization time-of-flight mass spectrometry (MALDI-TOF MS), as shown in Figure 1.7A.[66] This patterning method provides a means to create both smooth and punctate gradients while also being able to align and coupled multiple molecules to the same substrate.

Although photoprotected amines and carboxylic acids provide functional handles on a substrate, they are not bioorthogonal and intermediate coupling ligands are necessary for the immobilization of proteins and other biologically relevant molecules to these substrates. Thus, the development of bioorthogonal strategies for functionalizing surfaces has gained serious attention over the past few years. One strategy presented by Arumugam and Popik was to create a ligand that was photoactive while keeping the substrate inert. They first reported the use of 3-(hydroxymethyl)-2-naphthol (NQMP) derivatives, which when irradiated were converted to 2-napthoquinone-3-methides (*o*NQM).[67] These *o*NQM derivatives then underwent a Diels-Alder reaction with a surface bound alkene or were quickly hydrolyzed back to the starting material. As a proof-of-principle, they synthesized both a NQMP-biotin and NQMP-PEG derivative. The first step in the patterning process involved coupling the NQMP-biotin compound to the surface, which was done by immersing an alkene functionalized slide in a solution of NQMP-biotin followed by photoirradation though a shadow mask, Figure 1.7B. The next step was to remove the NQMP-biotin solution and replace it with the NQMP-PEG solution. The substrate was then flood irradiated to
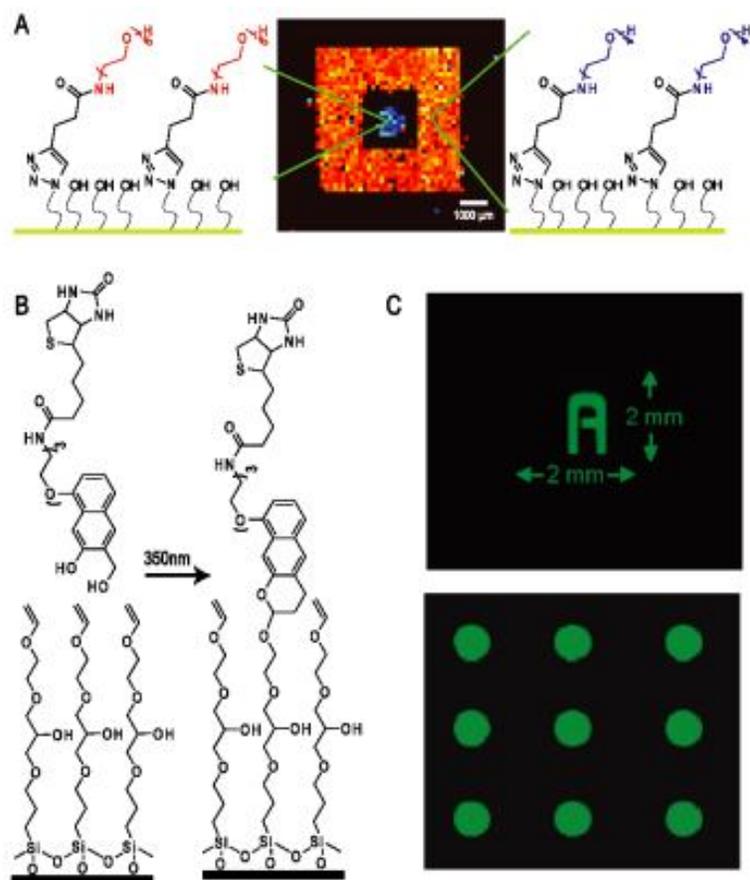
Figure 1.7. Photopatterning with ligand attachment. A) Heat maps generated after analysis for coupled molecules, reproduced from ref. 66. B) Schematic of patterning method utilized by Arumugam and Popik, adopted from ref. 40. C) Fluorescent images of fluorescently labeled avidin bound to the covalently coupled NQMP-biotin probe, circles are ~1mm, reproduced from ref. 67.

couple NQMP-PEG in the background, which resulted in protein resistance, as shown in Figure 1.7C. This patterning methodology was extended to include thiol functionalized slides, which upon prolonged exposure would react with the *o*NQMP-biotin compound by a 1,4 addition.[68] An additional interesting aspect of this work was that the thiol functionalized surfaces could be regenerated with prolonged exposure to UV irradiation in the absence of NQMP derivatives. This methodology provides an efficient way to pattern bioorthogonal ligands and to recycle substrates. An alternative method for patterning strained alkynes and

activated ketones is described in Chapter 4.

Besides thiols and alkenes, other bioorthogonal functional groups have been adapted for surface functionalization. Luo and Yousaf have reported a photo-protected hydroquinone (NVOC-H$_2$Q).[69] In their work, they created a mixed thiol monolayer composed of NVOC-H$_2$Q and a tetra(ethylene glycol) monomer. Upon irradiation, the photoprotecting group was cleaved to produce a hydroquinone moiety, which can electrochemically be oxidized to a quinone. The quinone was treated with an GRGDS peptide derivative containing an amino-oxy group. By combining this photochemistry with a gradient photomask and microcontact printing, Luo and Yousaf were able to create a mixed monolayer system to control Fibroblast cell growth. This work is not only an example of the versatility photochemistry patterning has to offer, but provides a glimpse at the complexity that can be achieved by merging multiple patterning strategies.

1.3.5 Microcontact Printing

Microcontact printing is another popular method for patterning substrates for use in biological applications.[5, 70] This method has been widely employed do to its simplicity and relatively low cost of production. The most labor intensive step in the patterning process is the fabrication of the master, which is outlined in Scheme 1.2. However, masters are commercially available, which removes the need for research groups to have access to clean room facilities and photolithography equipment. Once a master is created, it is used as a template to form multiple rounds of stamps, usually form poly(dimethylsiloxane)(PDMS). These stamps are then "inked" with a molecule, which is transferred to the substrate once the stamp makes physical contact, as shown in Scheme 1.3.
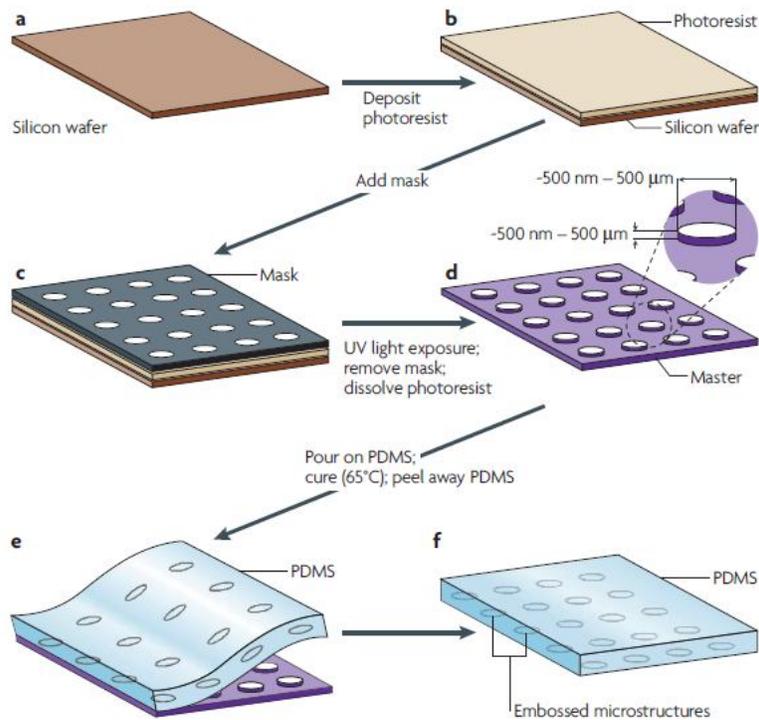
Scheme 1.2 Fabrication of a PDMS stamp, reproduced from ref. 32. A-B) Begin with a silicon wafer and spin coat on a thin layer of photoresist. C) A photomask is used to block the UV light from reaching certain regions of the substrate D) Non-cross-linked photoresist is then removed from the silicon wafer by placing the wafer in a developing solution. E) The master is then coated with PDMS and annealed to form a stamp. F) The resulting PDMS stamp fabricated during this process.
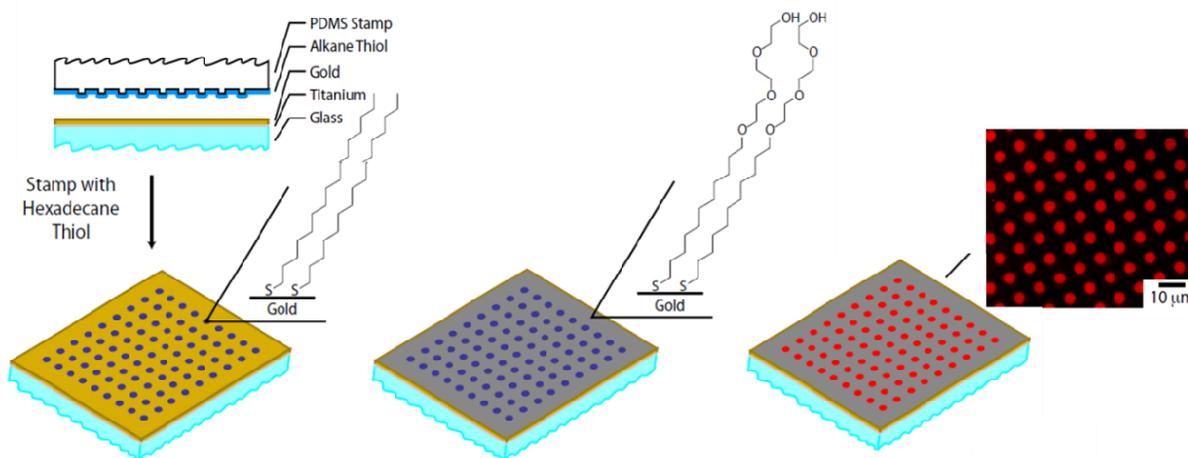
Scheme 1.3 Schematic of microcontact printing. A PDMS stamp is inked with hexadecane thiol and stamped onto a gold coated coverslip. The coverslip is then placed into a solution of a glycol-terminated thiol monomer for 12-14 hours to create a background that resists non-specific protein adsorption. Lastly, the pattern can be visualized by incubating the resulting substrate in a solution of fluorescently labeled protein.

1.4 Characterization Methods

Patterned SAMs have been characterized by a variety of methods including surface infrared (IR) spectroscopy, matrix-assisted laser desorption ionization time-of-flight mass spectrometry (MALDI-TOF MS), scanning probe microscopy (SPM), and surface plasmon resonance imaging (SPRi). Each method provides a unique piece of data about the substrate. Surface IR provides what functional groups are present on the substrate by detecting bond bending and stretching frequencies. This method was also employed to determine if a monolayer was "well-ordered" or not based on the C-H symmetric and asymmetric stretching frequencies. MALDI-TOF MS provides molecular weight information for molecules either coupled to or adsorbed to the surface. SPM is the most versatile of these characterization techniques due to the numerous imaging modes developed, which will be discuss below. SPRi, unlike the other techniques that detect the surface properties, measures interactions between a substrate and species of interest. Overall, each method provides a unique set of surface properties, but the combination of all four provides a complete picture of the substrate's structure and function.

MALDI-TOF MS is a characterization technique that provides molecular weight information of species that are located on a substrate. As indicated in the name, this method utilizes a matrix to facilitate the characterization. Briefly, a surface is coated with a thin layer of matrix, which is used to adsorb energy from the laser and transfer it to the molecules of interest. The molecules on the surface then become excited, detach from the surface, and become ionized. Charged particles are accelerated down the flight tube until they reach the detector. The time a particle takes to travel down the flight tube can be used to calculate its molecular weight. Additionally, molecules can also be desorbed from a substrate without the

need for matrix provided that the underlying metal adsorbs enough energy and can efficiently transfer this energy to ionize the molecules of interest. This technique is termed Laser Desorption Ionization TOF MS (LDI TOF MS).

MALDI-TOF MS is a great technique for determining what species exist on a surface, however knowing how these species affect the overall nanomechanical properties is also important. In order to gain this information, SPM was utilized. SPM is the most versatile of the characterization techniques mentioned due in part to the variety of scanning modes developed since it was introduced in 1986 by Binnig, Quate and Gerber.[71] One of the more recently commercialized modes is quantitative nanomechanical mapping (QNM). QNM provides six surface characterization properties; height, DMT modulus, log DMT modulus, adhesion, dissipation, and deformation. These properties are the result of a probe interacting with a substrate in semi-contact mode, which is outlined in Scheme 1.4. These properties are obtained from a force curve generated during the probe-sample interaction, as shown in Scheme 1.5. Briefly, the scanner begins at a predetermined distance from the surface. As the probe approaches the surface, van der Waals and electrostatic forces increase causing the probe to "jump" and make contact with the surface. This "jump" is noted by the small dip in the force curve on the approach side. The probe is then in contact with the surface. As the scanner extends, the cantilever begins to flex causing a signal change to occur on the detector. Once the signal reaches a predetermined set-point, the scanner begins to retract. As the scanner retracts, the signal drops below a certain threshold and the process begins again. Each full cycle produces a force curve, which can be used to calculate the nanomechanical properties of the substrate as outlined in Scheme 1.5.
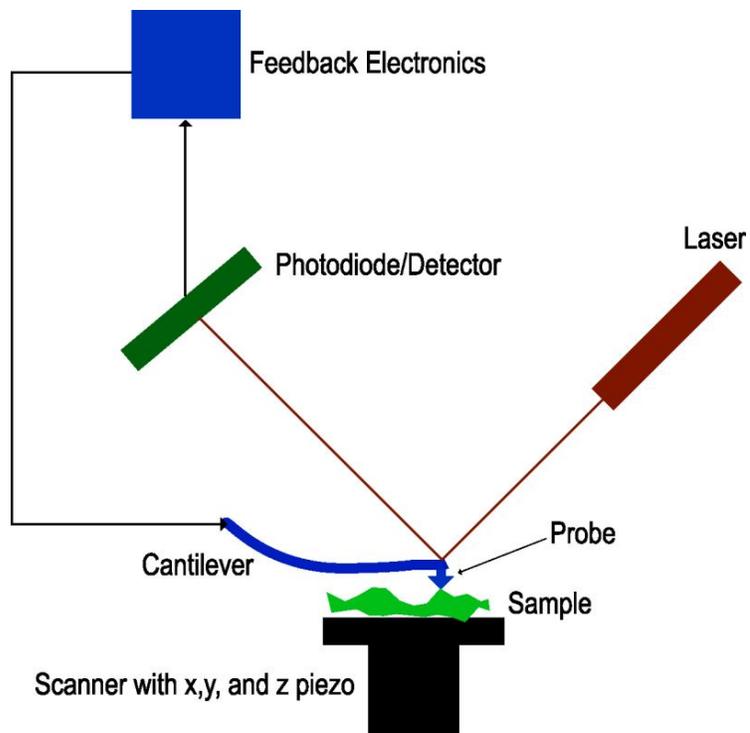
Scheme 1.4. SPM schematic for a stage scan system.
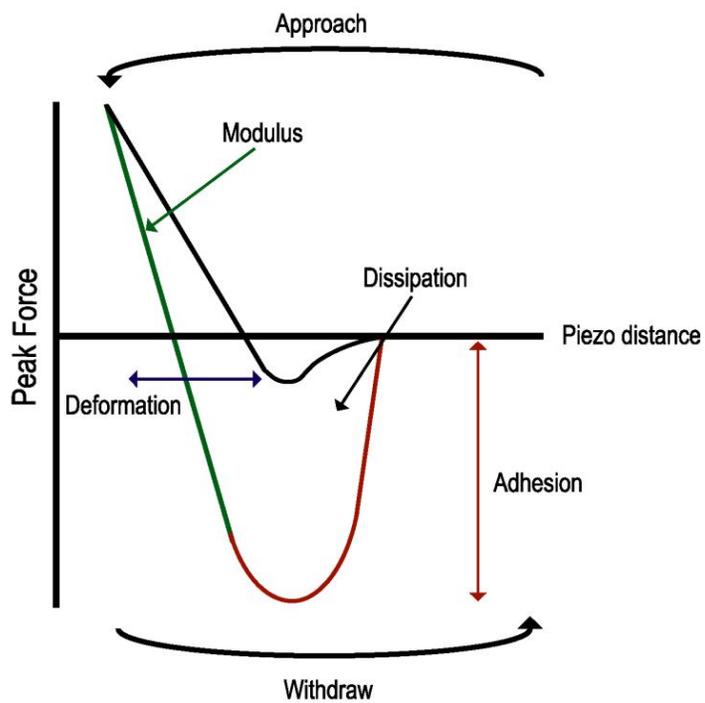
Scheme 1.5 QNM force curve generated from probe surface interaction

While SPM can provide nanomechanical properties of the surface, it cannot detect real-time binding to the surface. In order to obtain this data, SPRi was utilized to monitor protein binding to patterned substrates. Surface plasmons are a result of incident light making contact with a noble metal, in our system gold, and interacting with delocalized electrons.[72] This interaction induces an evanescent wave that extends hundreds of nanometers above the substrate and is very sensitive to changes in refractive indexes. When a compound binds to the surface, it changes the localized refractive index causing a shift in the signal, which is then detected by a camera. The schematic for this process is outline in Scheme 1.6A. The typical SPRi experiment conducted in this research involved equilibrating a patterned substrate, flowing over an analyte of interest, usually protein, and then rinsing the surface to remove any non-specifically bound material, as shown in Scheme 1.6B. After rinsing, a change in the SPR intensity is calculated based on the pixel intensities from the images captured by the CCD camera.
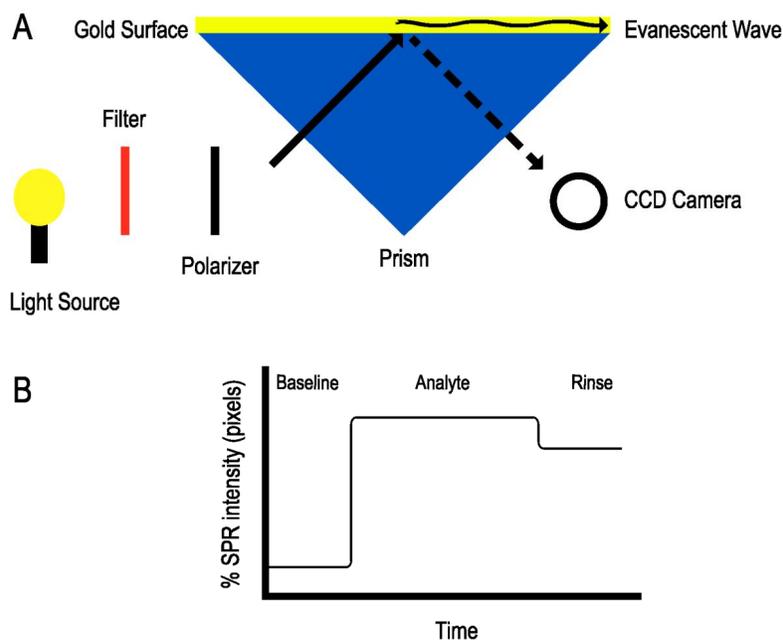
Scheme 1.6. SPRi Instrument Setup. A) Schematic for SPRi experiment. B) Generic SPRi trace.

1.5 Summary and Outlook

Here we describe recent developments in photopatterning substrates for biological applications and the techniques used to characterize them. These methods make use of SAMs and can be roughly divided into four categories; clean sweep, backbone cleavage, tail group degradation, and ligand attachment. This work will describe advances to both clean sweep and ligand attachment patterning strategies. Moreover, the required synthetic organic chemistry and substrate fabrication and characterization will also be addressed. Additionally, future advancements to these techniques and the field as a whole will be described in Chapter 5.

1.6 References

1.   Bain, C. D.; Troughton, E. B.; Tao, Y. T.; Evall, J.; Whitesides, G. M.; Nuzzo, R. G., Formation of monolayer films by the spontaneous assembly of organic thiols from solution onto gold. *Journal of the American Chemical Society* **1989,** 111, (1), 321-335.
2.   Ostuni, E.; Chapman, R. G.; Holmlin, R. E.; Takayama, S.; Whitesides, G. M., A Survey of Structure−Property Relationships of Surfaces that Resist the Adsorption of Protein. *Langmuir* **2001,** 17, (18), 5605-5620.
3.   Strulson, M. K.; Maurer, J. A., Microcontact Printing for Creation of Patterned Lipid Bilayers on Tetraethylene Glycol Self-Assembled Monolayers. *Langmuir* **2011,** 27, (19), 12052-12057.
4.   Wink, T.; J. van Zuilen, S.; Bult, A.; P. van Bennekom, W., Self-assembled Monolayers for Biosensors. *Analyst* **1997,** 122, (4), 43R-50R.
5.   Mrksich, M.; Whitesides, G. M., Patterning self-assembled monolayers using microcontact printing: A new technology for biosensors? *Trends in Biotechnology* **1995,** 13, (6), 228-235.
6.   Christophis, C.; Grunze, M.; Rosenhahn, A., Quantification of the adhesion strength of fibroblast cells on ethylene glycol terminated self-assembled monolayers by a microfluidic shear force assay. *Physical Chemistry Chemical Physics* **2010,** 12, (17), 4498-4504.
7.   Laibinis, P. E.; Fox, M. A.; Folkers, J. P.; Whitesides, G. M., Comparisons of self-assembled monolayers on silver and gold: mixed monolayers derived from HS(CH2)21X and HS(CH2)10Y (X, Y = CH3, CH2OH) have similar properties. *Langmuir* **1991,** 7, (12), 3167-3173.
8.   Laibinis, P. E.; Whitesides, G. M.; Allara, D. L.; Tao, Y. T.; Parikh, A. N.; Nuzzo, R. G., Comparison of the structures and wetting properties of self-assembled monolayers of n-alkanethiols on the coinage metal surfaces, copper, silver, and gold. *Journal of the American Chemical Society* **1991,** 113, (19), 7152-7167.

9.   Petrovykh, D. Y.; Kimura-Suda, H.; Opdahl, A.; Richter, L. J.; Tarlov, M. J.; Whitman, L. J., Alkanethiols on Platinum: Multicomponent Self-Assembled Monolayers. *Langmuir* **2006,** 22, (6), 2578-2587.

10.   Demoz, A.; Harrison, D. J., Characterization and extremely low defect density hexadecanethiol monolayers on mercury surfaces. *Langmuir* **1993,** 9, (4), 1046-1050.

11.   Nuzzo, R. G.; Korenic, E. M.; Dubois, L. H., Studies of the temperature-dependent phase behavior of long chain n-alkyl thiol monolayers on gold. *Journal of Chemical Physics* **1990,** 93, (1), 767.

12.   Porter, M. D.; Bright, T. B.; Allara, D. L.; Chidsey, C. E. D., Spontaneously organized molecular assemblies. 4. Structural characterization of n-alkyl thiol monolayers on gold by optical ellipsometry, infrared spectroscopy, and electrochemistry. *Journal of the American Chemical Society* **1987,** 109, (12), 3559-3568.

13.   Snyder, R. G.; Strauss, H. L.; Elliger, C. A., Carbon-hydrogen stretching modes and the structure of n-alkyl chains. 1. Long, disordered chains. *The Journal of Physical Chemistry* **1982,** 86, (26), 5145-5150.

14.   Sinniah, K.; Cheng, J.; Terrettaz, S.; Reutt-Robey, J. E.; Miller, C. J., Self-Assembled .omega.-Hydroxyalkanethiol Monolayers with Internal Functionalities: Electrochemical and Infrared Structural Characterizations of Ether-Containing Monolayers. *The Journal of Physical Chemistry* **1995,** 99, (39), 14500-14505.

15.   Dubois, L. H.; Zegarski, B. R.; Nuzzo, R. G., Molecular ordering of organosulfur compounds on Au(111) and Au(100): Adsorption from solution and in ultrahigh vacuum. *Journal of Chemical Physics* **1993,** 98, (1), 678.

16.   Strong, L.; Whitesides, G. M., Structures of self-assembled monolayer films of organosulfur compounds adsorbed on gold single crystals: electron diffraction studies. *Langmuir* **1988,** 4, (3), 546-558.

17.   Gouzman, I.; Dubey, M.; Carolus, M. D.; Schwartz, J.; Bernasek, S. L., Monolayer vs. multilayer self-assembled alkylphosphonate films: X-ray photoelectron spectroscopy studies. *Surface Science* **2006,** 600, (4), 773-781.

18.   McDermott, J. E.; McDowell, M.; Hill, I. G.; Hwang, J.; Kahn, A.; Bernasek, S. L.; Schwartz, J., Organophosphonate Self-Assembled Monolayers for Gate Dielectric Surface Modification of Pentacene-Based Organic Thin-Film Transistors: A Comparative Study†. *The Journal of Physical Chemistry A* **2007,** 111, (49), 12333-12338.

19.   Paz, Y., Self-assembled monolayers and titanium dioxide: From surface patterning to potential applications. *Beilstein Journal of Nanotechnology* **2011,** 2, 845-861.

20.   Jo, K.; Yu, H.-Z.; Yang, H., Formation kinetics and stability of phosphonate self-assembled monolayers on indium–tin oxide. *Electrochimica Acta* **2011,** 56, (13), 4828-4833.

21.   Hoque, E.; DeRose, J. A.; Kulik, G.; Hoffmann, P.; Mathieu, H. J.; Bhushan, B., Alkylphosphonate Modified Aluminum Oxide Surfaces. *The Journal of Physical Chemistry B* **2006,** 110, (22), 10855-10861.

22.   Gao, W.; Dickinson, L.; Grozinger, C.; Morin, F. G.; Reven, L., Self-Assembled Monolayers of Alkylphosphonic Acids on Metal Oxides. *Langmuir* **1996,** 12, (26), 6429-6435.

23.   Dubey, M.; Weidner, T.; Gamble, L. J.; Castner, D. G., Structure and Order of Phosphonic Acid-Based Self-Assembled Monolayers on Si(100). *Langmuir* **2010,** 26, (18), 14747-14754.

24.   Mendes, P.; Yeung, C.; Preece, J., Bio-nanopatterning of Surfaces. *Nanoscale Research Letters* **2007,** 2, (8), 373-384.

25.   Bengt, K., Biological surface science. *Surface Science* **2002,** 500, (1–3), 656-677.

26.   Yap, F. L.; Zhang, Y., Protein and cell micropatterning and its integration with micro/nanoparticles assembly. *Biosensors and Bioelectronics* **2007,** 22, (6), 775-788.

27.   Chiu, D. T.; Jeon, N. L.; Huang, S.; Kane, R. S.; Wargo, C. J.; Choi, I. S.; Ingber, D. E.; Whitesides, G. M., Patterned deposition of cells and proteins onto surfaces by using three-dimensional microfluidic systems. *Proceedings of the National Academy of Sciences* **2000,** 97, (6), 2408-2413.

28.   Mooney, J. F.; Hunt, A. J.; McIntosh, J. R.; Liberko, C. A.; Walba, D. M.; Rogers, C. T., Patterning of Functional Antibodies and Other Proteins by Photolithography of Silane Monolayers. *Proceedings of the National Academy of Sciences of the United States of America* **1996,** 93, (22), 12287-12291.

29.   Naiser, T.; Mai, T.; Michel, W.; Ott, A., Versatile maskless microscope projection photolithography system and its application in light-directed fabrication of DNA microarrays. *Review of Scientific Instruments* **2006,** 77, (6), 063711-11.

30.   Akbulut, O.; Yu, A. A.; Stellacci, F., Fabrication of biomolecular devices via supramolecular contact-based approaches. *Chemical Society Reviews* **2010,** 39, (1), 30-37.

31.   Wendeln, C.; Ravoo, B. J., Surface Patterning by Microcontact Chemistry. *Langmuir* **2012,** 28, (13), 5527-5538.

32.   Weibel, D. B.; DiLuzio, W. R.; Whitesides, G. M., Microfabrication meets microbiology. *Nature Reviews Microbiology* **2007,** 5, (3), 209-218.

33.   Wu, C.-C.; Reinhoudt, D. N.; Otto, C.; Subramaniam, V.; Velders, A. H., Strategies for Patterning Biomolecules with Dip-Pen Nanolithography. *Small* **2011,** 7, (8), 989-1002.

34.   Braunschweig, A. B.; Huo, F.; Mirkin, C. A., Molecular printing. *Nat Chem* **2009,** 1, (5), 353-358.

35.   Siegel, A. C.; Tang, S. K. Y.; Nijhuis, C. A.; Hashimoto, M.; Phillips, S. T.; Dickey, M. D.; Whitesides, G. M., Cofabrication: A Strategy for Building Multicomponent Microsystems. *Accounts of Chemical Research* **2010,** 43, (4), 518-528.

36.   Maerkl, S. J., Next generation microfluidic platforms for high-throughput protein biochemistry. *Current Opinion in Biotechnology* **2011,** 22, (1), 59-65.

37.   Liu, K.; Fan, Z. H., Thermoplastic microfluidic devices and their applications in protein and DNA analysis. *Analyst* **2011,** 136, (7), 1288-1297.

38.   Kolodziej, C. M.; Maynard, H. D., Electron-Beam Lithography for Patterning Biomolecules at the Micron and Nanometer Scale. *Chemistry of Materials* **2011,** 24, (5), 774-780.

39.   Ballav, N.; Terfort, A.; Zharnikov, M., Making Gradient Patterns by Electron-Beam Chemical Lithography with Monomolecular Resists. In *Soft Matter Gradient Surfaces*, John Wiley & Sons, Inc.: 2012; pp 199-227.

40.   Stenger, D. A.; Georger, J. H.; Dulcey, C. S.; Hickman, J. J.; Rudolph, A. S.; Nielsen, T. B.; McCort, S. M.; Calvert, J. M., Coplanar molecular assemblies of amino- and perfluorinated alkylsilanes: characterization and geometric definition of mammalian cell adhesion and growth. *Journal of the American Chemical Society* **1992,** 114, (22), 8435-8442.

41.   Dulcey, C. S.; Georger, J. H., Jr.; Krauthamer, V.; Stenger, D. A.; Fare, T. L.; Calvert, J. M., Deep UV Photochemistry of Chemisorbed Monolayers: Patterned Coplanar Molecular Assemblies. *Science* **1991,** 252, (5005), 551-554.

42.   Li, Y.; Huang, J.; McIver, R. T.; Hemminger, J. C., Characterization of thiol self-assembled films by laser desorption Fourier transform mass spectrometry. *Journal of the American Chemical Society* **1992,** 114, (7), 2428-2432.

43.   Ducker, R. E.; Janusz, S.; Sun, S.; Leggett, G. J., One-Step Photochemical Introduction of Nanopatterned Protein-Binding Functionalities to Oligo(ethylene glycol)-Terminated Self-Assembled Monolayers. *Journal of the American Chemical Society* **2007,** 129, (48), 14842-14843.

44.   Sun, S.; Thompson, D. G.; Graham, D.; Leggett, G. J., DNA nanofabrication by scanning near-field photolithography of oligo(ethylene glycol) terminated SAMs: Controlled scan-rate dependent switching between head group oxidation and tail group degradation. *Journal of Materials Chemistry* **2011,** 21, (37), 14173-14177.

45.   Shadnam, M. R.; Kirkwood, S. E.; Fedosejevs, R.; Amirfazli, A., Direct Patterning of Self-Assembled Monolayers on Gold Using a Laser Beam. *Langmuir* **2004,** 20, (7), 2667-2676.

46.   Feng, B.; Li, Z.; Zhang, X., Prediction of size effect on thermal conductivity of nanoscale metallic films. *Thin Solid Films* **2009,** 517, (8), 2803-2807.

47.   Slater, J. H.; Miller, J. S.; Yu, S. S.; West, J. L., Fabrication of Multifaceted Micropatterned Surfaces with Laser Scanning Lithography. *Advanced Functional Materials* **2011,** 21, (15), 2876-2888.

48.   Hynes, M. J.; Maurer, J. A., Photoinduced Monolayer Patterning for the Creation of Complex Protein Patterns. *Langmuir* **2012,** 28, (47), 16237-16242.

49.   Strulson, M. K.; Johnson, D. M.; Maurer, J. A., Increased Stability of Glycol-Terminated Self-Assembled Monolayers for Long-Term Patterned Cell Culture. *Langmuir* **2012,** 28, (9), 4318-4324.

50.   Lullo, G.; Leto, R.; Oliva, M.; Arnone, C., Multilevel pattern generation by GaN laser lithography: an application to beam shaper fabrication. **2006**, 62900A-62900A.

51.   Jun Nakanishi and Hidekazu Nakayama and Kazuo Yamaguchi and Andres, J. G. a. Y. H., Dynamic culture substrate that captures a specific extracellular matrix protein in response to light. *Science and Technology of Advanced Materials* **2011,** 12, (4), 044608.

52.   Kaneko, S.; Nakayama, H.; Yoshino, Y.; Fushimi, D.; Yamaguchi, K.; Horiike, Y.; Nakanishi, J., Photocontrol of cell adhesion on amino-bearing surfaces by reversible conjugation of poly(ethylene glycol) via a photocleavable linker. *Physical Chemistry Chemical Physics* **2011,** 13, (9), 4051-4059.

53.   Rolli, C. G.; Nakayama, H.; Yamaguchi, K.; Spatz, J. P.; Kemkemer, R.; Nakanishi, J., Switchable adhesive substrates: Revealing geometry dependence in collective cell behavior. *Biomaterials* **2012,** 33, (8), 2409-2418.

54.   Liu, V. A.; Jastromb, W. E.; Bhatia, S. N., Engineering protein and cell adhesivity using PEO-terminated triblock polymers. *Journal of Biomedical Materials Research* **2002,** 60, (1), 126-134.

55.   Nakanishi, J.; Kikuchi, Y.; Inoue, S.; Yamaguchi, K.; Takarada, T.; Maeda, M., Spatiotemporal Control of Migration of Single Cells on a Photoactivatable Cell Microarray. *Journal of the American Chemical Society* **2007,** 129, (21), 6694-6695.

56.   Edagawa, Y.; Nakanishi, J.; Yamaguchi, K.; Takeda, N., Spatiotemporally controlled navigation of neurite outgrowth in sequential steps on the dynamically photo-patternable surface. *Colloids and Surfaces B: Biointerfaces* **2012,** 99, (0), 20-26.

57.   Yamaguchi, S.; Yamahira, S.; Kikuchi, K.; Sumaru, K.; Kanamori, T.; Nagamune, T., Photocontrollable Dynamic Micropatterning of Non-adherent Mammalian Cells Using a

Photocleavable Poly(ethylene glycol) Lipid. *Angewandte Chemie International Edition* **2012,** 51, (1), 128-131.

58.   Adams, J.; Tizazu, G.; Janusz, S.; Brueck, S. R. J.; Lopez, G. P.; Leggett, G. J., Large-Area Nanopatterning of Self-Assembled Monolayers of Alkanethiolates by Interferometric Lithography. *Langmuir* **2010,** 26, (16), 13600-13606.

59.   Tizazu, G.; el Zubir, O.; Patole, S.; McLaren, A.; Vasilev, C.; Mothersole, D.; Adawi, A.; Hunter, C.; Lidzey, D.; Lopez, G.; Leggett, G., Micrometer and Nanometer Scale Photopatterning of Proteins on Glass Surfaces by Photo-degradation of Films Formed from Oligo(Ethylene Glycol) Terminated Silanes. *Biointerphases* **2012,** 7, (1), 1-9.

60.   Tizazu, G.; El-Zubir, O.; Brueck, S. R. J.; Lidzey, D. G.; Leggett, G. J.; Lopez, G. P., Large area nanopatterning of alkylphosphonate self-assembled monolayers on titanium oxide surfaces by interferometric lithography. *Nanoscale* **2011,** 3, (6), 2511-2516.

61.   Ahmad, S.; Leggett, G.; Hucknall, A.; Chilkoti, A., Micro- and Nanostructured Poly[oligo(ethylene glycol)methacrylate] Brushes Grown From Photopatterned Halogen Initiators by Atom Transfer Radical Polymerization. *Biointerphases* **2011,** 6, (1), 8-15.

62.   Barbey, R.; Kauffmann, E.; Ehrat, M.; Klok, H.-A., Protein Microarrays Based on Polymer Brushes Prepared via Surface-Initiated Atom Transfer Radical Polymerization. *Biomacromolecules* **2010,** 11, (12), 3467-3479.

63.   Mathieu, M.; Friebe, A.; Franzka, S.; Ulbricht, M.; Hartmann, N., Surface-Initiated Polymerization on Laser-Patterned Templates: Morphological Scaling of Nanoconfined Polymer Brushes. *Langmuir* **2009,** 25, (20), 12393-12398.

64.   Alang Ahmad, S. A.; Wong, L. S.; ul-Haq, E.; Hobbs, J. K.; Leggett, G. J.; Micklefield, J., Protein Micro- and Nanopatterning Using Aminosilanes with Protein-Resistant Photolabile Protecting Groups. *Journal of the American Chemical Society* **2011,** 133, (8), 2749-2759.

65.   Álvarez, M.; Alonso, J. M. a.; Filevich, O.; Bhagawati, M.; Etchenique, R.; Piehler, J.; del Campo, A. n., Modulating Surface Density of Proteins via Caged Surfaces and Controlled Light Exposure. *Langmuir* **2011,** 27, (6), 2789-2795.

66.   Hynes, M. J.; Maurer, J. A., Unmasking Photolithography: A Versatile Way to Site-Selectively Pattern Gold Substrates. *Angewandte Chemie International Edition* **2012,** 51, (9), 2151-2154.

67.   Arumugam, S.; Popik, V. V., Patterned Surface Derivatization Using Diels–Alder Photoclick Reaction. *Journal of the American Chemical Society* **2011,** 133, (39), 15730-15736.

68.   Arumugam, S.; Popik, V. V., Attach, Remove, or Replace: Reversible Surface Functionalization Using Thiol–Quinone Methide Photoclick Chemistry. *Journal of the American Chemical Society* **2012,** 134, (20), 8408-8411.

69.   Luo, W.; Yousaf, M. N., Tissue Morphing Control on Dynamic Gradient Surfaces. *Journal of the American Chemical Society* **2011,** 133, (28), 10780-10783.

70.   Perl, A.; Reinhoudt, D. N.; Huskens, J., Microcontact Printing: Limitations and Achievements. *Advanced Materials* **2009,** 21, (22), 2257-2268.

71.   Binnig, G.; Quate, C. F.; Gerber, C., Atomic Force Microscope. *Physical Review Letters* **1986,** 56, (9), 930-933.

72.   Pattnaik, P., Surface plasmon resonance. *Applied Biochemistry and Biotechnology* **2005,** 126, (2), 79-92.

Chapter 2

Photo-Induced Monolayer Patterning for the Creation of Complex Protein Patterns

2.1 Introduction

Well defined protein patterns are emerging as a critical tool for many biological applications, including, but not limited to, cell growth assays, biosensors, bioelectronics, and drug screening.[1-3] Substrates for these applications typically need to possess defined regions for protein attachment, while maintaining a bio-inert background that prevents non-specific protein and cell attachment. One of the most robust methods for creating substrates with these properties is the functionalization of gold substrates with thiol-terminated self-assembled monolayers (SAMs). SAMs on gold are easy to prepare while also providing a wide range of chemical functionality for further surface modification.[4, 5] Two of the most popular patterning techniques for SAMs are microcontact printing[6, 7] and dip pen nanolithography.[8] These techniques require physically placing a protein absorbent molecule in one region of the surface and then backfilling the remainder of the substrate with a protein resistant molecule to create a bio-inert background. Typically, this background region consists of glycol-terminated alkane thiols monomers, which have been shown to resist nonspecific protein adsorption.[9] While traditional glycol-terminated thiols have limited stability in cell culture, we have recently shown that amide-linked variants of the classical molecules are stable for up to five weeks in cell culture.[10, 11] Here we report a versatile non-contact method for directly patterning an amide-linked glycol-terminated monolayer, which allows us to create complex protein patterns, including smooth protein gradients with quantitative control over protein adsorption. To further demonstrate the versatility

28

of this method, we have adsorbed neutravidin to a pattern substrate and showed that neutravidin retains its ability to be recognized by an anti-avidin antibody.

Recently, non-contact based methods have been developed to directly pattern glycol-terminated monolayers. These methods can be divided into three main categories based on their mechanism of action; functional group modification, thermal desorption, and oxidation. The functional group modification method involves the inclusion of a photo-cleavable functional group within the backbone of the monomer, which when photo-irradiated produces regions for protein attachment.[12-15] Thermal desorption has most recently been reported by West and coworkers in the development of Laser Scanning Lithography (LSL).[16] In this work glycol–terminated monomers are thermally desorbed as a result of excitation into the plasmon band of the gold substrate. Using LSL, West created gradients by either controlling the iterations of the laser or by tipping the substrate to defocus the laser beam. However, West observed a dependence on gold thickness, as a result of hitting the plasmon band, which was consistent with previous reports[17] The principle oxidation methods are electron beam lithography (EBL)[18, 19] and scanning near-field photolithography (SNP).[20] EBL works by oxidation of the glycol tail, which creates regions that are no longer protein resistant. When these surfaces were exposed to protein solutions, proteins are able to absorb to the patterned regions. SNP also oxidizes the tail of glycol-terminated monolayers, but can also oxidize the thiol head group to a sulfonate. The sulfonate can then be readily replaced by another thiol in solution. Utilizing SNP, Leggett and coworkers were able to pattern features down to 9 nm, however to date no gradient patterns have been reported using this methodology. Here we report a versatile method for producing gradient patterns on protein resistant surfaces through photoinduced monolayer desorption of glycol-

terminated thiol monomers. Since we are utilizing a He-Cd laser operating at 325 nm, we facilitate thermal desorption by adsorbing into a resonance band that does not shift based on gold thickness.[17]

2.2 Experimental Methods

2.2.1 Materials and Instrumentation

All reagents were obtained from Sigma-Aldrich (St. Louis, MO) or VWR Scientific (Radnor, PA), were reagent grade or higher, and used as received unless otherwise indicated. ^{1}H NMR and ^{13}C NMR were collected on a 300 MHz Varian NMR (Agilent Technologies, Santa Barbra, CA). All NMR spectra are attached in Appendix B. Plasma oxidation of glass substrates was carried out in a Femto standard low-pressure plasma system (Diener electronic GmbH+Co. KG, Nagold). Gold substrates were prepared using a PVD 75 (Kurt J Lesker, Pittsburg, PA). Scanning Probe Microscopy (SPM) images were collected on a MultiMode 8 configured for quantum nanomechanical mapping (QNM) (Bruker Corporation, Santa Barbara, CA). Substrates were patterned using a direct-writer LaserWriter (Microtech, Palermo, Italy) system equipped with a 325 nm He:Cd laser operating at 15 mW and the beam was focused to 2 um^2 producing a laser spot intensity of ~7.5x10^5 W/cm^2. Surface plasmon resonance imaging (SPRi) was conducted on a SPRimager II (GWC Technologies, Madison, WI). Refractive indices of the ethanolic solutions used for SPRi calibration were measured on an Abbe 56 (Bausch & Lomb, Rochester, NY). Fluorescent images were captured on a Nikon TE2000-PFS microscope running NIS-Elements imaging software equipped with a Prior XY stage, and Photometrics CoolSNAP monochrome camera. Reflectance infrared spectra were collected on a Thermo

(Waltham, MA, USA) Nicolet Nexus 670 FT-IR with a Smart SAGA (Specular Apertured Grazing Angle) accessory with a nitrogen cooled mercury cadmium telluride (MCT/A) detector.

2.2.2 Substrate Preparation and Pattern Generation. Gold substrates were prepared by depositing 50 Å of titanium at 0.1 Å/sec followed by 425 Å of gold at 0.1 Å/sec on a glass coverslip. Gold substrates were soaked in a 1 mM ethanolic solution the glycol-terminated monomer for 12-14 hours. Slides were then rinsed with ethanol, water, and ethanol, and dried under a stream of nitrogen gas. Patterns were designed and generated using CleWin, a software layout editor, (WieWeb, Netherlands) or Adobe Illustrator. Substrates were then patterned using a commercial direct-write photolithography system (Microtech, Palermo, Italy), according to an uploaded 8-bit file in stage scan mode, between 0 and 100% power ($1.6x10^{12}$ photons/um^2). After photoablation, slides were rinsed with ethanol, water, ethanol, and dried under a stream of nitrogen. Freshly patterned substrates were used for protein adsorption studies.
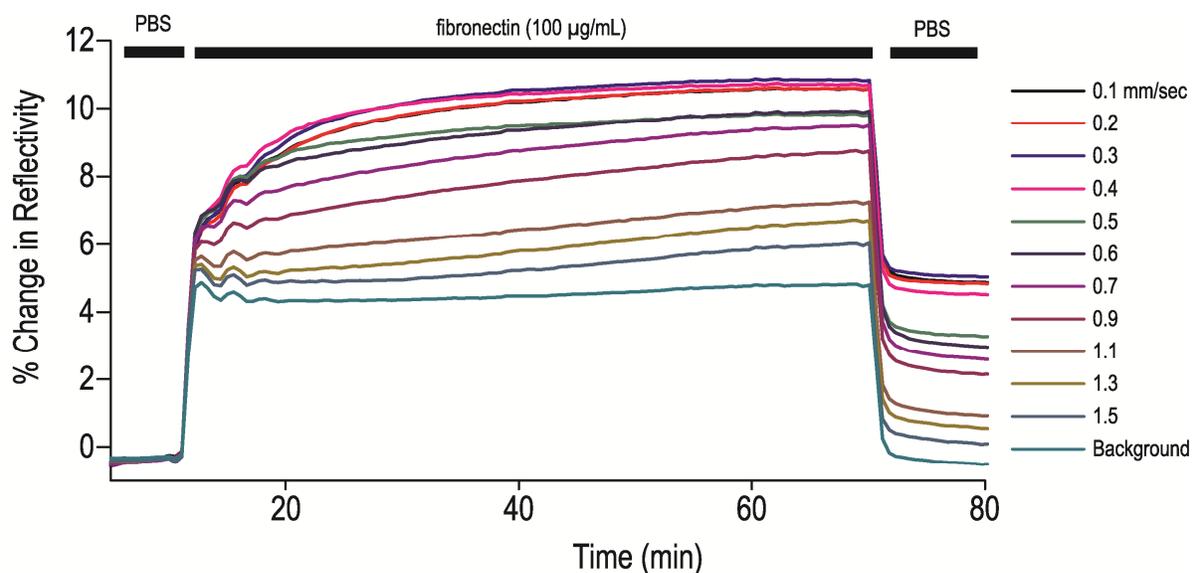
2.2.3 Surface Plasmon Resonance Imaging. Protein adsorption to patterned gradients was characterized using surface plasmon resonance imaging (SPRi) on a SPRimager II (GWC Technologies, Madison, WI).

2.2.4 Write Speed Optimization. In order to optimize the write speed of our direct-write photolithography system, glycol-terminated SAMs were prepared by soaking a gold slide (50 Å Ti, 425 Å Au) in an ethanolic solution of 1 mM glycol-terminated monomer for 12-14 hours. Slides were then rinsed with ethanol, water, and ethanol, and dried under a stream of nitrogen. Eleven lines of various speeds were patterned on the freshly prepared substrates with each line being 100 μm wide and 2000 μm long, **Figure 2.1**. As shown in **Figure 2.2**, as the write speed increased, the amount of fibronectin adsorbed decreased. By plotting the percent change in

31

reflectivity verse the log of number of photons for each patterned region, we were able to determine the minimal write speed for maximal protein adsorption, which was 0.3 mm/sec. Thus, a write speed of 0.3 mm/sec was used for all the studies reported here.
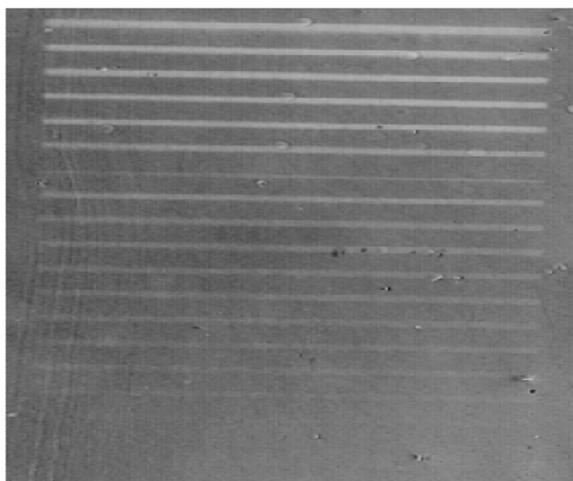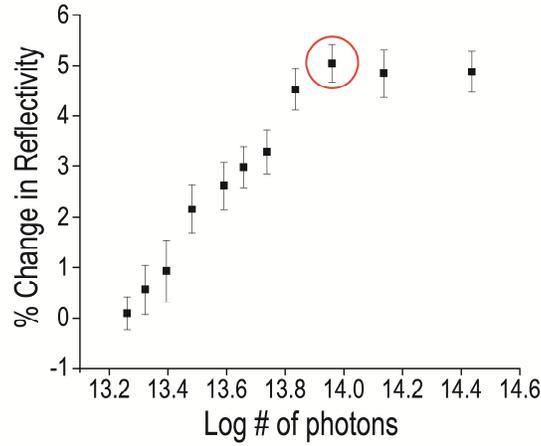

Figure 2.1. Difference imaged for write speed optimization.

Figure 2.2 SPRi trace of fibronectin adsorption to write speed optimization substrate. The substrate was equilibrated with PBS buffer and fibronectin was flowed over the substrate for approximately 1 hour to reach maximum adsorption before rinsing with PBS buffer.

Figure 2.3. Correlation between percent change in reflectivity of the substrate and laser intensity. A write speed of 0.3 mm/sec corresponded to the highest percent change in reflectivity (circled in red).

2.2.5 Surface Plasmon Resonance Calibration and Protein Concentration Calculations.

Protein adsorption to patterned gradients was characterized using surface plasmon resonance imaging (SPRi) on a SPRimager II (GWC Technologies, Madison, WI). The SPRi was calibrated as outlined by Shumaker-Parry and Campbell.[21] Briefly, the instrument sensitivity was calculated by flowing over a range of ethanol solutions in water to measure the percent change in reflectivity as a function of the refractive index of the solution. The slope of this line provided the sensitivity factor for the system, s. This calibration gave the curve, y=8235x, R^2=0.96.

From here, we can calculate the thickness of protein adsorbed on the surface using the equation **1**;

$$d = \left(\frac{l_d}{2}\right)\left[\frac{\Delta I}{s(n_a - n_s)}\right] \qquad (\mathbf{1})$$

where d is the thickness of protein adsorbed to the surface

33

l_d is the decay length of the evanescent field near the gold surface (typically 37 ± 13 % of the wavelength of light, our system operates at 800 nm)

ΔI is the measured reflected intensity shift at a high contrast angle

s is the instrument sensitivity factor. This value is gained from the slope of the calibration curve.

n_a is the index of refraction of the analyte being adsorbed

n_s is the index of refraction of the solvent

Thus for one fibronectin time point,

$$d = \left(\frac{296\ nm}{2}\right)\left[\frac{10.5}{8235(1.57 - 1.3339)}\right]$$

$$d = 0.799\ nm = 7.99\ x10^{-8} cm$$

Thickness can be converted to coverage using the specific density of the protein. Globular proteins range from 0.71 to 0.75 cm^3/g,[21] and we used 0.73 cm^3/g.

$$Coverage\left(\frac{g}{cm^2}\right) = 7.99x10^{-8} cm\ x\ \frac{1g}{0.73\ cm^3}$$

$$= 1.094\ x10^{-7}\frac{g}{cm^2}\ or\ 109.4\ \frac{ng}{cm^2}$$

$$Coverage\left(\frac{molecules}{cm^2}\right) = 1.094\ x10^{-7}\frac{g}{cm^2}\ x\ \frac{1\ mole}{440,000g}\ x\ \frac{6.02x10^{23} molecules}{1\ mole}$$

$$= 1.49x10^{11}\frac{molecules}{cm^2}$$

2.2.6 Scanning Probe Microscopy Analysis: Patterned gradients were characterized using quantitative nanomechanical mapping (QNM) on a MultiMode 8 scanning probe microscope (Bruker, Santa Barbara, CA). For QNM analysis, TAP150 probes (Bruker, Santa Barbara, CA) consisting of 1-10 Ohm-cm phosphorus doped silicon tip on a silicon nitride cantilever with

nominal force constants of 5.0 N/m were employed. Images were acquired in PeakForce QNM mode with a 150 μm scan area at a rate of 0.244 Hz with 2048 points per line with 2048 lines.

2.2.7 Reflectance infrared spectroscopy: SAMs used for reflectance IR studies were prepared by soaking a gold slide (4000 Å Ti, 100 Å Au) in an ethanolic solution of 1 mM either glycol-terminated thiol monomer, monomer 1, or monomer 2 for 12-14 hours. Substrates were then rinsed with ethanol, water, and ethanol and then dried under a stream of nitrogen. Photo-induced monolayer patterning was conducted on freshly prepared glycol-terminated substrates using a commercially available direct-write laser writer in stage scan mode operating at 325 nm with a write speed of 0.3 mm/sec. After patterning, each substrate was analyzed by reflectance IR with each spectrum containing 1024 scans with a data spacing of 0.964 cm^{-1}.
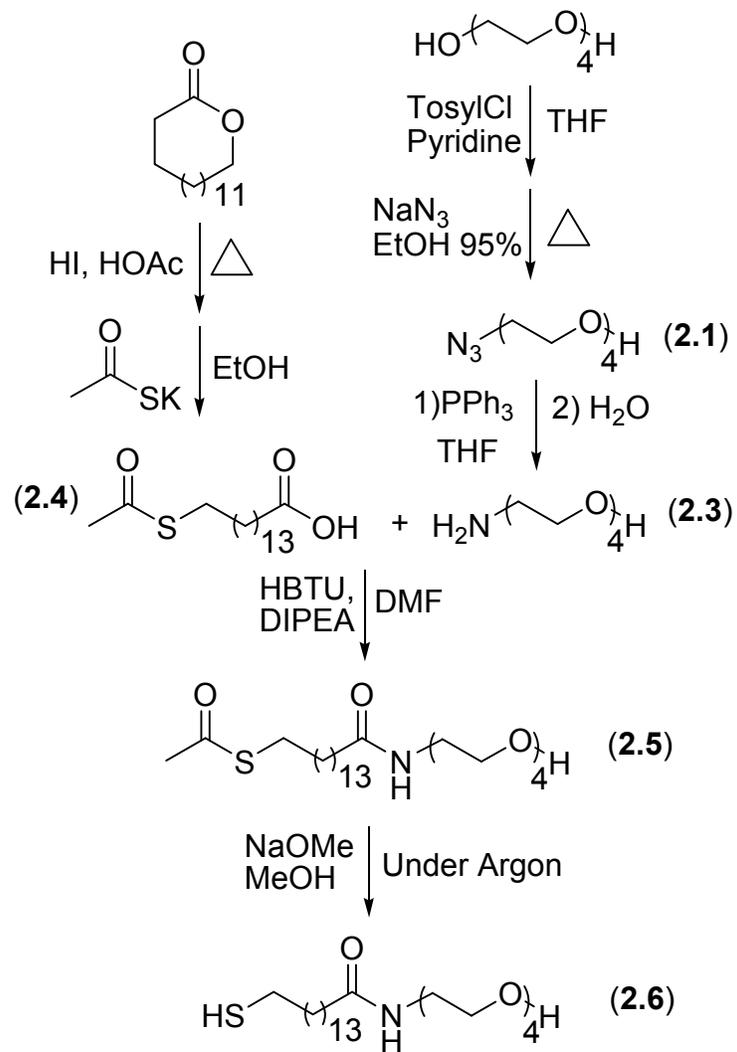
Scheme 2.1 Overall Synthetic Scheme for Monomer 2.6.

2.2.8 Synthetic Methods for 6

2-(2-(2-(2-azidoethoxy)ethoxy)ethoxy)ethanol **(2.1)** & 17-azido-3,6,9,12,15-pentaoxaheptadecan-1-ol **(2.2)**
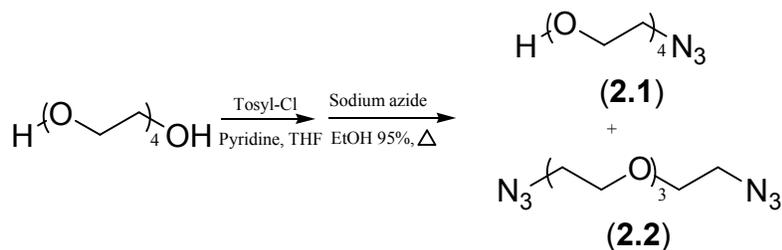
Tetraethylene glycol (7.002 g, 0.036 mol) was added to an oven dried round bottom flask and the flask was purged with argon. Dry tetrahydrofuran (THF) (30 mL), pyridine (9 mL, 0.310 mol) and recrystallized tosyl chloride (6.987 g, 0.036 mol) were added to the flask and the reaction was allowed to proceed for 2.5 hours at room temperature. The solution was concentrated via rotary evaporation and diluted with dichloromethane (CH_2Cl_2) (30 mL). The reaction was rinsed with 1 M sodium hydroxide (NaOH) (50 mL), 1 M hydrochloric acid (HCl) (50 mL), and brine (50 mL). The organic layers were then combined, dried over sodium sulfate, and concentrated to give a yellow oil. The oil was diluted with 95% ethanol (150 mL) and sodium azide (11.0081 g, 0.169 mol) was added to the flask and the reaction was allowed to reflux for 12 hours. The solvent was reduced by ~20 mL and 1 M NaOH (25 mL) was added to the flask. The reaction was then extracted with chloroform. The organic layer was dried over sodium sulfate and concentrated. The resulting oil was purified via flash column chromatography (50:40:10 CHCl$_3$:Hexanes:MeOH) to produce 3.9463 g (51%) of 2-(2-(2-(2-azidoethoxy)ethoxy)ethoxy)ethanol (**2.1**) and 1.3189 g (15%) of 17-azido-3,6,9,12,15-pentaoxaheptadecan-1-ol (**2.2**) as clear oils. For 2-(2-(2-(2-azidoethoxy)ethoxy)ethoxy)ethanol
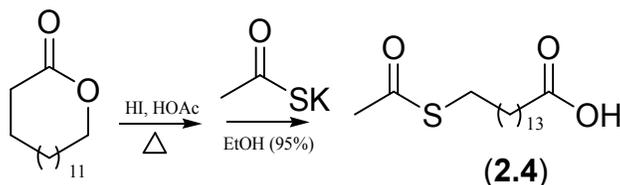
(2.1) ^{1}H NMR δ 3.36 (t, 2H), 3.36-3.70 (m, 14H); ^{13}C NMR δ 50.55, 61.61, 69.96, 70.24, 70.493, 70.56, 70.59, 72.84. MS (ESI+) cal. for $C_8H_{17}N_3O_4$ +H_1 220.13 found 220.12. For 17-azido-3,6,9,12,15-pentaoxaheptadecan-1-ol (2.2) ^{1}H NMR δ 3.40 (t, 4H), 3.65-3.69 (m, 12H) Contamination at 1.45 (t); ^{13}C NMR δ 50.17, 69.34, 69.55, 70.15. MS (ESI+) cal. for $C_8H_{17}N_3O_4$ +H_1 245.15 found 245.17.

2-(2-(2-(2-aminoethoxy)ethoxy)ethoxy)ethanol (2.3)
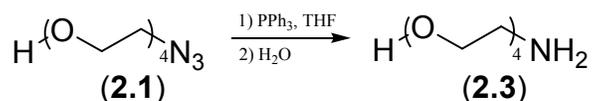
2-(2-(2-(2-azidoethoxy)ethoxy)ethoxy)ethanol (2.1) (1.4989 g, 6.83 mmol) was added to an oven dried round bottom flask and the flask was purged with argon. Dry THF (10 mL) and triphenylphoshpine (1.9703 g, 7.51 mmol) were added to the flask and the reaction was allowed to proceed at room temperature for 12 hours. Water (5 mL) was then added to the flask until a white precipitate formed. The organic layer was removed via rotary evaporation. The aqueous layer was rinsed twice with toluene (10 mL) and concentrated to give 1.2788 g (96.8%) of 2-(2-(2-(2-aminoethoxy)ethoxy)ethoxy)ethanol (2.3) as a clear oil. ^{1}H NMR δ 2.85 (t, 2H), 3.52 (t, 2H), 3.57-3.72 (m, 12H). DCM peak at 5.3. ^{13}C NMR δ 41.02, 61.13, 69.86, 70.01, 70.29, 70.386, 72.22, 72.78. MS (ESI+) cal. for $C_8H_{19}NO_4$ +H_1 194.13 found 194.13.

15-(acetylthio)pentadecanoic acid (2.4)

Pentadecanolide (16.0331 g, 0.066 moles) was added to a round bottom flask and diluted with hydroiodic acid (40 mL), acetic acid (20 mL), and the reaction was allowed to reflux overnight. The reaction mixture was cooled to room temperature, diluted with CH_2Cl_2 (50 mL), and rinsed with 10% sodium thiol sulfate. The organic layer was dried over sodium sulfate and concentrated via rotary evaporation to produce a yellow solid. The sample was diluted with 95% ethanol (100 mL), potassium thioacetate (11.5301 g, 0.100 moles) was added to the flask, and the reaction was allowed to proceed at room temperature for three hours. Ethanol was removed under reduced pressure and the resulting solid was diluted with CH_2Cl_2 (25 mL) and rinsed with 1 M HCl (25 mL). The organic layer was dried over sodium sulfate and concentrated via rotary evaporation to produce a yellow solid. The resulting solid was purified via flash column chromatography (10:90 ethyl acetate:hexanes) to produce 15.6667 g (75%) of 15-(acetylthio)pentadecanoic acid (**2.4**) as a yellowish solid. Melting point 68-70 °C. ^1H NMR δ 1.25 (m, 20H), 1.55 (m, 4H), 2.32 (s, 3H), 2.35 (t, 2H), 2.86 (t, 2H). Pentadecanolide contamination at 4.02 (t). ^{13}C NMR δ 24.88, 25.93, 29.02, 29.26, 29.31, 29.38, 29.43, 29.62, 29.67, 29.70, 29.75, 29.77, 29.80, 30.84, 34.22, 180.02. MS (ESI+) cal. for $C_{17}H_{32}O_3S + Na_1$ 339.20 found 338.75.

S-(1-hydroxy-13-oxo-3,6,9-trioxa-12-azaheptacosan-27-yl) ethanethioate (2.5)

15-(acetylthio)pentadecanoic acid (**2.4**) (2.112 g, 6.6 mmoles) was added to an oven dried round bottom flask and the flask was purged with argon. The sample was diluted with anhydrous

dimethylformamide (DMF) (10 mL) and CH_2Cl_2 (5 mL), Diisopropylethyl amine (DIPEA) (2 mL, 12.5 mmoles) and O-(Benzotriazol-1-yl)-N,N,N',N'-tetramethyluronium hexafluorophosphate (HBTU) (2.8016, 7.3 mmoles) were added to the flask and the reaction was allowed to proceed at room temperature for 1 hour.   2-(2-(2-(2-aminoethoxy)ethoxy)ethoxy)ethanol (2.3) (1.39 g, 7.2 mmoles) was added dropwise to the flask and the reaction was allowed to proceeded for 12 hours.   The solvent was removed under reduced pressure (20 mTorr). The resulting oil was diluted with CH_2Cl_2 (20 mL) and rinsed with 1 M NaOH (20 mL), 1 M HCl (20 mL), and brine (20 mL). The organic layers were combined, dried over sodium sulfate, and concentrated. The resulting oil was purified via flash column chromatography (5:20:75 MeOH:CHCl$_3$:ethyl acetate) to produce 2.758 g (85.1%) of S-(1-hydroxy-13-oxo-3,6,9-trioxa-12-azaheptacosan-27-yl) ethanethioate (2.5) as a yellowish solid. Melting point 59-60 °C. ^{1}H NMR δ 1.23 (m, 20H), 1.57 (m, 4H), 2.16 (t, 2H), 2.31 (s, 3H), 2.85 (t, 2H), 3.44 (t, 2H), 3.52 (t, 2H), 3.58-3.73 (m, 12H), 6.46 (s, 1H). Pentadecanolide contamination at 4.02 (t). ^{13}C NMR δ 25.96, 28.95, 29.24, 29.29, 29.54, 29.60, 29.62, 29.66, 29.70, 29.76, 30.77, 36.76, 39.20, 61.67, 70.14, 70.57, 70.78, 72.74, 173.66, 196.20. MS (ESI+) cal. for $C_{25}H_{48}NO_6S + H_1$ 492.34 found 492.33.

N-(2-(2-(2-(2-hydroxyethoxy)ethoxy)ethoxy)ethyl)-15-mercaptopentadecanamide (2.6)

(2.5)   **(2.6)**
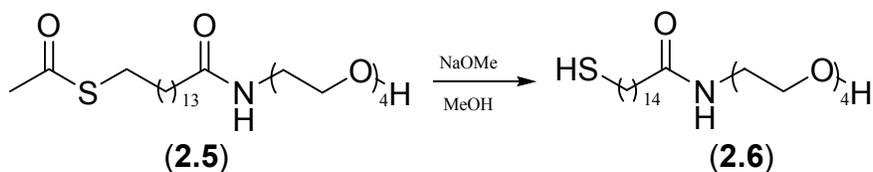
S-(1-hydroxy-13-oxo-3,6,9-trioxa-12-azaheptacosan-27-yl) ethanethioate (2.5) (1.7895 g, 3.6 mmoles) was added to an oven dried round bottom flask and the flask was purged with argon. The sample was diluted with methanol (20 mL), sodium methoxide 25% in methanol (1.7 mL,

7.2 mmoles) was added drop wise, and the reaction was allowed to proceed overnight. The reaction mixture was diluted with water, acidified to pH ~3 with concentrated HCl, and extracted with CH_2Cl_2 (20 mL). The organic layer was dried over sodium sulfate and concentrated. The resulting oil was purified via flash column chromatography (4:96 MeOH:ethyl acetate) to produce 1.2100 g (74%) of N-(2-(2-(2-(2-hydroxyethoxy)ethoxy)ethoxy)ethyl)-15-mercaptopentadecanamide (**2.6**) as a white solid. Melting point 50-52 °C. ^{1}H NMR δ 1.25 (m, 20H) 1.60 (m, 8H) 2.17 (t, 2H), 2.52 (q, 2H) 3.46 (t, 2H), 3.51-3.75 (m, 14H), 7.04 (s, 1H). ^{13}C NMR δ 24.79, 25.97, 28.52, 29.21, 29.56, 29.66, 29.72, 29.76, 34.20, 36.76, 39.19, 61.67, 70.13, 70.15, 70.54, 70.58, 70.79, 72.74, 173.63. MS (ESI+) cal. for $C_{25}H_{48}NO_6S + H_1$ 450.32 found 450.53.

2.3 Results and Discussion

With a commercial direct-write photolithography system,[22] we were able to remove amide-linked glycol-terminated thiol monomers from gold substrates, **Scheme 2.2**. Photoablation of glycol-terminated self-assembled monolayers has been reported to occur by both oxidative and thermal decay mechanisms. Oxidation can be further divided into tail group degradation or head group oxidation; however, sometimes these mechanisms operate in parallel. For tail group degradation, the glycol moiety is oxidized to aldehydes, ketones, and/or carboxylic acids with either excited oxygen or ozone. Once oxidized, these regions can no longer resist non-specific protein adsorption. As reported by Leggett and coworkers, tail group oxidation occurs faster than thiol head group oxidation.[23] The mechanism for thiol head group oxidation is strongly debated. Bohn and coworkers showed that oxidation resulted from the reaction of the thiol head group with ozone or singlet oxygen with ozone being an order of magnitude more efficient.[24] They also

41

reported the need to operate below 200 nm in order to adsorb into the cross section of oxygen, which would result in the formation of localized ozone or singlet oxygen. Later, work by Leggett and coworkers further investigated ozone involvement by utilizing an ozone free lamp operating at 254 nm.[25] They conclude that ozone was not necessarily the only mechanism to oxidize the thiol to a sulfonate and that slightly higher wavelengths could also be utilized. In a later report by Leggett and coworkers, they purposed an additional mechanism where photons are absorbed by the gold and the hot electrons are transferred into the anti-bonding orbitals of the thiol.[26] Once excited, the thiol could then undergo oxidation to a sulfonate, which is a weakly bound species that can be easily rinsed off the substrate.

Thermal decay, on the other hand, involves adsorption into the gold followed by thermal relaxation, which produces regions of localized heating and consequently breakage of the thiol-gold or gold-gold bonds.[16, 27] Previous work in this area showed a strong dependence on gold thickness, since adsorption was occurring in the plasmon band, which is thickness dependent.
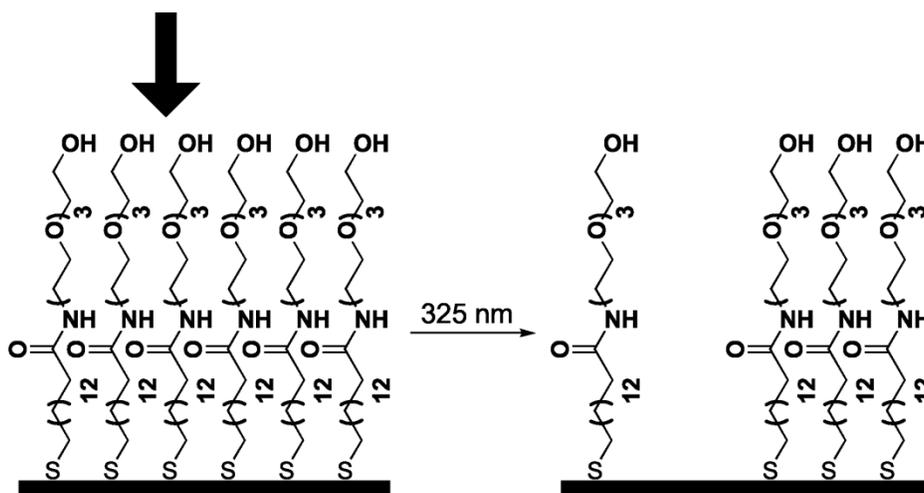
Scheme 2.2 Photoablation of amide-linked glycol monomer at 325 nm using a direct-write photolithography system.

42

In order to investigate which ablation mechanism was occurring in our system, we monitored changes in the surface chemistry by reflectance IR. Reflectance IR was chosen since it allows for analysis of which functional groups are present on the substrate, the overall "ordering" of the SAM, and the amount of material on the substrate. Substrates were prepared by depositing 400 nm of titanium followed by 100 Å of gold onto glass coverslips. Freshly prepared surfaces were immersed in a 1 mM ethanol solution of either the glycol-terminated thiol monomer, **1**, or **2**, Figure 2.4 D. Substrates were then rinsed with ethanol, water, and ethanol and then dried under a stream of nitrogen. Additionally, photo-induced monolayer patterning was carried out at 0.3 mm/sec to produce a 5 mm x 5 mm square.

Reflectance IR spectra were collected for the unpatterned glycol-terminated monolayer, the photopatterned glycol-terminated monolayer, and monolayers created from **1** and **2**, as shown in Figure 2.4. Each spectrum was an average of 1024 scans with a resolution of 2 and a data spacing of 0.964 cm^{-1} in single beam mode. The monolayer formed from **1** was used as a background sample and the symmetric and asymmetric peaks associated with the deuterated methylenes have been omitted for clarity. These peaks occur at ~2200 and 2100 cm^{-1}, in the region of the spectra that is not shown for clarity.

Oxidation of the glycol moiety would create additional carbonyls on the surface, thus having a profound effect on the IR spectra. If oxidation of the tail group were to occur, we would expect to observe additional peaks in the carbonyl region, 1500-1850 cm^{-1}, of the spectrum upon photopatterning. The resulting changes should be similar to the strong carbonyl stretch that is observed in Figure 2.4C for the carboxylic acid monolayer at 1720.62 cm^{-1}. However, no increase was observed between non-patterned and patterned samples, which

indicates that the glycol moiety is not undergoing oxidation to aldehydes, ketones, or carboxylic acids, Figure 2.4A and 2.4B. The only carbonyl peaks observed in the glycol-terminated monolayer correspond to the amide I and II peaks at 1557.65 and 1471.21 cm^{-1} for the non-patterned surface and 1559.77 and 1456.85 cm^{-1} for the patterned surface. The unusually low position of these peaks is due to the hydrogen bonding network formed by these monomers. To further confirm the glycol moiety is not undergoing degradation, we analyzed the alkane asymmetric and symmetric stretches. These stretching bands are often used to comment on monolayer "order" with "well ordered" exhibiting frequencies below 2920 and 2850 cm^{-1} for the asymmetric and symmetric stretches, respectfully, which correspond to the frequencies observed in crystalline long chain alkanes.[28] Monolayers formed from both the glycol-terminated monomer and **2** produce "well ordered" monolayers. However, a significant difference is observed when comparing the spectrum of an unpatterned glycol-terminated monolayer and one formed from **2**. In the glycol-terminated monolayer, a significant shoulder is observed for both the asymmetric and symmetric peaks, which is highlighted by an arrow in the spectrum. Since the glycol portion of the monomer does not pack tightly, this region remains disordered. This disorder results in C-H stretching occurring at higher wavenumbers than the C-H stretch of the straight chain alkanes, thus, the glycol C-H stretch manifests as a shoulder. As expected, the shoulder is present in both the non-patterned and patterned substrate, Figure 2.4A and 2.4B respectfully, but absent in the monolayer formed from **2**. This data indicates that the monolayer is not undergoing oxidation of the glycol tail, since this would result in a decrease in the relative intensity of the glycol tail.

Besides tail group degradation, head group oxidation must also be considered. Head group oxidation would result in the formation of two new S=O bounds on the surface, which have been detected by Leggett and coworkers.[26] Patterned substrates were analyzed directly after patterning to avoid losing any weakly bound species. The stretching frequency for S=O is a strong band around 1350 cm^{-1}, however, no strong bands were detected in the photopatterned substrate. Thus, no sulfonates were detected on our substrate, which suggests that the thiol head group is not being removed from the substrate by an oxidative mechanism.
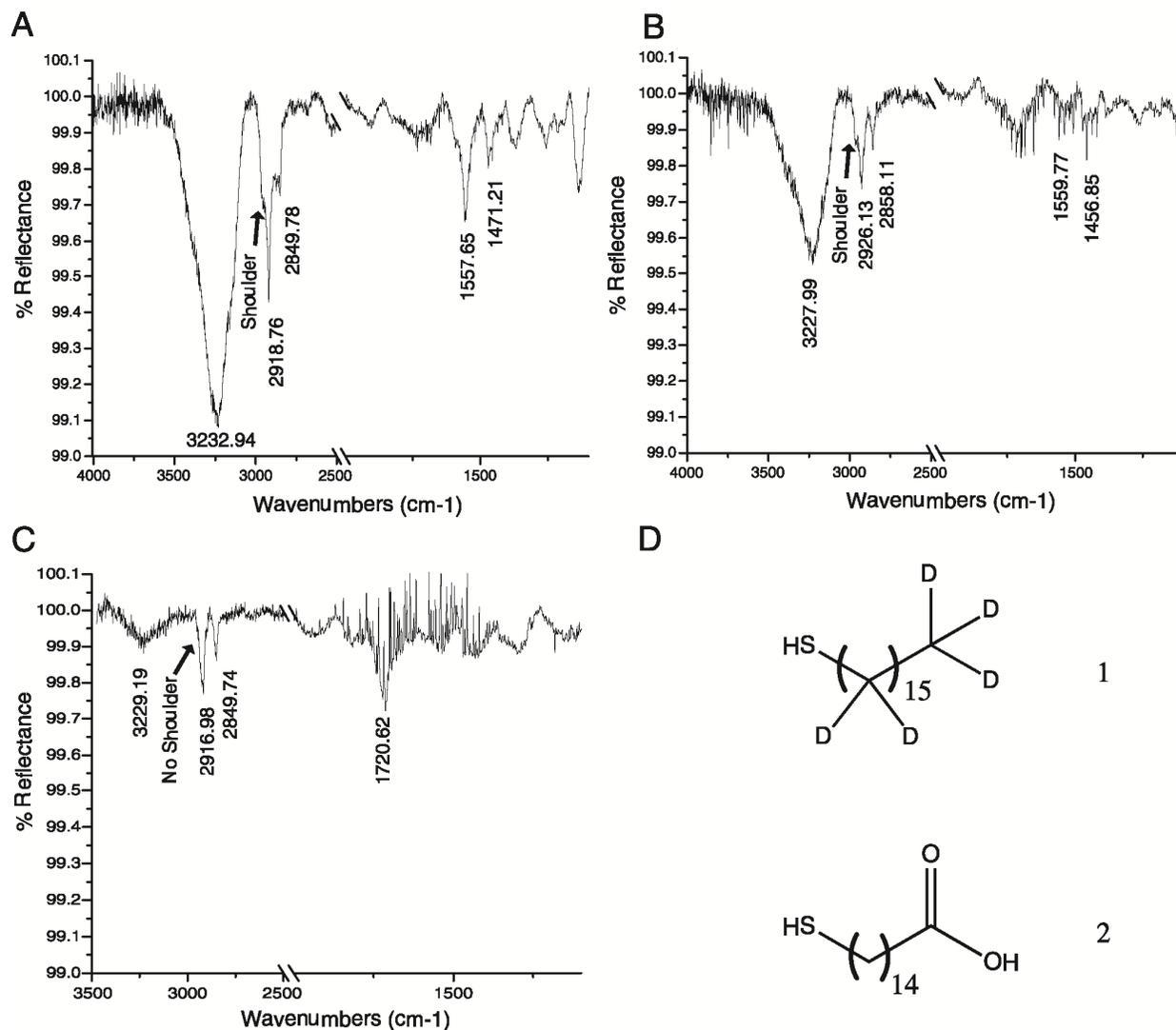
Figure 2.4. Reflectance IR data collected for three unique monolayers. A) Pristine glycol-terminated monolayer. B) Photo-induced monolayer patterned using direct-write photolithography. C) Monolayer formed from molecule **2**. D) Molecules used for comparison. (**1**) deuterated hexadecanethiol used as background and (**2**) 15-thiol-pentadecanoic acid carbonyl stretch.

The reflectance IR also provides two additional important pieces of information. First, we see a shift in the asymmetric and symmetric stretches, between the non-patterned, 2918.76 & 2849.78 cm^{-1}, and patterned, 2926.13/2858.11 cm^{-1}, substrates, which is consistent with complete monomer removal. Once sections of the monolayer are removed, the neighboring alkane chains

experience less van der Waals interactions and become disordered, which results in a shift to higher wavenumbers. Lastly, there is a clear decrease in the overall signal intensity between the non-pattered and patterned substrates. Since specular aperture grazing angle reflectance IR is a single bounce technique, the signal intensity can be correlated to the amount of material on the substrate. The non-patterned and patterned substrates have the same overall structure with a slight shift in the peak positions and intensities, which agrees with a thermal ablation mechanism where whole monomers are removed from the substrate.

During patterning, the laser intensity was modulated across the glycol substrate from 0 to 100% based on an 8-bit grayscale image, **Figure 2.5A**. This modulation provides a method of controlling the concentration of glycol-terminated monomers on the substrate, because as the laser intensity increases more glycol-terminated monomers are removed from the substrate. The removal of the monomers from the substrate was monitored by examining changes in the nanomechanical properties of the patterned substrates and surface infrared (IR) spectroscopy.

The relative difference in substrate stiffness was detected as changes in the LogDMT modulus measured using PeakForce quantitative nanomechanical mapping (QNM) scanning probe microscopy (SPM), **Figure 2.5B**. As expected, the surface modulus increased with higher laser intensities due to the removal of a greater number of compressible monomers. Significant changes were also observed in the adhesion of the silicon probe to the photopatterned gradient, **Figure 2.5C**, due to hydrogen bonding interactions between the glycol-termination and the probe. The more glycol-terminated monomers present, the great the interactions with the native silicon oxide layer on the probe. Thus, an increase in adhesion was observed as the laser power decreased, **Figure 2.5D**.
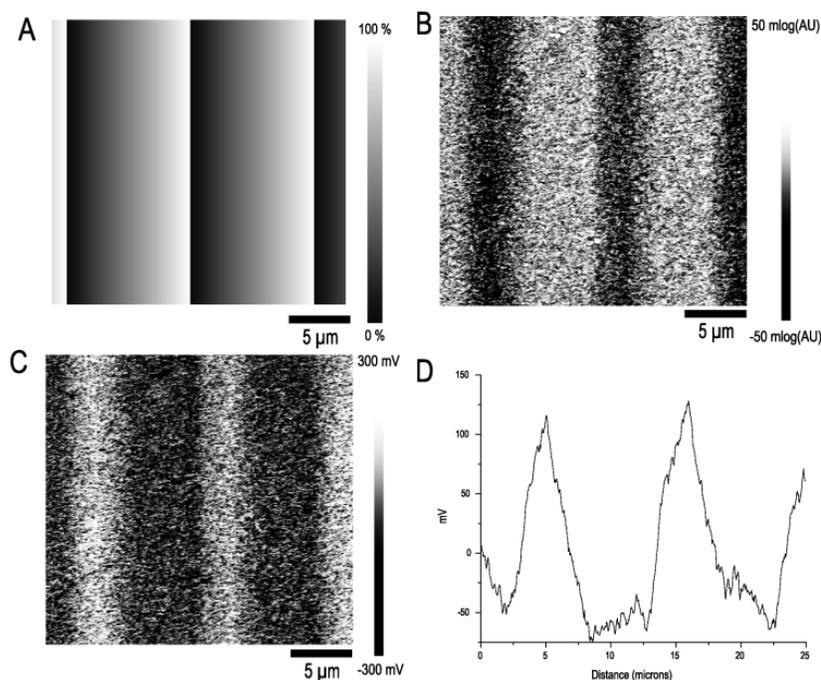
Figure 2.5. SPM Analysis of Ablated Substrates. (A) Eight-bit image patterned by direct-write photolithography (scale bar represents relative laser intensity). (B and C) The resulting LogMDTmodulus and adhesion channel for our patterned surface obtained using PeakForce QNM, respectively. (D) Cross-section analysis of the adhesion channel.

The direct-write laser writer also allows us to generate large complex patterns consisting of both punctate regions (STL letters) and smooth gradients (WU letters), **Figure 2.6A**. By using surface plasmon resonance imaging (SPRi), we have been able to quantitatively measure the amount of protein adsorbed to theses patterned regions. SPRi, which makes use of a CCD array for the simultaneous monitoring of SPR signals, was developed as a label-free method for detecting binding to DNA and protein microarrays,[29, 30] but serves as a powerful tool for quantitative low resolution imaging of protein adsorption to complex patterns. **Figure 2.6** shows the adsorption of neutravidin, fluorescently labeled with Oregon Green, to an ablated substrate monitored by SPRi and fluorescence. Maximum binding of neutravidin to the 100 % ablated region occurred over approximately one hour and was significantly greater than the binding of

the protein to the glycol background. As shown in **Figure 2.6C** and **2.6D**, the regions patterned

with higher laser intensities, which consequently contained less glycol-terminated monomers,

adsorbed a greater amount of neutravidin.
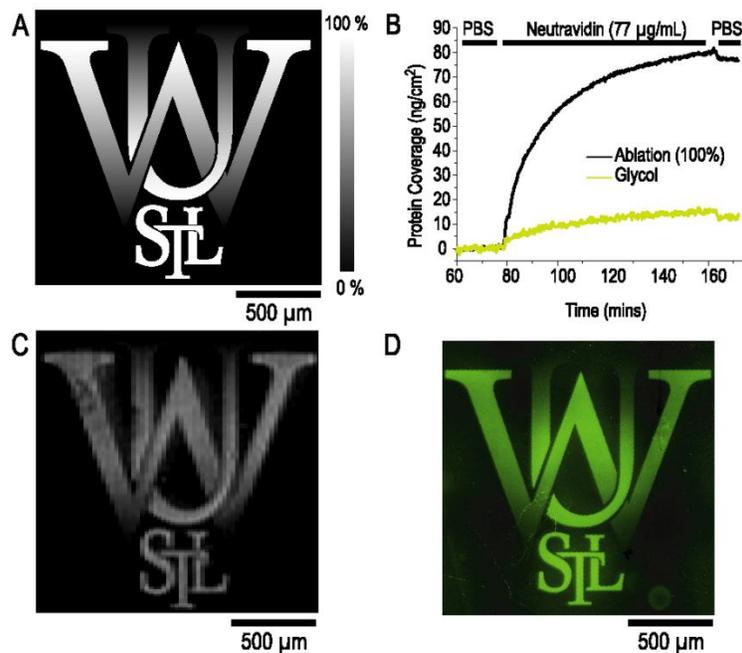
Figure 2.6. Complex Protein Gradients (A) Eight-bit image patterned by direct-write photolithography (scale bar represents relative laser intensity). (B) SPRi trace of Neutravidin in phosphate buffered saline (PBS) binding to ablated substrate. (C) Difference imaged obtained from final SPRi signal frame minus initial SPRi signal frame. (D) Fluorescent image of substrate after PBS rinsing.

Fibronectin was also adsorbed to a photopatterned substrate and its adsorption to a

monolayer patterned using ten discrete power intensities was quantified. As shown in **Figure**

2.7A, laser intensities ranging from 10% to 100% were investigated. As with neutravidin

binding, the amount of fibronectin adsorbed to each region increased with increasing laser

intensity, which can be seen in both the SPRi difference image and the resulting fluorescent

image, **Figure 2.7B** and **2.7C** respectively. A consistent trend between the SPRi signal and the

fluorescent signal can be clearly seen in **Figure 2.7D**. The SPRi signal fit to a Boltzmann function, which gives further evidence that the mechanism of action involves thermal desorption. By determining the Boltzmann function, we can now quantitatively control the concentration of fibronectin on a photopatterned glycol-terminated substrate by simply setting the gray-level in the eight-bit image.
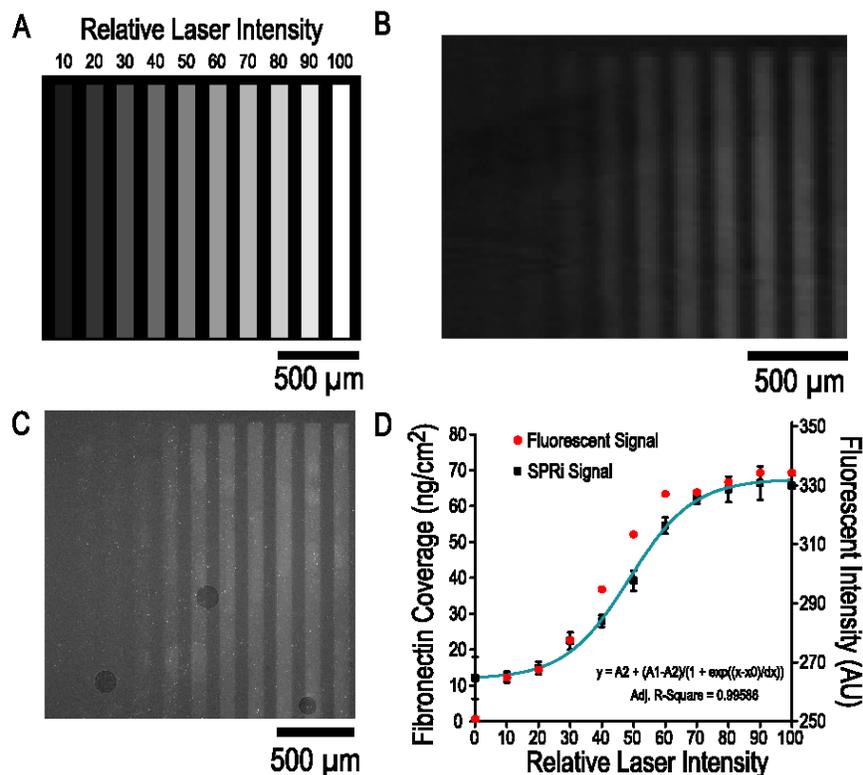
Figure 2.7 Boltzmann Correlation between Fibronectin adsorption and Laser Intensity. (A) Eight-bit image patterned by direct-write lithography. (B) Difference image obtained during SPRi experiment. (C) Fluorescent image of substrate after PBS rinsing. (D) Overlay of SPRi signal fit to a Boltzmann function and the fluorescent signal.

A neutravidin binding assay was conducted to further demonstrate the versatility of this method using a commercial signal amplification kit (Sigma B9655). A section of the substrate was patterned with hexadecanethiol by microcontact printing, which has been shown to adsorb

functional proteins. The substrate was then backfilled with the glycol-terminated monomer and patterned using photo-induced desorption. The resulting substrate contained twelve unique regions to probe neutravidin binding and recognition; Background (0%), 10%, 20%, 30%, 40%, 50%, 60%, 70%, 80%, 90%, 100% laser power, and hexadecanethiol, which can be seen in **Figure 2.8**. As shown in **Figure 2.9**, neutravidin was adsorbed to the substrate followed by anti-avidin binding. Anti-avidin selectively bound to the patterned region where neutravidin was adsorbed. This binding shows that anti-avidin could still recognize neutravidin after it had adsorbed to the substrate. The anti-avidin used in this study contained multiple biotin tags, which allowed for further amplification of the binding signal by flowing neutravidin over the substrate for a second time. As a result, the substrate had a neutravidin, Anti-avidin, neutravidin sandwich formation. Lastly, a statistical difference was observed in the neutravidin binding assay between each laser intensity from 0–70%, however no statistical difference was observed between hexadecanethiol and laser powers above 70 %, **Figure 2.10**.
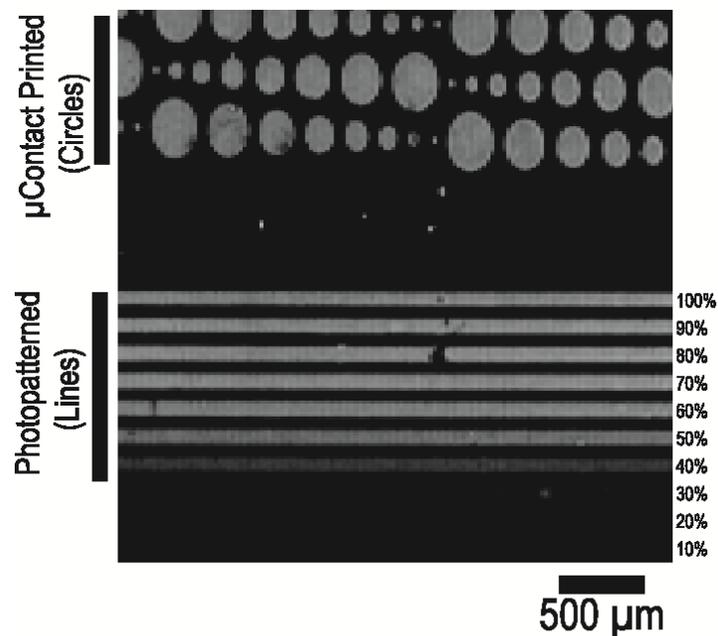
Figure 2.8. Difference imaged for stamping correlation study. The image was obtained from the final SPRi signal frame minus the initial SPRi signal frame from the neutravidin binding assay. The circle pattern was generated by microcontact printing hexadecanethiol onto the gold substrate. The line pattern was generated by photo-induced desorption of the glycol-terminated monolayer. The black region represents the nonpatterned region.
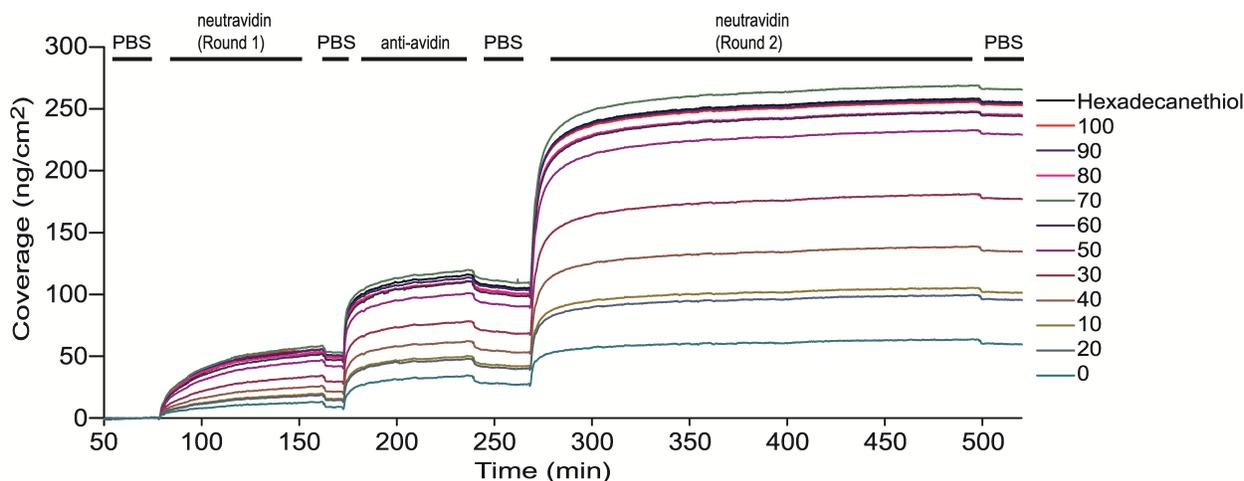
Figure 2.9. SPRi trace of neutravidin binding assay. The black line above the SPRi trace indicates what solution was flowing over the substrates. Briefly, neutravidin (77 μm/mL) was flowed over a patterned substrate at 150 μL/min for 80 minutes before the substrate was rinsed with PBS. Anti-avidin (22 μg/mL) was then flowed over the substrate for 65 mins and binding monitored. The substrate was rinsed again with PBS and neutravidin was flowed over the substrate for a second time.

52
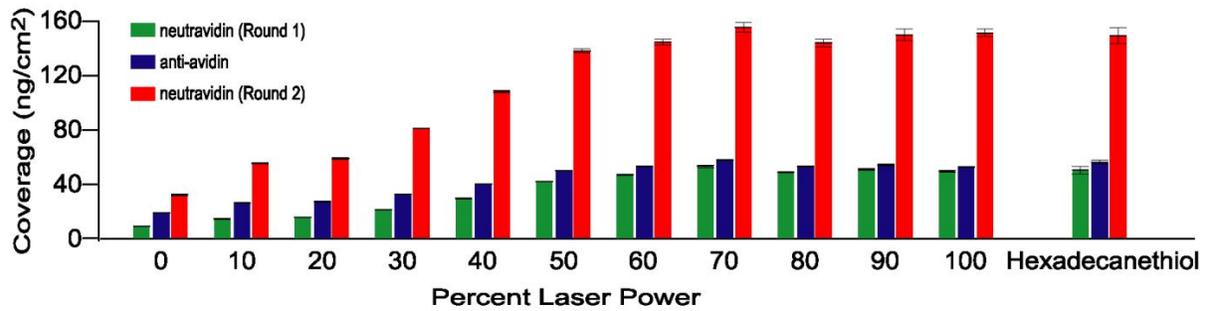
Figure 2.10. Quantitative analysis of neutravidin and anti-avidin binding to the twelve unique regions of the substrate.

2.4 Conclusions

Here, we demonstrate a versatile method for creating complex protein gradients and punctate protein regions on a single substrate using photo-induced monolayer patterning by thermal desorption. Patterning of glycol-terminated SAMs was achieved by using gray-scale photolithography and characterization of the changes in the nanomechanical properties and surface chemistry were analyzed by QNM and surface IR. Protein attachment to these patterns was quantified by SPRi and the amount of protein adsorption was found to be directly dependent on laser power and fit to a Boltzmann function. Protein adsorption was also quantified by fitting fibronectin adsorption to a Boltzmann function. Finally, neutravidin absorbed in this study could still be recognized by an anti-avidin antibody.

2.5 References

1.   Mendes, P.; Yeung, C.; Preece, J., Bio-nanopatterning of Surfaces. *Nanoscale Research Letters* **2007,** 2, (8), 373-384.
2.   Bengt, K., Biological surface science. *Surface Science* **2002,** 500, (1–3), 656-677.
3.   Yap, F. L.; Zhang, Y., Protein and cell micropatterning and its integration with micro/nanoparticles assembly. *Biosensors and Bioelectronics* **2007,** 22, (6), 775-788.
4.   Love, J. C.; Estroff, L. A.; Kriebel, J. K.; Nuzzo, R. G.; Whitesides, G. M., Self-Assembled Monolayers of Thiolates on Metals as a Form of Nanotechnology. *Chemical Reviews* **2005,** 105, (4), 1103-1170.
5.   Milan, M., Using self-assembled monolayers to model the extracellular matrix. *Acta Biomaterialia* **2009,** 5, (3), 832-841.
6.   Kane, R. S.; Takayama, S.; Ostuni, E.; Ingber, D. E.; Whitesides, G. M., Patterning proteins and cells using soft lithography. *Biomaterials* **1999,** 20, (23–24), 2363-2376.
7.   Alom Ruiz, S.; Chen, C. S., Microcontact printing: A tool to pattern. *Soft Matter* **2007,** 3, (2).
8.   Piner, R. D.; Zhu, J.; Xu, F.; Hong, S.; Mirkin, C. A., "Dip-Pen" Nanolithography. *Science* **1999,** 283, (5402), 661-663.
9.   Pale-Grosdemange, C.; Simon, E. S.; Prime, K. L.; Whitesides, G. M., Formation of self-assembled monolayers by chemisorption of derivatives of oligo(ethylene glycol) of structure HS(CH2)11(OCH2CH2)mOH on gold. *Journal of the American Chemical Society* **1991,** 113, (1), 12-20.
10.   Strulson, M. K.; Johnson, D. M.; Maurer, J. A., Increased Stability of Glycol-Terminated Self-Assembled Monolayers for Long-Term Patterned Cell Culture. *Langmuir* **2012,** 28, (9), 4318-4324.
11.   Johnson, D. M.; Maurer, J. A., Recycling and reusing patterned self-assembled monolayers for cell culture. *Chemical Communications* **2011,** 47, (1), 520-522.
12.   Yamaguchi, S.; Yamahira, S.; Kikuchi, K.; Sumaru, K.; Kanamori, T.; Nagamune, T., Photocontrollable Dynamic Micropatterning of Non-adherent Mammalian Cells Using a Photocleavable Poly(ethylene glycol) Lipid. *Angewandte Chemie International Edition* **2012,** 51, (1), 128-131.
13.   Herbert, C. B.; McLernon, T. L.; Hypolite, C. L.; Adams, D. N.; Pikus, L.; Huang, C. C.; Fields, G. B.; Letourneau, P. C.; Distefano, M. D.; Hu, W.-S., Micropatterning gradients and controlling surface densities of photoactivatable biomolecules on self-assembled monolayers of oligo(ethylene glycol) alkanethiolates. *Chemistry & Biology* **1997,** 4, (10), 731-737.
14.   Krakert, S.; Ballav, N.; Zharnikov, M.; Terfort, A., Adjustment of the bioresistivity by electron irradiation: self-assembled monolayers of oligo(ethyleneglycol)-terminated alkanethiols with embedded cleavable group. *Physical Chemistry Chemical Physics* **2010,** 12, (2), 507-515.
15.   Cheng, N.; Cao, X., Photoactive SAM surface for control of cell attachment. *Journal of Colloid and Interface Science* **2010,** 348, (1), 71-79.
16.   Slater, J. H.; Miller, J. S.; Yu, S. S.; West, J. L., Fabrication of Multifaceted Micropatterned Surfaces with Laser Scanning Lithography. *Advanced Functional Materials* **2011,** 21, (15), 2876-2888.

17.   Doron-Mor, I.; Barkay, Z.; Filip-Granit, N.; Vaskevich, A.; Rubinstein, I., Ultrathin Gold Island Films on Silanized Glass. Morphology and Optical Properties. *Chemistry of Materials* **2004,** 16, (18), 3476-3483.

18.   Ballav, N.; Thomas, H.; Winkler, T.; Terfort, A.; Zharnikov, M., Making Protein Patterns by Writing in a Protein-Repelling Matrix. *Angewandte Chemie International Edition* **2009,** 48, (32), 5833-5836.

19.   Kolodziej, C. M.; Maynard, H. D., Electron-Beam Lithography for Patterning Biomolecules at the Micron and Nanometer Scale. *Chemistry of Materials* **2011,** 24, (5), 774-780.

20.   Montague, M.; Ducker, R. E.; Chong, K. S. L.; Manning, R. J.; Rutten, F. J. M.; Davies, M. C.; Leggett, G. J., Fabrication of Biomolecular Nanostructures by Scanning Near-Field Photolithography of Oligo(ethylene glycol)-Terminated Self-Assembled Monolayers. *Langmuir* **2007,** 23, (13), 7328-7337.

21.   Shumaker-Parry, J. S.; Campbell, C. T., Quantitative Methods for Spatially Resolved Adsorption/Desorption Measurements in Real Time by Surface Plasmon Resonance Microscopy. *Analytical Chemistry* **2004,** 76, (4), 907-917.

22.   Lullo, G.; Leto, R.; Oliva, M.; Arnone, C., Multilevel pattern generation by GaN laser lithography: an application to beam shaper fabrication. *Proc. SPIE* **2006,** 6290, 62900A.

23.   Ducker, R. E.; Janusz, S.; Sun, S.; Leggett, G. J., One-Step Photochemical Introduction of Nanopatterned Protein-Binding Functionalities to Oligo(ethylene glycol)-Terminated Self-Assembled Monolayers. *Journal of the American Chemical Society* **2007,** 129, (48), 14842-14843.

24.   Zhang, Y.; Terrill, R. H.; Bohn, P. W., Ultraviolet Photochemistry and ex Situ Ozonolysis of Alkanethiol Self-Assembled Monolayers on Gold. *Chemistry of Materials* **1999,** 11, (8), 2191-2198.

25.   Brewer, N. J.; Rawsterne, R. E.; Kothari, S.; Leggett, G. J., Oxidation of Self-Assembled Monolayers by UV Light with a Wavelength of 254 nm. *Journal of the American Chemical Society* **2001,** 123, (17), 4089-4090.

26.   Brewer, N. J.; Janusz, S.; Critchley, K.; Evans, S. D.; Leggett, G. J., Photooxidation of Self-Assembled Monolayers by Exposure to Light of Wavelength 254 nm: A Static SIMS Study. *The Journal of Physical Chemistry B* **2005,** 109, (22), 11247-11256.

27.   Shadnam, M. R.; Kirkwood, S. E.; Fedosejevs, R.; Amirfazli, A., Direct Patterning of Self-Assembled Monolayers on Gold Using a Laser Beam. *Langmuir* **2004,** 20, (7), 2667-2676.

28.   Snyder, R. G.; Strauss, H. L.; Elliger, C. A., Carbon-hydrogen stretching modes and the structure of n-alkyl chains. 1. Long, disordered chains. *The Journal of Physical Chemistry* **1982,** 86, (26), 5145-5150.

29.   Li, Y.; Lee, H. J.; Corn, R. M., Detection of Protein Biomarkers Using RNA Aptamer Microarrays and Enzymatically Amplified Surface Plasmon Resonance Imaging. *Analytical Chemistry* **2007,** 79, (3), 1082-1088.

30.   Kanda, V.; Kariuki, J. K.; Harrison, D. J.; McDermott, M. T., Label-Free Reading of Microarray-Based Immunoassays with Surface Plasmon Resonance Imaging. *Analytical Chemistry* **2004,** 76, (24), 7257-7262.

Chapter 3

Unmasking Photolithography: A Versatile Way to Site-Selectively Pattern Gold Substrates

3.1 Introduction

Patterned substrates with well-defined micro- and nanoscale features are central to the development of a broad range of applications and fields, including, but not limited to, microelectronics,[1-3] solar cell development,[4] and biotechnology.[5] Typically, these applications require the functionalization of inorganic substrates to meet the specific demands of an application. While this is classically achieved using photoresist, lift-off techniques, and chemical etching, one of the methods that has emerged for direct conjugation of active molecules to substrates is thiol terminated self-assembled monolayers (SAMs) on gold, silver, copper, palladium, and platinum substrates.[6] These substrates are especially useful for biological applications and have been employed in a wide variety of studies ranging from basic cell biology[7-9] to biosensing.[10] SAMs are an ideal platform for direct functionalization because the monomers covalently bind to substrates through the thiol "head" group and self-assemble via van der Waals packing interactions between adjacent long-chain alkane "tail" groups. This packing orients the terminal functional group to create a new interface with defined chemistry. As a result, many techniques have been developed to pattern SAMs, including soft photolithography,[11-16] photooxidation,[13, 17] and dip-pen nanolithography.[18] However, the development of a single technique to create smooth gradients of functional groups and for patterning multiple molecules on a single substrate remains a major challenge in pattern generation. For example, functional group gradients have been generated by diffusing two molecules across a substrate[19] or through photolithographic methods, including gradient

56

photomasks[11] and controlling light exposure.[12, 20] While molecular diffusion produces defined gradients, in its most basic form, it does not allow for pattern generation. Patterned gradients can be prepared using microfluidic devices;[21-25] however traditional polydimethylsiloxane devices are susceptible to monomer leeching and solvent swelling that can lead to pattern distortion and limits precise molecular control. While gradient photomasks have previously been used to reveal functional groups on a surface,[26] the production of high quality gradient masks are expensive. Moreover, controlling the overall light exposure to a surface has produced regions of varying functional group densities;[11, 12, 27, 28] however these methods have failed to produce a continuous gradient. Another major shortfall of all these methods is the inability to provide a simple method for pattering multiple molecules on a single substrate. By utilizing a commercial direct-write grayscale photolithography system, we have removed the need for the tradition photomask which provides us with two distinct advantages; we can produce smooth, complex functional group gradients on a surface and patterned multiple molecules sequentially on the same substrate

3.2 Experimental Methods

3.2.1 Materials and Instrumentation

All reagents were obtained from Sigma-Aldrich (St. Louis, MO) or VWR Scientific (Radnor, PA), were reagent grade or higher, and used as received unless otherwise indicated. ^{1}H NMR and ^{13}C NMR were collected on a 300 MHz Varian NMR (Agilent Technologies, Santa Barbra, CA). All NMR spectra are attached in Appendix C. Electrospray ionization (ESI) Mass spectrums were collected on a Thermo LCQ Deca Plus (ThermoFisher Scientific, Waltham, MA) operating in positive mode. Melting points were collected on a Stuart SMP10 (Keison Products, England) melting point apparatus. Gold substrates were prepared using a PVD 75 (Kurt J Lesker, Pittsburg, PA). Scanning Probe Microscopy (SPM) images were collected on a

MultiMode 8 configured for quantum nanomechanical mapping (QNM) (Bruker Corporation, Santa Barbara, CA). Matrix Assisted Laser Desorption Ionization Mass Spectrums (MALDI-MS) were collected on an Applied Biosystems 4700 MALDI TOF-TOF (Applied Biosystems, Carlsbad, CA) with a Nitrogen laser (337 nm) operating in reflectance mode. Substrates were patterned using a direct-writer LaserWriter (Microtech, Palermo, Italy) system equipped with a 325 nm He:Cd laser operating at 19 mW.

3.2.2 Substrate Preparation and Patterning: Gold substrates were prepared by depositing 50 Å of titanium at 0.1 Å/sec followed by 100 Å of gold 0.1 Å/sec on a glass coverslip. For SPM experiments, gold substrates were soaked in a 1 mM ethanol:acetonitrile (9:1) solution of molecule **12** for 1 hour. For surface coupling experiments, gold substrates were soaked in a 1 mM ethanol:THF (9:1) solution of molecules **6** and **12** (3:1 respectively) for 14 hours. Slides were then rinsed with ethanol, water, and ethanol, and dried under a stream of nitrogen gas. Patterns were generated in CleWin (WieWeb, Netherlands) or Adobe Illustrator and lithography was carried out in beam scan mode between 0 and 100% power ($1.6x10^{12}$ photons/um^2). After photopatterning, samples were rinsed with ethanol, water, and ethanol, and dried under a stream of nitrogen.

3.2.3 Two molecule coupling procedure

Photoreactive SAMs for surface coupling studies were prepared by soaking a freshly prepared gold slide in an ethanolic solution of 0.25 mM of glycol-terminated photoprotected carboxylic acid monomer (**12**) and 0.75 mM of hydroxyl terminated glycol monomer. Substrates were then photodeprotected using our direct-write photolithography system according to the uploaded 8-bit file in beam scan mode. After photodeprotection, slides were rinsed with ethanol, water, and ethanol, and dried under a stream of nitrogen. The freshly exposed carboxylate groups were then

activated with 1 mL of 5 mM 1-ethyl-3-(3-diemthylaminopropyl) carbodiimide (EDC•HCl) in

anhydrous CH_2Cl_2 for 1 minute followed by the addition of 1 mL of 2.5 mM 1-hydroxy-7-aza-

benzotriazole (HOAt) in anhydrous $DMF:CH_2Cl_2$ (1:1). The reaction was allowed to proceed

with shaking at 200 rpm for 15 minutes before 1 mL of 1.5 mM hexaethylene glycol amine in

anhydrous DMF was added. The reaction was allowed to proceed for an additional hour. Slides

were then removed from the reaction mixture and rinsed with ethanol, water, and ethanol, and

dried under nitrogen. Three rounds of activation and coupling were carried out before the process

was repeated for tetraethylene glycol.

3.2.4 Scanning Probe Microscopy Analysis: Patterned gradients were characterized using

quantitative nanomechanical mapping (QNM) and Kevin Probe Microscopy (KFM) on a

MultiMode 8 scanning probe microscope (Bruker, Santa Barbara, CA). For QNM analysis,

SNL10 probes (Bruker, Santa Barbara, CA) consisting of a silicon tip on a silicon nitride

cantilever with nominal force constants of 0.06 N/m or 0.32N/m were employed. Images were

acquired in PeakForce QNM mode with a 150 μm scan area at a rate of 0.244 Hz with 2048

points per line with 2048 lines. For KFM analysis, MESP probes (Bruker, Santa Barbara, CA),

0.01-0.025 Ohm-cm Antimony (n) doped silicone with force constants between 1-5 N/m were

used. Prior to analysis, the gold surfaces were connected to a metal SPM puck with copper tape.

Images were acquired in surface potential mode with an amplitude set point of 8 V, a 150 μm

scan size, a rate of 0.5 Hz, 2560 points per line, and 2560 lines.

3.2.5 MALDI-MS Characterization. Patterned coverslips were coated with 200 μL of 20

mg/mL 2,5-dihydroxybenzoic acid (DHB) and dried under vacuum for 10 minutes to obtain

uniform matrix coverage. Samples were then imaged in positive reflectance mode using an ABI

4700 with a source voltage of 20 kV, grid voltage of 14 kV, Mirror 1 voltage of 14.281 kV, and

Mirror 2 voltage of 20.480 kV. Imaging was carried out using 100 µm spots spaced 250 µm

apart (center to center), and each spectrum consisted of 20 averaged spectra containing 50 shots

collected with a center bias. Spectra were processed using 4000 Series Explorer software

(Applied Biosystems, Carlsbad, CA) and analyzed for peaks with a mass-to-charge ratio of the

imaged molecules within ± 0.3 m/z and with a signal to noise ratio greater than four. The

resulting area under the peak was used to generate contour plots using Origin 8 (OriginLab,

Northampton, MA).
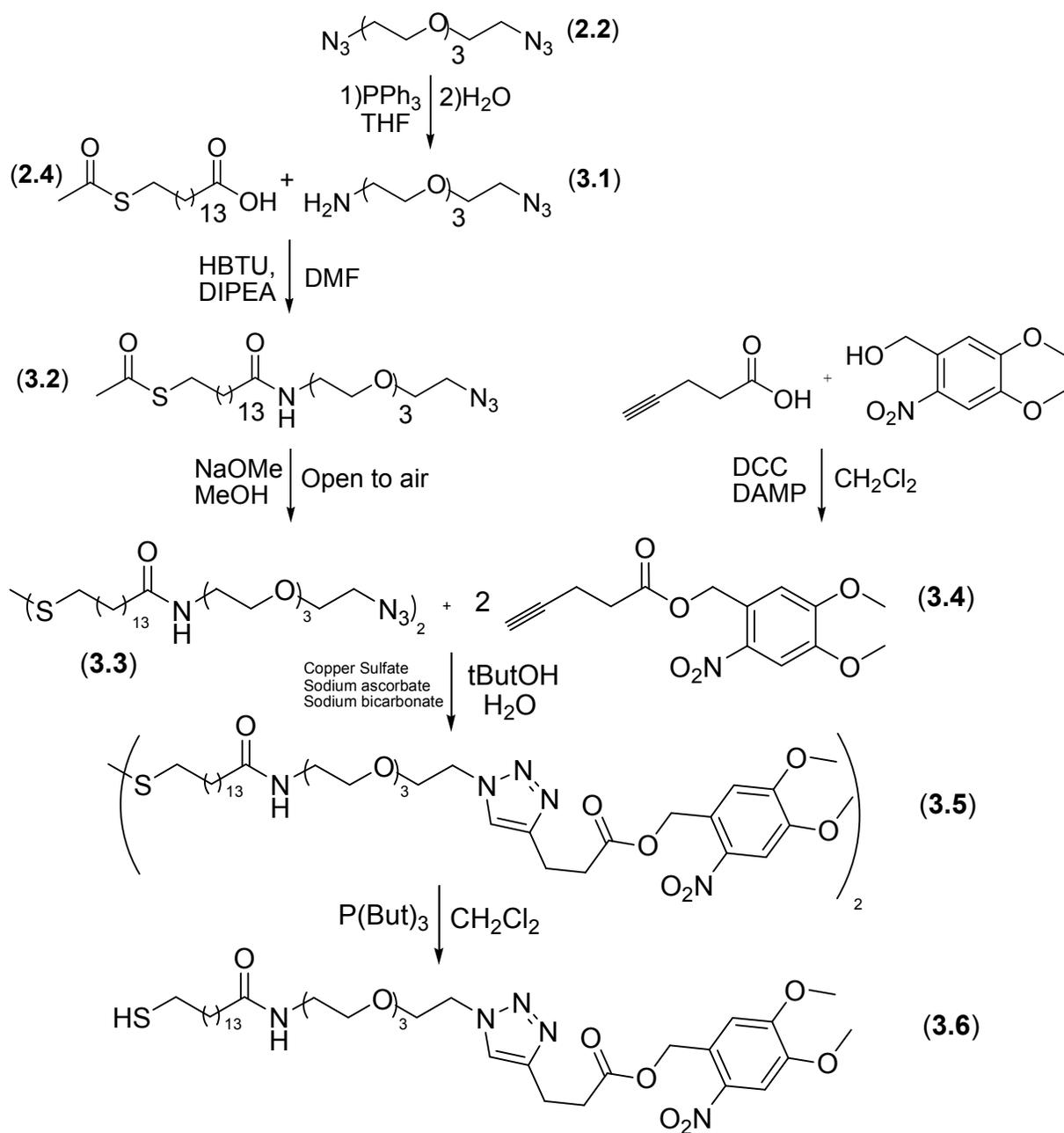
Scheme 3.1 Overall Synthetic Scheme for Monomer 3.6.

3.2.6 Synthetic Methods for 3.6

2-(2-(2-(2-azidoethoxy)ethoxy)ethoxy)ethanamine (3.1)

$$N_3 \overset{}{\underset{3}{\frown O}} N_3 \xrightarrow[\text{2) H}_2\text{O}]{\text{1) PPh}_3\text{, THF}} N_3 \overset{}{\underset{3}{\frown O}} NH_2$$

(2.2)   **(3.1)**
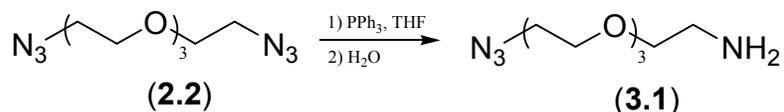
17-azido-3,6,9,12,15-pentaoxaheptadecan-1-ol (**2.2**) (2.9876 g, 12.2 mmoles) was added to an

oven dried flask and the flask was purged with argon. Dry THF (15 mL) and triphenylphoshpine

(2.967 g, 11.3 mmol) were added to the flask and the reaction was allowed to proceed at room

temperature for 12 hours. Water (5 mL) was added to the flask until a white precipitate formed.

The organic layer was removed via rotary evaporation. The sample was rinsed twice with

toluene (10 mL) to produce a yellow oil, which was purified via flash column chromatography

(15:85 MeOH:CHCl$_3$) to give 0.9808 g (37%) of 2-(2-(2-(2-azidoethoxy)ethoxy)ethoxy)

ethanamine (**3.1**) as an clear oil. ^{1}H NMR δ 2.93 (t, 2H), 3.41 (t, 2H), 3.52 (t, 2H), 3.52-3.69 (m,

10H). ^{13}C NMR δ 41.13, 50.49, 69.83, 70.03, 70.13, 70.39, 70.45, 72.05. MS (ESI+) cal. for

C$_8$H$_{18}$N$_4$O$_4$ +H$_1$ 219.15 found 219.34.

S-(1-azido-13-oxo-3,6,9-trioxa-12-azaheptacosan-27-yl) ethanethioate (3.2)

$$\text{(2.4)} \quad + \quad \text{H}_2\text{N} \overset{}{\underset{3}{\frown O}} N_3 \xrightarrow[\text{DMF}]{\text{HBTU, DIPEA}} \text{(3.2)}$$

(2.4)   **(3.1)**   **(3.2)**
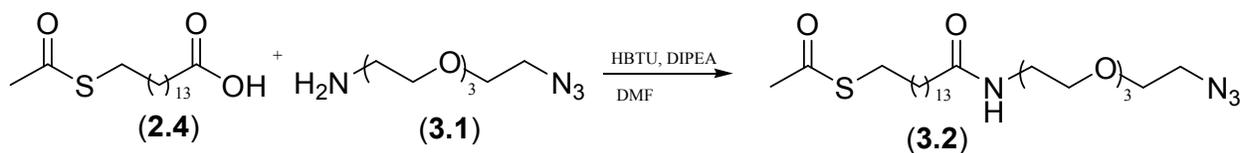
15-(acetylthio)pentadecanoic acid (**4**) (1.5103 g, 3.43 mmoles) was added to an oven dried round

bottom flask and the flask was purged with argon. Dry DMF (10 mL), CH$_2$Cl$_2$ (5

mL),diisopropylethyl amine (3.5 mL, 22.0 mmoles) and HBTU (1.4008 g, 3.69 mmoles) were

added to the flask and the reaction was allowed to proceed for 1 hour. 2-(2-(2-(2-

azidoethoxy)ethoxy)ethanamine (**3.1**) (0.8688 g, 3.98 mmoles) was added drop wise to

the flask and the reaction was allowed to proceed for 12 hours.   Solvent was removed under

reduced pressure (20 mTorr). The resulting oil was diluted with CH_2Cl_2 (20 mL) and rinsed with

1 M NaOH (25 mL), 1 M HCl (25 mL), and brine (25 mL). The organic layers were combined,

dried over sodium sulfate, and concentrated. The resulting oil was purified via flash column

chromatography (50:50, 30:60, and 0:100 hexanes:ethyl acetate) to produce 0.9665 g (56 %) of

S-(1-azido-13-oxo-3,6,9-trioxa-12-azaheptacosan-27-yl) ethanethioate (**3.2**) as a yellowish oil.

^{1}H NMR δ 1.2-1.4 (m, 20H), 1.5-1.7 (m, 4H) 2.17 (t, 2H), 2.32 (s, 3H), 2.86 (t, 2H), 3.40 (t,

2H), 3.46 (t, 2H), 3.56 (t, 2H), 3.62-3.70 (m, 10H), 5.99 (s, 1H). ^{13}C NMR δ 25.86, 28.93,

29.06, 29.22, 29.27, 29.35, 29.45, 29.50, 29.58, 29.61, 29.67, 29.72, 30.75, 36.87, 39.23, 50.78,

70.11, 70.18, 70.34, 70.68, 70.73, 70.82, 173.36, 196.13. MS (ESI+) cal. for $C_{25}H_{48}N_4O_5S + Na_1$

539.32 found 538.40.

15,15'-disulfanediylbis(N-(2-(2-(2-(2-azidoethoxy)ethoxy)ethoxy)ethyl)pentadecanamide)

(3.3)
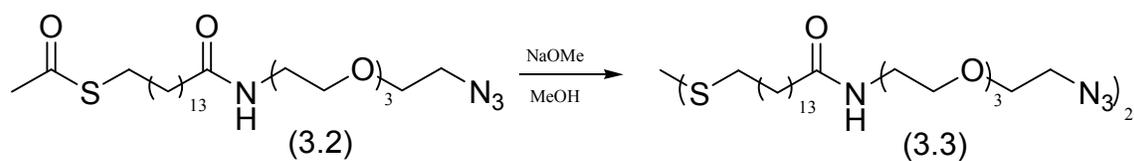
S-(1-azido-13-oxo-3,6,9-trioxa-12-azaheptacosan-27-yl) ethanethioate (**3.2**) (0.3286 g, 0.63

mmoles) was added to a round bottom flask and the flask was left open to air. Methanol (5 mL)

and sodium methoxide 25% in methanol (1.5 mL) were added to the flask and the reaction was

allowed to proceed for 12 hours. The reaction mixture was diluted with water, acidified to pH

~3 with concentrated HCl, and extracted with CH_2Cl_2 (20 mL). The resulting oil was purified

via flash column chromatography (4:96 MeOH:ethyl acetate) to produce 0.6018 g (99%) of

15,15'-disulfanediylbis(N-(2-(2-(2-(2-azidoethoxy)ethoxy)ethoxy)ethyl)pentadecanamide) (**3.3**) as an off white solid. Melting point 84-86 °C. ^{1}H NMR δ 1.2-1.4 (m, 40H), 1.6-1.7 (m, 8H), 2.16 (t, 4H), 2.66 (t, 4H), 3.38 (t, 4H), 3.45 (q, 4H), 3.54 (t, 4H), 3.6-3.7 (m, 20H), 6.02 (s, 1H). ^{13}C NMR δ 25.64, 28.39, 29.09, 29.11, 29.21, 29.28, 29.39, 29.47, 29.51, 36.54, 39.02, 42.62, 50.52, 69.76, 69.94, 70.10, 70.44, 70.48, 70.56, 71.23, 173.16. MS (ESI+) cal. for $C_{46}H_{90}N_8O_8S_2$ + H_1 947.64 found 947.87.

4,5-dimethoxy-2-nitrobenzyl pent-4-ynoate (3.4)

(**3.4**)
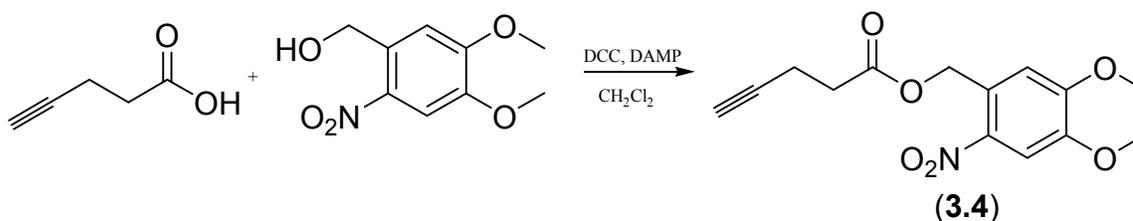
4-Pentynoic acid (98.6 mg, 1.0 mmoles) was added to an oven dried round bottom flask and the flask was purged with argon. The sample was diluted with CH_2Cl_2 (5 mL) and N,N-Dicyclohexyl carbodiimide (DCC, 0.4170 g, 2.0 mmoles), 4-(Dimethyl amino)-pyridine (DMAP, 0.2525 g, 2.0 mmoles), and 6-nitroveratryl alcohol (0.3536 g, 1.6 mmoles) were added to the flask. The reaction was allowed to proceed overnight. The reaction mixture was rinsed with 1 M HCl (25 mL). The organic layers were combined, dried over sodium sulfate, concentrated, and purified via flash column chromatography (10:15:75 CHCl$_3$:ethyl acetate:hexanes) to produce 0.2918 g (99%) of 4,5-dimethoxy-2-nitrobenzyl pent-4-ynoate (**3.4**) as a yellow powder. Melting point 90-91 °C. ^{1}H NMR δ 1.98 (t, 1H), 2.57 (t, 2H), 2.66 (t, 2H), 3.96 (s, 3H), 3.99 (s, 3H), 5.55 (s, 2H), 7.02 (s,1H), 7.73 (s, 1H). ^{13}C NMR δ 14.42, 33.39, 56.49, 56.55, 63.53, 69.39,

82.41, 108.28, 110.53, 126.88, 140.02, 148.35, 153.57, 171.15. MS (ESI+) cal. for $C_{14}H_{15}O_6N +$

Na_1 316.08 found 316.00.

bis(4,5-dimethoxy-2-nitrobenzyl) 3,3'-(1,1'-(13,44-dioxo-3,6,9,48,51,54-hexaoxa-28,29-dithia-12,45-diazahexapentacontane-1,56-diyl)bis(1H-1,2,3-triazole-4,1-diyl))dipropanoate (3.5)

(**3.3**)   (**3.4**)

Copper Sulfate
Sodium Ascorbate   t-ButOH/H₂O

(**3.5**)
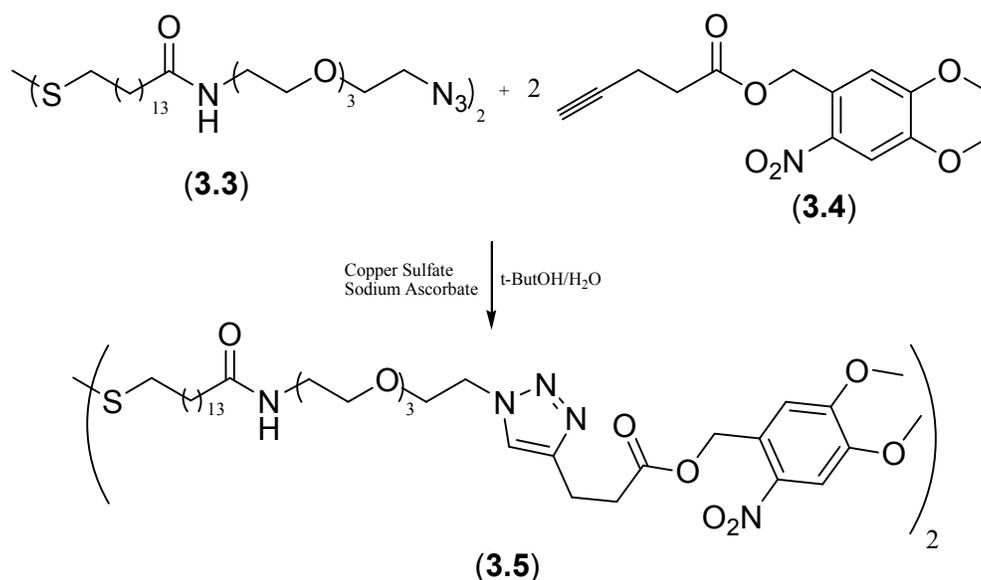
15,15'-disulfanediylbis(N-(2-(2-(2-(2-azidoethoxy)ethoxy)ethoxy)ethyl)pentadecanamide) (**3.3**)

(95.8 mg, 0.101 mmoles) was added to a round bottom flask and diluted with *tert*-butanol (1

mL), water (1 mL), and THF (1 mL). Sodium ascorbate (16.4 mg, 0.102 mmoles), copper

sulfate (16.4 mg, 0.102 mmoles), and 4,5-dimethoxy-2-nitrobenzyl pent-4-ynoate (**3.4**) (58.2 mg,

0.198 mmoles) were added to the flask. The reaction was allowed to proceed for 12 hours. The

reaction mixture was concentrated, diluted with CH_2Cl_2 (10 mL), and rinsed with water (10 mL).

The organic layer was dried over sodium sulfate and concentrated to produce a yellow solid.

The yellow solid was purified via flash column chromatography (5:95 MeOH:ethyl acetate) to

produce 85.2 mg (54%) of bis(4,5-dimethoxy-2-nitrobenzyl) 3,3'-(1,1'-(13,44-dioxo-

3,6,9,48,51,54-hexaoxa-28,29-dithia-12,45-diazahexapentacontane-1,56-diyl)bis(1H-1,2,3-triazole-4,1-diyl))dipropanoate (**3.5**) as yellowish solid. Melting point 60-62 °C. ^{1}H NMR δ 1.2-1.4 (m, 40H), 1.58-1.68 (m, 8H), 2.16 (t, 4H) 2.67 (t, 4H), 2.89 (t, 4H), 3.08 (t, 4H), 3.45 (q, 4H), 3.52-3.60 (m, 20H) 3.83 (t, 4H), 3.95 (s, 6H), 3.98 (s, 6H), 4.48 (t, 4H), 5.51 (s, 4H), 6.03 (s, 1H), 6.99 (s, 2H), 7.53 (s, 2H), 7.71 (s, 2H). ^{13}C NMR δ 20.97, 25.82, 28.59, 29.28, 29.30, 29.42, 29.47, 29.58, 29.66, 29.70, 33.54, 36.77, 39.16, 39.24, 50.16, 56.47, 56.62, 63.34, 69.56, 70.01, 70.23, 70.47, 70.56, 70.60, 108.24, 110.35, 122.55, 127.15, 139.86, 145.88, 148.29, 153.71, 172.20, 173.35. MS (ESI+) cal. for $C_{74}H_{120}N_{10}O_{20}S_2 + H_1$ 1533.82 found 1533.53.

4,5-dimethoxy-2-nitrobenzyl 3-(1-(27-mercapto-13-oxo-3,6,9-trioxa-12-azaheptacosyl)-1H-1,2,3-triazol-4-yl)propanoate (3.6)
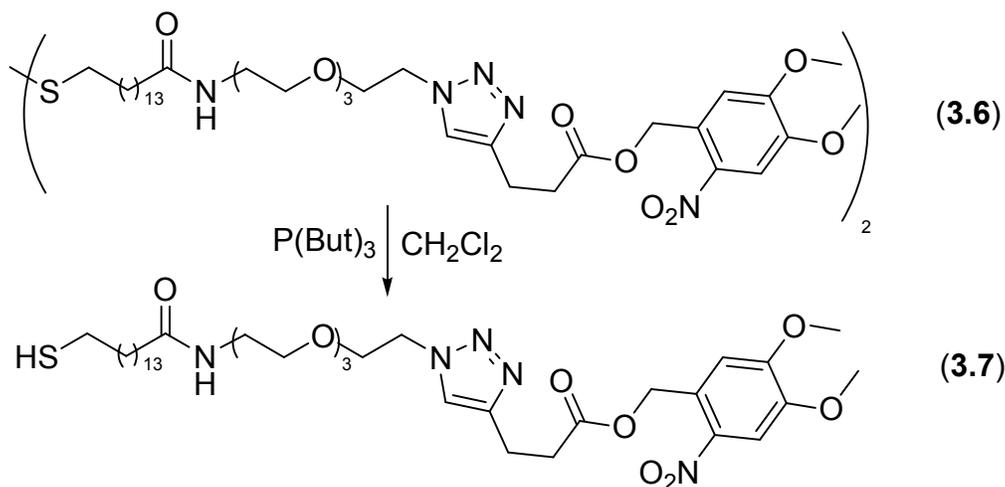
bis(4,5-dimethoxy-2-nitrobenzyl) 3,3'-(1,1'-(13,44-dioxo-3,6,9,48,51,54-hexaoxa-28,29-dithia-12,45-diazahexapentacontane-1,56-diyl)bis(1H-1,2,3-triazole-4,1-diyl))dipropanoate (**3.6**) (47.7 mg, 0.031 mmoles) was added to an oven dried round bottom flask and the flask was purged with argon. Dichloromethane (5 mL) and tributylphosphine (0.4 mL of a 0.4 mmoles/mL solution, 0.162 mmoles) were added to the flask and the reaction was allowed to proceed for 1.5

hours. Solvent was removed under reduced pressure and reaction mixture was purified via flash

column chromatography (5: 95 MeOH:ethyl acetate) to produce a yellow wax. The resulting

wax was further purified under reduced pressure (20 mTorr) to produce 44.6 mg (94 %) of 4,5-

dimethoxy-2-nitrobenzyl 3-(1-(27-mercapto-13-oxo-3,6,9-trioxa-12-azaheptacosyl)-1H-1,2,3-

triazol-4-yl)propanoate (**3.7**) a yellow solid. Melting point 43-45 °C. ^{1}H NMR δ 1.24-1.55 (m,

20 H), 1.55-1.71 (m, 4H), 2.16 (t, 2H), 2.52 (q, 2H), 2.89 (t, 2H), 3.08 (t, 2H), 3.43 (q, 2H), 3.53-

3.60 (m, 10H), 3.83 (t, 2H), 3.95 (s, 3H), 3.98 (s, 3H), 4.48 (t, 2H) 5.51 (s, 2H), 6.00 (s, 1H),

6.99 (s, 1H), 7.53 (s, 1H), 7.71 (s, 1H). ^{13}C NMR δ 13.86, 21.11, 23.98, 24.45, 24.63, 24.88,

25.96, 27.48, 28.34, 28.59, 29.29, 29.57, 29.61, 29.72, 29.80, 29.84, 33.69, 34.27, 36.98, 39.30,

50.32, 56.64, 63.52, 69.73, 70.19, 70.39, 70.65, 70.72, 70.76, 108.38, 110.43, 122.70, 127.31,

146.05, 153.84, 172.37, 173.43. MS (ESI+) cal. for $C_{37}H_{61}N_5O_{10}S_1 + H_1$ 768.42 found 768.27.

3.2.7 Synthesis of Hexaethylene Glycol Amine
17-azido-3,6,9,12,15-pentaoxaheptadecan-1-ol (3.7)
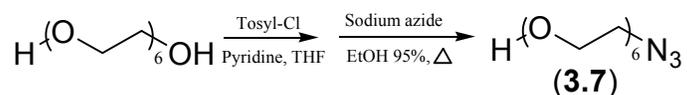
Hexaethylene glycol (1.0796 g, 3.8 mmol) was added to an oven dried round bottom flask and

the flask was purged with argon. Dry THF (15 mL), pyridine (0.5 mL, 6.2 mmol), and

recrystallized tosyl chloride (0.6446 g, 3.3 mmol) were added to the RBF and the reaction was

allowed to stir for 2.5 hours. The solution was concentrated via rotary evaporation and diluted

with CH_2Cl_2 (20 mL). The sample was rinsed with 1 M NaOH (25 mL), 1 M HCl (25 mL), and

brine (25 mL). The organic layers were then combined, dried over sodium sulfate, and

concentrated to produce a yellow oil. The oil was diluted with 95% ethanol (30 mL), and

sodium azide (0.6446 g, 9.9 mmoles) was added to the flask, and the reaction was allowed to

reflux overnight The sample was concentrated and rinsed with 1 M NaOH (25 mL), 1 M HCl

(25 mL), and brine (25 mL). The organic layers were combined, dried over sodium sulfate, and

concentrated to produce a yellow oil. The oil was purified via flash column chromatography to

produce 0.5320 g (51% overall) of 17-azido-3,6,9,12,15-pentaoxaheptadecan-1-ol (**3.7**) as a clear

oil. ^{1}H NMR δ 3.38 (t, 2H), 3.36-3.70 (m, 22H). ^{13}C NMR δ 50.25, 61.12, 69.62, 69.91, 70.12,

70.18, 70.22 (m), 72.26. MS (ESI+) cal. for $C_{12}H_{25}N_3O_7$ +H_1 330.16 found 330.07.

17-amino-3,6,9,12,15-pentaoxaheptadecan-1-ol (3.8)
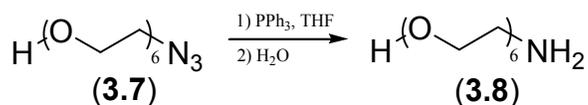
17-azido-3,6,9,12,15-pentaoxaheptadecan-1-ol (**3.7**) (0.532 g, 1.7 mmol) was added to an oven

dried round bottom flask and the flask was purged with argon.   Dry THF (10 mL) and

triphenylphoshpine (0.6523 g, 2.4 mmol) were added to the flask and the reaction was allowed to

proceed at room temperature for 12 hours.   Water (5 mL) was added to the flask until a white

precipitate formed. The organic layer was then removed via rotary evaporation. The sample was

rinsed twice with toluene (15 mL) and concentrated to produce 0.4113 g (86%) of 17-amino-

3,6,9,12,15-pentaoxaheptadecan-1-ol (**3.8**) as a clear oil. ^{1}H NMR δ 2.87 (t, 2H), 3.54 (t, 2H),

3.58-3.73 (m, 20H). ^{13}C NMR δ 41.12, 61.30, 70.15, 70.45 (m), 70.51, 70.58, 71.79, 72.98. MS

(ESI+) cal. for $C_{12}H_{25}NO_6$ +H_1 282.19 found 281.53.

3.3 Results and Discussion

In order to produce continuous gradients using direct-write photolithography, a glycol-terminated photoprotected carboxylic acid monomer was synthesized, shown in **Scheme 3.2** attached to a gold substrate. The nitroveratryl photoprotecting group was employed for our monomer, since it has sufficient absorption and reactivity at 325 nm[29] to allow for rapid photodeprotection by the He-Cd laser in our commercial direct-write photolithography system. Gradient patterns were created from 8-bit gray scale bitmap images with black representing 100% exposure and white representing 0% exposure (**Figure 3.1A** and **3.1C**). These images were directly read by the photolithography system and transferred to the photoprotected SAM using beam scan direct-write photolithography. In this mode, the laser power is tightly controlled using a mirror mounted on a piezoelectric actuator that rasters the beam across the surface in one-dimension.[29] The second writing dimension is achieved with a high-resolution linear encoded motorized stage. After gradient patterns were generated with the direct-write system, they were imaged using scanning probe microscopy (SPM).
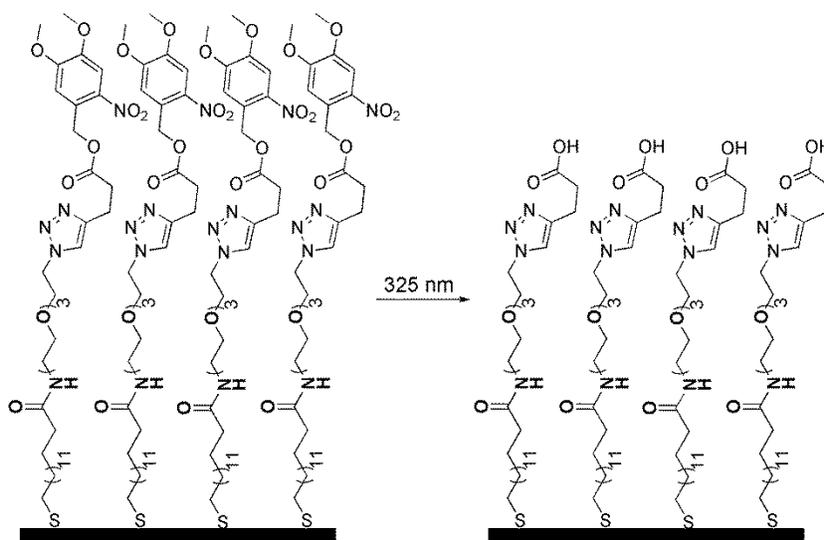
Scheme 3.2 Photodeprotection of glycol-terminated photoprotected carboxylic acid monomer at 325 nm.
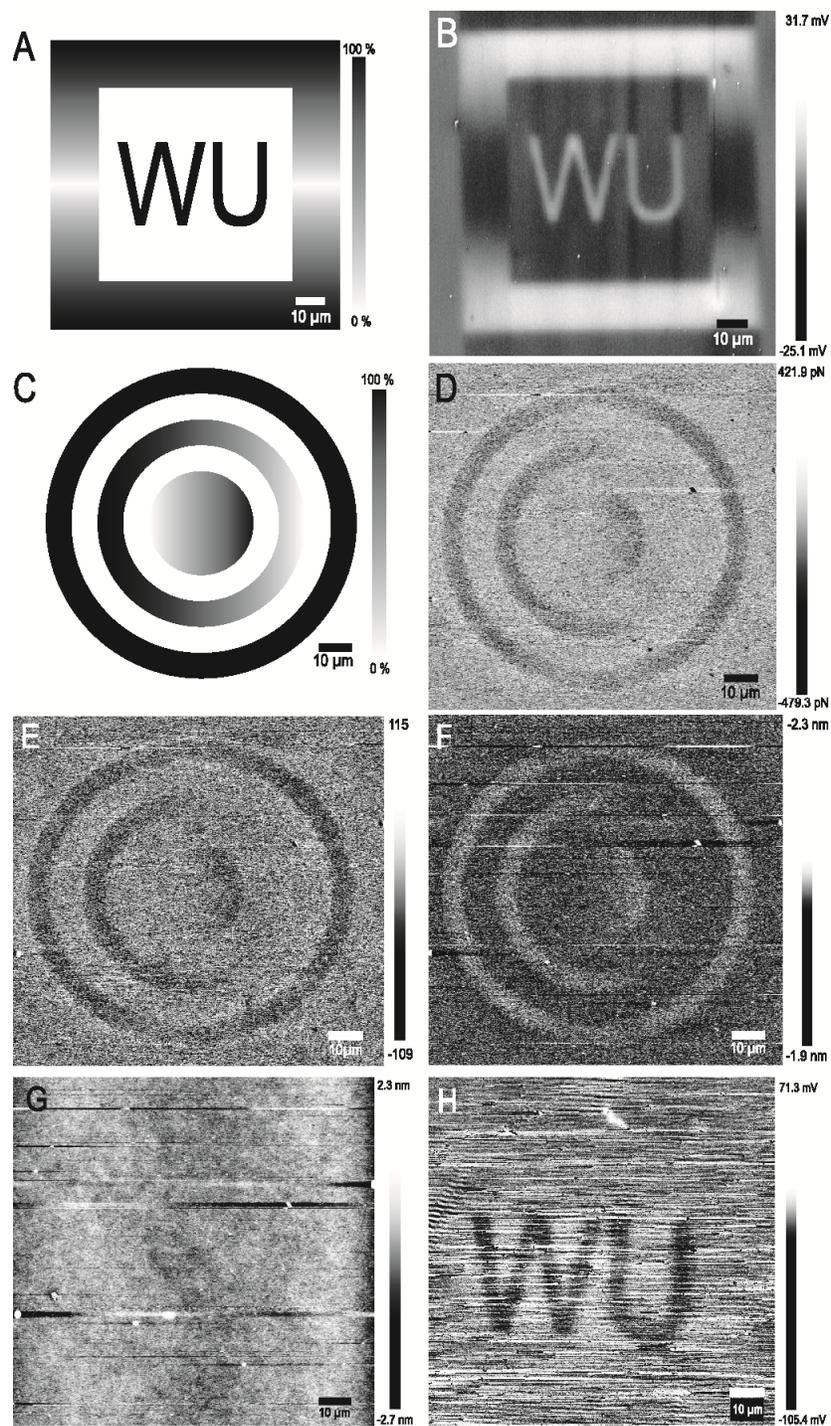
Figure 3.1 SPM Analsysis of Nitroveratryl Pattern Substrates (A and C) 8-bit images patterned by direct-write lithography (scale bar represents relative laser intensity). (B) The resulting KFM image after deprotection. (D, E, F, & G) The adhesion, dissipation, deformation, and height channel, respectively for our patterned surface using PeakForce QNM. (H) Frictional force image generated using LFM.

In order to image our gradient patterns, we have taken advantage of the chemical differences that result upon photodeprotection. One of the most pronounced changes that we would expect to occur upon photodeprotection is a change in surface potential. Upon deprotection, we reveal highly polar carboxylic acids in a relatively hydrophobic monolayer background. As a result, we would expect regions with exposed carboxylic acids to have a larger surface potential than the background monolayer. Moreover, the observed surface potential should be related to the number of free carboxylate groups. Kelvin probe microscopy (KFM), an SPM technique, allowed us to directly measure surface potential. As shown in **Figure 3.1B**, our gradient pattern is clearly visible using KFM with white representing the relative amount of carboxylic acid in a particular region, which is consistent with the image patterned on the surface, **Figure 3.1A**. As expected, the regions of high carboxylate concentrate gave a larger surface potential than the non-patterned region.

While KFM allows us to clearly visualize our molecular gradients, it requires the use of a relatively large SPM probes (20 nm) compared to high resolution probes (1-2 nm). However, by utilizing quantitative nanomechanical mapping (QNM), we can image changes in the mechanical properties that result upon photodeprotection using high resolution SPM probes. Upon photodeprotection, we remove a hydrophobic portion of the molecule that alters the mechanical properties of the underlying structure with the magnitude of the change being proportional to the amount of carboxylic acids revealed. Using QNM SPM, we observe changes in adhesion, dissipation, and deformation (**Figure 3.1D**, **3.1E**, and **3.1F** respectively). In **Figure 3.1D**, the patterned regions show a lower adhesion signal (darker) than the nonpatterned regions due to a greater adhesion force between the probe and the nitroveratryl monomer compared to a free

carboxylic acid. The observed images are a result of both changes in the bulk nanomechanical properties and in tip-sample interactions that result from protecting group cleavage.

Classically, SPM is used to measure height differences; however the height difference that would occur upon deprotection of our carboxylic acid (~1 nm) is too small to be easily measured for a soft material, such as a monolayer fabricated on a gold coated glass coverslip. We anticipated that gradient deprotection of the surface would result in regions that have small local changes on the atomic level that cannot be discerned with a 2 nm SPM probe. As a result, we do not observe our patterns directly in the height channel using PeakForce QNM mode, **Figure 3.1G**.

Monolayer patterns consisting of regions of hexadecanethiol and glycol-terminated thiol have previously been imaged using contact mode lateral force microscopy (LFM), another SPM technique, with functionalized probes.[30] Utilizing LFM, we were able to visualize our patterns in the frictional force channel, **Figure 3.1H**, using standard SPM probes. However, one down side of this technique is the appearance of streaks generated from dragging the probe across this surface. As a result, we have primarily utilized other non-contact images techniques, which will also provide additional properties of our surfaces.

Another major advantage of our methodology is the ability to pattern two molecules on the same surface. To accomplish this, photolithography was carried out using two distinct overlaid patterns with each pattern encoding the spatial distribution of a different amine molecule as shown in **Scheme 3.3**. Briefly, a circle was patterned on the substrate producing free carboxylic acids, which were subsequently activated with EDC/HOAt. Hexaethylene glycol amine was then added to the solution, which resulted in it becoming coupled to the substrate. After coupling the first amine, a frame was patterned around the circle. The newly formed carboxylic acids were

activated with EDC/HOAt and tetraethylene glycol amine was coupled to the substrate. This multimolecule pattern was designed to highlight the flexibility of maskless photolithography, since at least two masks would need to be fabricated to produce this image using traditional methods and the alignment would be extremely difficult.

Patterned samples were characterized by imaging matrix assisted laser desorption-ionization time of flight mass spectrometry (MALDI-TOF MS),[31] to ensure that only site-selective deprotection and coupling had occurred. Imaging was carried out using 100 μm spots spaced 250 μm apart (center to center) with each spectrum consisting of 20 averaged spectra containing 50 shots. The resulting spectra were then analyzed for the molecular weights of the coupled products (**1** and **2**), the disulfide of the glycol (**3**), the photoprotected monomer, and the corresponding heat maps were generated (**Figure 3.2**). As shown in **Figure 3.2A**, a bright circle was produced when analyzing for **1** which is consistent with our patterning scheme. A bright frame was produced when analyzing for **2**, **Figure 3.2B**. However there is a small amount of **1** observed in the circle region, which is a result of steric packing of the acids limiting ester formation. In addition, we observed a loss in signal when analyzing for the photoprotected monomer as shown in **Figure 3.2C**. This result is expected since the photoprotected monomer is converted to a coupled
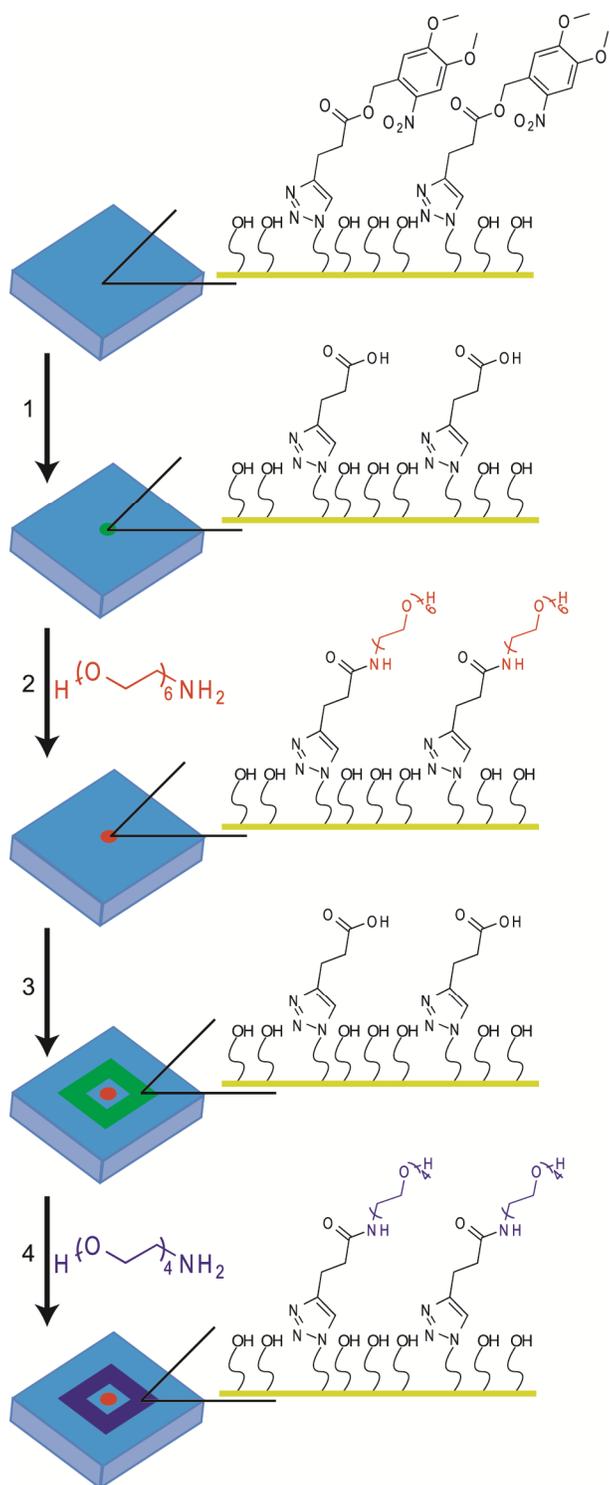
Scheme 3.3 Two molecule patterning scheme. (1) Pattern circle, (2) Activate carboxylic acid with EDC/HOAt and couple hexaethylene glycol amine, (3) Pattern frame around circle, (4) Activate carboxylic acid with EDC/HOAt and couple tetraethylene glycol amine.
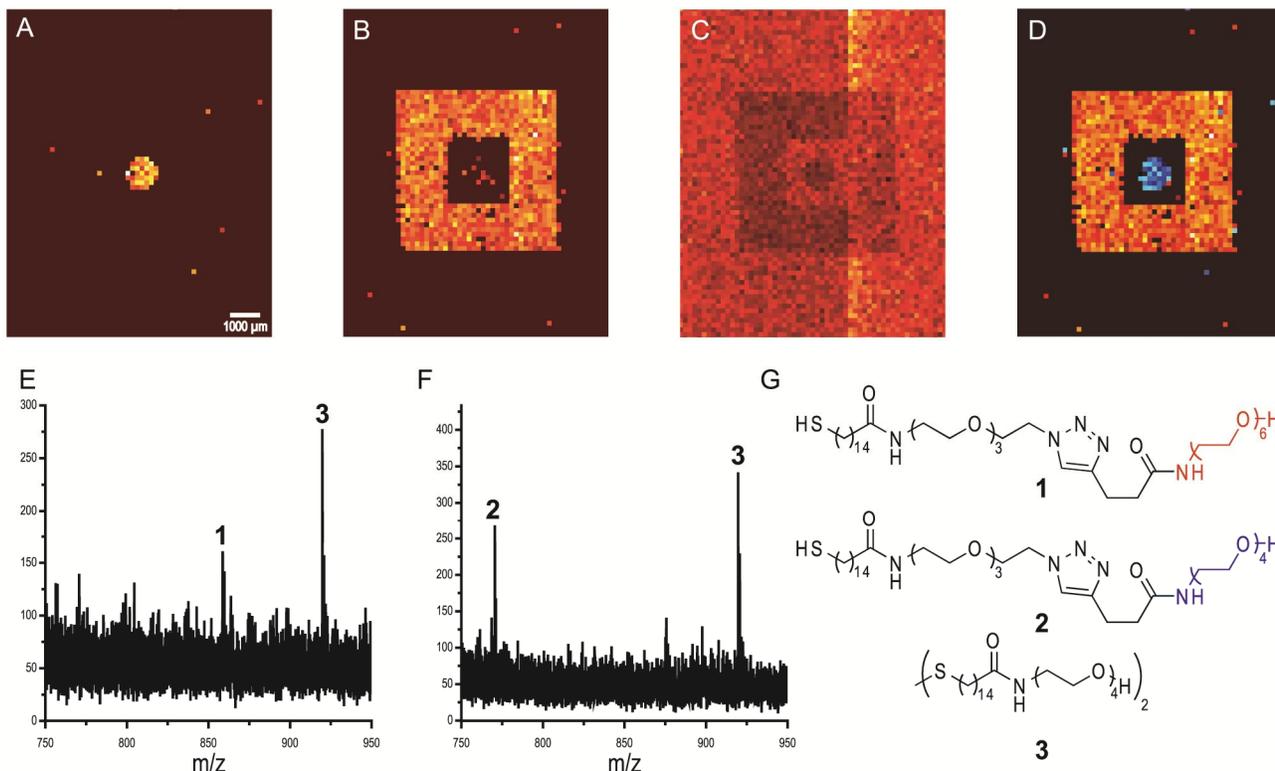
Figure 3.2. MALDI TOF Analysis of two molecule coupling substrate. (A,B,C) Heat maps generated after analysis for molecule **1**, **2**, and glycol-terminated photoprotected carboxylic acid monomer glycol, respectively. (D) Overlay of A and B. (E, F) Representative MALDI-TOF spectra for the circle and frame region, respectively. (G) Molecules analyzed for in MALDI-TOF spectrum.

product in the patterned regions. The versatility of this method is shown in **Figure 2D**, which is an overlay of the two heat maps generated from the coupled molecules **1** and **2** showing that two distinct molecules were coupled to the same substrate in a site-specific manner using our patterning methodology.

3.4 Conclusions

Here we have developed a versatile method for patterning multiple molecules on a single substrate at defined molecular densities using direct-write photolithography. Smooth molecular gradients were straightforward to generate using grayscale photolithography and could be

characterized using SPM in KPM, QNM, and LFM modes. The alignment of two molecules on a single substrate was implemented using multilayer photolithography. In conclusion, the methodology developed here is broadly applicable to the development of patterned molecular substrates for materials applications and is especially pertinent to the development of biosensors and cell-based assays.

3.5 References

1.   Yamada, H.; Imahori, H.; Nishimura, Y.; Yamazaki, I.; Ahn, T. K.; Kim, S. K.; Kim, D.; Fukuzumi, S., Photovoltaic Properties of Self-Assembled Monolayers of Porphyrins and Porphyrin−Fullerene Dyads on ITO and Gold Surfaces. *Journal of the American Chemical Society* **2003,** 125, (30), 9129-9139.

2.   Kuo, C.-H.; Liu, C.-P.; Lee, S.-H.; Chang, H.-Y.; Lin, W.-C.; You, Y.-W.; Liao, H.-Y.; Shyue, J.-J., Effect of surface chemical composition on the work function of silicon substrates modified by binary self-assembled monolayers. *Physical Chemistry Chemical Physics* **2011,** 13, (33), 15122-15126.

3.   Mandler, D.; Kraus-Ophir, S., Self-assembled monolayers (SAMs) for electrochemical sensing. *Journal of Solid State Electrochemistry* **2011,** 15, (7), 1535-1558.

4.   Khodabakhsh, S.; Sanderson, B. M.; Nelson, J.; Jones, T. S., Using Self-Assembling Dipole Molecules to Improve Charge Collection in Molecular Solar Cells. *Advanced Functional Materials* **2006,** 16, (1), 95-100.

5.   Falconnet, D.; Csucs, G.; Michelle Grandin, H.; Textor, M., Surface engineering approaches to micropattern surfaces for cell-based assays. *Biomaterials* **2006,** 27, (16), 3044-3063.

6.   Love, J. C.; Estroff, L. A.; Kriebel, J. K.; Nuzzo, R. G.; Whitesides, G. M., Self-Assembled Monolayers of Thiolates on Metals as a Form of Nanotechnology. *Chemical Reviews* **2005,** 105, (4), 1103-1170.

7.   Herbert, C. B.; McLernon, T. L.; Hypolite, C. L.; Adams, D. N.; Pikus, L.; Huang, C. C.; Fields, G. B.; Letourneau, P. C.; Distefano, M. D.; Hu, W.-S., Micropatterning gradients and controlling surface densities of photoactivatable biomolecules on self-assembled monolayers of oligo(ethylene glycol) alkanethiolates. *Chemistry & Biology* **1997,** 4, (10), 731-737.

8.   Johnson, D. M.; Maurer, J. A., Recycling and reusing patterned self-assembled monolayers for cell culture. *Chemical Communications* **2011,** 47, (1), 520-522.

9.   Yanker, D. M.; Maurer, J. A., Direct printing of trichlorosilanes on glass for selective protein adsorption and cell growth. *Molecular BioSystems* **2008,** 4, (6), 502-504.

10.   Samanta, D.; Sarkar, A., Immobilization of bio-macromolecules on self-assembled monolayers: methods and sensor applications. *Chemical Society Reviews* **2011,** 40, (5), 2567-2592.

11.   Dillmore, W. S.; Yousaf, M. N.; Mrksich, M., A Photochemical Method for Patterning the Immobilization of Ligands and Cells to Self-Assembled Monolayers. *Langmuir* **2004,** 20, (17), 7223-7231.

12.   Álvarez, M.; Alonso, J. M. a.; Filevich, O.; Bhagawati, M.; Etchenique, R.; Piehler, J.; del Campo, A. n., Modulating Surface Density of Proteins via Caged Surfaces and Controlled Light Exposure. *Langmuir* **2011,** 27, (6), 2789-2795.

13.   Huang, J.; Hemminger, J. C., Photooxidation of thiols in self-assembled monolayers on gold. *Journal of the American Chemical Society* **1993,** 115, (8), 3342-3343.

14.   Han, X.; Pradeep, S. N. D.; Critchley, K.; Sheikh, K.; Bushby, R. J.; Evans, S. D., Supported Bilayer Lipid Membrane Arrays on Photopatterned Self-Assembled Monolayers. *Chemistry – A European Journal* **2007,** 13, (28), 7957-7964.

15.   Alonso, J. M.; Reichel, A.; Piehler, J.; del Campo, A., Photopatterned Surfaces for Site-Specific and Functional Immobilization of Proteins. *Langmuir* **2007,** 24, (2), 448-457.

16.   Alang Ahmad, S. A.; Wong, L. S.; ul-Haq, E.; Hobbs, J. K.; Leggett, G. J.; Micklefield, J., Protein Micro- and Nanopatterning Using Aminosilanes with Protein-Resistant Photolabile Protecting Groups. *Journal of the American Chemical Society* **2011,** 133, (8), 2749-2759.

17.   Ducker, R. E.; Janusz, S.; Sun, S.; Leggett, G. J., One-Step Photochemical Introduction of Nanopatterned Protein-Binding Functionalities to Oligo(ethylene glycol)-Terminated Self-Assembled Monolayers. *Journal of the American Chemical Society* **2007,** 129, (48), 14842-14843.

18.   Piner, R. D.; Zhu, J.; Xu, F.; Hong, S.; Mirkin, C. A., "Dip-Pen" Nanolithography. *Science* **1999,** 283, (5402), 661-663.

19.   Liedberg, B.; Tengvall, P., Molecular Gradients of .omega.-Substituted Alkanethiols on Gold: Preparation and Characterization. *Langmuir* **1995,** 11, (10), 3821-3827.

20.   Burgos, P.; Geoghegan, M.; Leggett, G. J., Generation of Molecular-Scale Compositional Gradients in Self-Assembled Monolayers. *Nano Letters* **2007,** 7, (12), 3747-3752.

21.   Jeon, N. L.; Dertinger, S. K. W.; Chiu, D. T.; Choi, I. S.; Stroock, A. D.; Whitesides, G. M., Generation of Solution and Surface Gradients Using Microfluidic Systems. *Langmuir* **2000,** 16, (22), 8311-8316.

22.   Dertinger, S. K. W.; Jiang, X.; Li, Z.; Murthy, V. N.; Whitesides, G. M., Gradients of substrate-bound laminin orient axonal specification of neurons. *Proceedings of the National Academy of Sciences* **2002,** 99, (20), 12542-12547.

23.   Jiang, X.; Xu, Q.; Dertinger, S. K. W.; Stroock, A. D.; Fu, T.-m.; Whitesides, G. M., A General Method for Patterning Gradients of Biomolecules on Surfaces Using Microfluidic Networks. *Analytical Chemistry* **2005,** 77, (8), 2338-2347.

24.   Westcott, N. P.; Lamb, B. M.; Yousaf, M. N., Electrochemical and Chemical Microfluidic Gold Etching to Generate Patterned and Gradient Substrates for Cell Adhesion and Cell Migration. *Analytical Chemistry* **2009,** 81, (9), 3297-3303.

25.   Lamb, B. M.; Park, S.; Yousaf, M. N., Microfluidic Permeation Printing of Self-Assembled Monolayer Gradients on Surfaces for Chemoselective Ligand Immobilization Applied to Cell Adhesion and Polarization. *Langmuir* **2010,** 26, (15), 12817-12823.

26.   Ryan, D.; Parviz, B. A.; Linder, V.; Semetey, V.; Sia, S. K.; Su, J.; Mrksich, M.; Whitesides, G. M., Patterning Multiple Aligned Self-Assembled Monolayers Using Light. *Langmuir* **2004,** 20, (21), 9080-9088.

27.   del Campo, A.; Boos, D.; Spiess, H. W.; Jonas, U., Surface Modification with Orthogonal Photosensitive Silanes for Sequential Chemical Lithography and Site-Selective Particle Deposition. *Angewandte Chemie International Edition* **2005,** 44, (30), 4707-4712.

28.   Bhagawati, M.; Lata, S.; Tampé, R.; Piehler, J., Native Laser Lithography of His-Tagged Proteins by Uncaging of Multivalent Chelators. *Journal of the American Chemical Society* **2010,** 132, (17), 5932-5933.

29.   Lullo, G.; Leto, R.; Oliva, M.; Arnone, C., Multilevel pattern generation by GaN laser lithography: an application to beam shaper fabrication. *Proc. SPIE* **2006,** 6290, 62900A.

30.   Sasaki, K.; Koike, Y.; Azehara, H.; Hokari, H.; Fujihira, M., Lateral force microscope and phase imaging of patterned thiol self-assembled monolayer using chemically modified tips. *Applied Physics A: Materials Science & Processing* **1998,** 66, (0), 1275-1277.

31.   Henke, C.; Steinem, C.; Janshoff, A.; Steffan, G.; Luftmann, H.; Sieber, M.; Galla, H.-J., Self-Assembled Monolayers of Monofunctionalized Cyclodextrins onto Gold: A Mass Spectrometric Characterization and Impedance Analysis of Host−Guest Interaction. *Analytical Chemistry* **1996,** 68, (18), 3158-3165.

Chapter 4

Phototriggered Cyclooctyne Formation for the Patterning of Peptides, Proteins, and Small Molecules

4.1 Introduction

The ability to immobilize peptides and proteins site-selectively on two dimensional substrates is critical to the development of protein and peptide arrays, biosensors, drug discovery, cell growth assays, and other areas of biotechnology.[1-5] As a result, many bioorthogonal chemical reactions, which were originally developed for protein and cell labeling in solution, are now being utilized to anchor biological molecules to patterned surfaces.[1, 6] These techniques include the Staudinger[7] and oximine[8, 9] ligations, the Diels-Alder[10, 11] and thiol-ene[12, 13] reactions, and Cu(I) catalyzed[14, 15] and Cu-free strain-promoted[16] [3+2] azide-alkyne cycloadditions, termed "click" chemistry. One of the most versatile patterning strategies for arraying reactive functional groups site-selectively is photolithography. Photolithography provides a non-contact based patterning strategy that is compatible with large scale production and results in less contamination issues than classical contact methods including dip-pen nanolithography and microcontact printing.[17] Additionally, photolithography provides a high degree of spatial and temporal control through the use of conventional photolithography instrumentation.[18] As a result, photochemical variants of oximine ligations,[19] the Diels-Alder[20] and thiol-ene[21] reactions, and the Cu(I) catalyzed [3+2] azide-alkyne cycloaddition[5] have been developed to couple either biotin or the RGD peptide to functionalized surfaces. However, to date, no report exists that utilizes the versatility of photolithography and the selectivity of Cu-free strain-promoted [3+2] azide-alkyne cycloadditions for patterning these molecules. Here, we report the development of such a system that is compatible with protein resistant self-assembled monolayers (SAMs).

79

4.2 Experimental Methods

4.2.1 Materials and Instrumentation

All reagents used for synthesis were obtained from Sigma-Aldrich (St. Louis, MO) or VWR Scientific (Radnor, PA), were reagent grade or higher, and used as received unless otherwise indicated. The anti-avidin antibody, B-9655, was purchased from Sigma-Aldrich (St. Louis, MO). The azido-biotin monomer was purchased from Click Chemistry Tools (Scottsdale, AZ). The azido-cRGD peptide was purchased from Peptides International (Louisville, KY). The rabbit anti-RGD peptide, bs-2039R, was purchased from BIOSS (Wuborn, MA). The donkey anti-rabbit antibody, A10039, was purchased from Invitrogen (Grand Island, NY). Neutravidin was purchased from Thermo Fisher (Waltham, MA). ^{1}H NMR and ^{13}C NMR were collected on a 300 MHz Varian NMR (Agilent Technologies, Santa Barbra, CA) and referenced to residual deuterated solvent peaks. All NMR spectra are attached in Appendix D. Electrospray ionization (ESI) Mass spectrums were collected on a Thermo LCQ Deca Plus (Thermo Fisher Scientific, Waltham, MA) operating in positive mode. Melting points were collected on a Stuart SMP10 (Keison Products, England) melting point apparatus. Gold substrates were prepared using a PVD 75 with a four pocket electron beam module (Kurt J Lesker, Pittsburg, PA). Matrix Assisted Laser Desorption Ionization Mass Spectrums (MALDI-MS) were collected on a Voyager DE-STR MALDI TOF-TOF (Applied Biosystems, Carlsbad, CA) with a Nitrogen laser (337 nm) operating in positive reflectance mode. Substrates were patterned using a direct-writer LaserWriter (Microtech, Palermo, Italy) system equipped with a 325 nm He:Cd laser operating at 15 mW with a 90% neutral density filter. Fluorescent and bright field images were obtained using a Nikon TE2000-PFS microscope running NIS-Elements imaging software and equipped

with a Prior XY stage, EXFO X-Cite series 120PC UV illuminator, Photometrics CoolSNAP monochrome camera, and In Vivo Scientific incubation system.

4.2.2 Substrate Preparation and Patterning: Gold substrates were prepared by electron beam deposition of 50 Å of titanium at 0.1 Å/sec followed by 100 Å of gold 0.1 Å/sec without venting between layers. Gold substrates were soaked in a 1 mM ethanolic solution of the indicated thiol monomers for 12 hours. The relative concentration of thiol monomers was varied depending on the application. Slides were then rinsed with ethanol, water, and ethanol, and dried under a stream of nitrogen gas. Patterns were created using CleWin (WieWeb, Netherlands) or Adobe Illustrator. Photolithography was carried out using a direct-write laser writer in beam scan mode between 0 and 100% laser intensity with a full laser power of 1200 mJ/cm^2 under an argon atmosphere. After photopatterning samples were rinsed with ethanol, water, and ethanol, and dried under a stream of nitrogen.

4.2.3 Surface Coupling. Freshly patterned substrates were placed into a 0.1 mM solution of an azide terminated molecule (either azido-biotin or azido-cRGD peptide) in 10 mM phosphate buffer at pH 8.05 (PB) for 2 hours at room temperature. Substrates were removed, rinsed with water and ethanol, and dried under a stream of nitrogen.

4.2.4 Characterization of monolayers with MALDI-MS. Patterned coverslips were coated with 200 μL of 10 mg/mL 2,5-dihydroxybenzoic acid (DHB) in THF and dried under vacuum for 10 minutes to obtain uniform matrix coverage. Samples were then imaged in positive reflectance mode using a Voyager DE-STR with an accelerating voltage of 15 kV, grid voltage of 66%, mirror voltage ratio 1.12 and an average delay time of 150 nsec. Each spectrum consisted of 20 averaged spectra containing 100 shots. Spectra were processed using Data

Explorer software (Applied Biosystems, Carlsbad, CA). Spectra were baseline corrected and passed through a noise filter with a correlation factor of 0.7.

4.2.5 Biotin amplification assay. Fluorescent labeling of neutravidin. To 50 µL of Neutravidin (1mg/mL) in sterile water was added 1 µL of 1 M sodium bicarbonate in sterile water and 2 µL of Oregon Green 488 carboxylic acid, succinimidyl ester (5 mg/mL in DMF, Invitrogen). The reaction was allowed to proceed at room temperature for 1 h. The reaction was quenched by addition of 3 µL of 1.5 M hydroxyl amine in 1 N sodium hydroxide.

Amplification assay. Gold substrates functionalized with a 0.1 % photoprotected cyclooctyne monomer solution were used for the biotin amplification assay. Freshly coupled biotin slides were placed into a solution of fluorescently labeled neutravidin (50 µg/mL) for 1 hour at 37 °C. Slides were rinsed with PB and incubated with a solution of biotin labeled anti-avidin antibody (22 µg/mL) for 1 h at 37 °C. The slide was then rinsed and incubated with fresh fluorescently labeled neutravidin for 1 h at 37 °C. The entire amplification process was repeated to bring the fluorescent signal out from background. The final substrate was imaged using an inverted microscope and the mean fluorescent pixel intensities for each of the eleven regions, **Figure 4.2C**, were extracted using NIS Elements.

4.2.6 Immunohistochemistry. Gold substrates functionalized with a 1.0 % photoprotected cyclooctyne monomer solution were used for the immunohistochemistry assay. Freshly coupled azido-cRGD coupled slides were incubated with a primary rabbit anti-RGD antibody (20 µg/mL) solution for 1 hour at 37 °C. Subsequently, the substrates were rinsed with PB, to remove nonspecifically adsorbed antibody, and incubated with a fluorescently labeled donkey anti-rabbit secondary antibody (10 µg/mL) for 1 hour at 37 °C. The substrate was rinsed and imaged using an inverted microscope.

4.2.7 Cell Culture. A patterned coverslips, coupled with azido-cRGD peptide, in a Teflon cell culture chamber were equilibrated with Dulbecco's Modified Eagle Medium for NIH/3T3 (DMEM, high glucose 1X, glutamax, 1g/L D-glucose, 110 mg/L sodium pyruvate, 50 mL Fetal calf serum (FCS), 5 mL penicillin/streptomycin (10,000 units/mL Penicillin G Sodium and 10,000 µg/mL Streptomycin Sulfate in 0.85% saline), Invitrogen). NIH/3T3 cells (ATCC, Manassas, VA) were separated using TrypLE Express (Invitrogen), followed by resuspension in medium and counted using a TC10 automated cell counter with trypan blue dye (Bio-Rad, Hercules, CA). Approximately 50,000 cells were applied in 1 mL of DMEM and cultures grown at 37°C, 5% CO_2, for 2 hours. Substrates were then rinsed to remove nonspecifically attached cells. Live cultures were visualized and images captured by inverted microscopy in brightfield after 5 days in culture.
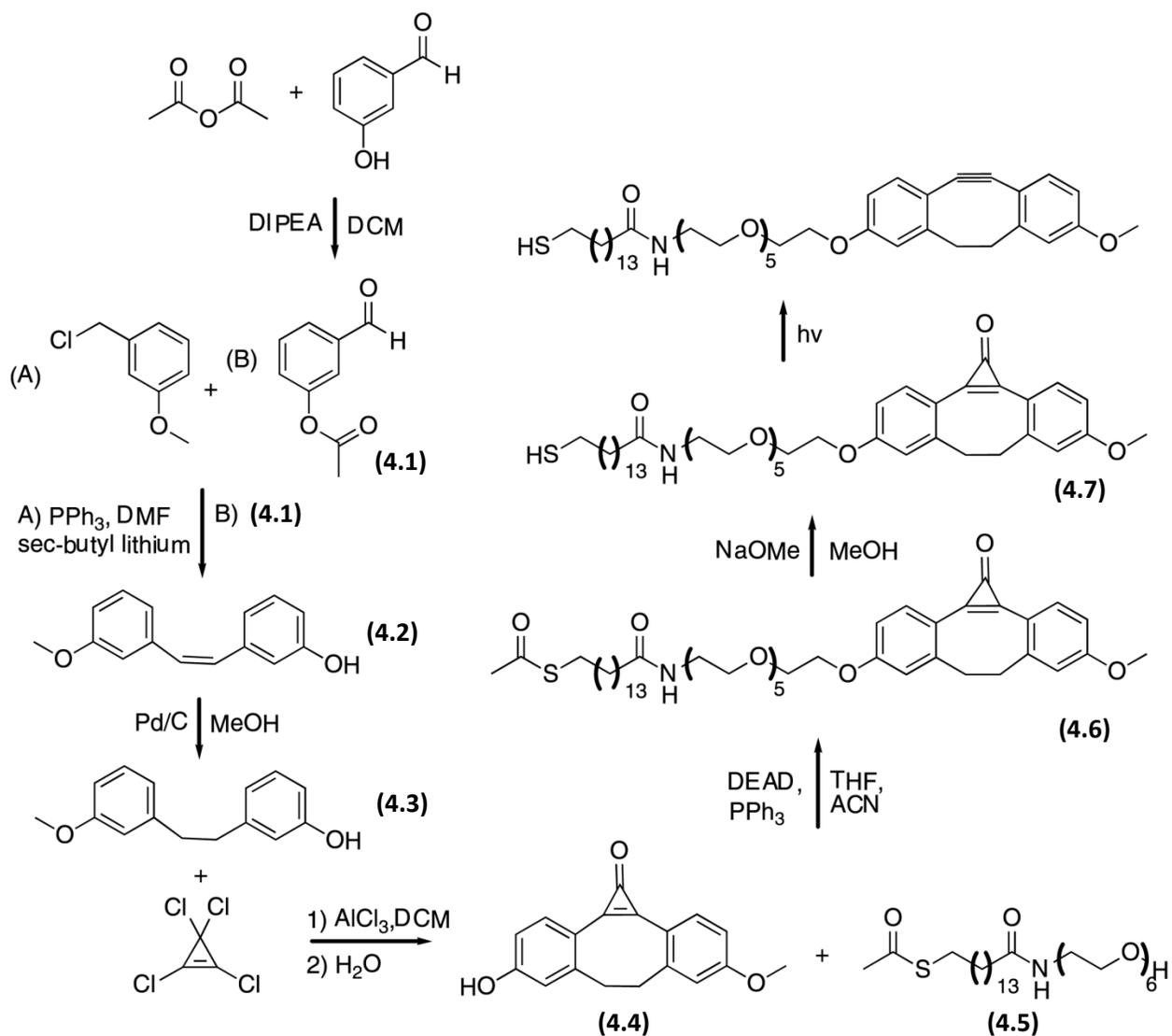
Scheme 4.1 Overall Synthetic Scheme for the Cyclopropenone Monomer

4.2.8 Synthetic Methods for 4.4

3-formylphenyl acetate (4.1)
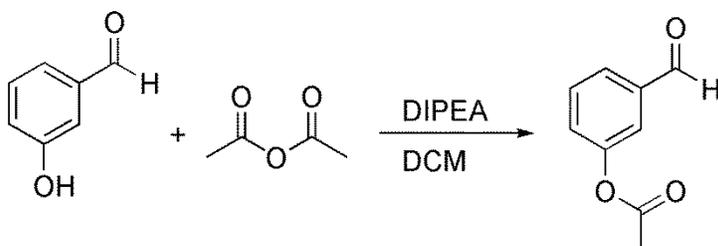
3-hydroxylbenzaldehyde (12.3512 g, 0.101 moles) was added to an oven dried round bottom flask and the flask was purged with argon. The sample was diluted with anhydrous tetrahydrofuran (THF) (30 mL) and diisopropylethyl amine (DIPEA) (50 mL, 0.314 moles). Acetic anhydride (12.0 mL, 0.129 mmoles) was added to the round bottom flask and allowed to proceed at room temperature for 12 hours. THF was removed under reduced pressure and the resulting oil was diluted with DCM and rinsed with 0.5 M NaOH (25 mL, 3 times). The organic layers were combined, dried over sodium sulfate, and concentrated to produce 12.1395 g (73%) of 3-formylphenyl acetate (**4.1**) as a yellow oil. ^{1}H NMR δ 2.34 (s, 3H), 7.37 (dd,1H), 7.56 (t, 1H), 7.62 (t, 1H), 7.76 (t, 1H) 10.00 (1H). ^{13}C NMR δ 21.11, 122.28, 122.36, 127.44, 127.85, 130.25, 137.81, 151.31, 169.23, 191.26. MS (ESI+) cal. for $C_9H_8O_3$ +H 165.00 found 165.05 m/z.

(Z)-3-(3-methoxystyryl)phenol and (E)-3-(3-methoxystyryl)phenol
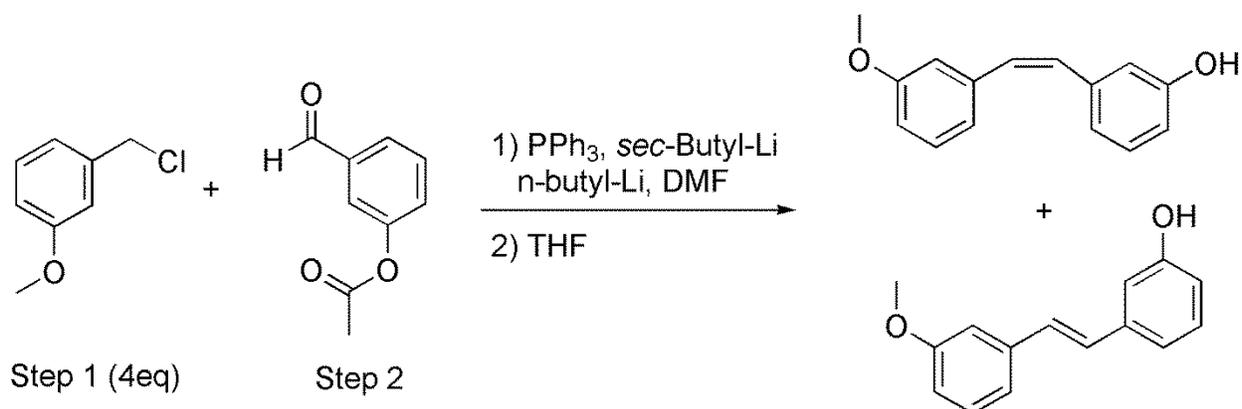
Triphenylphosphine (PPh₃) (5.6445 g, 0.0216 moles) was added to an oven dried round bottom flask and the flask was purged with argon. The round bottom flask was placed in a warm oil bath (110 °C) and the PPh₃ melted. 3-methoxybenzyl chloride (3.0 mL, 0.0206 moles) was added dropwise and the reaction was allowed to proceed for 20 minutes before the mixture solidified. The sample was diluted with dry DMF (25 mL) and cooled to -78 °C in a dry ice/acetone bath. sec-Butyl lithium (8 mL, 0.0112 moles) and n-butyl lithium (6 mL, 0.015 moles) was added dropwise and the reaction was allowed to proceed for 30 minutes before 3-formylphenyl acetate (**4.1**) (1.1916 g, 7.2 mmoles) was added dropwise. The reaction mixture was allowed to slowly come to room temperature (12 hours total). The solvent was removed under reduced pressure (20 mTorr). The resulting oil was diluted with CH_2Cl_2 (20 mL) and rinsed with 1 M NaOH (20 mL), 1 M HCl (20 mL), and brine (20 mL). The organic layers were combined, dried over sodium sulfate, and concentrated. The resulting oil was purified via flash column chromatography (15:20:65 MeOH:CHCl₃:Hexanes) to produce 1.830 g (99%) a mixture of both (Z)-3-(3-methoxystyryl)phenol and (E)-3-(3-methoxystyryl)phenol (**4.2**) as a yellow oil. ¹H NMR δ 3.66 (s, 3H), 6.56 (s, 2H), 6.78 (m, 6H), 7.14 (m, 2H). ¹³C NMR δ 55.28, 113.55, 113.94,114.03, 114.39, 115.58, 115.68, 121.81, 129.45, 129.73, 130.17, 130.22, 130.28, 130.60,

130.65, 130.71, 138.61, 139.02, 155.51, 159.47. MS (ESI+) cal. for $C_{15}H_{14}O_2$ +K 265.06 found

265.33 m/z.

3-(3-methoxyphenethyl)phenol (4.3)
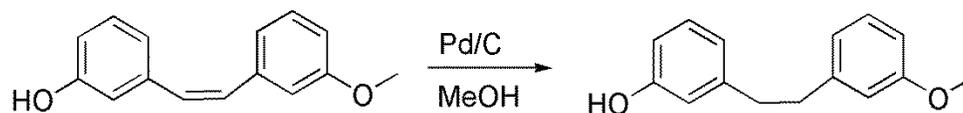
The mixture of (Z)-3-(3-methoxystyryl)phenol and (E)-3-(3-methoxystyryl)phenol (**4.2**) (1.800

g, 7.9 mmoles) was added to a round bottom flask and purged with argon. Palladium on

activated carbon (10%, approx 50 mg) was added to the round bottom flask. The round bottom

flask was then purged with hydrogen and the reaction was allowed to proceed for 12 hours in a

hydrogen atmosphere. The sample was then filtered through celite and the organic layers were

concentrated to produce 1.611 g (89%) of 3-(3-methoxyphenethyl)phenol (**4.3**) as a yellow oil.

^{1}H NMR δ 2.88 (s, 4H), 3.79 (s, 3H), 6.73 (m, 6H), 7.18 (m, 2H). ^{13}C NMR δ 37.83, 51.37,

111.49, 113.01, 114.34, 114.45, 115.53, 115.63, 121.10, 129.52, 129.72, 143.53, 143.86, 155.73,

159.68. MS (ESI+) cal. for $C_{15}H_{16}O_2$ +H 229.12 found 229.22.

4-hydroxy-9-methoxy-6,7-dihydro-1H-dibenzo[a,e]cyclopropa[c][8]annulen-1-one (4.4)
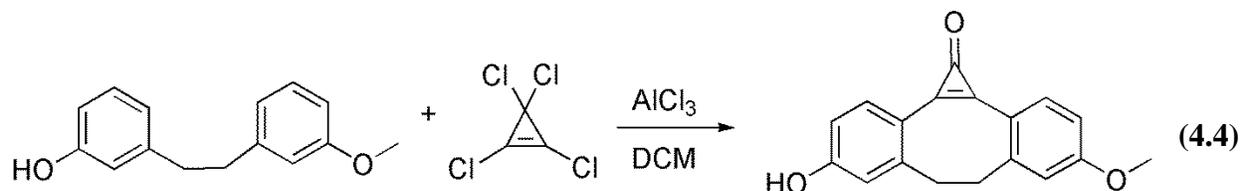
Aluminum chloride (1.5623 g, 11.7 mmoles) was added to an oven dried round bottom flask and

the flask was purged with argon. Tetrachlorocyclopropene (0.90 mL, 7.3 mmoles) was added to

the flask. The reaction mixture was diluted with anhydrous DCM (15 mL) and placed in a 40 °C

oil bath for 30 minutes. The sample was then placed in an ice water bath and 3-(3-methoxyphenethyl)phenol (**4.3**) (1.611 g, 7.05 mmoles) was added dropwise. The reaction mixture was allowed to proceed for an additional 4 hours before being slowly quenched with water. The reaction mixture was further diluted with water and extracted in DCM. The organic layers were combined, dried over sodium sulfate, and concentrated. The resulting oil was purified via flash column chromatography (2:98 MeOH:EthylAceate) to produce 0.5493 g (28 %) of 4-hydroxy-9-methoxy-6,7-dihydro-1H-dibenzo[a,e]cyclopropa[c][8]annulen-1-one (**4.4**) as a yellow solid. Melting Point; 68-70 °C. ^{1}H NMR δ 2.48 (s, 3H), 3.35 (d, 2H), 3.88 (d, 2H), 6.91 (ddd, 2H), 6.98 (dd, 2H), 7.73 (dd, 2H) 10.48 (s, 1H). ^{13}C NMR (DMSO) δ 36.83, 56.10, 74.99, 104.99, 112.88, 114.43, 114.97, 116.14, 116.58, 117.49, 135.26, 135.71, 141.27, 148.41, 148.66, 152.46, 161.56, 162.40. MS (ESI+) cal. for $C_{18}H_{14}O_3$ +H 279.10 found 279.20 m/z.

S-(1-hydroxy-19-oxo-3,6,9,12,15-pentaoxa-18-azatritriacontan-33-yl) ethanethioate (4.5)
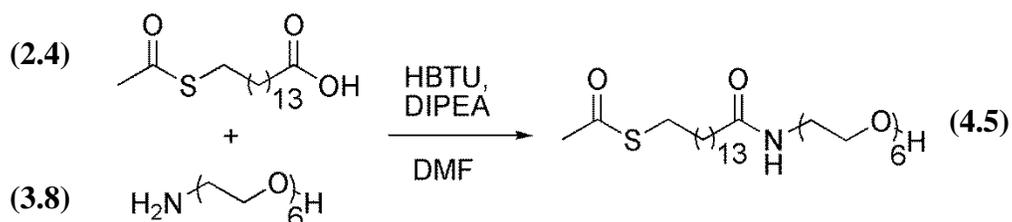
15-(acetylthio)pentadecanoic acid (**2.4**) (1.0632g, 3.3 mmoles) was added to an oven dried round bottom flask and the flask was purged with argon. The sample was diluted with anhydrous dimethylformamide (DMF) (10 mL) and CH_2Cl_2 (5 mL), Diisopropylethyl amine (DIPEA) (1.5 mL, 9.4 mmoles) and O-(Benzotriazol-1-yl)-N,N,N',N'-tetramethyluronium hexafluorophosphate (HBTU) (1.23 g, 3.2 mmoles) were added to the flask and the reaction was allowed to proceed at room temperature for 1 hour. 17-amino-3,6,9,12,15-pentaoxaheptadecan-1-ol (**3.8**) (0.7370 g, 2.2 mmoles) was added dropwise to the flask and the reaction was allowed

to proceeded for 12 hours. The solvent was removed under reduced pressure (20 mTorr). The resulting oil was diluted with CH_2Cl_2 (20 mL) and rinsed with 1 M NaOH (20 mL), 1 M HCl (20 mL), and brine (20 mL). The organic layers were combined, dried over sodium sulfate, and concentrated. The resulting oil was purified via flash column chromatography (5:20:75 MeOH:CHCl$_3$:ethyl acetate) to produce 1.0993 g (72%) of S-(1-hydroxy-19-oxo-3,6,9,12,15-pentaoxa-18-azatritriacontan-33-yl) ethanethioate (**4.5**) an off-white solid. Melting point 52-53 °C. ^{1}H NMR δ 1.27 (m, 28H), 1.56 (m, 6H), 2.18 (t, 2H), 2.32 (s, 3H), 2.86 (t, 2H) 3.45 (t, 2H) 3.66 (m, 30H), 6.41 (broad, 1H). ^{13}C NMR δ 25.95, 28.98, 29.27, 29.31, 29.54, 29.58, 29.63, 29.69, 29.73, 29.78, 30.82, 36.84, 39.31, 61.81, 64.84, 70.67, 70.70, 70.76, 72.76, 173.59, 196.28. MS (ESI+) cal. for $C_{12}H_{25}NO_6$ +K 602.37 found 602.60 m/z.

S-(1-((9-methoxy-1-oxo-6,7-dihydro-1H-dibenzo[a,e]cyclopropa[c][8]annulen-4-yl)oxy)-19-oxo-3,6,9,12,15-pentaoxa-18-azatritriacontan-33-yl) ethanethioate (4.6)
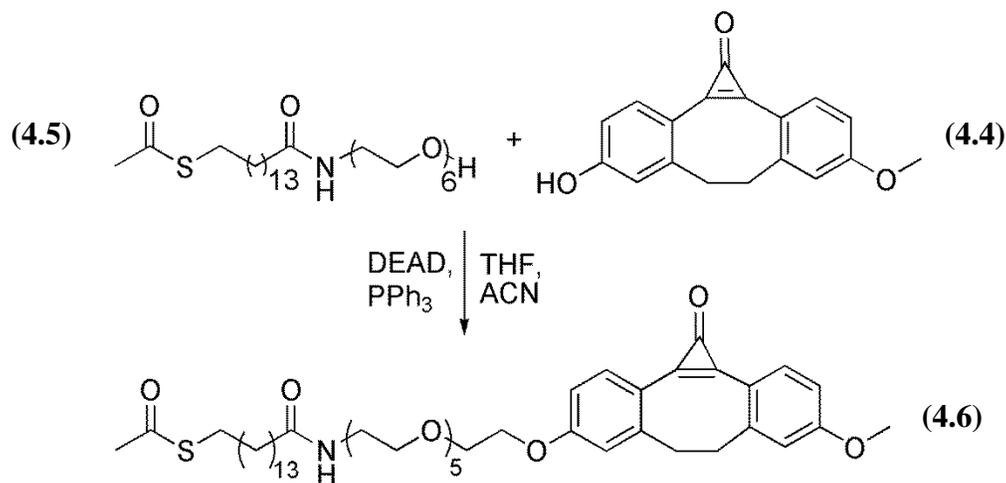
S-(1-hydroxy-19-oxo-3,6,9,12,15-pentaoxa-18-azatritriacontan-33-yl) ethanethioate (**4.5**) (0.2708 g, 0.467 mmoles) was added to an oven dried round bottom flask and the flask was purged with argon. 4-hydroxy-9-methoxy-6,7-dihydro-1H-dibenzo[a,e]cyclopropa[c][8]annulen-1-one (**4.4**) (0.1634 g, 0.58 mmoles) and triphenyl phosphine (0.2630 g, 1.00 mmoles) were added to the round bottom flask and diluted with anhydrous tetrahydrofuran (5 mL) and acetonitrile (5 mL). Diethyl azodicarboxylate (DEAD) was added dropwise to the reaction mixture and placed in a warm 50 °C oil bath for 12 hours. Solvent was removed under reduced pressure and the resulting oil was diluted with DCM and rinsed with 1 M HCl (20 mL). The organic layer was dried over sodium sulfate, and concentrated. The resulting oil was purified via flash column chromatography (7:10:83 MeOH:CHCl$_3$:EthylAceate) to produce 0.2144 g (55 %) of S-(1-((9-methoxy-1-oxo-6,7-dihydro-1H-dibenzo[a,e]cyclopropa[c][8]annulen-4-yl)oxy)-19-oxo-3,6,9,12,15-pentaoxa-18-azatritriacontan-33-yl) ethanethioate (**4.6**) as an oil. ^{1}H NMR δ 1.24 (m, 30H), 1.60 (m, 6H), 2.28 (t, 2H), 2.32 (s, 3H), 2.64 (d, 2H), 2.85 (t, 2H), 3.36 (d, 2H), 3.59 (m, 2H), 3.56 (t, 2H), 3.67 (m, 24H), 3.88 (t, 6H), 4.04 (t, 2H), 4.22 (t, 2H), 6.81 (dd, 4H), 7.99 (dd, 2H). ^{13}C NMR δ 25.68, 25.81, 28.71, 29.01, 29.03, 29.15, 29.27, 29.32, 29.37, 29.42, 29.47, 29.52, 30.54, 30.58, 36.56, 37.05, 39.05, 55.42, 55.47, 67.60, 69.42, 69.81, 70.10, 70.433, 70.47, 70.53, 70.77, 111.83, 112.35, 115.63, 115.69, 116.27, 116.40, 135.56, 142.08, 142.21, 147.71, 147.74, 161.57, 162.36, 173.25, 195.88, MS (ESI+) cal. for C$_{47}$H$_{70}$NO$_{10}$S+H 840.47 found 840.67 m/z.

15-mercapto-N-(17-((9-methoxy-1-oxo-6,7-dihydro-1H-ibenzo[a,e]cyclopropa[c][8]annulen-4-yl)oxy)3,6,9,12,15-pentaoxaheptadecyl)pentadecanamide (4.7)
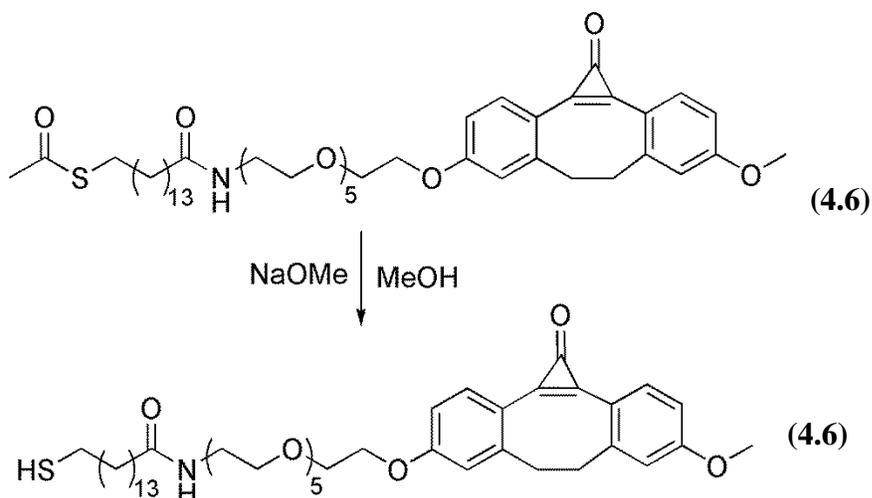
(4.6)

NaOMe | MeOH

(4.6)

S-(1-((9-methoxy-1-oxo-6,7-dihydro-1H-dibenzo[a,e]cyclopropa[c][8]annulen-4-yl)oxy)-19-oxo-3,6,9,12,15-pentaoxa-18-azatritriacontan-33-yl) ethanethioate (**4.6**) (0.1030 g, 0.122 mmoles) was added to an oven dried round bottom flask and the flask was purged with argon. The sample was then diluted with MeOH (10 mL) and sodium methoxide (32 µL, 0.18 mmoles) was added to the reaction. The mixture was allowed to proceed for 12 hours. The sample was acidified with 1 M HCl (200 µL) and extracted into DCM (2x 25 mL). The organic layer were dried over sodium sulfate and concentrated. The resulting oil was purified via flash column chromatography (10:10:80 MeOH:CHCl$_3$:EthylAceate) to produce 50.3 mg (52 %) of 15-mercapto-N-(17-((9-methoxy-1-oxo-6,7-dihydro-1H-dibenzo[a,e]cyclopropa[c][8]annulen-4-yl)oxy)-3,6,9,12,15-pentaoxaheptadecyl)pentadecanamide (**4.7**) as a yellow oil. ^{1}H NMR δ 1.24 (m, 29H), 1.60 (m, 6H), 2.18 (t, 2H), 2.51 (q, 2H), 2.63 (d, 2H), 3.34 (d, 2H), 3.45 (q, 2H), 3.65 (m, 24H), 3.89 (t, 6H), 4.21 (t, 2H), 6.25 (broad, 1H), 6.91 (dd, 4H), 7.94 (dd, 2H). ^{13}C NMR δ 24.88, 25.99, 28.58, 29.28, 29.57, 29.62, 29.73, 29.79, 29.84, 34.26, 36.88, 37.37, 39.37, 55.754, 67.88, 69.74, 70.15, 70.41, 70.72, 70.74, 70.77, 70.84, 71.09, 105.18, 112.04, 112.57, 116.03,

116.60, 116.78, 135.99, 136.07, 142.40, 142.56, 148.03, 153.95, 161.84, 162.66, 173.58. MS (ESI+) cal. for $C_{45}H_{67}NO_9S$ +H 798.46 found 798.47 m/z.

4.3 Results and Discussion

We have chosen biotin and an RGD peptide as demonstration molecules for patterning because they are critical tools for biotechnology. Biotin is significant due to its high binding affinity for avidin proteins (Ka ~ 2.5×10^{13} M^{-1}), which is one of the strongest noncovalent protein-ligand interactions measured.[22] This strong interaction makes it an ideal candidate for non-covalently anchoring molecules to substrates because minimal dissociation is observed. Additionally, avidin proteins contain multiple biotin binding pockets and have been genetically engineered for an array of biotechnology applications.[23, 24] Furthermore, a common signal amplification assay combines biotin labeled anti-avidin antibodies and alternating rounds of biotin-avidin binding.[25] On the other hand, the RGD peptide is important because it promotes integrin mediated cell adhesion to peptide-modified substrates.[26, 27] Since cell adhesion is promoted by the RGD peptide interacting with cell surface integrins, patterning RGD provides a facile means to control cell adhesion and ultimately cell growth.[28] Thus, patterning both biotin and the RGD peptide creates versatile and highly functional substrates that can be directly applied to a variety of applications in biotechnology. Additionally, the patterning of two molecules that are chemically very different demonstrates the generality and versatility of our strained alkyne monomer.

Copper-free strain-promoted [3+2] azide-alkyne cycloadditions are an important class of bioorthogonal reactions due to their tremendous selectivity and biocompatability.[29, 30] Copper-free reactions are achieved by destabilizing the ground state of the alkyne relative to the transition state through ring strain, which leads to increased reaction rates verse linear alkynes.[31] These reactions are high yielding making them ideal candidates to be used for biomaterials[29] and

the removal of copper from the reaction is critical for many biological applications, since copper has been shown to be highly toxic to cells.[32, 33] Due to the many advantages of Cu-free strain-promoted [3+2] azide-alkyne cycloadditions and photolithography, we have developed a cyclopropenone monomer that undergoes photoconversion to give a strained cyclooctyne. To show the versatility of this monomer, both azido-biotin and azido-cyclicRGD (cRGD) peptide derivatives were coupled to different patterned surfaces. Biotin functionalized surfaces were used to create neutravidin gradients. Coupled cRGD substrates were detected using traditional immunohistochemistry. Moreover, cRGD surfaces were used to pattern NIH/3T3 cells.

A thiol-terminated cyclopropenone monomer was developed for the formation of mixed monolayers that could be patterned using standard photolithographic equipment. Previous reports have shown that upon expose to UV light, cyclopropenones produce alkynes.[34-36] The synthesis of this monomer is outlined in **Scheme 4.1**. Briefly, the cyclopropenone was formed by a Wittig reaction between 3-methoxybenzyl chloride and 3-formylphenyl acetate (**4.1**), followed by reduction of both the E and Z products to produce 3-(3-methoxyphenethyl)phenol (**4.2**). Compound **4.2** was then reduced using palladium on activated carbon in a hydrogen rich atmosphere to form 3-(3-methoxyphenethyl)phenol (**4.3**). After reduction, **4.3** was subjected to a Friedel-Crafts acylation with tetrachlorocyclopropene to form the photoprotected cyclooctyne (**4.4**) in 20.4% overall yield. The yield limiting step of this reaction scheme is the Friedel-Crafts acylation, which is consistent with literature precedent.[37, 38] The photoprotected cyclooctyne was then directly coupled to the thiol acetate monomer (**4.5**), via a Mitsunobu reaction. The synthesis of **4.5** was conducted according to our previous methods.[39] After removal of the acetate group from **4.6**, the thiol-terminated cyclopropenone monomer (**4.7**) could then be used for mixed monolayer formation. Mixed monolayers of **4.7** and an amide-linked glycol-terminated thiol

monomer (**2.6**) were formed on gold coated glass coverslips (50 Å Ti/100 Å Au) from solutions containing a total thiol concentration of 1 mM with between 0.1% and 100% of **4.7**. For convenience, surfaces will be referred to by the solution concentration of monomers used for formation. Monolayers were set for 12 hours at room temperature and subsequently used in photopatterning and coupling experiments.

To verify that our monomer could be deprotected to the strained cyclooctyne photochemically, **Scheme 4.1**, and then undergo a Cu-free strain-promoted [3+2] azide-alkyne cycloaddition on the surface, an azido-biotin derivative was coupled to a patterned surface containing 100% of **4.7**. A 6x6 mm square was patterned in the center of the slide using a commercial direct-write lithography system containing a He-Cd laser operating at 325 nm.[40] After patterning, the slide was incubated in a 0.1 mM solution of an azido-biotin derivative in 10 mM phosphate buffer pH 8.05 (PB) for 2 hours. After rinsing, the substrate was analyzed by matrix-assisted laser desorption/ionization time-of-flight mass spectrometry (MALDI-TOF MS). The coupled product, **Figure 4.1A**, was detected as shown in **Figure 4.1B**, which confirmed our cyclooctyne monomer could be deprotected at 325 nm and then undergo a Cu-free strain-promoted [3+2] azide-alkyne cycloaddition when exposed to an azide moiety. Moreover, exposure of a nonpatterned cyclopropenone monolayer to the azide moiety under identical conditions did not lead to the observation of any coupled product. One of the main advantages of photolithographic patterning over contact methods is the ability to control precisely the extent of photodeprotection and therefore the concentration of reactive functional groups available on the surface.
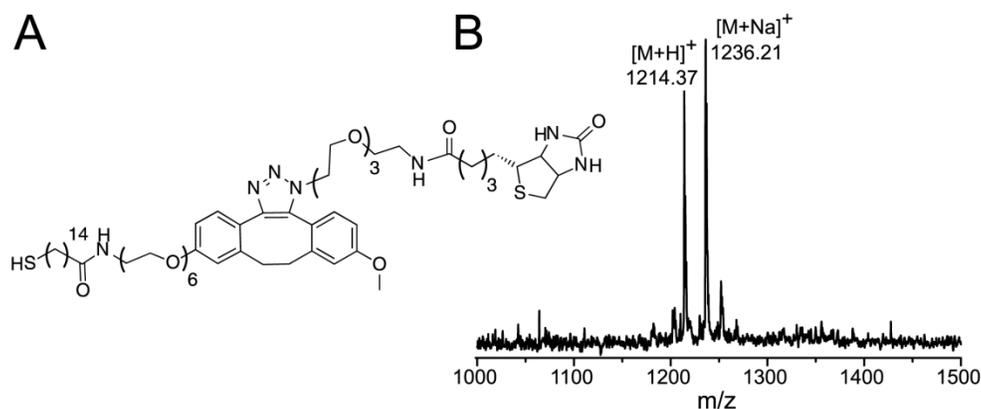
Figure 4.1 Biotin functionalized substrates. A) The coupled product detected using MALDI-TOF MS. B) Representative mass spectrum of functionalized substrate.
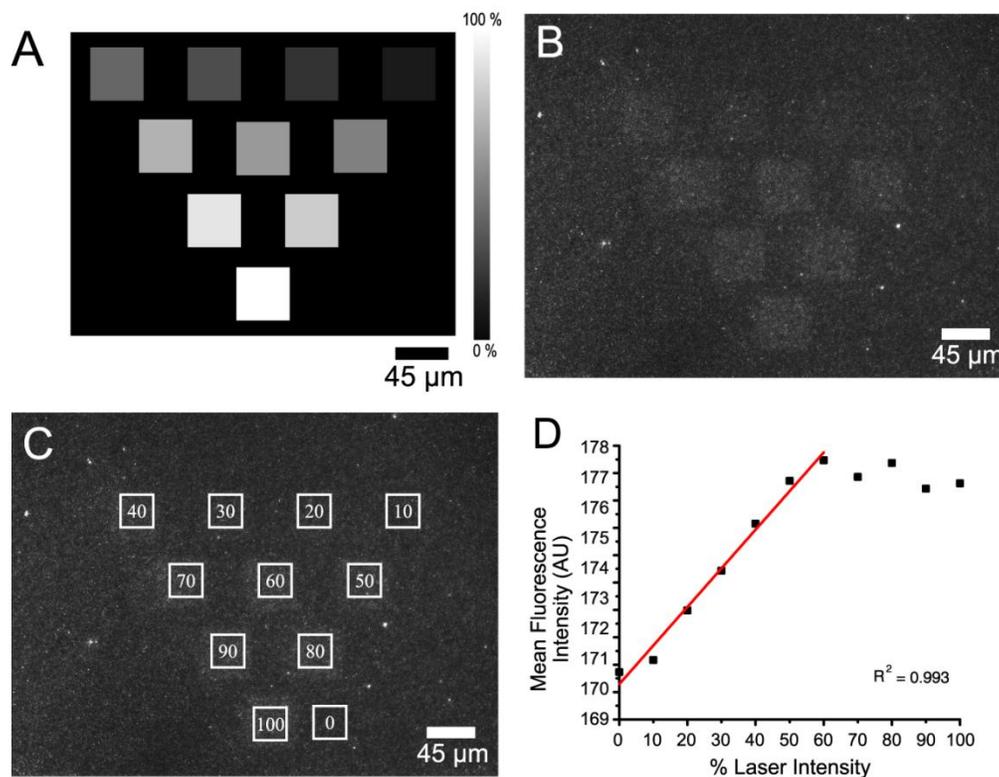
Figure 4.2. Fluorescent image from neutravidin binding assay. A) The 8-bit gradient image patterned by direct-write lithography for amplification assay (scale bar is relative laser intensity). B) Fluorescent image of labeled neutravidin binding to a 0.1% biotin coupled surface after two rounds of signal amplification. C) The white boxes represent the regions of interest (ROI) used to extract the mean fluorescent signal intensity for each of the relative laser intensities used, which is given by the number inside. D) Mean fluorescence intensity for the eleven regions of the substrate, background 0% -100%, after signal enhancement.

Neutravidin   Anti-Avidin with biotin tags
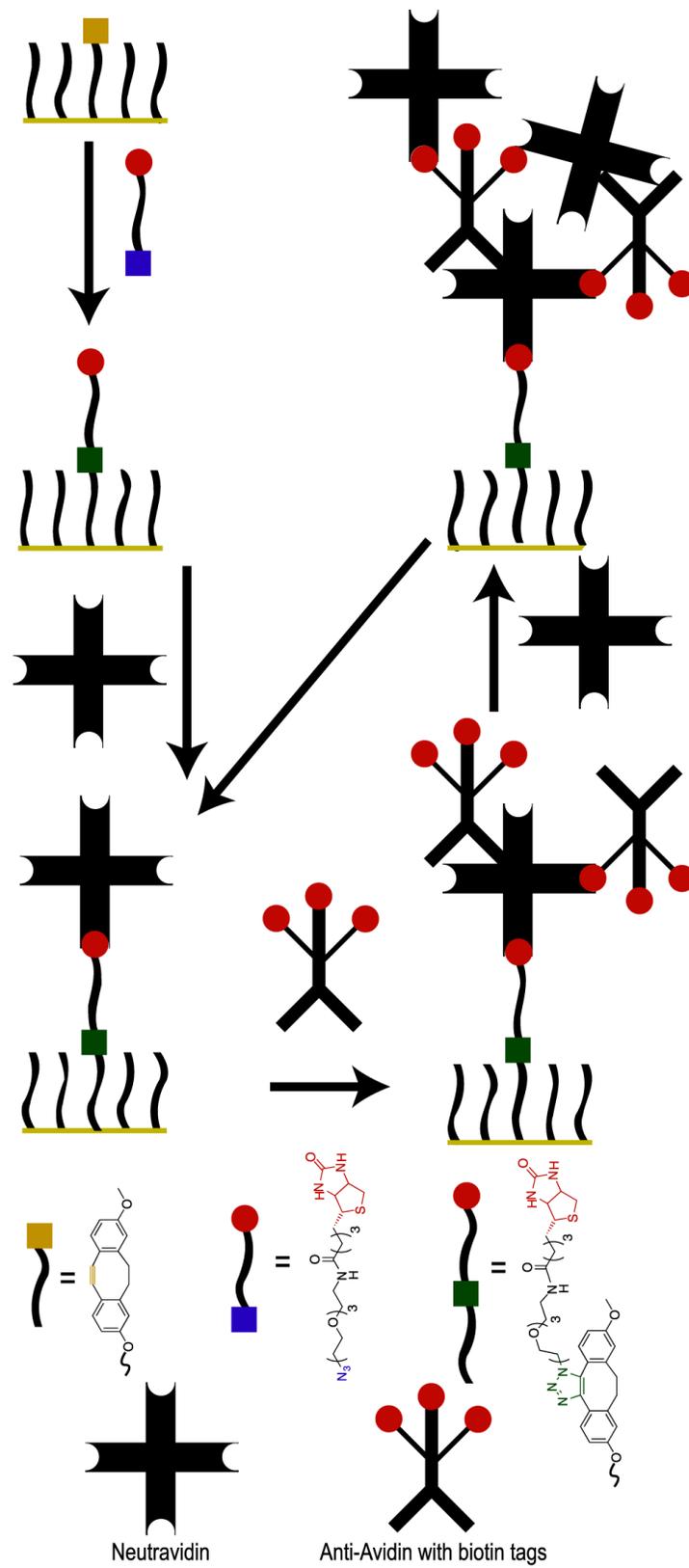
Scheme 4.2 Biotin/neutravidin Amplification Scheme

In the case of biotin, this allows for precise control over the two-dimensional concentration of avidin proteins. To demonstrate the versatility of patterning **4.7** using direct-write photolithography, we produced precise protein gradients. For this application, a mixed monolayer system containing **4.7** and **2.6** was used to minimize nonspecific protein adsorption, since glycol-terminated alkane thiols have been shown to resist nonspecific protein adsorption.[41] Additionally, an extremely low concentration of the functional monomer, 0.1%, was used to prevent further nonspecific protein adsorption to the surface. The surface was patterned according to an 8-bit gray scale bitmap image with black representing 0% laser intensity and white representing 100% laser intensity, **Figure 4.1C**. A 100% laser intensity correlates to 1200 mJ/cm^2, which is an order of magnitude lower laser power than we had previously observed was required to deprotect a nitroveratryl protected carboxylic acid monomer.[39] Biotin was coupled to the surface as described above and neutravidin (50 µg/mL) bound to the biotin. In order to visualize the neutravidin binding, an amplification scheme, **Scheme 4.2**, was required, since even at full deprotection the surface concentration of avidin was on average one alkyne per 215 nm^2 and at the lowest deprotection values shown was on average one alkyne per 2,150 nm^2. Neutravidin binding was accomplished by coupling fluorescently labeled neutravidin (50 µg/mL) to the surface in PB for 1 h at 37 °C. The slide was then rinsed; however no fluorescent signal was detected above background. To distinguish the fluorescent signal from the background an amplification assay was conducted by coupling a biotin labeled anti-avidin antibody (22 µg/mL) to the surface (1 h at 37 °C). The slide was then rinsed and fresh fluorescently labeled neutravidin was added and the entire amplification process was repeated to bring the fluorescent signal out from background. The final substrate was imaged using an inverted microscope and the mean fluorescent pixel intensities for each of the eleven regions were extracted using NIS

Elements, **Figure 4.2**. As the laser intensity increases, the relative number of strained cyclooctynes produced on the surface should increase linearly resulting in a linear increase in the amount of biotin on the surface after coupling. Therefore, neutravidin bound to the surface both before and after amplification should be directly proportional to the laser intensity used for patterning. Since we are operating at low fluorescent levels, this results in a direct linear relationship between laser intensity and observed fluorescence intensity. We observed this relationship up to 50 % laser intensity with an R^2 value of 0.993. The leveling off in fluorescence intensity for laser intensities greater than 50% is the result of complete surface deprotection being achieved at 50% laser intensity. Thus, deprotecting **4.7** with a direct-write laser writer provides a facile means to produce precise protein gradients. Moreover, neutravidin coupled to a surface using this monomer can still be recognized by primary antibodies and used for amplification assays.

Besides proteins, peptides can also be couple to our functionalized surfaces by utilizing commercially available azido amino acid derivatives. Peptide anchoring was confirmed by coupling an azido-cRGD peptide to a patterned mixed monolayer system that contained 25% of **4.7** in a background of **2.6**. Peptide coupling was achieved by incubating the patterned surface in a 0.11 mM solution of the azido-cRGD peptide in PB for 2 hours. The disulfide of the coupled product with the glycol monomer, **Figure 4.3A**, was detected by MALDI TOF MS, **Figure 4.3B**.

In addition to detection by MALDI-TOF MS, the patterned peptide could be visualized using traditional immunohistochemistry and a primary anti-RGD antibody. A mixed monolayer system formed from a 1% solution of **4.7** was patterned using an 8-bit image, **Figure 4.3C**, and labeled with cRGD peptide as described above. These substrates were then rinsed and incubated with a primary rabbit anti-RGD antibody solution (20 μg/mL in PB) for 1 hour at 37 °C.

Subsequently, the substrates were rinsed with PB, to remove nonspecifically adsorbed antibody, and incubated with a fluorescently labeled donkey anti-rabbit secondary antibody (10 µg/mL in PB). The substrate was imaged using an inverted microscope, which clearly showed the anticipated pattern, **Figure 4.3D**, even at the relatively low 1% peptide density. The ability to use classical immunohistochemistry in surface analysis is critical to a wide variety of applications in biotechnology and cell biology. Moreover, this allows other surfaces to be directly incorporated into existing technological applications without the development of novel sensing technology.
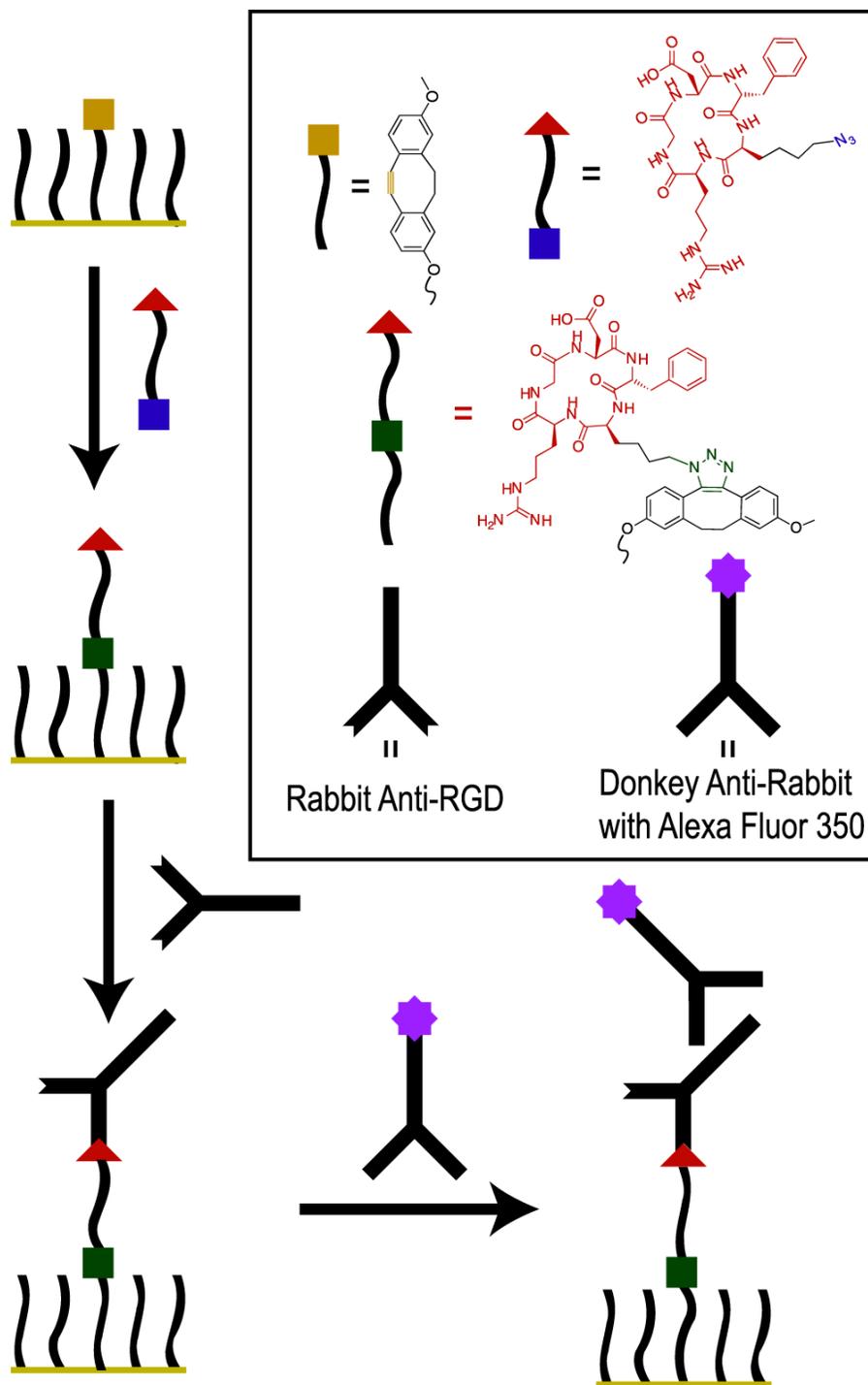
Scheme 4.3. cRGD immunohistochemistry. A) Overall scheme for cRDG coupling and sequential detection by rabbit anti-RGD. The rabbit antibody was detected by fluorescently labeled donkey anti-rabbit antibody. For each antibody coupling, the substrate was incubated for 1 hour at 37 °C.
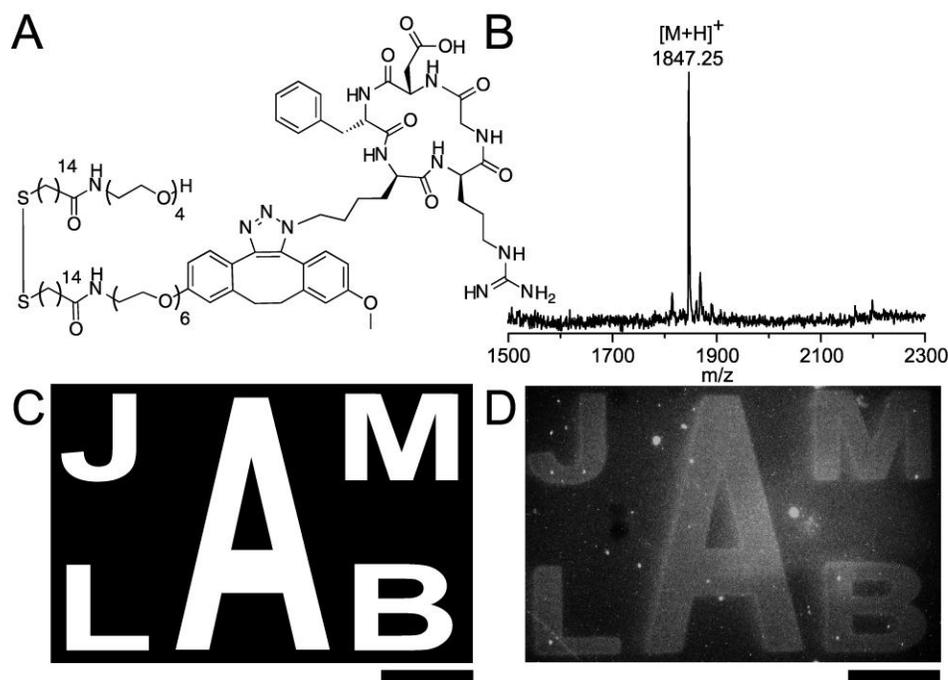
Figure 4.3 cRGD functionalized substrates. A) The disulfide of the coupled product with the amide-linked glycol-terminated monomer that was detected using MALDI-TOF MS. B) Representative MALDI-TOF spectrum of the functionalized substrate. C) The 8-bit image patterned for antibody detection assay (100% laser intensity). D) Fluorescent image of the substrate after rinsing. Scale bar = 100 μm.

Besides antibody detection, we wanted to ensure the cRGD coupled to our functionalized substrates could support cell growth. As mentioned above, one of the advantages of Cu-free strain-promoted [3+2] azide-alkyne cycloadditions is its compatibility with cell culture. To demonstrate our monomer system can support cell growth, substrates were prepared by soaking in varying concentrations of **4.7** (1%, 0.25%, and 0.1%) with background monomer **2.6**, which we have shown to be stable for up to 5 weeks under cell culture conditions.[42] A 3x3 mm square was patterned in the center of the substrate and cRGD was coupled to the newly formed SAMs. Coupled substrates were then rinsed and used for cell culture studies. NIH/3T3 cells were seeded on these substrates, 50,000 cells/mL, for 2 h at 37 °C and rinsed to remove any nonspecifically adhered cells. NIH/3T3 cells were allowed to grow and representative images

were captured on day 5 in culture. As shown in **Figure 4.4A**, which is the right hand side of the pattern, the 1% cRGD surface clearly shows cell attachment in the patterned region with no cell growth in the non patterned region, right side of the image. After rinsing, non-strongly adhered cells were removed from the surface as shown in **Figure 4.4B**, which was taken from the left hand side of the patterned substrate. All three surfaces concentrations did support cell growth, but cell adhesion was strongest to the 1% surfaces. This result is consistent with previous reports that investigated RGD density and cell adhesion.[11, 13, 14]
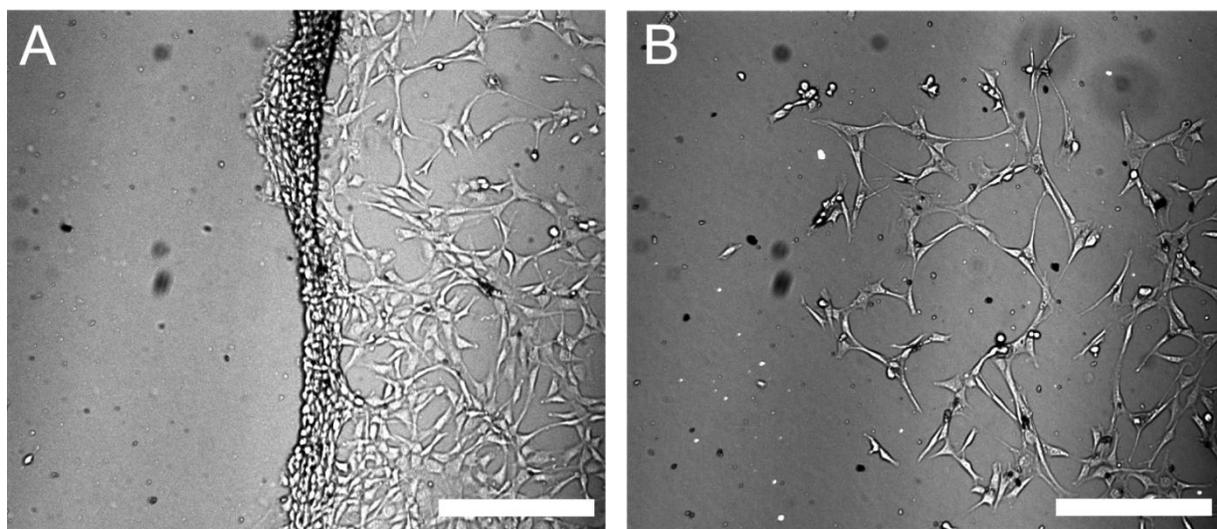
Figure 4.4. NIH/3T3 cells adhered to a 1% cRGD surface. A) Representative image of NIH/3T3 cells on the surface 5 days in culture before rinsing (cRGD on the left portion) B) After rinsing (cRGD on the right portion) Scale bar = 500 μm.

4.4 Conclusions

Here we have reported the synthesis of a versatile thiol terminated monomer incorporating a photoprotected strained cyclooctyne. After photodeprotection, the strained alkyne can undergo Cu-free strain-promoted [3+2] azide-alkyne cycloadditions with azide functionalized molecules making this photopatterning strategy broadly applicable to a wide array of applications ranging from biotechnology, to the development of a new materials for industrial applications, including

energy storage and harvesting. We have further shown that deprotected substrates can support peptide and protein attachment. Additionally, using grey scale lithography, precise protein gradients can be formed on a substrate. Furthermore, extremely low protein concentrations can be detected using classical amplification schemes and the patterned substrates are amenable to immunohistochemical analysis. Moreover, we showed that patterned cell growth on a substrate can be achieved by coupling an azido-cRGD peptide to the surface.

4.5 References

1.   Chen, Y.-X.; Triola, G.; Waldmann, H., Bioorthogonal Chemistry for Site-Specific Labeling and Surface Immobilization of Proteins. *Accounts of Chemical Research* **2011,** 44, (9), 762-773.
2.   Yap, F. L.; Zhang, Y., Protein and cell micropatterning and its integration with micro/nanoparticles assembly. *Biosensors and Bioelectronics* **2007,** 22, (6), 775-788.
3.   Bengt, K., Biological surface science. *Surface Science* **2002,** 500, (1–3), 656-677.
4.   Mendes, P.; Yeung, C.; Preece, J., Bio-nanopatterning of Surfaces. *Nanoscale Research Letters* **2007,** 2, (8), 373-384.
5.   Adzima, B. J.; Tao, Y.; Kloxin, C. J.; DeForest, C. A.; Anseth, K. S.; Bowman, C. N., Spatial and temporal control of the alkyne-azide cycloaddition by photoinitiated Cu(II) reduction. *Nat. Chem.* **2011,** 3, (3), 256-259.
6.   Arnold, R. M.; Huddleston, N. E.; Locklin, J., Utilizing click chemistry to design functional interfaces through post-polymerization modification. *Journal of Materials Chemistry* **2012,** 22, (37), 19357-19365.
7.   Soellner, M. B.; Dickson, K. A.; Nilsson, B. L.; Raines, R. T., Site-Specific Protein Immobilization by Staudinger Ligation. *Journal of the American Chemical Society* **2003,** 125, (39), 11790-11791.
8.   Lempens, E. H. M.; Helms, B. A.; Merkx, M.; Meijer, E. W., Efficient and Chemoselective Surface Immobilization of Proteins by Using Aniline-Catalyzed Oxime Chemistry. *ChemBioChem* **2009,** 10, (4), 658-662.
9.   Kolodziej, C. M.; Kim, S. H.; Broyer, R. M.; Saxer, S. S.; Decker, C. G.; Maynard, H. D., Combination of Integrin-Binding Peptide and Growth Factor Promotes Cell Adhesion on Electron-Beam-Fabricated Patterns. *Journal of the American Chemical Society* **2011,** 134, (1), 247-255.
10.   de Araújo, A. D.; Palomo, J. M.; Cramer, J.; Köhn, M.; Schröder, H.; Wacker, R.; Niemeyer, C.; Alexandrov, K.; Waldmann, H., Diels–Alder Ligation and Surface Immobilization of Proteins. *Angewandte Chemie International Edition* **2006,** 45, (2), 296-301.
11.   Kato, M.; Mrksich, M., Using Model Substrates To Study the Dependence of Focal Adhesion Formation on the Affinity of Integrin−Ligand Complexes†. *Biochemistry* **2004,** 43, (10), 2699-2707.

12.   Shabbir, S. H.; Eisenberg, J. L.; Mrksich, M., An Inhibitor of a Cell Adhesion Receptor Stimulates Cell Migration. *Angewandte Chemie International Edition* **2010,** 49, (42), 7706-7709.
13.   Kilian, K. A.; Mrksich, M., Directing Stem Cell Fate by Controlling the Affinity and Density of Ligand–Receptor Interactions at the Biomaterials Interface. *Angewandte Chemie International Edition* **2012,** 51, (20), 4891-4895.
14.   Hudalla, G. A.; Murphy, W. L., Using "Click" Chemistry to Prepare SAM Substrates to Study Stem Cell Adhesion. *Langmuir* **2009,** 25, (10), 5737-5746.
15.   Hudalla, G. A.; Murphy, W. L., Immobilization of Peptides with Distinct Biological Activities onto Stem Cell Culture Substrates Using Orthogonal Chemistries. *Langmuir* **2010,** 26, (9), 6449-6456.
16.   Kuzmin, A.; Poloukhtine, A.; Wolfert, M. A.; Popik, V. V., Surface Functionalization Using Catalyst-Free Azide−Alkyne Cycloaddition. *Bioconjugate Chemistry* **2010,** 21, (11), 2076-2085.
17.   Barbulovic-Nad, I.; Lucente, M.; Yu, S.; Mingjun, Z.; Wheeler, A. R.; Bussmann, M., Bio-Microarray Fabrication Techniques—A Review. *Critical Reviews in Biotechnology* **2006,** 26, (4), 237-259.
18.   Hynes, M. J.; Maurer, J. A., Lighting the path: photopatternable substrates for biological applications. *Molecular BioSystems* **2013,** 9, (4), 559-564.
19.   Pauloehrl, T.; Delaittre, G.; Bruns, M.; Meißler, M.; Börner, H. G.; Bastmeyer, M.; Barner-Kowollik, C., (Bio)Molecular Surface Patterning by Phototriggered Oxime Ligation. *Angewandte Chemie International Edition* **2012,** 51, (36), 9181-9184.
20.   Dillmore, W. S.; Yousaf, M. N.; Mrksich, M., A Photochemical Method for Patterning the Immobilization of Ligands and Cells to Self-Assembled Monolayers. *Langmuir* **2004,** 20, (17), 7223-7231.
21.   Jonkheijm, P.; Weinrich, D.; Köhn, M.; Engelkamp, H.; Christianen, P. C. M.; Kuhlmann, J.; Maan, J. C.; Nüsse, D.; Schroeder, H.; Wacker, R.; Breinbauer, R.; Niemeyer, C. M.; Waldmann, H., Photochemical Surface Patterning by the Thiol-Ene Reaction. *Angewandte Chemie International Edition* **2008,** 47, (23), 4421-4424.
22.   Chilkoti, A.; Stayton, P. S., Molecular Origins of the Slow Streptavidin-Biotin Dissociation Kinetics. *Journal of the American Chemical Society* **1995,** 117, (43), 10622-10628.
23.   Laitinen, O. H.; Hytönen, V. P.; Nordlund, H. R.; Kulomaa, M. S., Genetically engineered avidins and streptavidins. *Cellular and Molecular Life Sciences CMLS* **2006,** 63, (24), 2992-3017.
24.   Sardo, A.; Wohlschlager, T.; Lo, C.; Zoller, H.; Ward, T. R.; Creus, M., Burkavidin: A novel secreted biotin-binding protein from the human pathogen Burkholderia pseudomallei. *Protein Expression and Purification* **2011,** 77, (2), 131-139.
25.   Hynes, M. J.; Maurer, J. A., Photoinduced Monolayer Patterning for the Creation of Complex Protein Patterns. *Langmuir* **2012,** 28, (47), 16237-16242.
26.   Bellis, S. L., Advantages of RGD peptides for directing cell association with biomaterials. *Biomaterials* **2011,** 32, (18), 4205-4210.
27.   Hersel, U.; Dahmen, C.; Kessler, H., RGD modified polymers: biomaterials for stimulated cell adhesion and beyond. *Biomaterials* **2003,** 24, (24), 4385-4415.
28.   Ruoslahti, E.; Pierschbacher, M. D., New perspectives in cell adhesion: RGD and integrins. *Science (Washington, D. C., 1883-)* **1987,** 238, (4826), 491-7.
29.   Jewett, J. C.; Bertozzi, C. R., Cu-free click cycloaddition reactions in chemical biology. *Chemical Society Reviews* **2010,** 39, (4), 1272-1279.

30.   Lutz, J.-F., Copper-Free Azide–Alkyne Cycloadditions: New Insights and Perspectives. *Angewandte Chemie International Edition* **2008,** 47, (12), 2182-2184.

31.   Shea, K. J.; Kim, J. S., Influence of strain on chemical reactivity. Relative reactivity of torsionally strained double bonds in 1,3-dipolar cycloadditions. *Journal of the American Chemical Society* **1992,** 114, (12), 4846-4855.

32.   Gaetke, L. M.; Chow, C. K., Copper toxicity, oxidative stress, and antioxidant nutrients. *Toxicology* **2003,** 189, (1–2), 147-163.

33.   Agard, N. J.; Prescher, J. A.; Bertozzi, C. R., A Strain-Promoted [3 + 2] Azide−Alkyne Cycloaddition for Covalent Modification of Biomolecules in Living Systems [J. Am. Chem. Soc. 2004, 126, 15046−15047]. *Journal of the American Chemical Society* **2005,** 127, (31), 11196-11196.

34.   Ciabattoni, J.; Nathan, E. C., Di-tert-butylcyclopropenone and substituted di-tert-butyl-cyclopropenyl cations. *Journal of the American Chemical Society* **1969,** 91, (17), 4766-4771.

35.   Poloukhtine, A.; Popik, V. V., Highly Efficient Photochemical Generation of a Triple Bond: Synthesis, Properties, and Photodecarbonylation of Cyclopropenones. *The Journal of Organic Chemistry* **2003,** 68, (20), 7833-7840.

36.   Orski, S. V.; Poloukhtine, A. A.; Arumugam, S.; Mao, L.; Popik, V. V.; Locklin, J., High Density Orthogonal Surface Immobilization via Photoactivated Copper-Free Click Chemistry. *Journal of the American Chemical Society* **2010,** 132, (32), 11024-11026.

37.   Nacsa, E. D.; Lambert, T. H., Cyclopropenone Catalyzed Substitution of Alcohols with Mesylate Ion. *Organic Letters* **2012,** 15, (1), 38-41.

38.   West, R.; Zecher, D. C.; Goyert, W., Triarylcyclopropenium ions and diarylcyclopropenones from trichlorocyclopropenium ion. *Journal of the American Chemical Society* **1970,** 92, (1), 149-154.

39.   Hynes, M. J.; Maurer, J. A., Unmasking Photolithography: A Versatile Way to Site-Selectively Pattern Gold Substrates. *Angewandte Chemie International Edition* **2012,** 51, (9), 2151-2154.

40.   Lullo, G.; Leto, R.; Oliva, M.; Arnone, C., Multilevel pattern generation by GaN laser lithography: an application to beam shaper fabrication. *Proc. SPIE* **2006**, 62900A-62900A.

41.   Prime, K. L.; Whitesides, G. M., Adsorption of proteins onto surfaces containing end-attached oligo(ethylene oxide): a model system using self-assembled monolayers. *Journal of the American Chemical Society* **1993,** 115, (23), 10714-10721.

42.   Strulson, M. K.; Johnson, D. M.; Maurer, J. A., Increased Stability of Glycol-Terminated Self-Assembled Monolayers for Long-Term Patterned Cell Culture. *Langmuir* **2012,** 28, (9), 4318-4324.

Chapter 5

Conclusion and Future Work

5.1 Complete monomer removal

Chapter 2 describes a versatile patterning method for creating complex protein gradients on traditionally protein resistant SAMs. Patterning was achieved by utilizing a commercial direct-write photolithography system that contained a He-Cd laser operating at 325 nm. Freshly prepared SAMs were irradiated at 325 nm and monomers were site-selectively desorbed from the surface creating defect sites in the monolayer. When patterned surfaces were placed into a protein solution, proteins adsorbed into the defect sites of the monolayer. Protein adsorption was quantified using SPRi and a correlation was observed between protein attachment and the patterning laser intensity. Additionally, neutravidin adsorbed to these surfaces could still be recognized by a commercial biotin labeled anti-avidin antibody.

During the course of this work, the mechanism for monolayer removal was investigated using surface IR. Surface IR showed clear evidence that monomers were being completely removed from the surface as supposed to undergoing glycol degradation. However, complete monomer removal can occur either by gold-gold or thiol-gold bond cleavage. Determining exactly which bonds were cleaved was beyond the scope of this chapter, but by conducting the correct set of experiments could be determined. Additionally, monomer desorption has been extensively used in MALDI TOF MS as a surface analysis technique.[1] Typically, SAMs are coated with a thin layer of matrix and analyzed. Monomers are either detected as free thiols or as disulfides depending on laser intensity. However, when freshly prepared glycol-terminated monolayers were analyzed in negative mode without using matrix, similar to conditions used for

photo-induced monolayer patterning, thiol oxidation was observed, **Figure 5.1**. Oxidation was unexpected since the system was under high vacuum, 10^{-7} torr, which should have resulted in most of the molecular oxygen being removed. Understanding the desorption mechanism under MALDI TOF MS conditions, might provide further insights into the desorption mechanism that occurs under a variety of photo-induced monolayer patterning conditions.

In order to better understand the source of oxygen, a series of isotope experiments could be conducted. The first variable to consider would be the isotopic labeling of water adsorbed during SAM formation, since it is possible that water molecules become molecularly entangled during this process and cannot be removed from the monolayer under high vacuum. To determine if water was the oxygen source, SAMs could be formed in degassed ethanol that contained a trace amount of $H_2^{18}O$. Consequently, to determine if molecular oxygen was the oxygen source, ethanol could first be degasses and then $^{18}O_2$ bubbled through the solution. Additionally, these substrates would need to be set in an $^{18}O_2$ atmosphere to ensure minimal oxygen exchange. Analysis of these surfaces would indicate if the oxygen of the sulfonate was a result of trapping water or molecular oxygen during SAM formation. Based on the fact that molecular oxygen is highly soluble in nonpolar organic,[2] similar to the alkane chains present in SAMs, one would expect that the source of oxygen is a result of adsorbed molecular oxygen during SAM formation. Thus, an increase of six mass units would be expected when these surfaces are analyzed by MALDI TO MS.

Photo-induced monolayer pattering could be applied to study cell growth with particular emphasis on cellular responses to protein gradients. One cell type that is of particular interest is the neuron, since neuronal networks are central for proper brain development and learning.[3]

Neuronal cells have also been shown to be manipulated by surface chemistry particularly laminin, fibronectin, and gelatin functionalized surfaces.[4] This work showed that functionalized surfaces play a key role in changes to pheonotypic, electrophysiological, and molecular characteristics. However, this study failed to provide control over protein concentration or spatial distribution. We have shown in Chapter 2 that photo-induced monolayer patterning can produce precise control over fibronectin gradients on complex patterned surfaces. Since both fibronectin and laminin are glycoproteins, it is reasonable to expect that they would have similar surface adsorption characteristics. This hypothesis could be confirmed by adsorbing laminin to a gradient patterned surface while monitoring by SPRi, which is the same experiment that was conducted for fibronectin. SPRi would then give a quantitative value for the amount of laminin adsorbed to the surface. The amount of adsorbed laminin could then be correlated to the laser intensity. After this relationship was determined, complex gradients of both fibronectin and laminin could be used to further investigate their role in neuronal development and as a platform to culture neuronal networks.
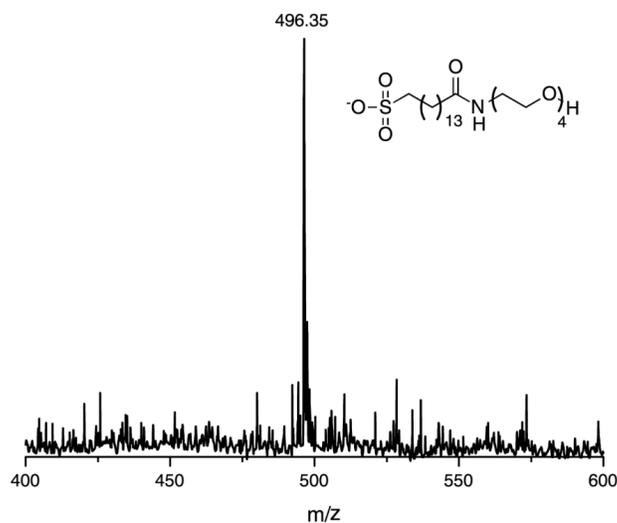
Figure 5.1. Representative MALDI TOF MS spectrum of a nonpatterned amide-linked glycol-terminated monolayer analyzed in negative mode without using matrix.

This work could also be applied to studying enzymatic activity, particularly in the development of new enzyme-linked immuno sorbet assays (ELISA). This method would allow for precise control of an initial antibody adsorption to the surface, which is a current limitation of this technique. These substrates could then be used in traditional amplification assays using horseradish peroxidase, [5-7] which would demonstrate the compatibility of this patterning method with a wide array of common detection assays. Thus, photo-induced monolayer patterning can be applied to many areas of biotechnology research.

5.2 Functional Group Modification

Chapters 3 and 4 describe the synthesis and functionalization of two novel monomers that contain derivatized glycol tails. In Chapter 3, this tail consisted of a nitroveratryl protected carboxylic acid. Utilizing direct-write photolithography, this tail was able to be removed site-selectively to produce both punctate and smooth functional group gradients. Functional group density was initially characterized by Kelvin Probe Force Microscopy (KPFM), which measures the relative surface potential across the substrate. As expected, the patterned regions with freshly exposed carboxylic acids contained a higher surface potential than the nonpatterned regions. Additionally, changes in the nanomechanical properties of the substrate were characterized using PeakForce Quantitative Nanomechanical Mapping (QNM). The most pronounced nanomechanical property change occurred in the adhesion channel, which was a result of the probe interacting with the nitroveratryl monomer stronger than the freshly prepared carboxylic acids. Moreover, two unique amine molecules were coupled site-selectively to freshly prepared carboxylic acids in a circle in box pattern.

This monomer system was successful at patterning amine molecules; however it does have a few limitations. The first limitation is the inefficiency of surface coupling, which was detected by the cross coupling of the second amine. This result comes from the fact that three transformations need to occur in order to achieve final coupling; 1) activation with EDC, 2) formation of an activated ester with HOAt, and 3) coupling with an amine molecule. During steps 1 and 2, the functional group can undergo hydrolysis back to the carboxylic acid. Additionally, being attached to the surface induces an additional steric effect. The monomer system also does not allow for multiple proteins or peptides containing glutamate or aspartate or non-protected C-terminus to be coupled to the surface since a second round of activating would not only activate the surface carboxylic acids, but would result is the carboxylic acids of the proteins being activated. Activation of the protein carboxylic acids would lead to protein-protein cross coupling. As a result of these limitations, a high yielding bioorthogonal monomer was designed and utilized for surface patterning, which is the focus of Chapter 4.

Chapter 4 describes the synthesis and functionality of a cyclopropenone monomer. When the cyclopropenone monomer is irradiated with UV light, under an argon atmosphere, a cyclooctyne is produced. Cyclooctynes can undergo Cu-free strained promoted [3+2] cycloadditions with azide terminated molecules, which are not only highly efficient reactions, but also bioorthogonal.[8-11] Additionally, azide functionalities can be easily incorporated into unnatural amino acids, which can be used for site-directed protein and/or peptide mutagenesis. We have shown that both an azido-biotin and azido-cRGD peptide derivatives can be coupled to a patterned substrate. Biotin functionalized slides were used to produce precise neutravidin gradients with a direct relationship between protein adsorption and laser intensity. cRGD functionalized slides were used for both traditional immunohistochemistry and supported

NIH/3T3 cell growth. Combined with direct-write photolithography, this monomer system provides a facile means to pattern azide terminated molecules site-selectively.

Initial studies to pattern the cyclopropenone monomer and couple an azido molecule to the surface were unsuccessful. These studies included increasing the azido concentration in solution and changing the coupling solution from aqueous to organics. Cu-free strained promoted [3+2] cycloadditions, however, have been reported under various solvent conditions,[12] which led us to investigate the laser intensity, **Scheme 5.1**. Low intensities were studied to minimize side reactions. After patterning, slides were rinsed with ethanol and the large 6x6 mm square was visible to the naked eye when ethanol evaporated, however no coupling was observed by MALDI TOF MS. In an attempt to reproduce the literature precedent,[13] a handheld UV lamp with a 365 nm bulb was used to irradiate functionalized substrates. Interestingly, coupling was
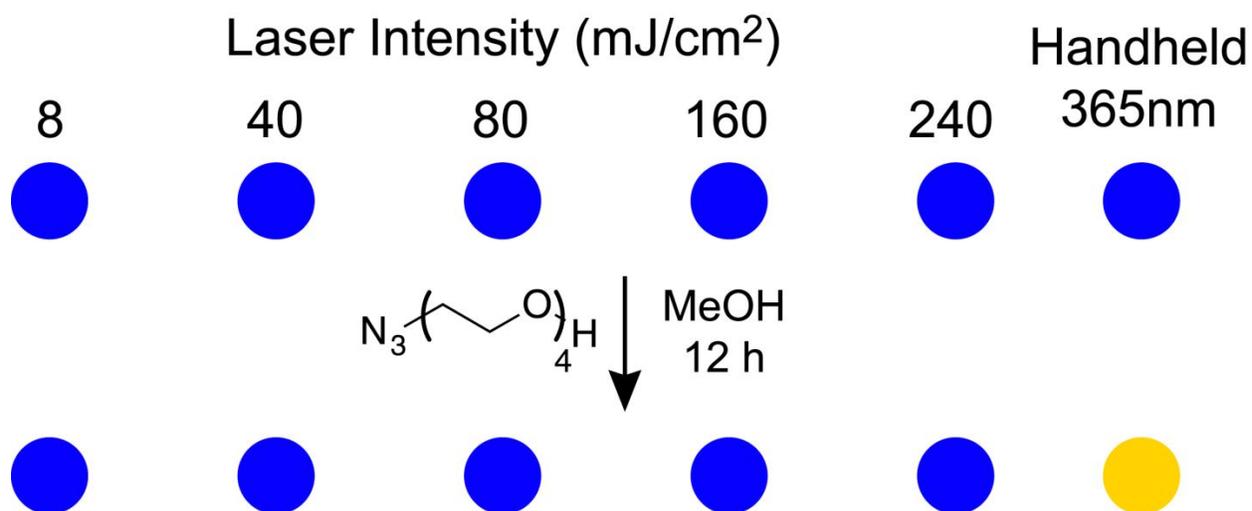
Scheme 5.1. Initial surface patterning conditions for the cyclopropenone monomer. A 6x6 mm square was patterned on 100% cyclopropenone functionalized slides using the direct-write laser writer in beam scan mode. For the sample patterned with the handheld UV lamp, the entire slide was irradiated. After patterning, substrates were immersed in a 1 mM ethanolic solution of azido functionalized glycol (**2.1**) for 12 h before analysis by MALDI TOF MS. Only the sampled patterned using the handheld UV lamp show coupling.

observed on the 100% surface, shown in **Scheme 5.1**. These findings led to a model solution based study so that the reaction could be monitored by UV-Vis and the resulting products characterized by ^{1}H and ^{13}C NMR and ESI MS.

In order to investigate the difference between the handheld UV lamp and the direct-write laser writer, a model cyclopropenone compound (**5.1**) was synthesis to mimic the surface deprotection, **Figure 5.2**. This monomer was irradiated with the handheld UV lamp at 325 nm for 150 minutes and the reaction was monitored by UV-Vis, **Figure 5.3**. A parallel reaction was also conducted at 365 nm and monitored by UV-Vis for 150 minutes, **Figure 5.4**. **Figure 5.3** clearly shows the addition of a new spectrum with a max absorbance at 285 nm. This sample was concentrated and analyzed using ^{1}H and ^{13}C NMR and ESI MS, which indicated a diphenyl diketone (**5.3**), was formed, **Figure 5.2**. After isolating the major products of the cyclopropenone irradiation, a representative UV-Vis trace was obtained for each compound, **Figure 5.5**, and the overall conversion from **5.1** to the cyclooctyne (**5.2**) and finally to **5.3** was calculated for each wavelength, **Figure 5.6**.
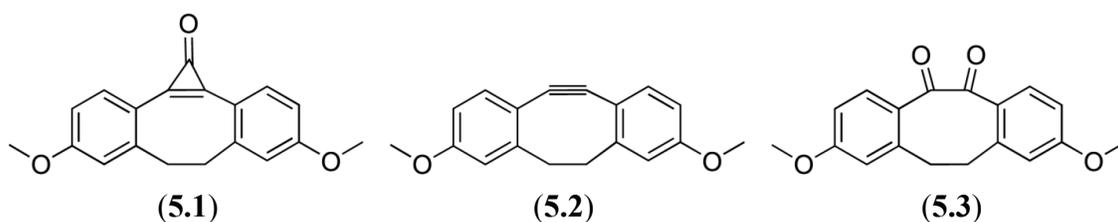
Figure 5.2. Compounds characterized in model cyclopropenone monomer study. **5.1** – model cyclopropenone, **5.2** – strained cyclooctyne, **5.3** – diphenyl diketone.
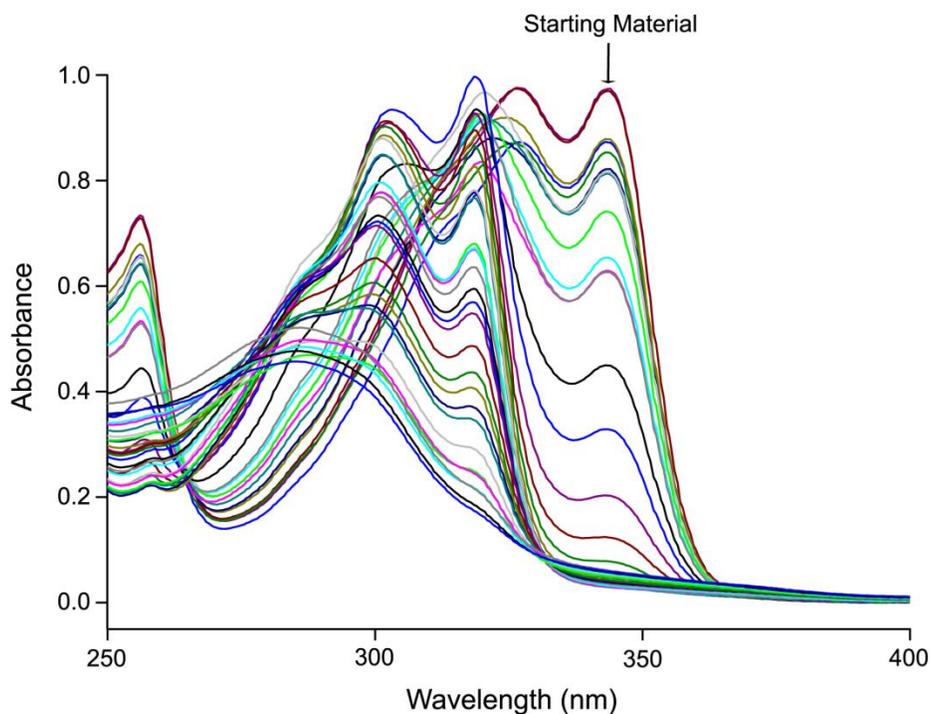
Figure 5.3. UV-Vis traces of **5.1** after irradiation at 325 nm over 150 minutes. Aliquots were removed from the reaction mixture, diluted with acetonitrile, and analyzed by UV-Vis.
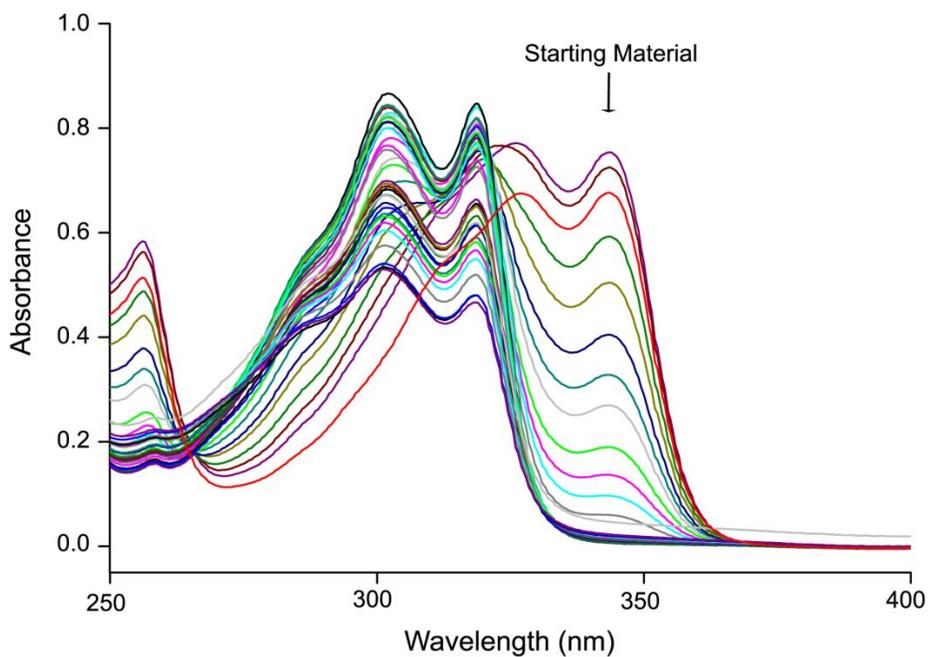
Figure 5.4. UV-Vis traces of **5.1** after irradiation at 365 nm over 150 minutes. Aliquots were removed from the reaction mixture, diluted with acetonitrile, and analyzed by UV-Vis.
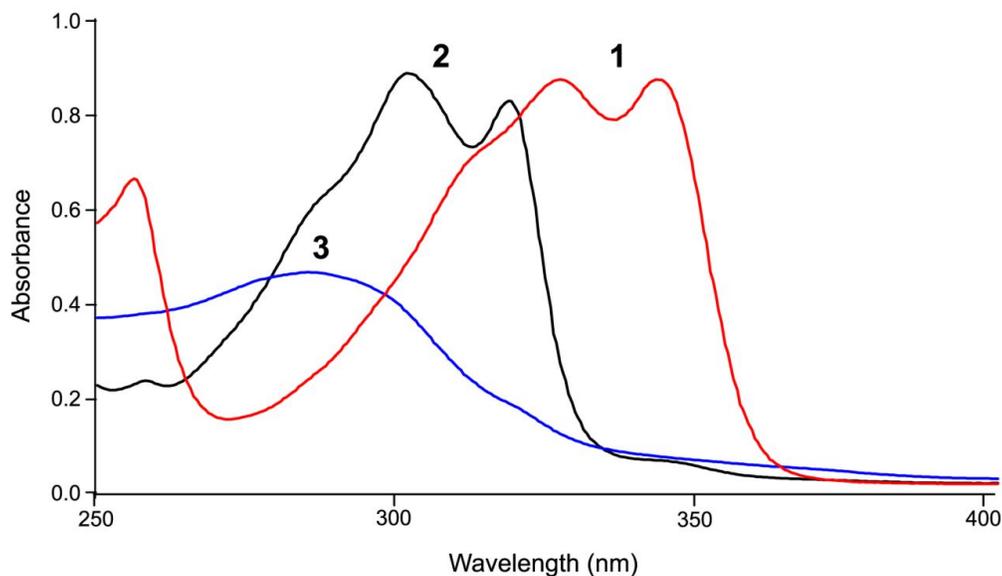
Figure 5.5. UV-Vis traces of compounds **5.1, 5.2,** and **5.3**.

The conversion of **5.1** to **5.3** occurred more rapidly at 325 nm do to the significant absorbance of **5.2** at 325 nm. At 325 nm, **5.2** could be excited into the triplet state and consequently react with oxygen that was absorbed in solution, which is shown in **Scheme 5.2**. As a result of this finding, a gas chamber was designed to be used with the direct-write laser writer so that surfaces could be patterned under an inert atmosphere. Purging the system with argon resulted in only cyclooctyne formation after patterning. The goal for this project was to produce a photoprotected bioorthogonal group, however serendipitously this monomer system actually produces two bioorthogonal functionalities depending on the deprotecting conditions. Under argon, a cyclooctyne monomer is produced, which can couple azido functionalized molecules. However under atmospheric conditions, a diphenyl diketone monomer is produced, which can be use to couple aminooxy groups and hydrazidines groups, **Scheme 5.3**.[14-16]
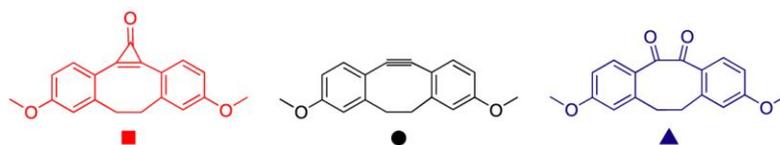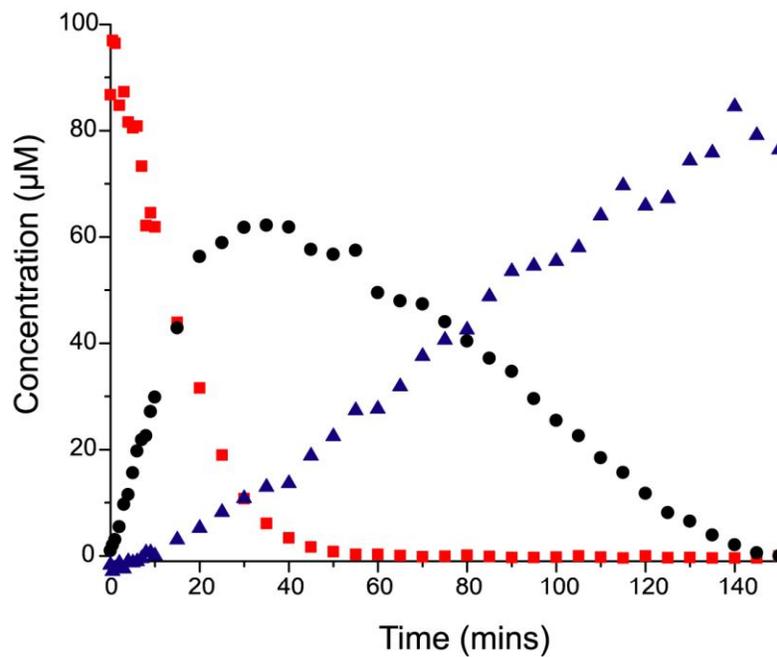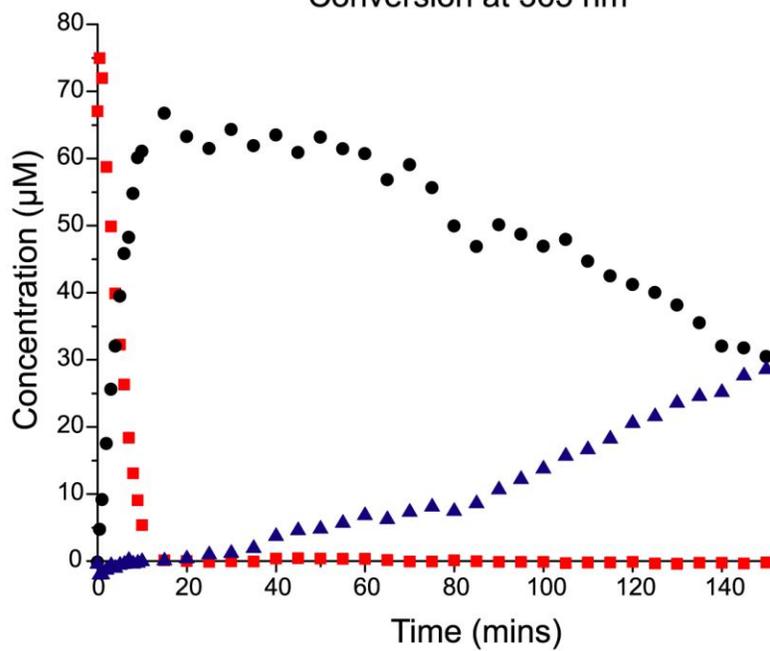
Figure 5.6. Conversion of compound **5.1**
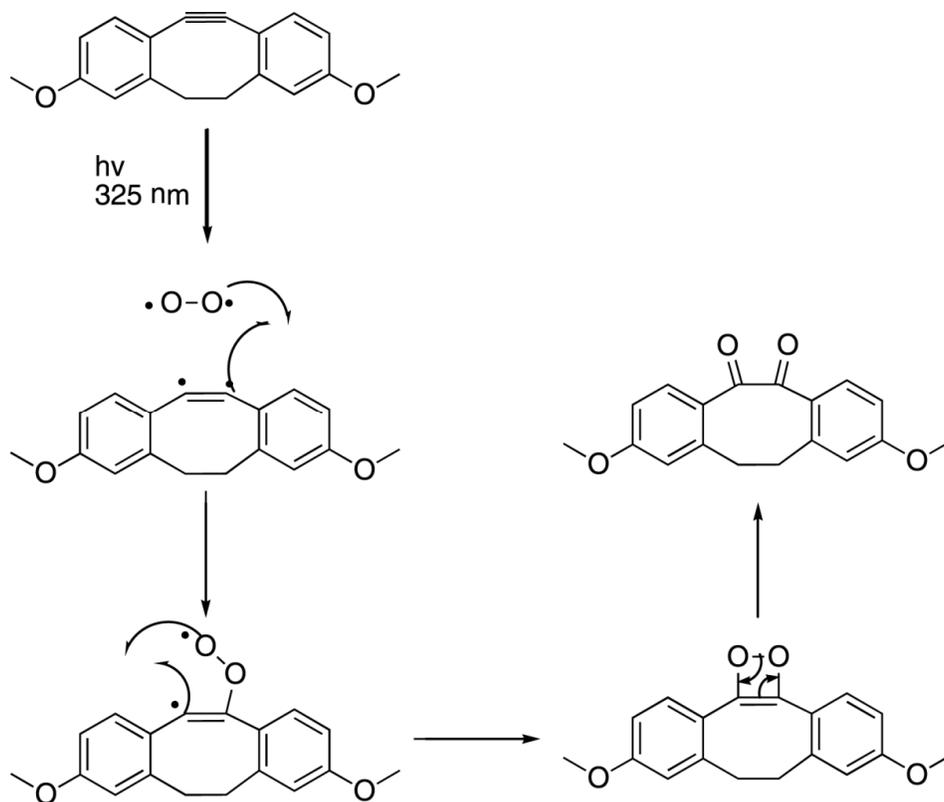
Scheme 5.2. Conversion of cyclooctyne to diphenyl diketone.
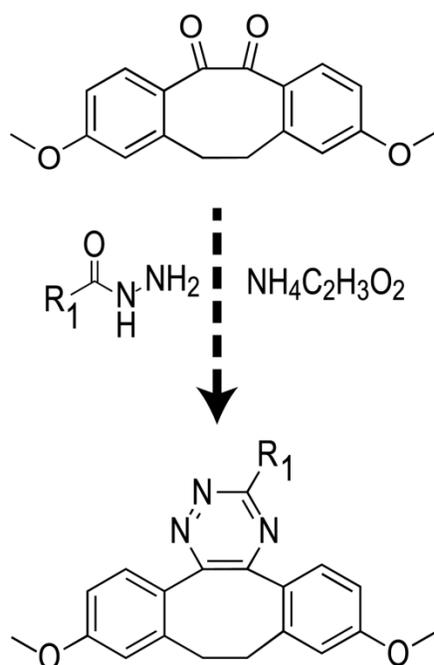
Scheme 5.3. Hydrazide reaction with the diphenyl diketone with ammonium acetate.

In addition to the cyclooctyne and diphenyl diketone functionalities, cyclopropenones also undergo a variety of nonphotochemical reactions.[17] Many of these are compatible with ketones and cyclooctynes. As a result, this monomer system has the capability to produce three distinct functional groups from the same monomer. Creating functional group arrays is important for many applications, in particular cell growth assays. This work then could be applied to studying cell responses to functional group gradients. One of the earliest investigation of 2D substrates to support neuronal growth involved the use of polylysine pretreated surfaces.[18] This work showed that amine functionalized slides could support neuronal attachment and outgrowth; however the concentration of polylysine on the surface was not control. Later work utilized masked photolithography to control localized amine concentrations.[19] These findings have led many groups to investigate how neurons respond to other chemical functionalities, including hydroxyl (-OH), sulfonic ($-SO_3H$), amino ($-NH_2$), carboxyl (-COOH), mercapto (-SH), methyl ($-CH_3$).[20] Additionally, mesenchymal stem cells have also been exposed to surfaces containing a variety of functional groups including; methy, amino, mercapto, hydroxyl, and carboxyl.[21] Each functional group affected stem cell adhesion and differentiation to a different extent. By utilizing direct-write photolithography and the cyclopropenone monomer system, we have the capability to precisely pattern 3 functional groups on a single substrate. This versatility has never been shown before for surface chemistry.

5.3 References

1.	Mrksich, M., Mass Spectrometry of Self-Assembled Monolayers: A New Tool for Molecular Surface Science. *ACS Nano* **2008,** 2, (1), 7-18.
2.	Battino, R.; Rettich, T. R.; Tominaga, T., The Solubility of Oxygen and Ozone in Liquids. *Journal of Physical and Chemical Reference Data* **1983,** 12, (2), 163-178.
3.	Clem, R. L.; Barth, A., Pathway-Specific Trafficking of Native AMPARs by In Vivo Experience. *Neuron* **2006,** 49, (5), 663-670.
4.	Goetz, A. K.; Scheffler, B.; Chen, H.-X.; Wang, S.; Suslov, O.; Xiang, H.; Brüstle, O.; Roper, S. N.; Steindler, D. A., Temporally restricted substrate interactions direct fate and specification of neural precursors derived from embryonic stem cells. *Proceedings of the National Academy of Sciences* **2006,** 103, (29), 11063-11068.
5.	Sinniah, K.; Cheng, J.; Terrettaz, S.; Reutt-Robey, J. E.; Miller, C. J., Self-Assembled .omega.-Hydroxyalkanethiol Monolayers with Internal Functionalities: Electrochemical and Infrared Structural Characterizations of Ether-Containing Monolayers. *The Journal of Physical Chemistry* **1995,** 99, (39), 14500-14505.
6.	Jia, J.; Wang, B.; Wu, A.; Cheng, G.; Li, Z.; Dong, S., A Method to Construct a Third-Generation Horseradish Peroxidase Biosensor: Self-Assembling Gold Nanoparticles to Three-Dimensional Sol−Gel Network. *Analytical Chemistry* **2002,** 74, (9), 2217-2223.
7.	Yu, X.; Munge, B.; Patel, V.; Jensen, G.; Bhirde, A.; Gong, J. D.; Kim, S. N.; Gillespie, J.; Gutkind, J. S.; Papadimitrakopoulos, F.; Rusling, J. F., Carbon Nanotube Amplification Strategies for Highly Sensitive Immunodetection of Cancer Biomarkers. *Journal of the American Chemical Society* **2006,** 128, (34), 11199-11205.
8.	Varga, B. R.; Kállay, M.; Hegyi, K.; Béni, S.; Kele, P., A Non-Fluorinated Monobenzocyclooctyne for Rapid Copper-Free Click Reactions. *Chemistry – A European Journal* **2012,** 18, (3), 822-828.
9.	Wendeln, C.; Singh, I.; Rinnen, S.; Schulz, C.; Arlinghaus, H. F.; Burley, G. A.; Ravoo, B. J., Orthogonal, metal-free surface modification by strain-promoted azide-alkyne and nitrile oxide-alkene/alkyne cycloadditions. *Chemical Science* **2012,** 3, (8), 2479-2484.
10.	Chang, P. V.; Prescher, J. A.; Sletten, E. M.; Baskin, J. M.; Miller, I. A.; Agard, N. J.; Lo, A.; Bertozzi, C. R., Copper-free click chemistry in living animals. *Proceedings of the National Academy of Sciences* **2010,** 107, (5), 1821-1826.
11.	Kuzmin, A.; Poloukhtine, A.; Wolfert, M. A.; Popik, V. V., Surface Functionalization Using Catalyst-Free Azide−Alkyne Cycloaddition. *Bioconjugate Chemistry* **2010,** 21, (11), 2076-2085.
12.	Jewett, J. C.; Bertozzi, C. R., Cu-free click cycloaddition reactions in chemical biology. *Chemical Society Reviews* **2010,** 39, (4), 1272-1279.
13.	Orski, S. V.; Poloukhtine, A. A.; Arumugam, S.; Mao, L.; Popik, V. V.; Locklin, J., High Density Orthogonal Surface Immobilization via Photoactivated Copper-Free Click Chemistry. *Journal of the American Chemical Society* **2010,** 132, (32), 11024-11026.
14.	Zhao, Z.; Leister, W. H.; Strauss, K. A.; Wisnoski, D. D.; Lindsley, C. W., Broadening the scope of 1,2,4-triazine synthesis by the application of microwave technology. *Tetrahedron Letters* **2003,** 44, (6), 1123-1127.
15.	Palimkar, S. S.; Siddiqui, S. A.; Daniel, T.; Lahoti, R. J.; Srinivasan, K. V., Ionic Liquid-Promoted Regiospecific Friedlander Annulation: Novel Synthesis of Quinolines and Fused Polycyclic Quinolines. *The Journal of Organic Chemistry* **2003,** 68, (24), 9371-9378.

16.   Potewar, T. M.; Lahoti, R. J.; Daniel, T.; Srinivasan, K. V., Efficient Synthesis of 3,5,6-Trisubstituted-1,2,4-triazines in the Brønsted Acidic Ionic Liquid, 1-n-Butylimidazolium Tetrafluoroborate ([Hbim]BF4). *Synthetic Communications* **2007,** 37, (2), 261-269.

17.   Potts, K. T.; Baum, J. S., Chemistry of cyclopropenones. *Chemical Reviews* **1974,** 74, (2), 189-213.

18.   Yavin, E.; Yavin, Z., ATTACHMENT AND CULTURE OF DISSOCIATED CELLS FROM RAT EMBRYO CEREBRAL HEMISPHERES ON POLYLYSINE-COATED SURFACE. *The Journal of Cell Biology* **1974,** 62, (2), 540-546.

19.   Kleinfeld, D.; Kahler, K. H.; Hockberger, P. E., Controlled outgrowth of dissociated neurons on patterned substrates. *The Journal of Neuroscience* **1988,** 8, (11), 4098-4120.

20.   Ren, Y.-J.; Zhang, H.; Huang, H.; Wang, X.-M.; Zhou, Z.-Y.; Cui, F.-Z.; An, Y.-H., In vitro behavior of neural stem cells in response to different chemical functional groups. *Biomaterials* **2009,** 30, (6), 1036-1044.

21.   Curran, J. M.; Chen, R.; Hunt, J. A., The guidance of human mesenchymal stem cell differentiation in vitro by controlled modifications to the cell substrate. *Biomaterials* **2006,** 27, (27), 4783-4793.

Appendix A

Glycol-terminated Phosphonate Monomer Synthesis to Functionalize Titanium Dioxide Surfaces*

*The surface patterning conducted in this Appendix was conducted by Kevin Wacker under my guidance.

A.1 Introduction

Surface functionalization with SAMs has traditionally been carried out using either thiols on precious metals or silanes on oxide surfaces.[1, 2] These systems have many advantages. One of these advantages is easy substrate preparation, however there are also numerous limitations associated with them. Thiols require the use of expensive precious metals and only form a single covalent bond with the surface, which can lead to limited monolayer stability under harsh conditions.[3] Additionally, not all applications are compatible with the use of precious metals since they are soft and conducting. Conversely, silanes have been used to functionalized oxide substrates.[4-7] However, silane derivatives, trichlorosilanes and trialkylsilanes, are not easily synthesized do to the high reactivity. Additionally, silanes display limited stability due to reaction with atmospheric water leading to gel formation. This same reactivity and lead to monomer cross-linking on the substrate and reduce monolayer stability. As a result, only a limited number of functionalized silane monomers have been prepared. To address these limitations, a number of phosphonates monomers have been developed.[4, 8, 9] Phosphonates are an interesting class of compounds since they are can form ordered SAMs on many oxide substrates.[10-14] Here we report the synthesis of a glycol-terminated phosphonate monomer that can be used to functionalize titanium dioxide substrates.

120

A.2 Experimental Methods

A.2.1 Materials and Instrumentation

All reagents were obtained from Sigma-Aldrich (St. Louis, MO) or VWR Scientific (Radnor, PA), were reagent grade or higher, and used as received unless otherwise indicated. Plasma oxidation of glass and titanium dioxide substrates was carried out in a Femto standard low-pressure plasma system (Diener electronic GmbH+Co. KG, Nagold). Titanium dioxide slides were prepared using a PVD 75 (Kurt J Lesker, Pittsburg, PA). Substrates were patterned using a direct-writer LaserWriter (Microtech, Palermo, Italy) system equipped with a 325 nm He:Cd laser operating at 15 mW and the beam was focused to 2 um^2 producing a laser spot intensity of ~7.5x10^5 W/cm^2. Fluorescent images were captured on a Nikon TE2000-PFS microscope running NIS-Elements imaging software equipped with a Prior XY stage, and Photometrics CoolSNAP monochrome camera. Transmittance infrared spectra were collected on a Thermo (Waltham, MA, USA) Nicolet Nexus 670 FT-IR with a DTGS detector.

A.2.2 Substrate Preparation: Titanium dioxide (TiO$_2$) samples were prepared by depositing 50 Å of titanium at 0.1 Å/sec followed by 150 Å of TiO$_2$ at 0.1 Å/sec. TiO$_2$ substrates were cleaned for 20 minutes in oxygen plasma prior to use. Substrates were then soaked in a 1 mM solution the glycol-terminated phosphonate monomer (**A.5**) in anhydrous THF for 48 hours at 40 °C and annealed at 100 °C for 1 hour in an oven. Substrates were rinsed with ethanol, water, and ethanol and then dried under a stream of nitrogen.

A.2.3 Transmittance Infrared Spectroscopy: Substrates were analyzed by transmittance IR with each spectrum consisting of 1024 scans collected with a data spacing of 1.8 cm^{-1}.

A.2.3 Substrate Patterning: The line pattern was generated using CleWin (WieWeb, Netherlands). Substrates were then patterned using a commercial direct-write photolithography

system (Microtech, Palermo, Italy), at 100% power (1.6×10^{12} photons/um^2). After photoablation, slides were rinsed with ethanol, water, ethanol, and dried under a stream of nitrogen. Freshly patterned substrates were used for protein adsorption studies.

A.3 Results and Discussion

A glycol-terminated phosphonate monomer was synthesized to functionalize oxide substrates for biological applications. The phosphonate head group was installed via an Arbuzov reaction and deprotection achieved using bromotrimethylsilane. The glycol tail was chosen since glycol-terminated SAMs have been shown to resist non-specific protein adsorption.[15]

Monolayer formation was characterized by transmittance IR. In general, monolayers are considered well ordered when the asymmetric and symmetric methylene stretches in the monolayer approach 2920 and 2850 cm^{-1} respectively, which are the values observed for crystalline alkanes.[16, 17] The asymmetric and symmetric shifts observed for glycol-terminated phosphonate monolayers that were prepared by soaking at elevated temperature (40 °C) and annealing at 100 °C were 2919.74 and 2850.32 cm^{-1}, respectively, **Figure A.1**. This suggests that the resulting monolayers are well ordered, since the asymmetric and symmetric stretches for the non-ordered methylene region of the glycol portion of the monolayer broadens these stretching bands and causes a slight shift to higher wavenumbers. A number of other monolayer formation conditions, including Tethered By Aggregated Growth (T-BAG),[18] were attempted, but these conditions did not result in well ordered monolayers.

Monolayers were patterned using photo-induced monomer desorption. We anticipated that photo-induced patterning would be successful due to the large absorbance of titanium dioxide at 325 nm.[19] As shown in **Figure A.2**, fibronectin could be specifically absorbed to the ablated regions on the substrate. This first proof-of-concept experiment suggests that monolayers formed from phosphonates might be able to be thermally desorbed from the substrate similar to what was observed for thiols on gold in Chapter 2.
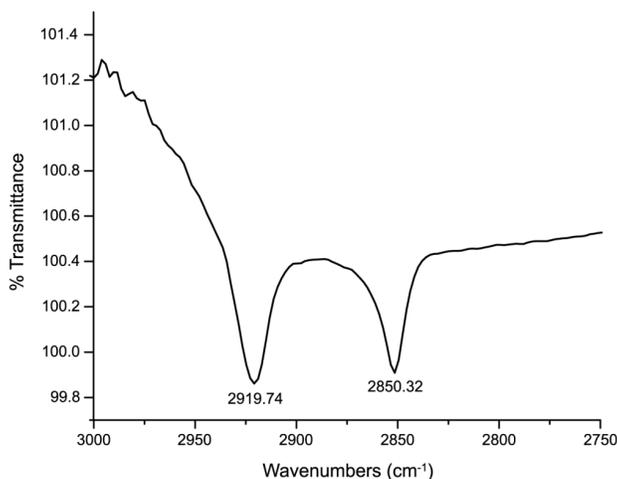
Figure A.1. Transmittance IR of monolayer formed from **A1.5** on TiO_2.
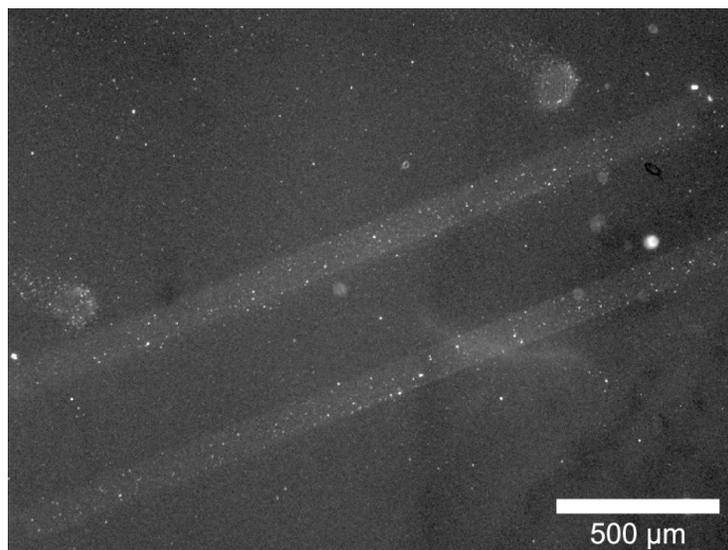
Figure A.2. Fluorescent image of fibronectin adsorbed to a patterned monolayer formed from **A.5** on TiO_2 using direct-write photolithography.

To generate a robust patterning method the write speed must be optimized to ensure complete monomer removal, while also minimizing the time necessary to pattern each sample. This optimization could be performed the same way as described in Chapter 2 for thiols on gold. Additionally, ablated monolayers need to be characterized and confirmed by IR and various scanning probe microscopy techniques, including PeakForce QNM and KPFM. Quantitative protein adsorption to these patterned substrates could also be analyzed using SPRi, if a thin layer of TiO_2 was deposited on top of the gold substrate.

It is anticipated that these substrates will be compatible with cell culture conditions and will allow for patterned cell culture due to the presence of the protein-resistant glycol-portion of the monomer. Moreover, removing the gold layer, which acts a fluorescent quencher, should allow for lower concentrations of proteins or fluorescent probes to be detected by fluorescence microscopy. This reduction could eliminate the amplification assays that were conducted in chapter 2 and 4 and were necessary to visualize some patterns.

In conclusion, we have developed a straight forward synthesis for a glycol-terminated phosphonate monomer. These monomers can produce well ordered SAMs, by transmittance IR characterization and protein patterns can be formed by phosphonate ablation. Since many implantable medical devices are made out of titanium and its alloys an contain a native oxide coating, these methods have the potential of revolutionizing how specific cellular connections are formed with medical devices.
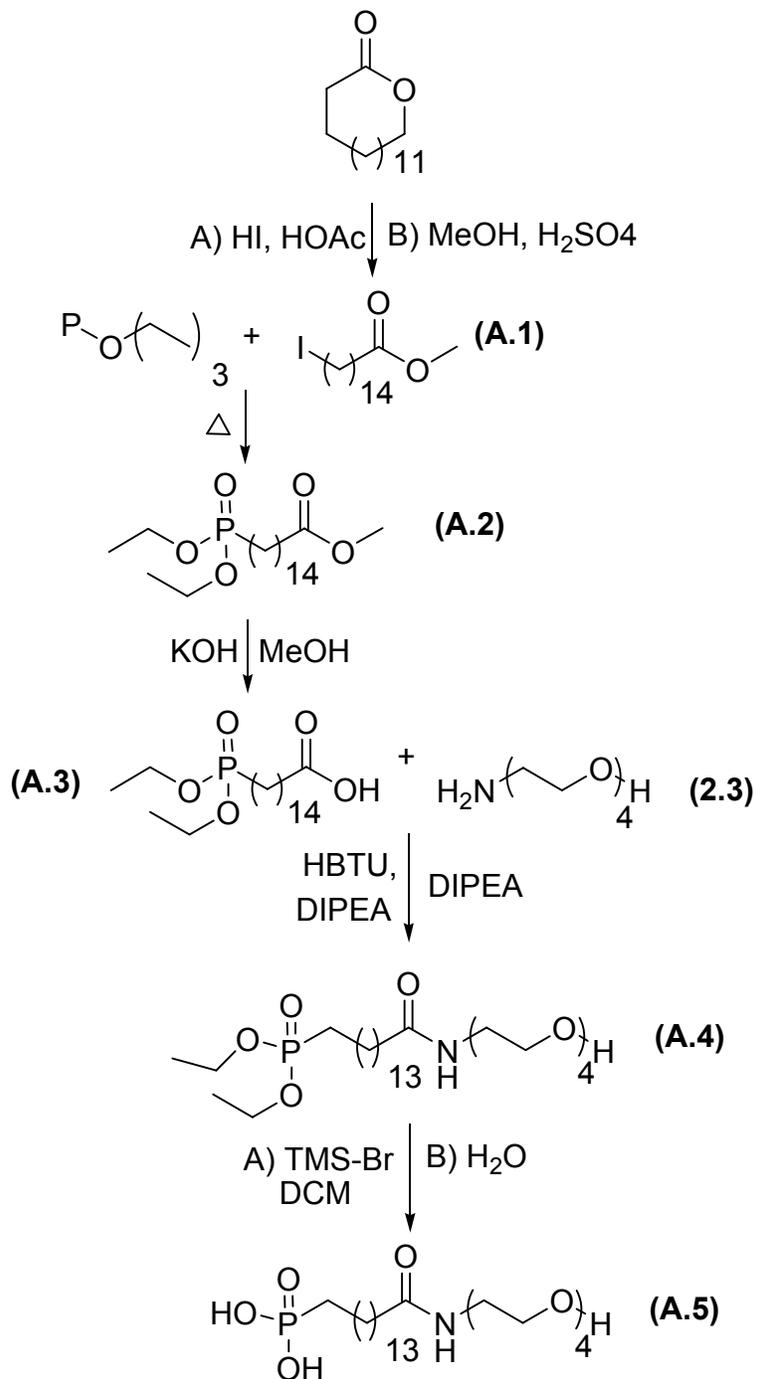
Scheme A.1 Overall Synthetic Scheme for Monomer A.5

Methyl 15-iodopentadecanoate (A.1)
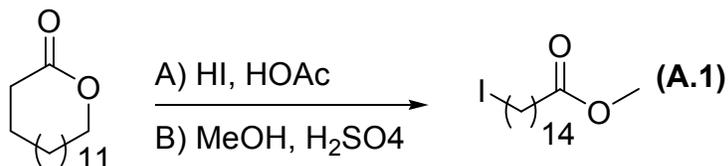
Pentadecanolide (16.0008 g, 0.066 moles) was added to a round bottom flask and diluted with

hydroiodic acid (40 mL), acetic acid (80 mL), and the reaction was allowed to reflux overnight.

The reaction mixture was cooled to room temperature, diluted with CH_2Cl_2 (50 mL), and rinsed

with 10% sodium thiol sulfate. The organic layer was dried over sodium sulfate and

concentrated via rotary evaporation to produce a yellow solid. The sample was then diluted with

methanol (100 mL) and concentrated sulfuric acid (200 uL) and refluxed for 12 hours. Methanol

was removed under reduced pressure and the resulting oil was purified via flash column

chromatography (1:4 ethyl acetate:hexanes) to produce 22.2417 g (88 %) of methyl 15-

iodopentadecanoate (**A.1**) as a yellow solid. ^{1}H NMR δ 1.23 (m, 24H), 1.60 (m, 4H), 1.8 (m,

2H), 2.30 (t, 2H), 3.19 (t, 2H), 3.60 (s, 3H).

Methyl 15-(diethoxyphosphoryl)pentadecanoate (A.2)
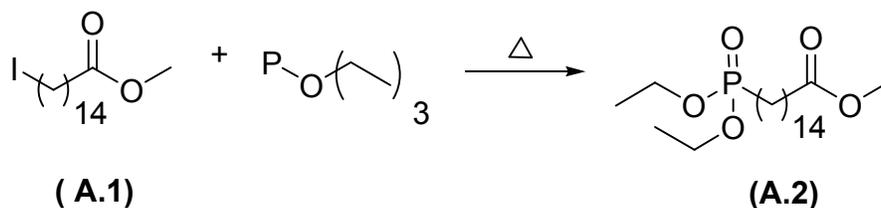
Methyl 15-iodopentadecanoate (**A.1**) (4.2087g, 11.0 mmoles) was added to a round bottom flask

and purged with argon. The reaction mixture was placed in a 100 °C oil bath and triethyl

phoshite (12 mL, 69.9 mmoles) was added dropwise (1 mL/50 min) using a syringe pump. The

solution was stirred for 12 hours. Excess triethylphosphite was removed under reduced pressure

and the resulting product was purified by flash column chromatography (4:1

ethylacetate:hexanes) to produce 4.0163 g (93 %) of methyl 15-

(diethoxyphosphoryl)pentadecanoate (**A.2**) as a yellow solid. ^{1}H NMR δ 1.21 (m, 24H), 1.62 (m, 6H), 2.27 (t, 2H), 3.60 (s, 3H), 4.10 (m, 4H).

15-(diethoxyphosphoryl)pentadecanoic acid (A.3)

(A.2)   **(A.3)**
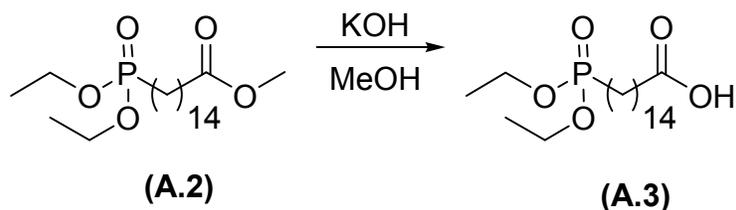
Methyl 15-(diethoxyphosphoryl)pentadecanoate (**A.2**) (1.0038 g, 2.55 mmoles) was added to a round bottom flask. The sample was diluted with methanol (25 mL), potassium hydroxide (0.3540 g, 3.4 mmoles) was added, and refluxed for 3 hours. The reaction mixture was cooled to room temperature and acidified with concentrated HCl (0.80 mL). Methanol was then removed under reduced pressure and the resulting solid was purified by flash column chromatography (5:95 MeOH:CHCl$_3$) to produce 0.8954 g (92.3%) of 15-(diethoxyphosphoryl)pentadecanoic acid (**A.3**) as yellow solid. ^{1}H NMR δ 1.21 (m, 24H), 1.62 (m, 6H), 2.32 (t, 2H), 4.10 (m, 4H).

diethyl (1-hydroxy-13-oxo-3,6,9-trioxa-12-azaheptacosan-27-yl)phosphonate (A.4)
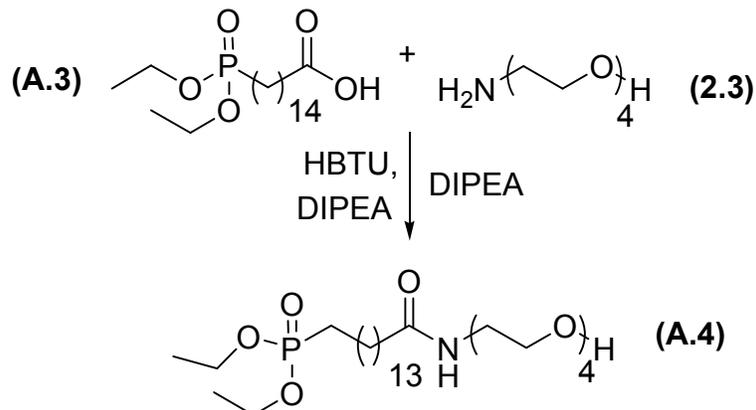
15-(diethoxyphosphoryl)pentadecanoic acid **(A.3)** (1.2019 g, 3.17 mmoles) was added to an oven dried round bottom flask and the flask was purged with argon. The sample was diluted with anhydrous dimethylformamide (DMF) (10 mL) and CH_2Cl_2 (5 mL), Diisopropylethyl amine (DIPEA) (1.6 mL, 10.1 mmoles) and O-(Benzotriazol-1-yl)-N,N,N',N'-tetramethyluronium hexafluorophosphate (HBTU) (1.4642, 3.88 mmoles) were added to the flask and the reaction was allowed to proceed at room temperature for 1 hour.   2-(2-(2-(2-minoethoxy)ethoxy)ethoxy) ethanol **(2.3)** (0.5264 g, 2.7 mmoles) was added dropwise to the flask and the reaction was allowed to proceeded for 12 hours.   The solvent was removed under reduced pressure (20 mTorr). The resulting oil was diluted with CH_2Cl_2 (20 mL) and rinsed with 1 M NaOH (20 mL), 1 M HCl (20 mL), and brine (20 mL). The organic layer was dried over sodium sulfate, and concentrated. The resulting oil was purified via flash column chromatography (10:40:50 MeOH:ethyl acetate:$CHCl_3$) to produce 0.5119 g (34 %) of diethyl (1-hydroxy-13-oxo-3,6,9-trioxa-12-azaheptacosan-27-yl)phosphonate **(A.4)** as a yellow oil. ^{1}H NMR δ 1.21 (m, 24H), 1.62 (m, 6H), 2.15 (t, 2H), 3.44 (t, 2H), 3.52 (t, 2H), 3.62 (m, 12H), 4.10 (m, 4H), 6.98 (s, 1H).

(1-hydroxy-13-oxo-3,6,9-trioxa-12-azaheptacosan-27-yl)phosphonic acid (A.5)
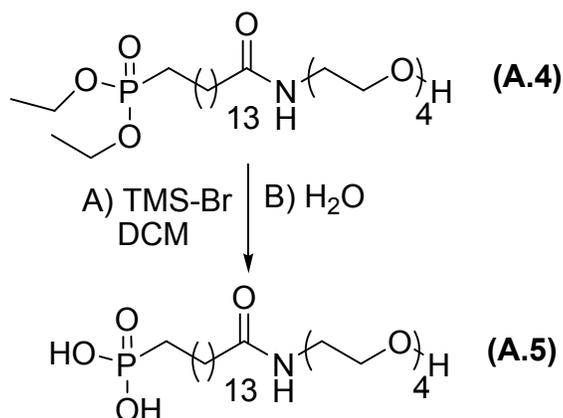
Diethyl (1-hydroxy-13-oxo-3,6,9-trioxa-12-azaheptacosan-27-yl)phosphonate **(A.4)** (89.6 mg, 0.16 mmoles) was added to an oven dried round bottom flask and the flask was purged with argon. The sample was diluted with DCM (5 mL) and bromotrimethylsilane (0.1 mL, 0.36 mmoles) was added. The reaction mixture was placed in a 40 °C oil bath and stirred for 3 hours. Solvent and byproducts were removed under reduced pressure to produce 88.1 mg of (1-hydroxy-13-oxo-3,6,9-trioxa-12-azaheptacosan-27-yl)phosphonic acid **(A.5)** as a yellow oil. ^{1}H NMR (DMSO-d6) δ 1.23 (m, 24H), 1.45 (m, 6H), 2.05 (t, 2H), 3.40 (t, 2H), 3.52 (t, 2H), 3.62 (m, 12H), 7.8 (s, 1H).

^{1}H NMR of molecule **A.1**

(A.2)

^{1}H NMR of molecule **A.2**

ppm (f1)

(A.3)

^{1}H NMR of molecule **A.3**

ppm (f1)
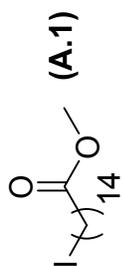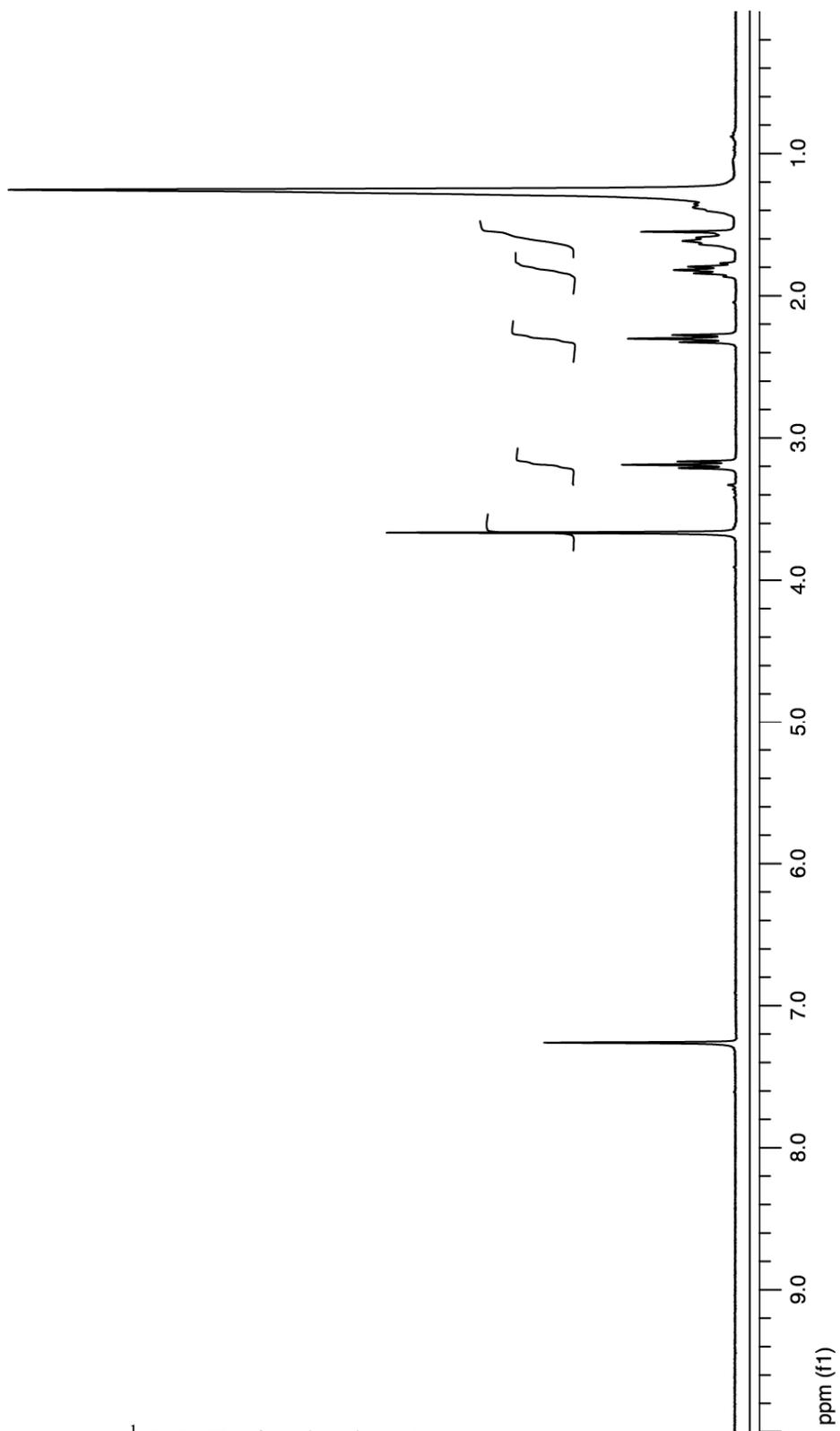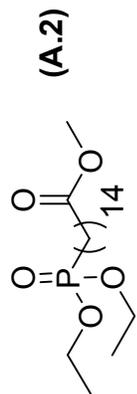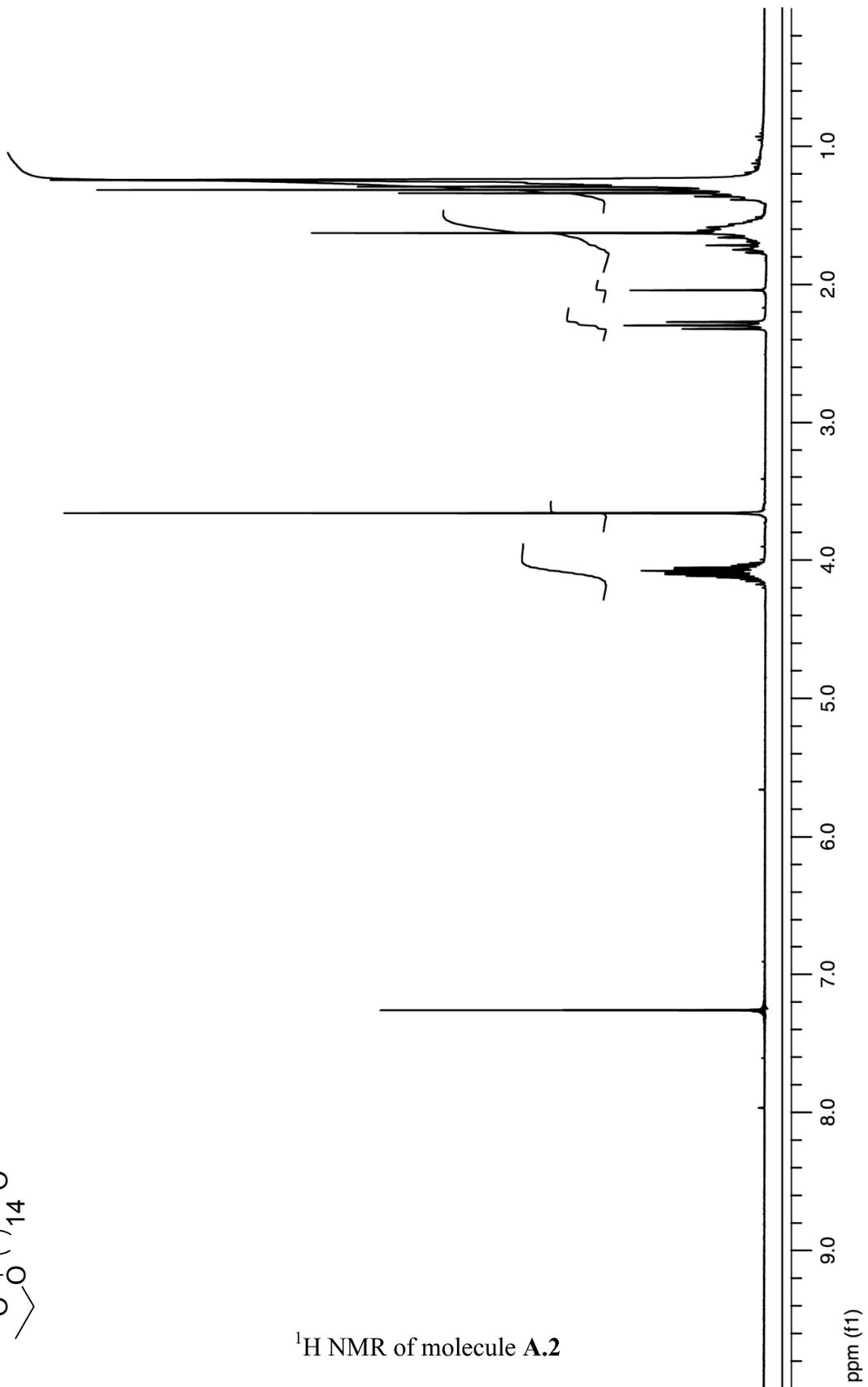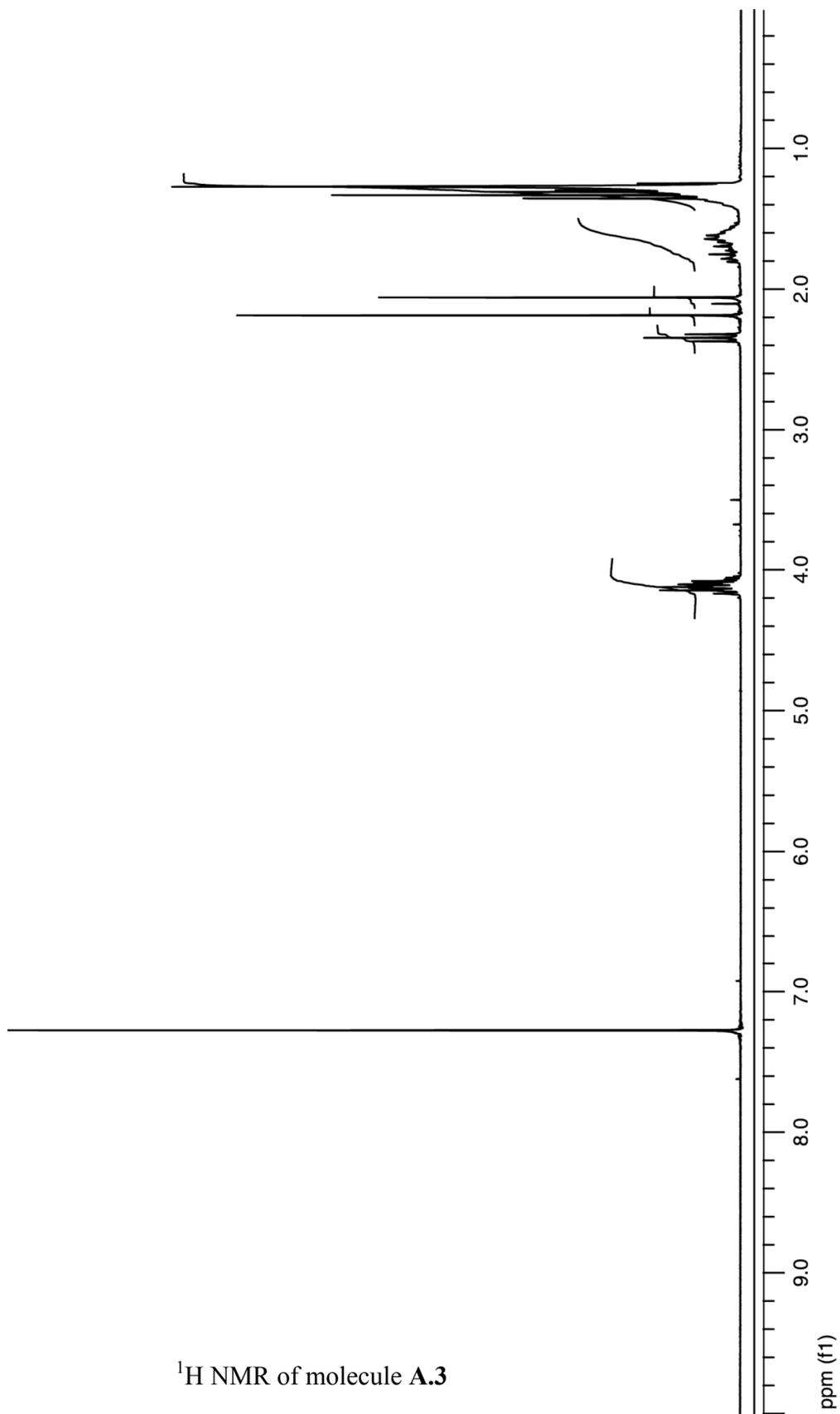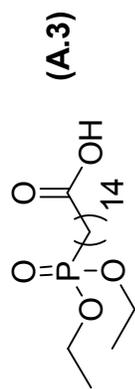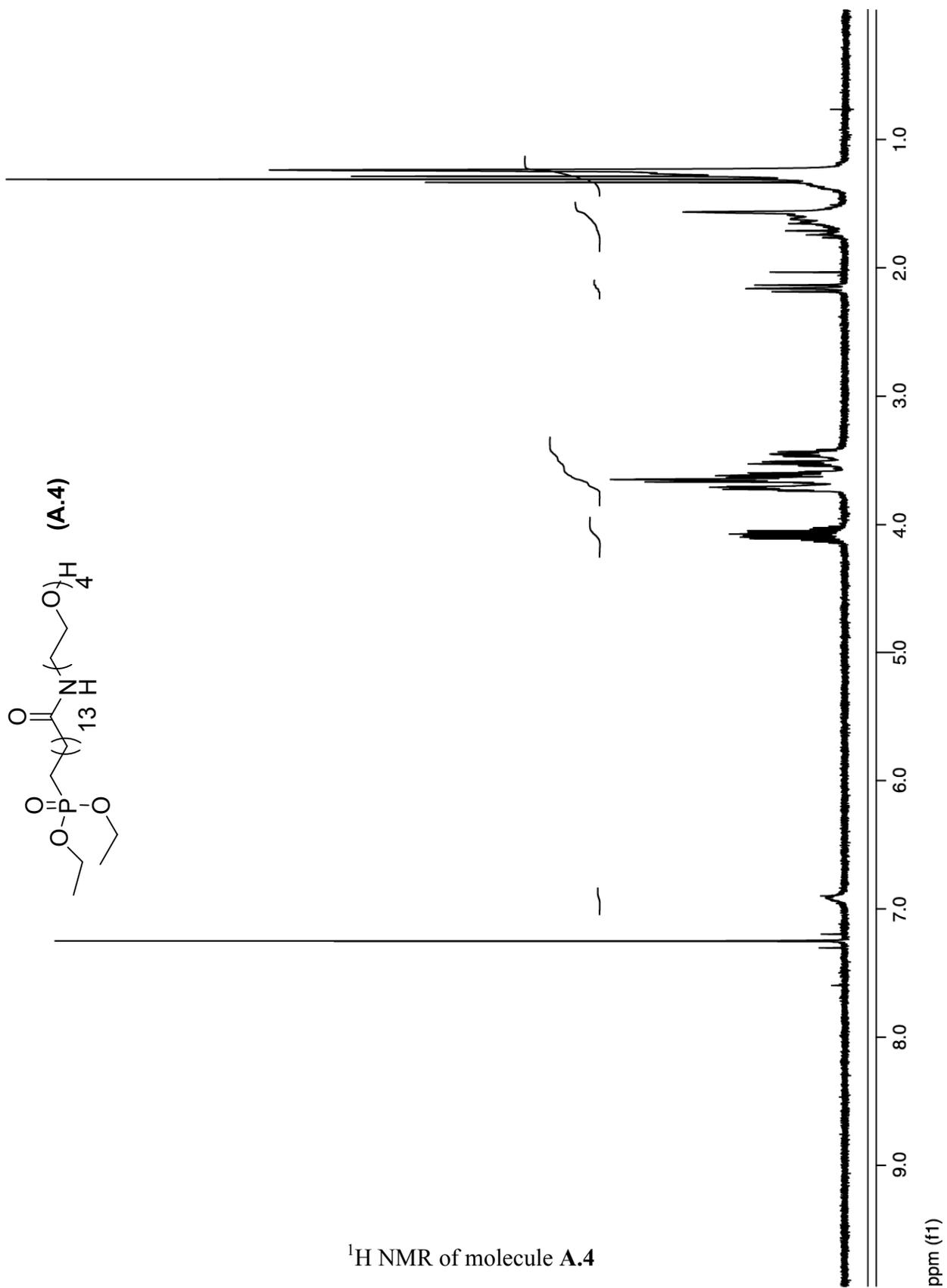
^{1}H NMR of molecule **A.4**
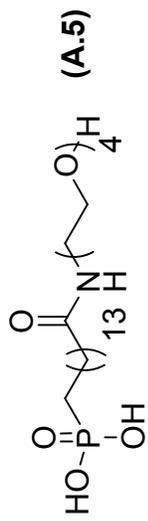
^{1}H NMR of molecule **A.5**
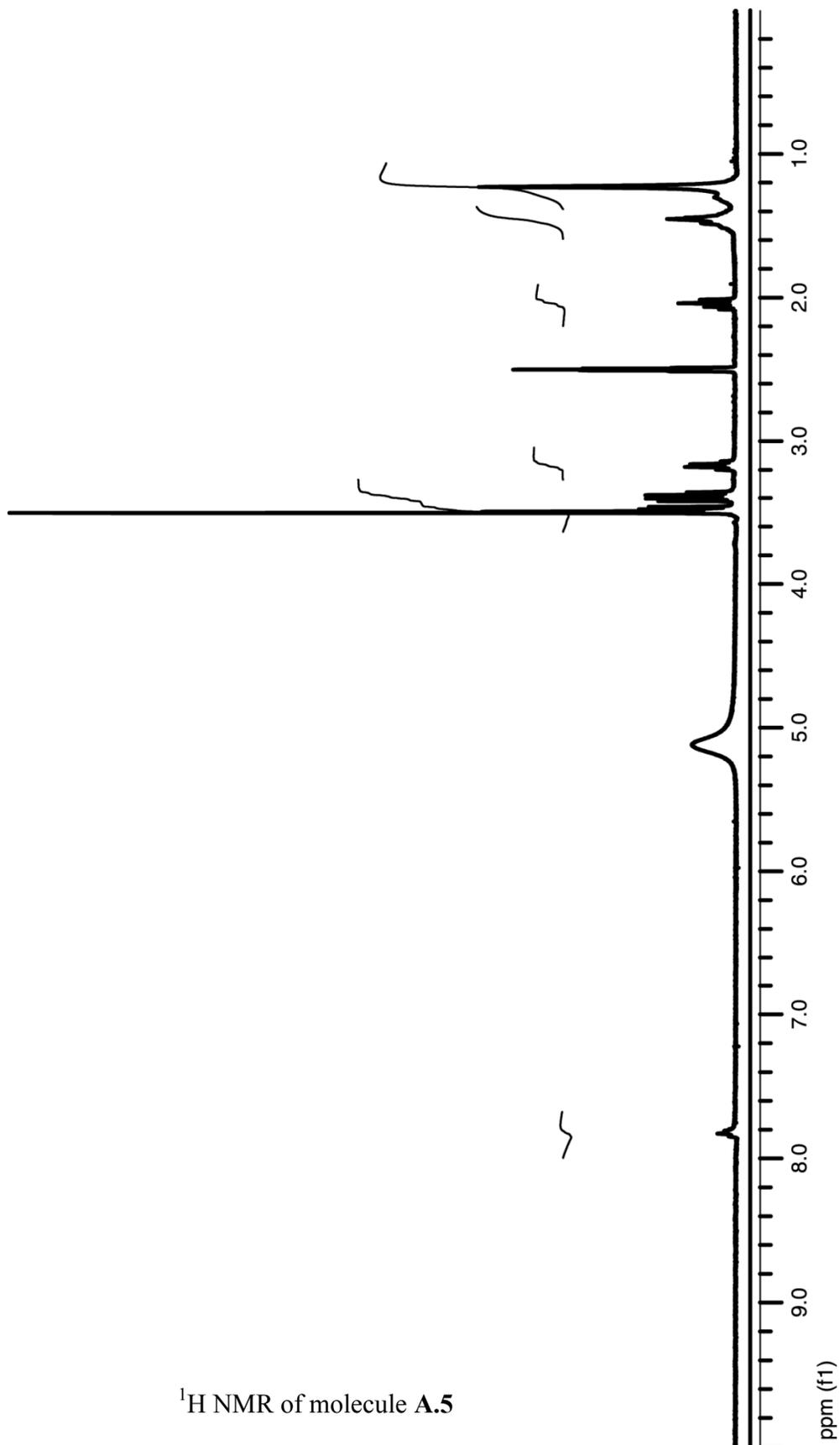
A.4 References

1.   Kumar, A.; Biebuyck, H. A.; Whitesides, G. M., Patterning Self-Assembled Monolayers: Applications in Materials Science. *Langmuir* **1994,** 10, (5), 1498-1511.

2.   Tsukruk, V. V.; Bliznyuk, V. N., Adhesive and Friction Forces between Chemically Modified Silicon and Silicon Nitride Surfaces. *Langmuir* **1998,** 14, (2), 446-455.

3.   Mani, G.; Johnson, D. M.; Marton, D.; Dougherty, V. L.; Feldman, M. D.; Patel, D.; Ayon, A. A.; Agrawal, C. M., Stability of Self-Assembled Monolayers on Titanium and Gold. *Langmuir* **2008,** 24, (13), 6774-6784.

4.   Helmy, R.; Fadeev, A. Y., Self-Assembled Monolayers Supported on TiO2: Comparison of C18H37SiX3 (X = H, Cl, OCH3), C18H37Si(CH3)2Cl, and C18H37PO(OH)2. *Langmuir* **2002,** 18, (23), 8924-8928.

5.   Marcinko, S.; Fadeev, A. Y., Hydrolytic Stability of Organic Monolayers Supported on TiO2 and ZrO2. *Langmuir* **2004,** 20, (6), 2270-2273.

6.   Marcinko, S.; Helmy, R.; Fadeev, A. Y., Adsorption Properties of SAMs Supported on TiO2 and ZrO2. *Langmuir* **2003,** 19, (7), 2752-2755.

7.   Fadeev, A. Y.; Helmy, R.; Marcinko, S., Self-Assembled Monolayers of Organosilicon Hydrides Supported on Titanium, Zirconium, and Hafnium Dioxides. *Langmuir* **2002,** 18, (20), 7521-7529.

8.   Bozzini, S.; Petrini, P.; Tanzi, M. C.; Zürcher, S.; Tosatti, S., Poly(ethylene glycol) and Hydroxy Functionalized Alkane Phosphate Mixed Self-Assembled Monolayers to Control Nonspecific Adsorption of Proteins on Titanium Oxide Surfaces. *Langmuir* **2009,** 26, (9), 6529-6534.

9.   Mallouk, T. E.; Kim, H.-N.; Ollivier, P. J.; Keller, S. W. In *Ultrathin films based on layered materials*, 1996; Elsevier: 1996; pp 189-217.

10.   Tizazu, G.; El-Zubir, O.; Brueck, S. R. J.; Lidzey, D. G.; Leggett, G. J.; Lopez, G. P., Large area nanopatterning of alkylphosphonate self-assembled monolayers on titanium oxide surfaces by interferometric lithography. *Nanoscale* **2011,** 3, (6), 2511-2516.

11.   Hähner, G.; Hofer, R.; Klingenfuss, I., Order and Orientation in Self-Assembled Long Chain Alkanephosphate Monolayers Adsorbed on Metal Oxide Surfaces. *Langmuir* **2001,** 17, (22), 7047-7052.

12.   Hofer, R.; Textor, M.; Spencer, N. D., Alkyl Phosphate Monolayers, Self-Assembled from Aqueous Solution onto Metal Oxide Surfaces. *Langmuir* **2001,** 17, (13), 4014-4020.

13.   Textor, M.; Ruiz, L.; Hofer, R.; Rossi, A.; Feldman, K.; Hähner, G.; Spencer, N. D., Structural Chemistry of Self-Assembled Monolayers of Octadecylphosphoric Acid on Tantalum Oxide Surfaces. *Langmuir* **2000,** 16, (7), 3257-3271.

14.   Gouzman, I.; Dubey, M.; Carolus, M. D.; Schwartz, J.; Bernasek, S. L., Monolayer vs. multilayer self-assembled alkylphosphonate films: X-ray photoelectron spectroscopy studies. *Surface Science* **2006,** 600, (4), 773-781.

15.   Prime, K. L.; Whitesides, G. M., Adsorption of proteins onto surfaces containing end-attached oligo(ethylene oxide): a model system using self-assembled monolayers. *Journal of the American Chemical Society* **1993,** 115, (23), 10714-10721.

16.   Snyder, R. G.; Strauss, H. L.; Elliger, C. A., Carbon-hydrogen stretching modes and the structure of n-alkyl chains. 1. Long, disordered chains. *The Journal of Physical Chemistry* **1982,** 86, (26), 5145-5150.

17.   Sinniah, K.; Cheng, J.; Terrettaz, S.; Reutt-Robey, J. E.; Miller, C. J., Self-Assembled .omega.-Hydroxyalkanethiol Monolayers with Internal Functionalities: Electrochemical and Infrared Structural Characterizations of Ether-Containing Monolayers. *The Journal of Physical Chemistry* **1995,** 99, (39), 14500-14505.

18.   Hanson, E. L.; Schwartz, J.; Nickel, B.; Koch, N.; Danisman, M. F., Bonding Self-Assembled, Compact Organophosphonate Monolayers to the Native Oxide Surface of Silicon. *Journal of the American Chemical Society* **2003,** 125, (51), 16074-16080.

19.   Yang, H.; Zhu, S.; Pan, N., Studying the mechanisms of titanium dioxide as ultraviolet-blocking additive for films and fabrics by an improved scheme. *Journal of Applied Polymer Science* **2004,** 92, (5), 3201-3210.

Appendix B

^{1}H and ^{13}C NMR for Chapter 2
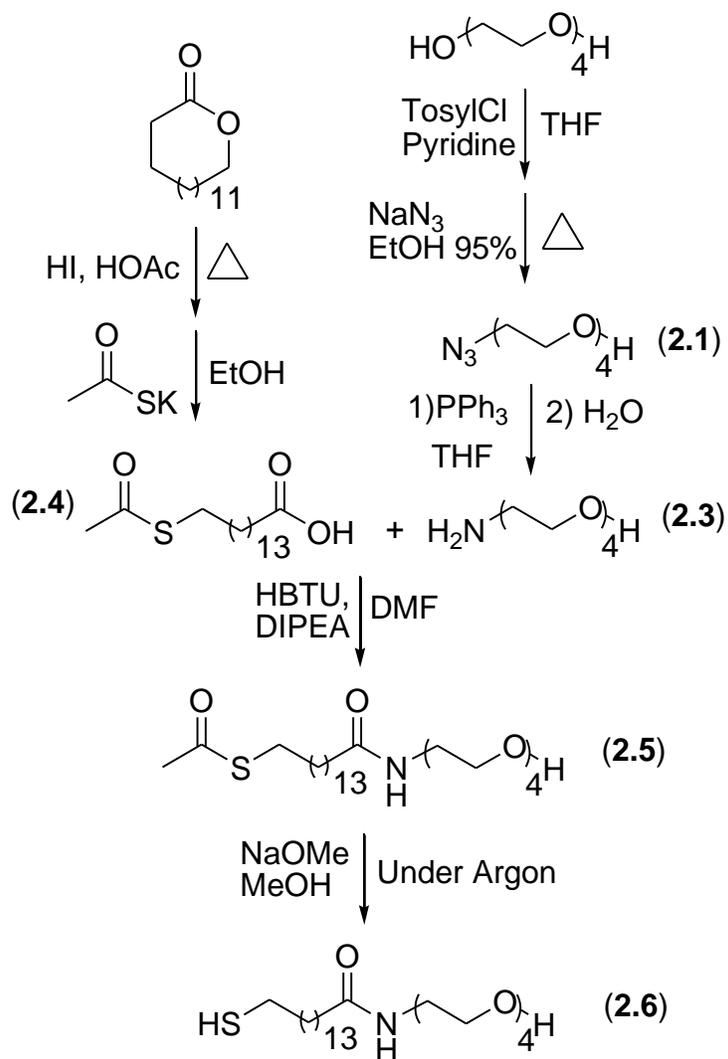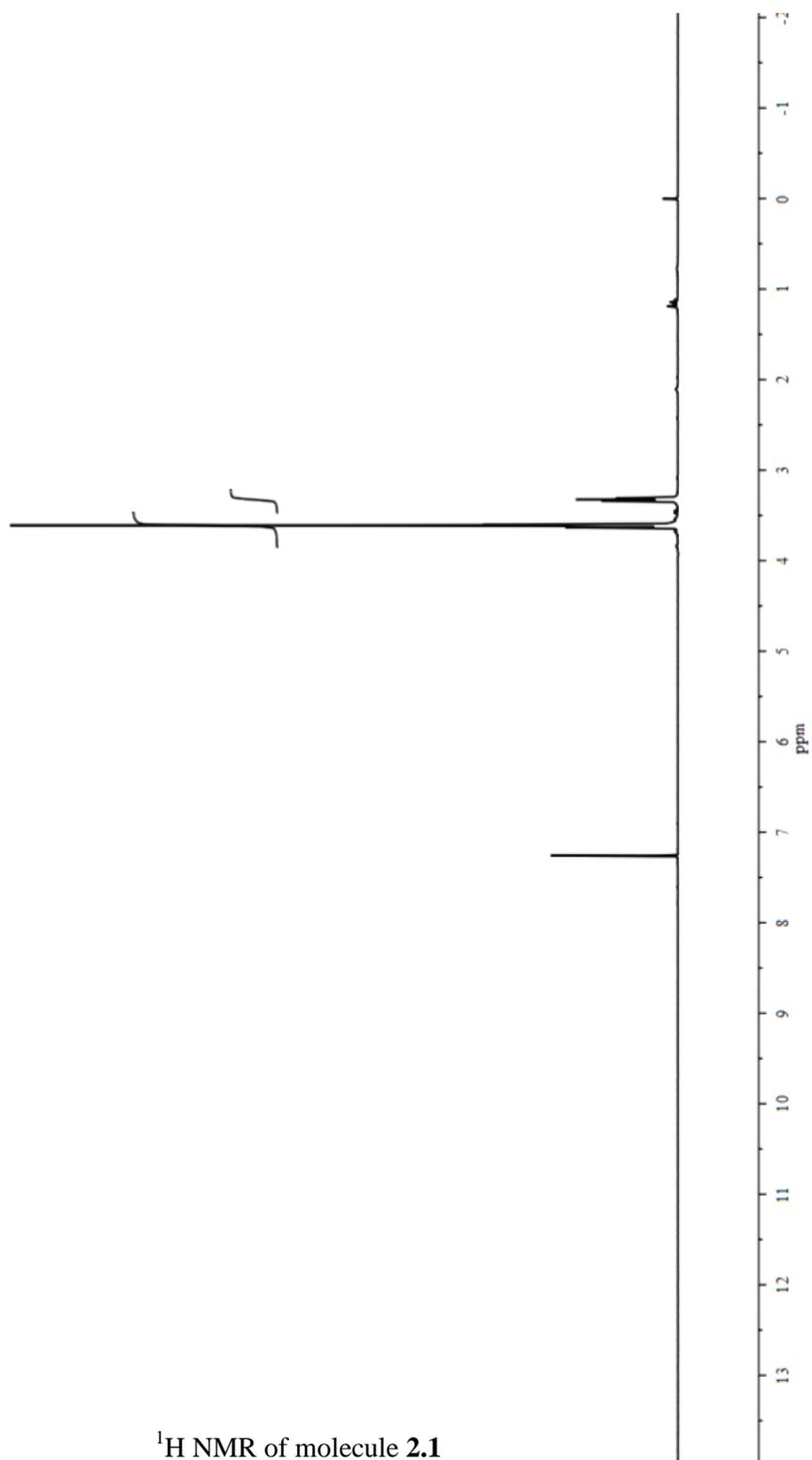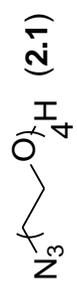
^{1}H NMR of molecule **2.1**
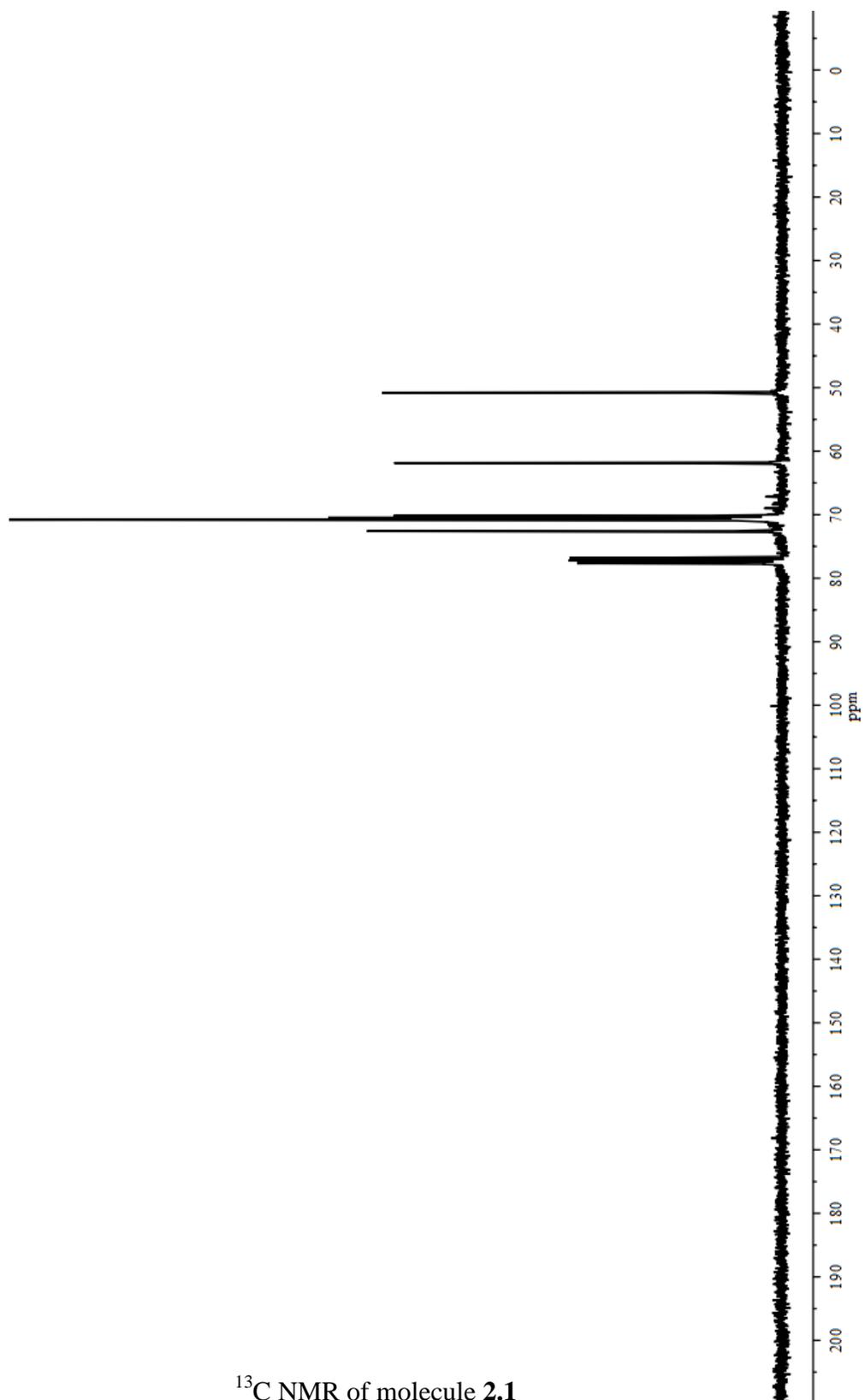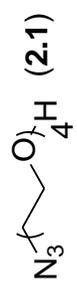
^{13}C NMR of molecule **2.1**
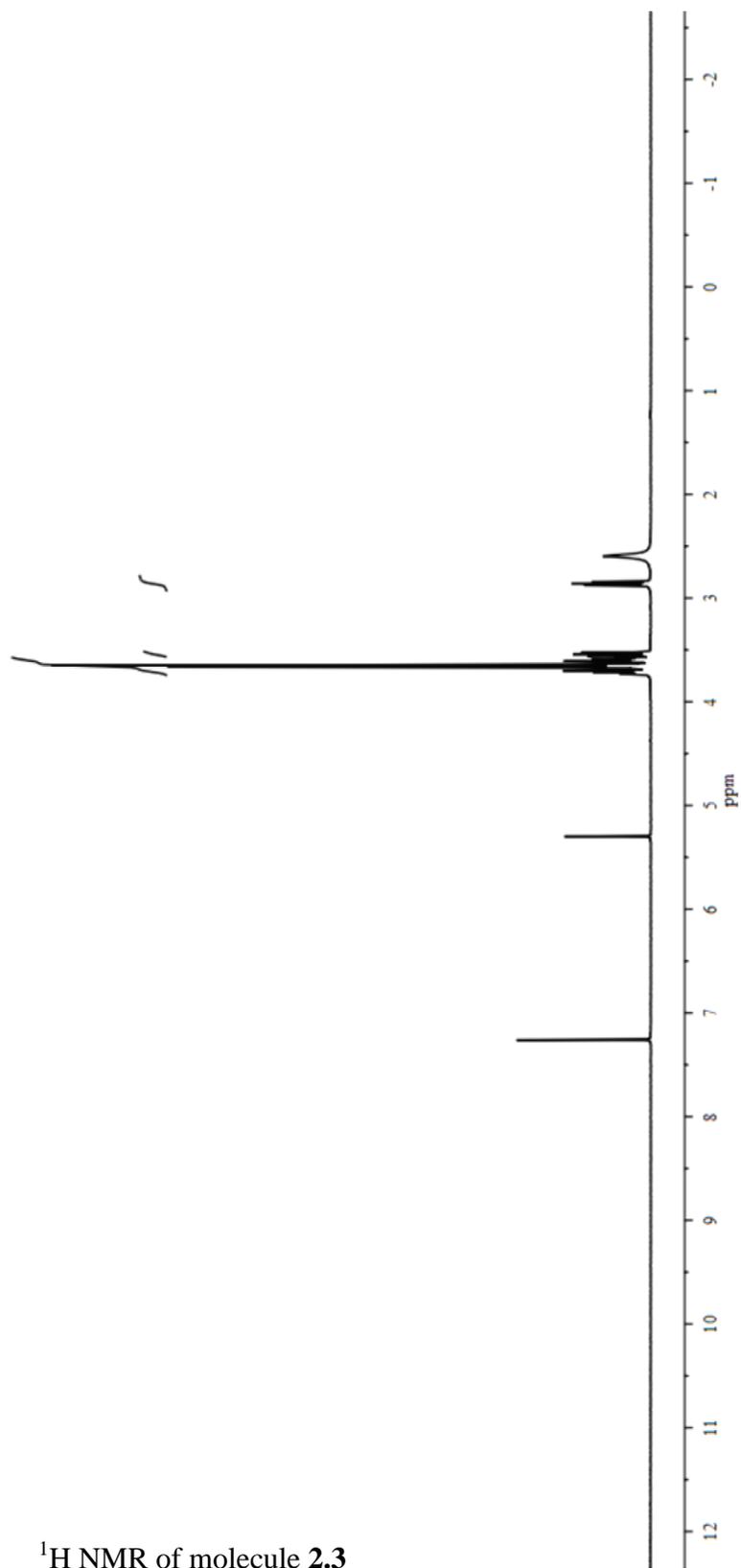
^{1}H NMR of molecule **2.3**
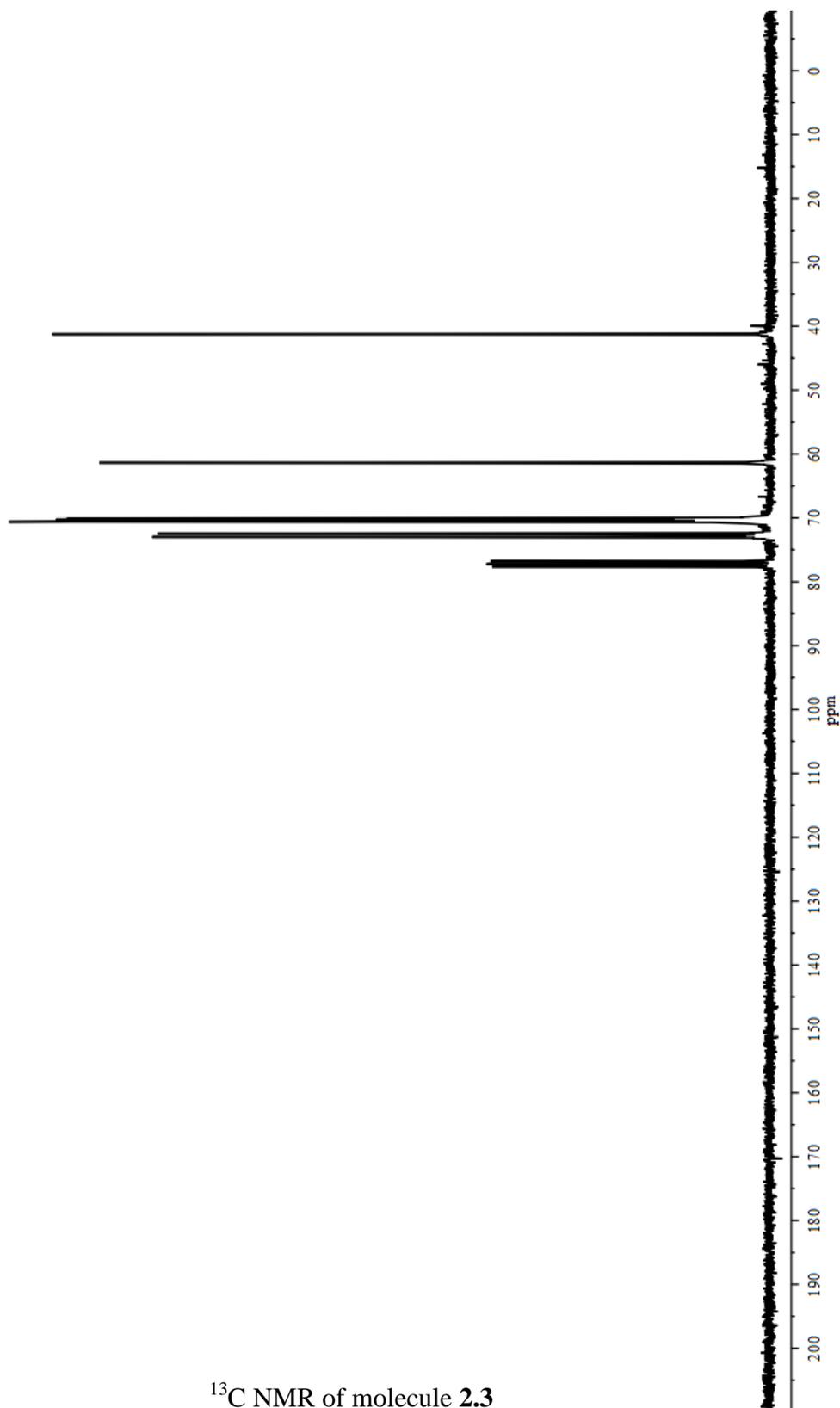
^{13}C NMR of molecule **2.3**
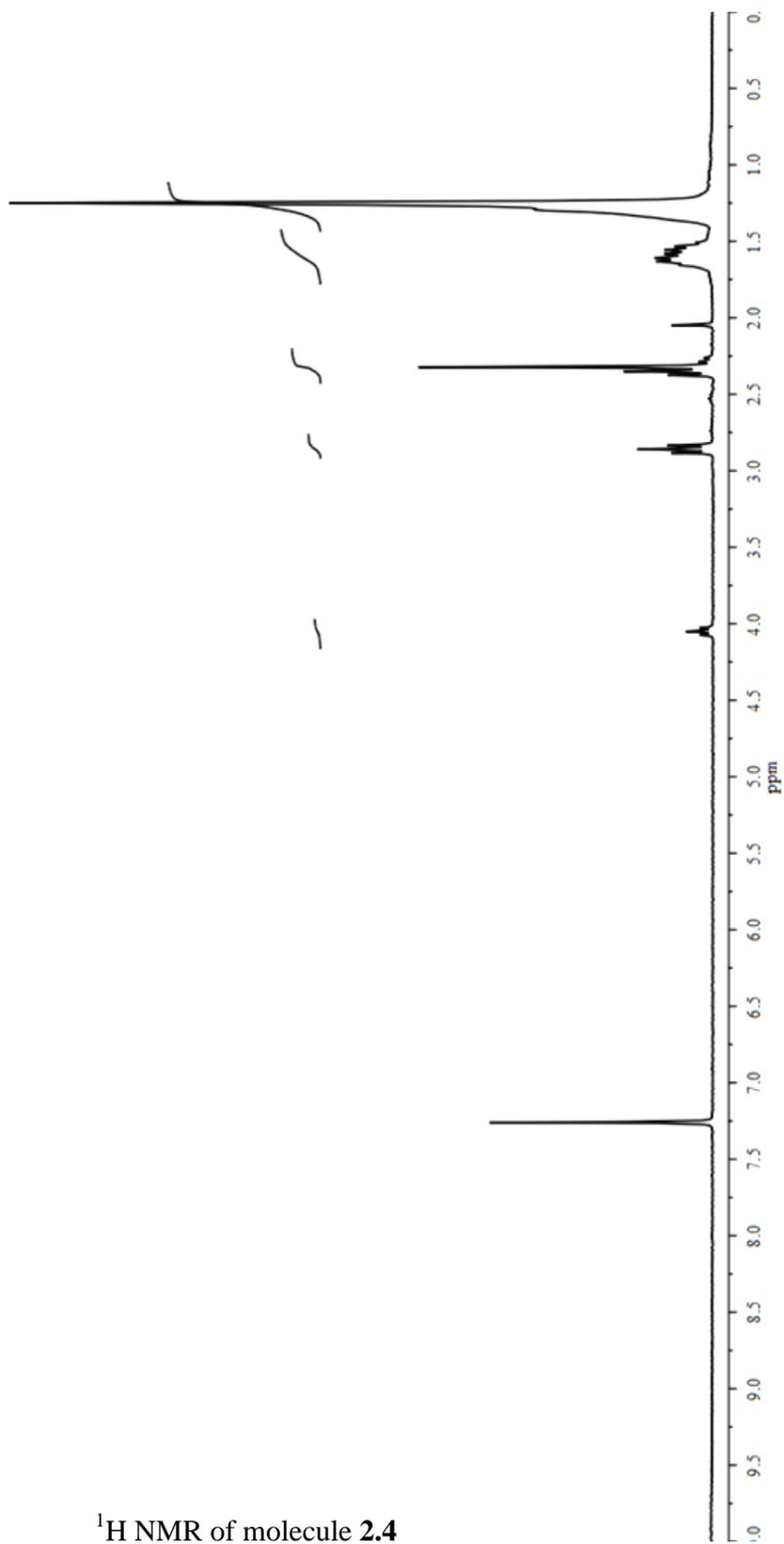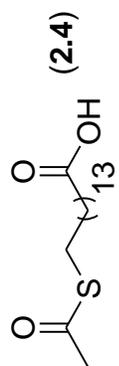
^{1}H NMR of molecule **2.4**
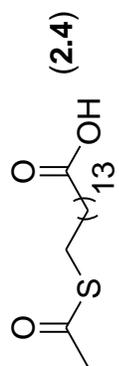
^{13}C NMR of molecule **2.4**
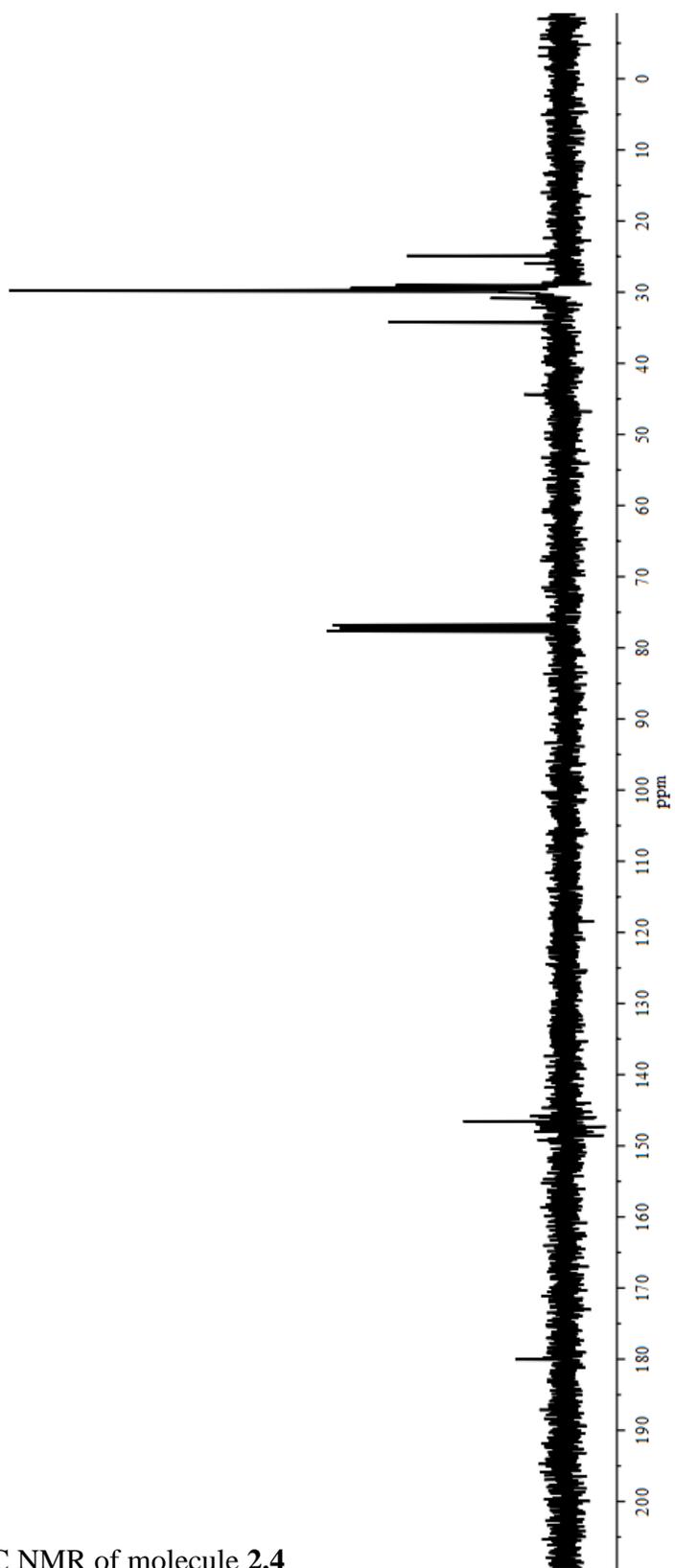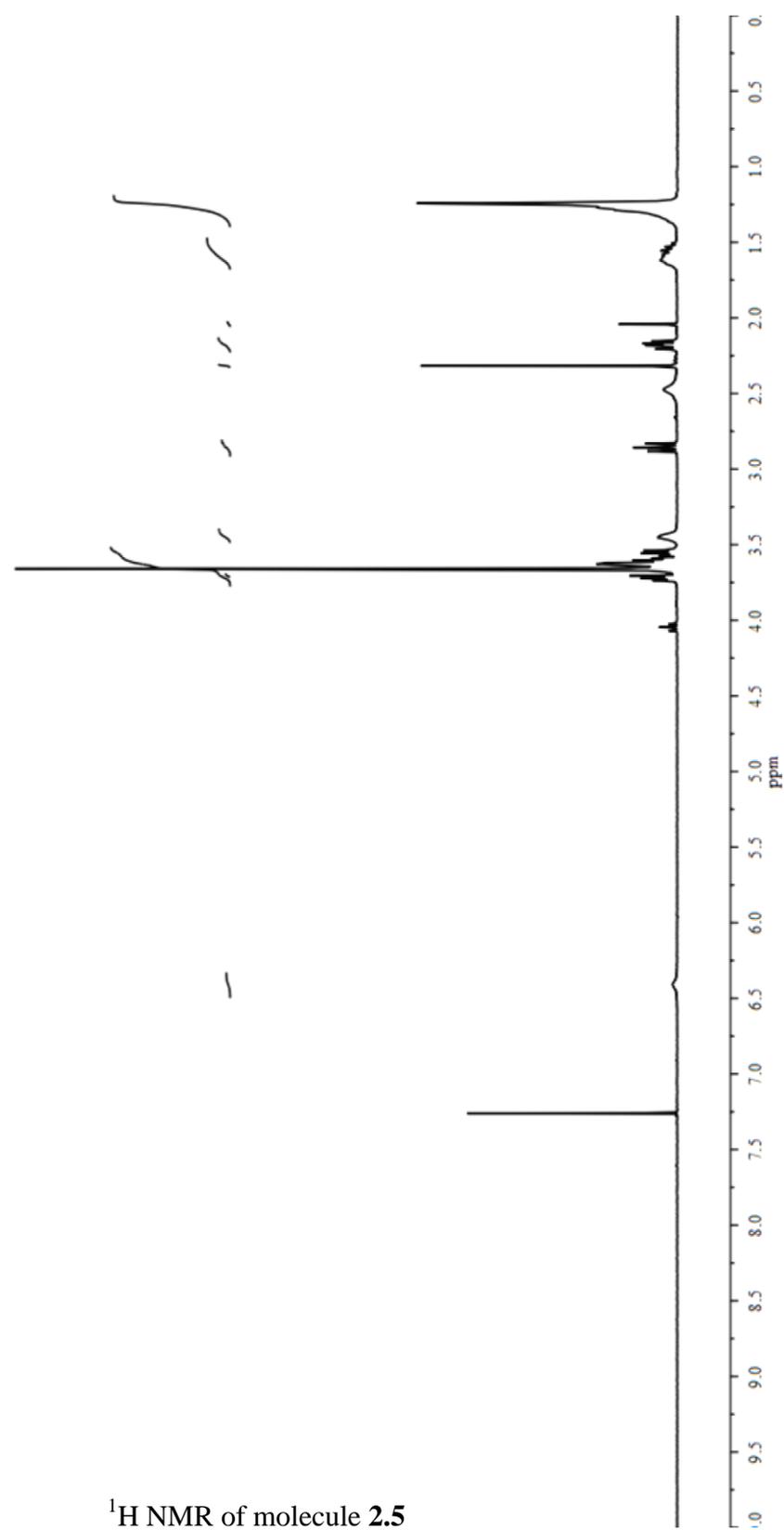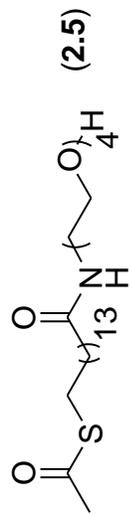
^{1}H NMR of molecule **2.5**

^{13}C NMR of molecule **2.5**
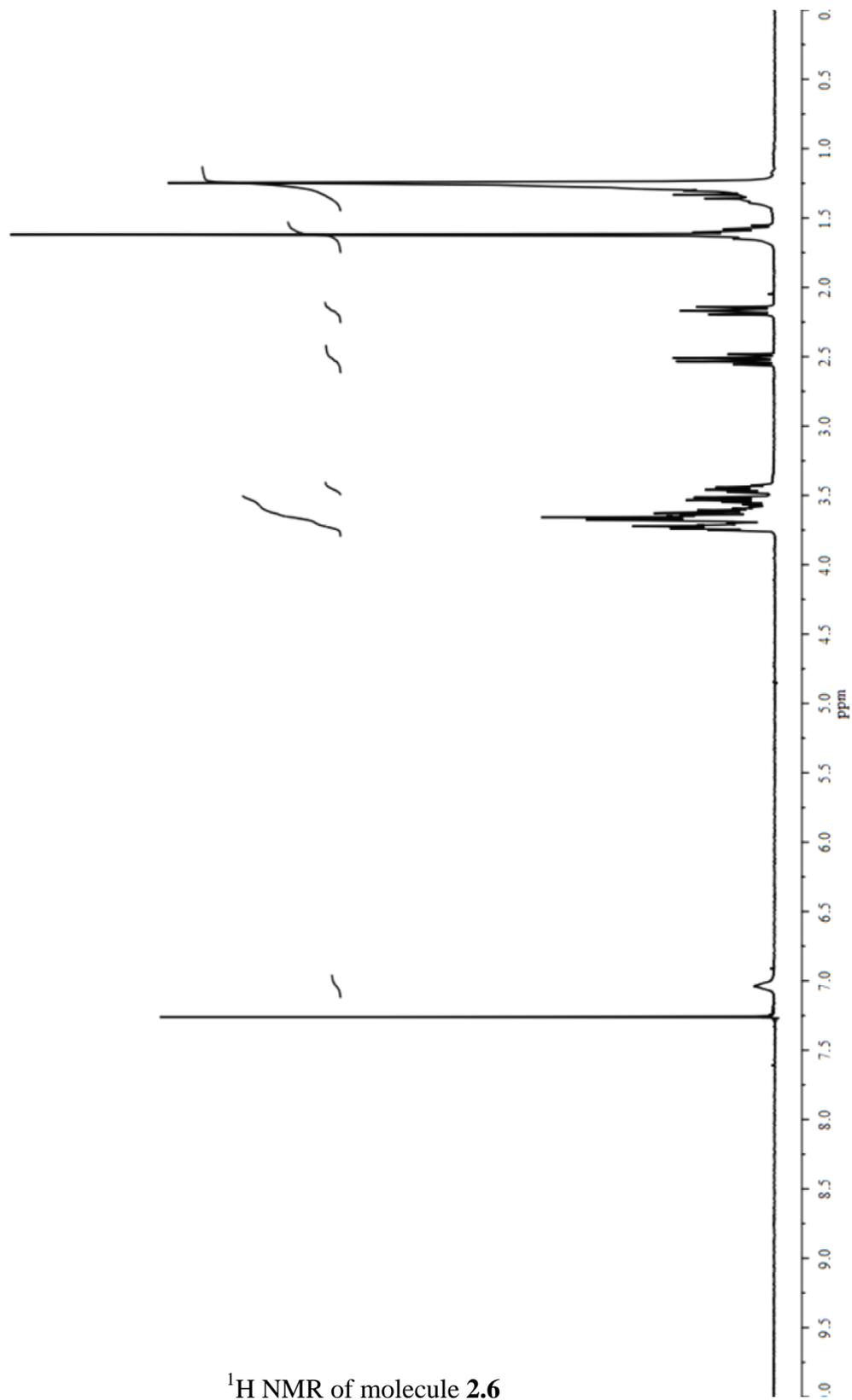
^{1}H NMR of molecule **2.6**
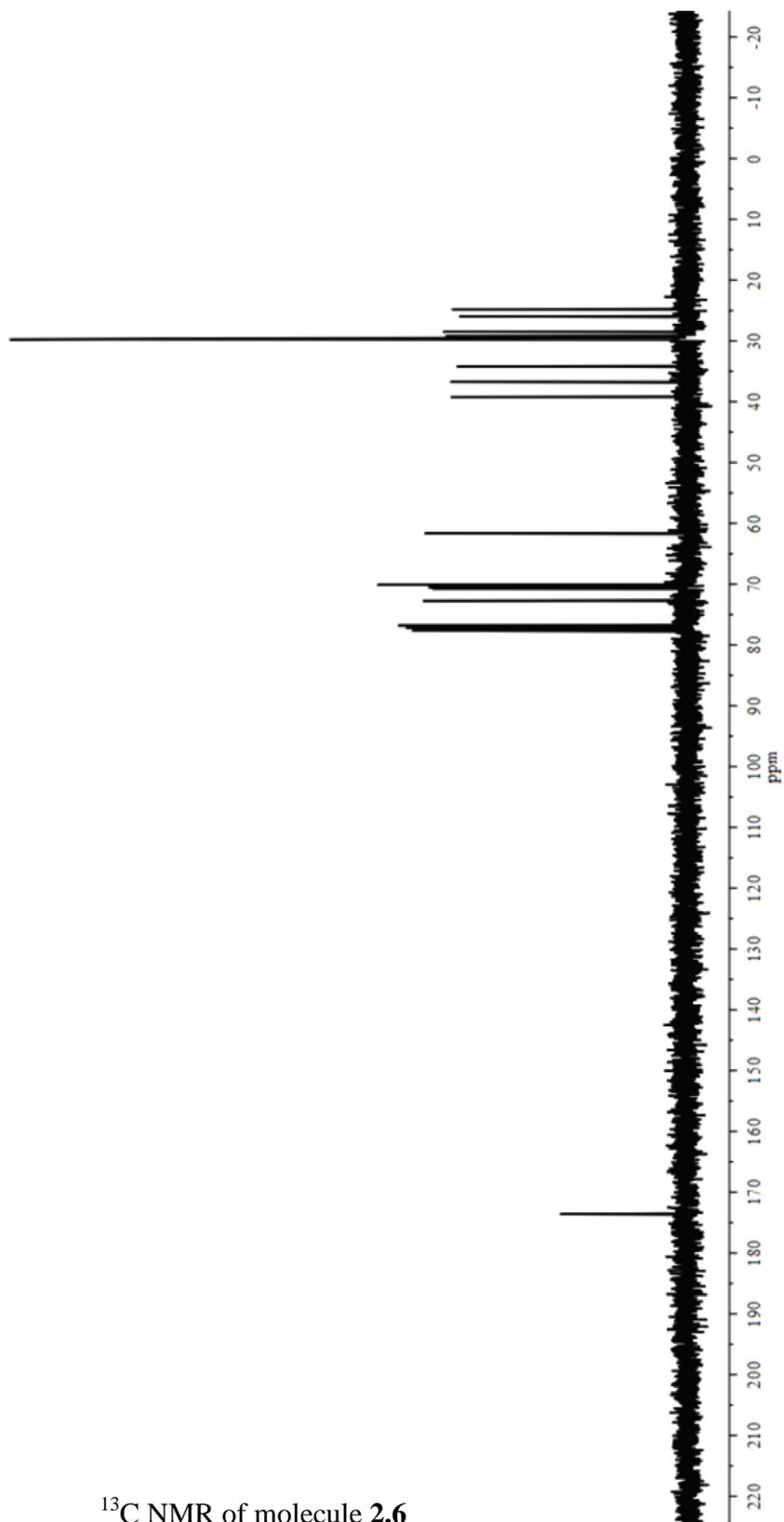
^{13}C NMR of molecule **2.6**

Appendix C

¹H and ¹³C NMR for Chapter 3
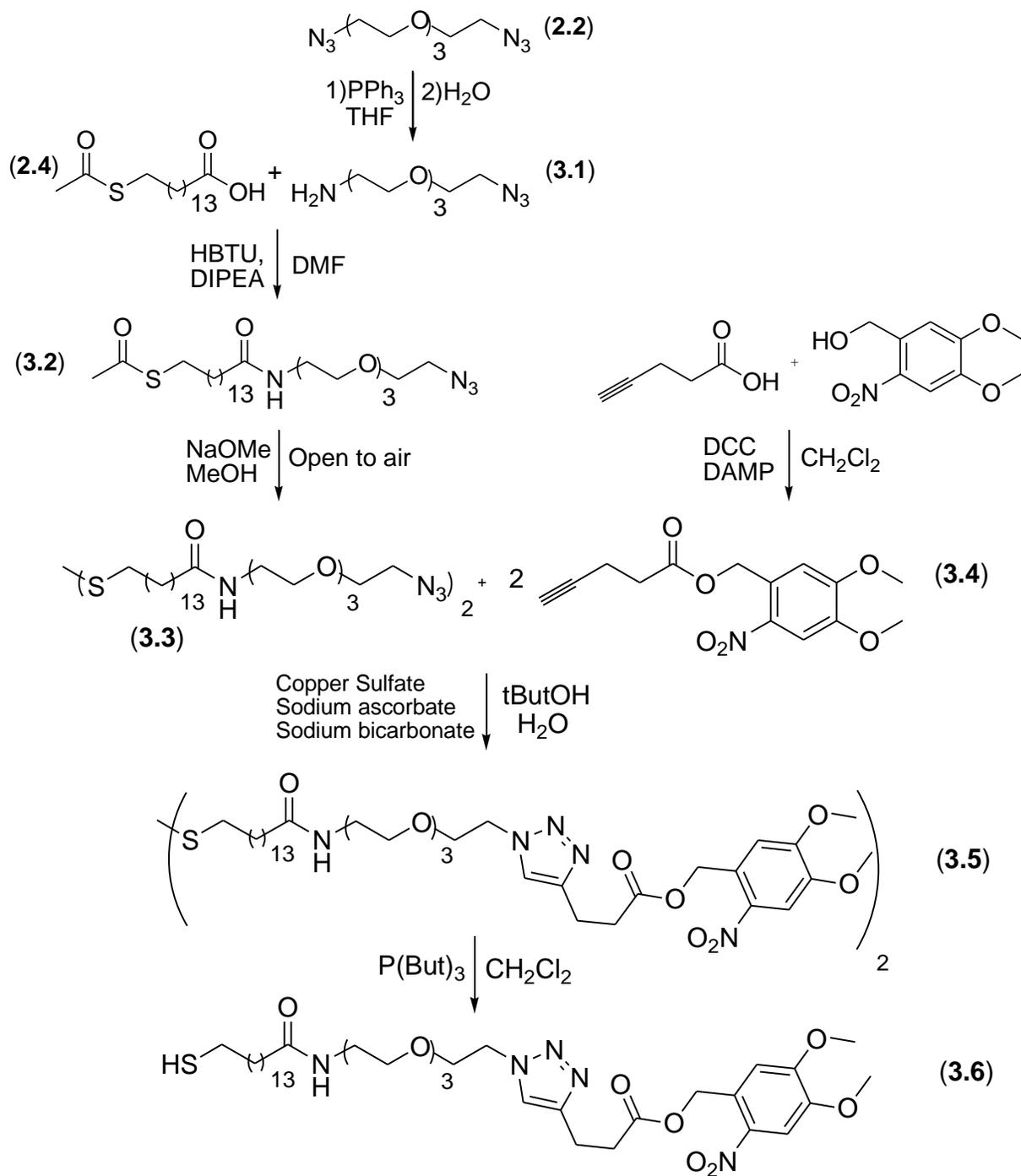
Scheme C.1. Overall Synthetic Scheme for 3.6.
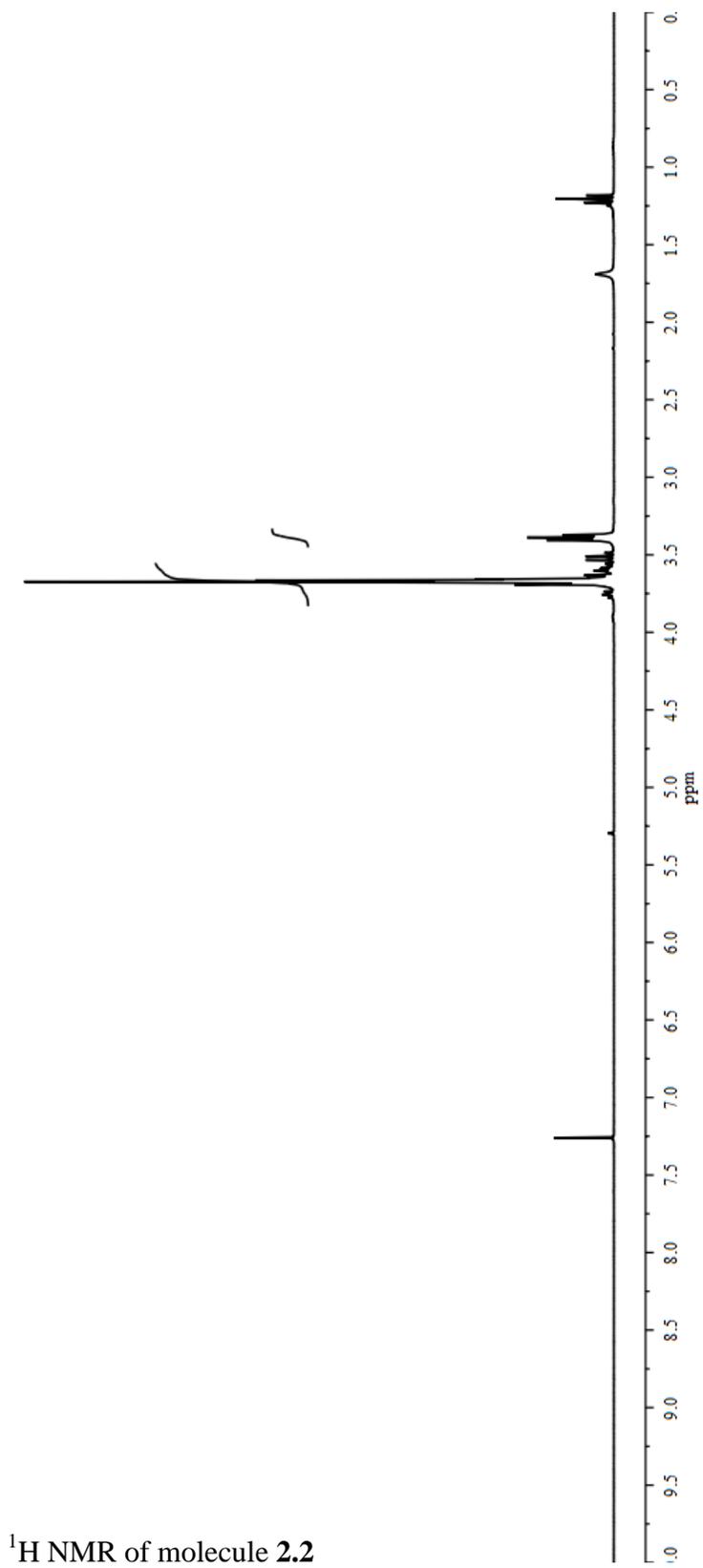
^{1}H NMR of molecule **2.2**
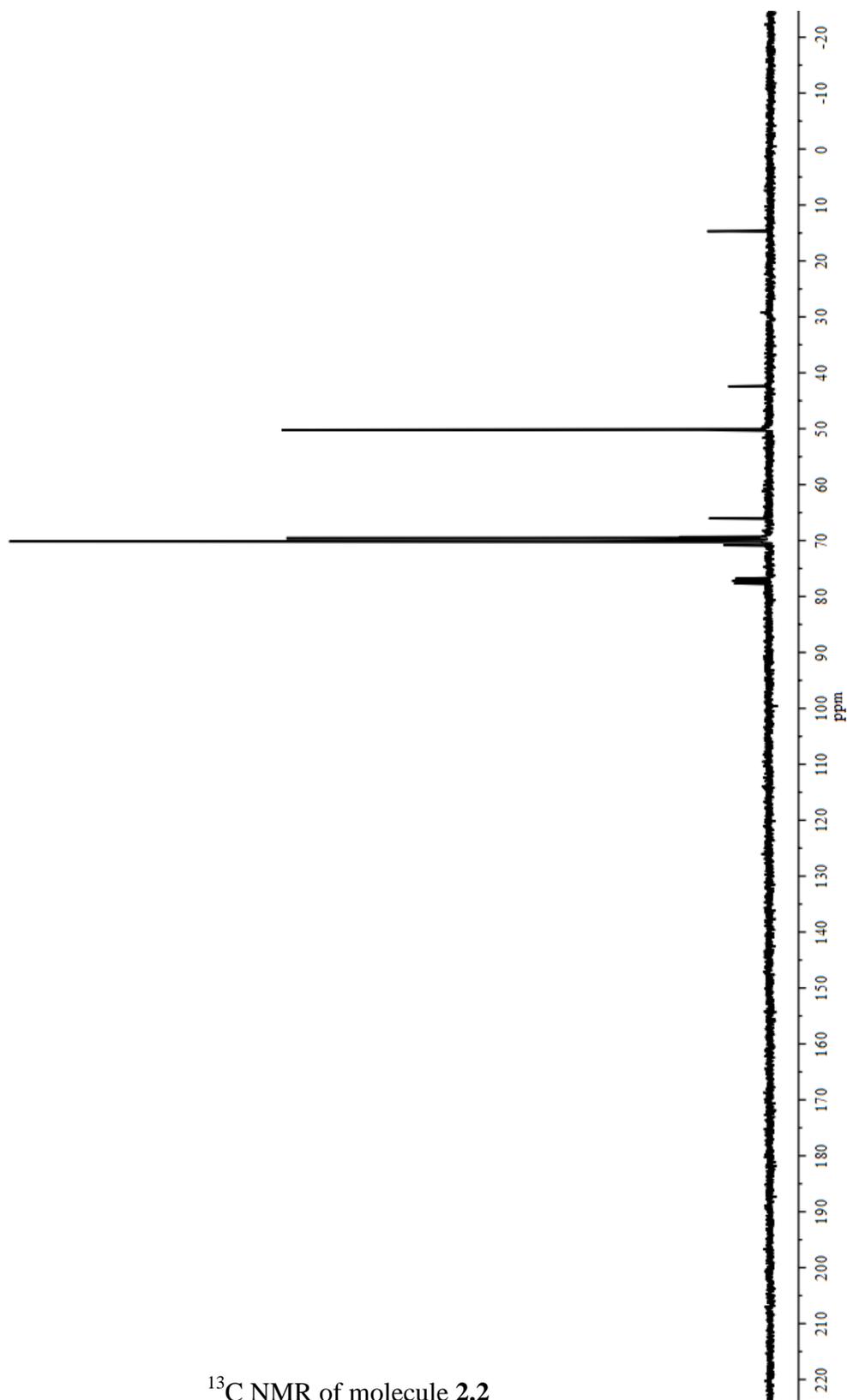
^{13}C NMR of molecule **2.2**
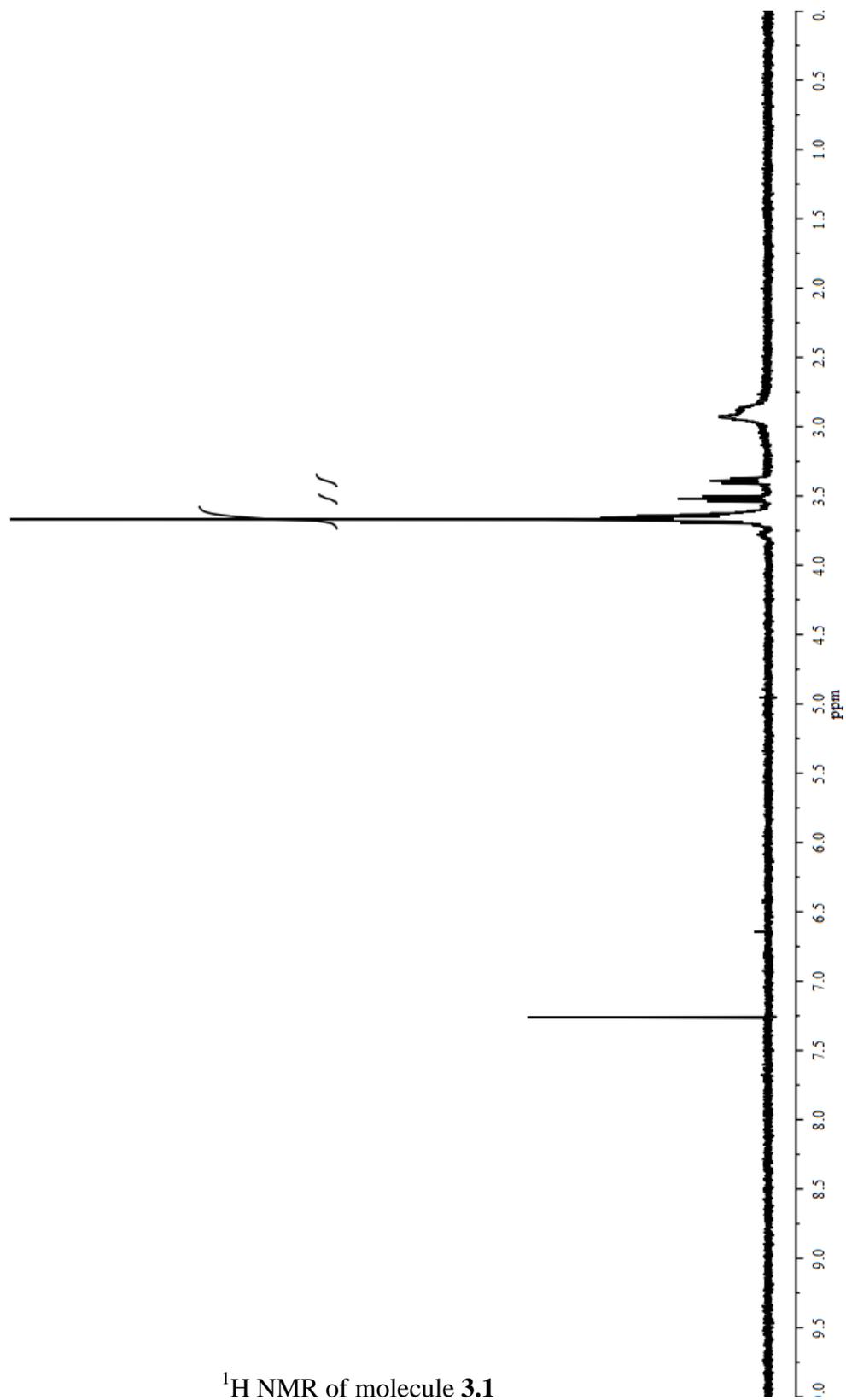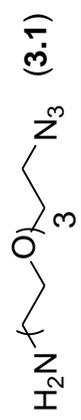
^{1}H NMR of molecule **3.1**
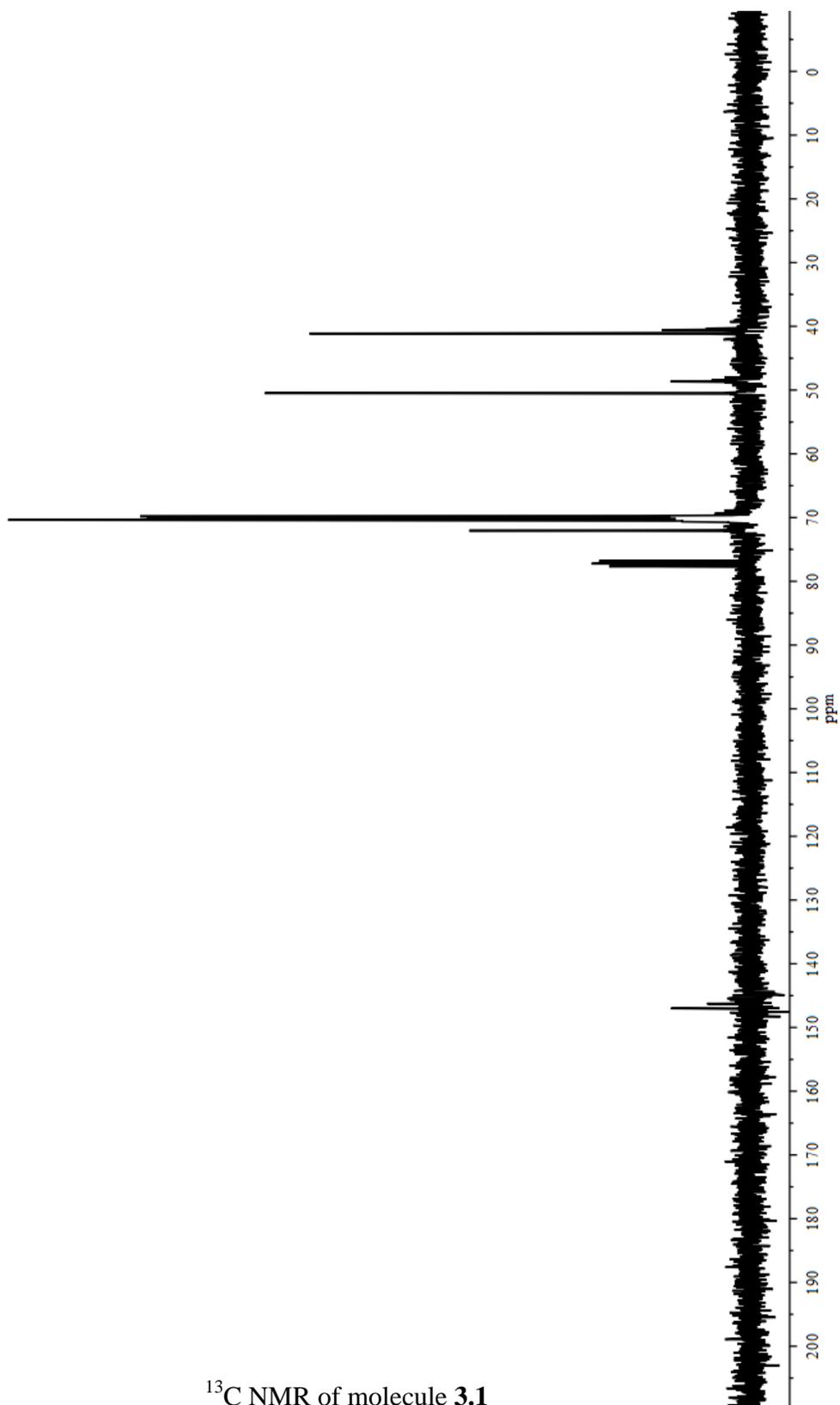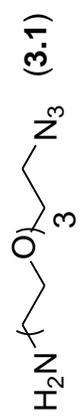
^{13}C NMR of molecule **3.1**
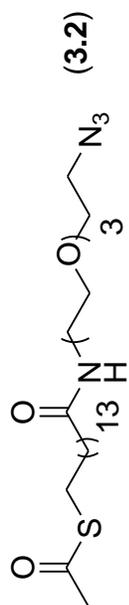
^{1}H NMR of molecule **3.2**

153
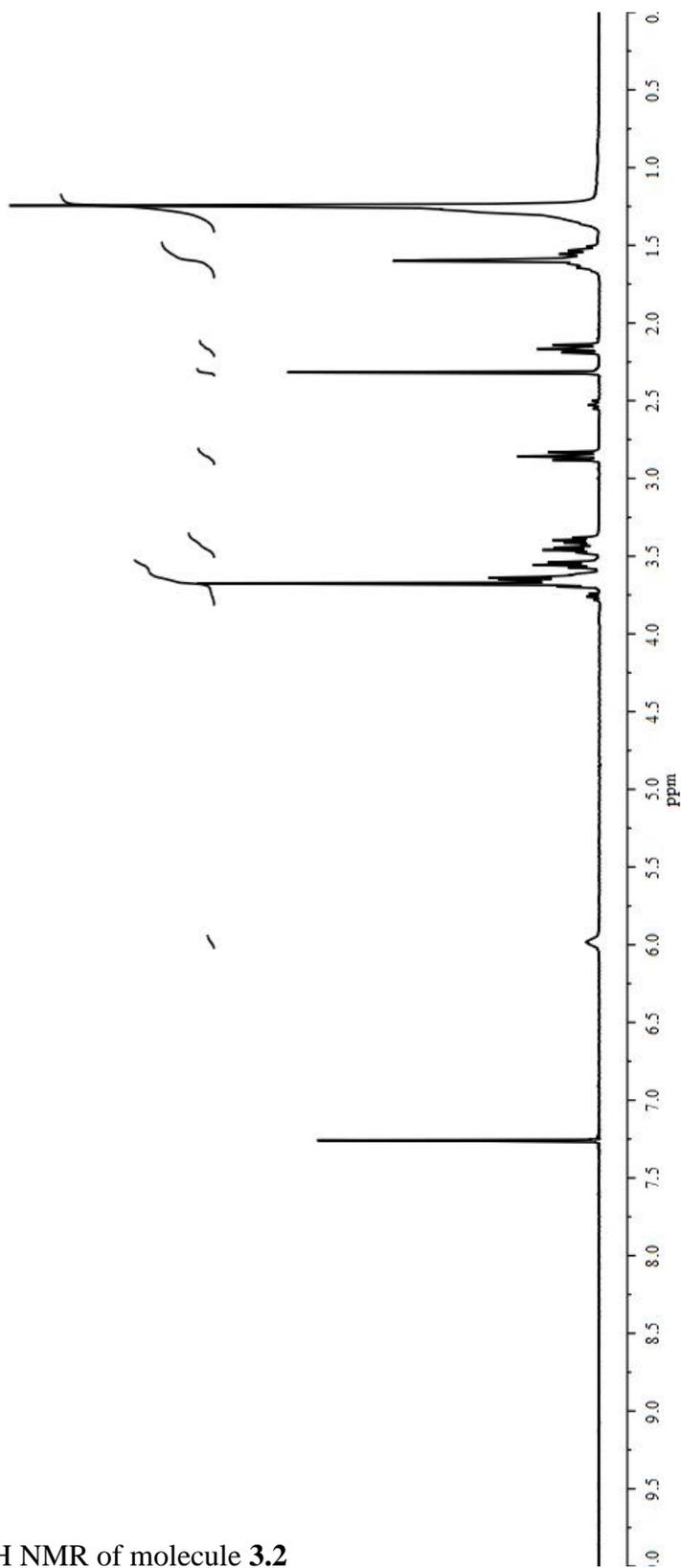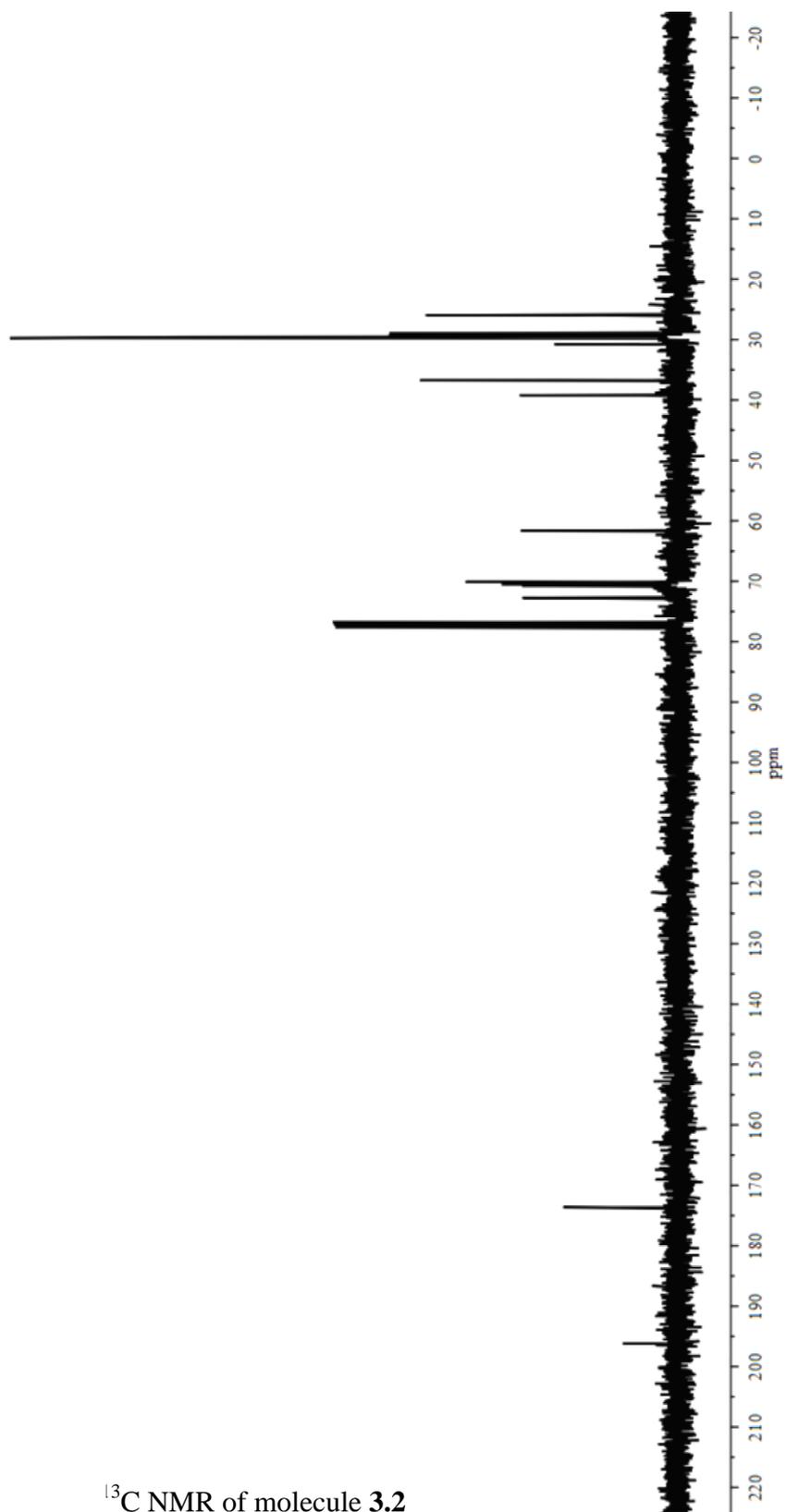
^{13}C NMR of molecule **3.2**
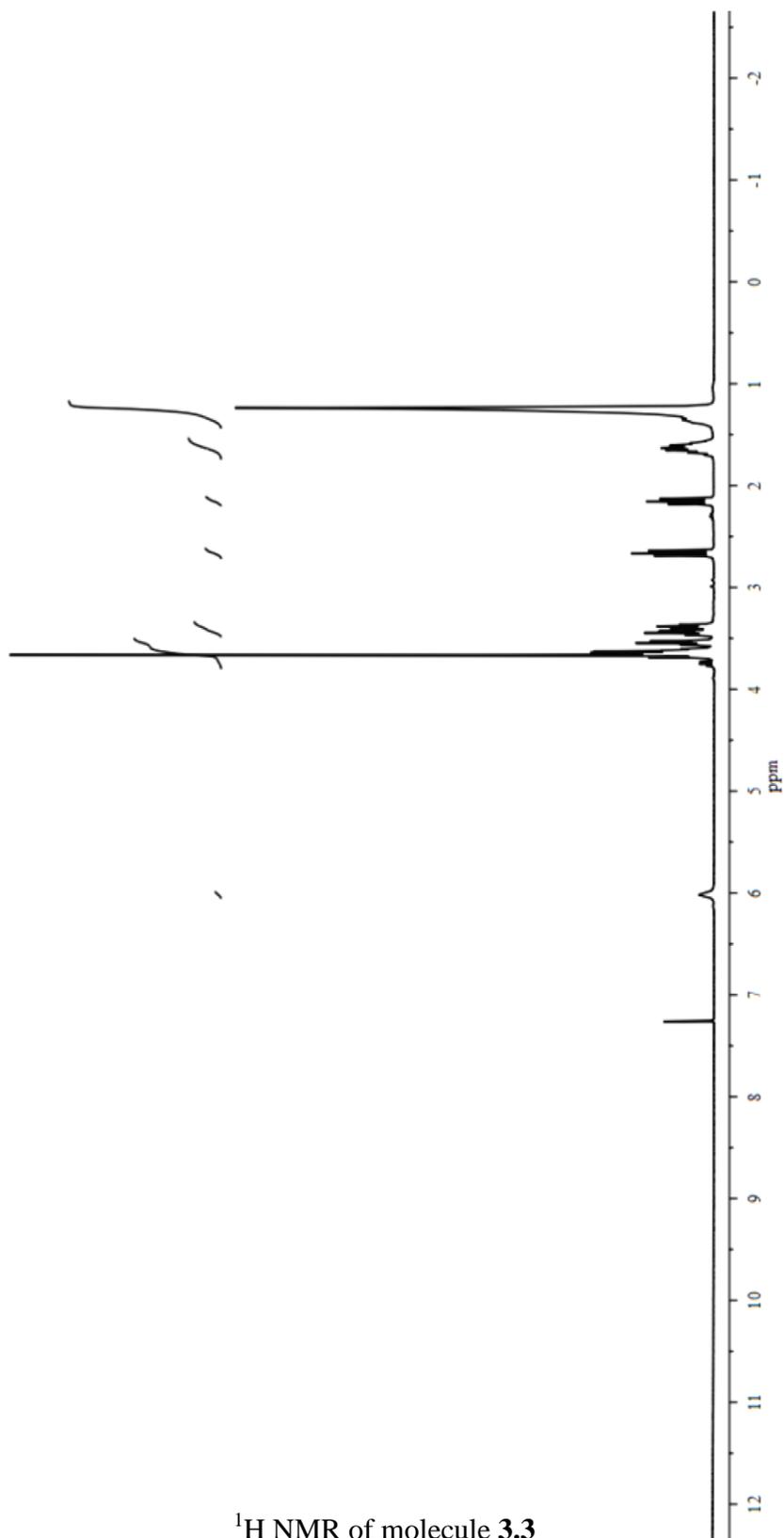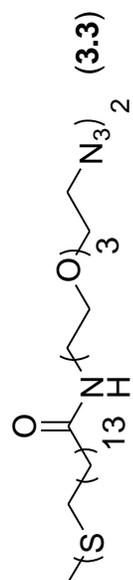
^{1}H NMR of molecule **3.3**
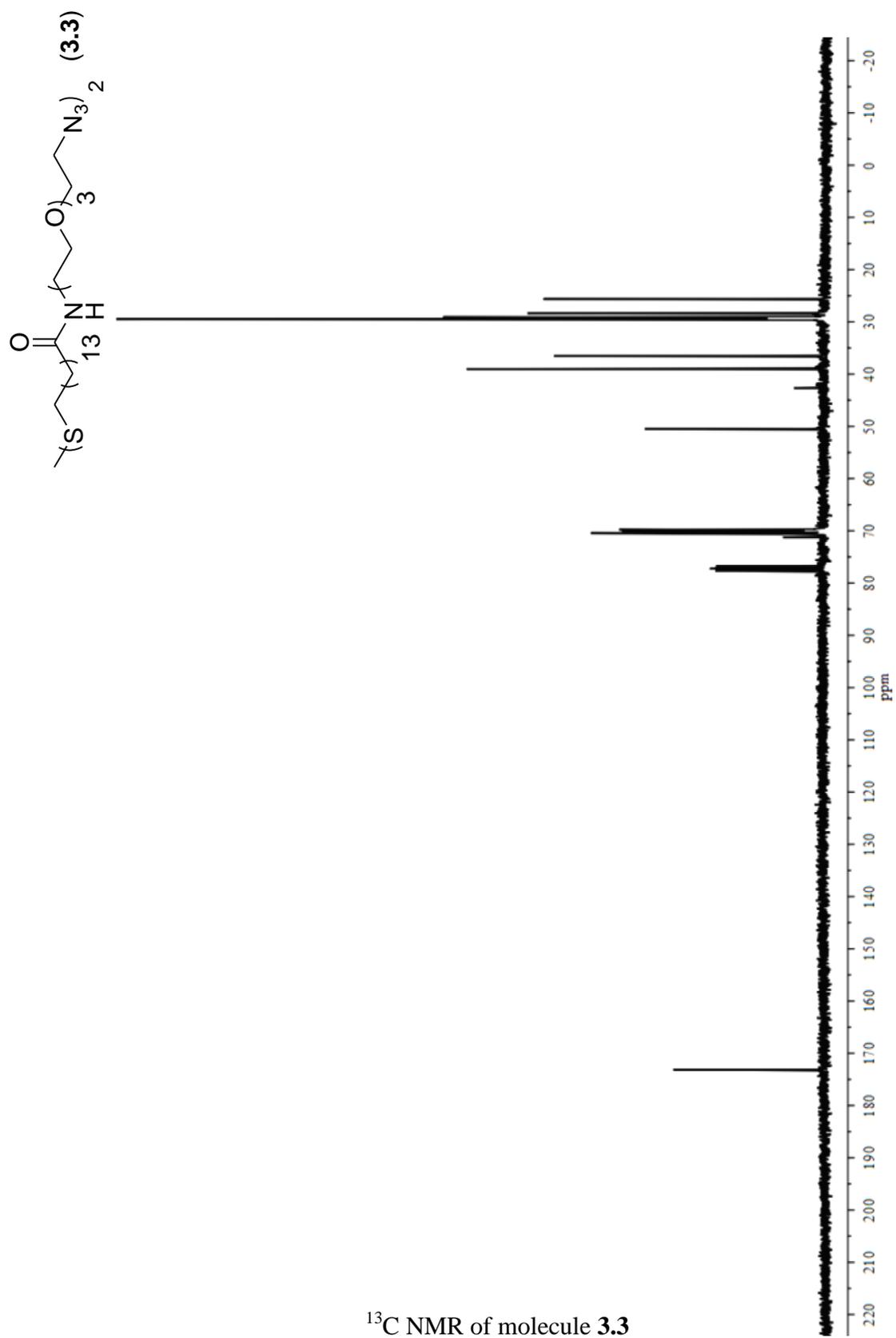
^{13}C NMR of molecule **3.3**
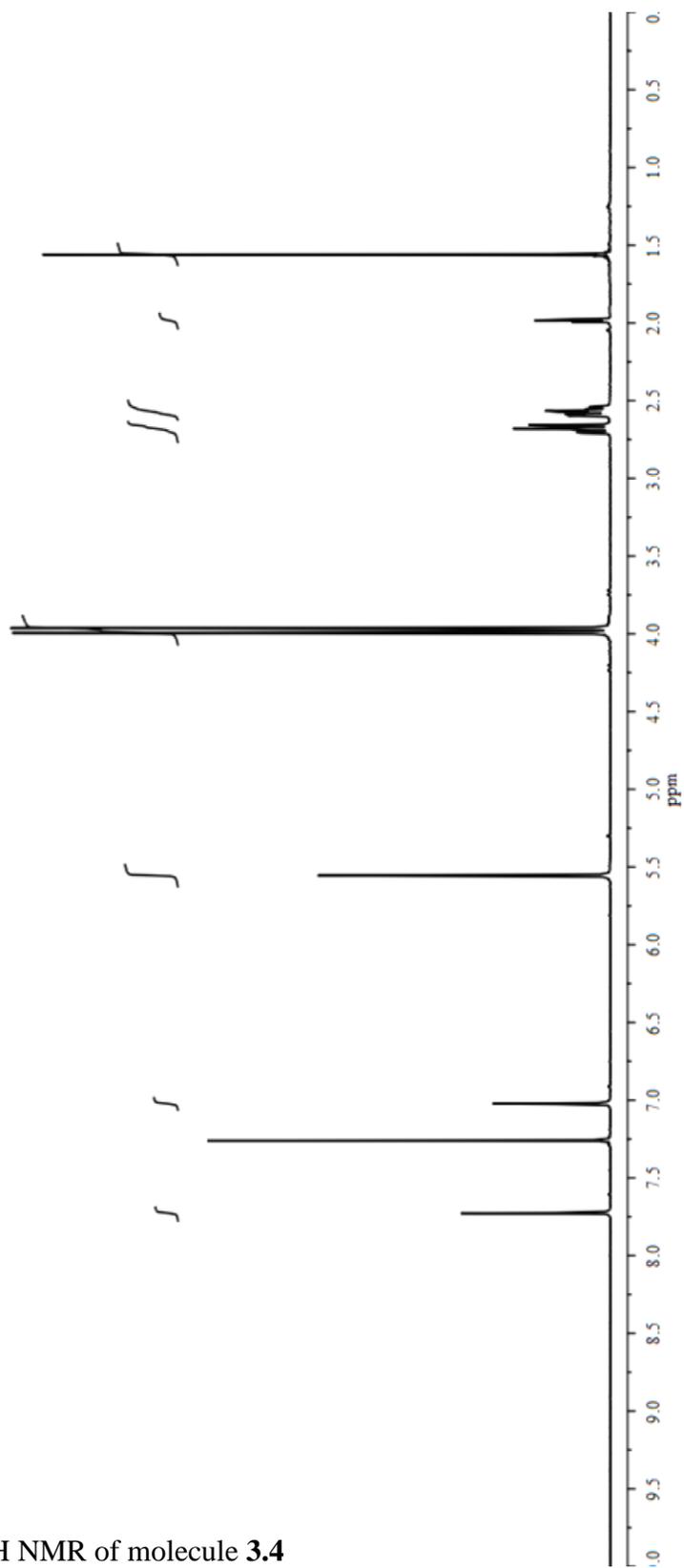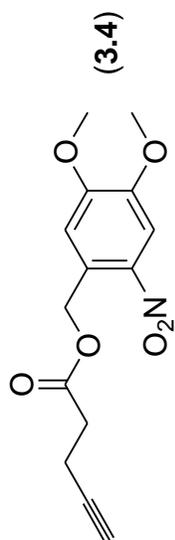
^{1}H NMR of molecule **3.4**
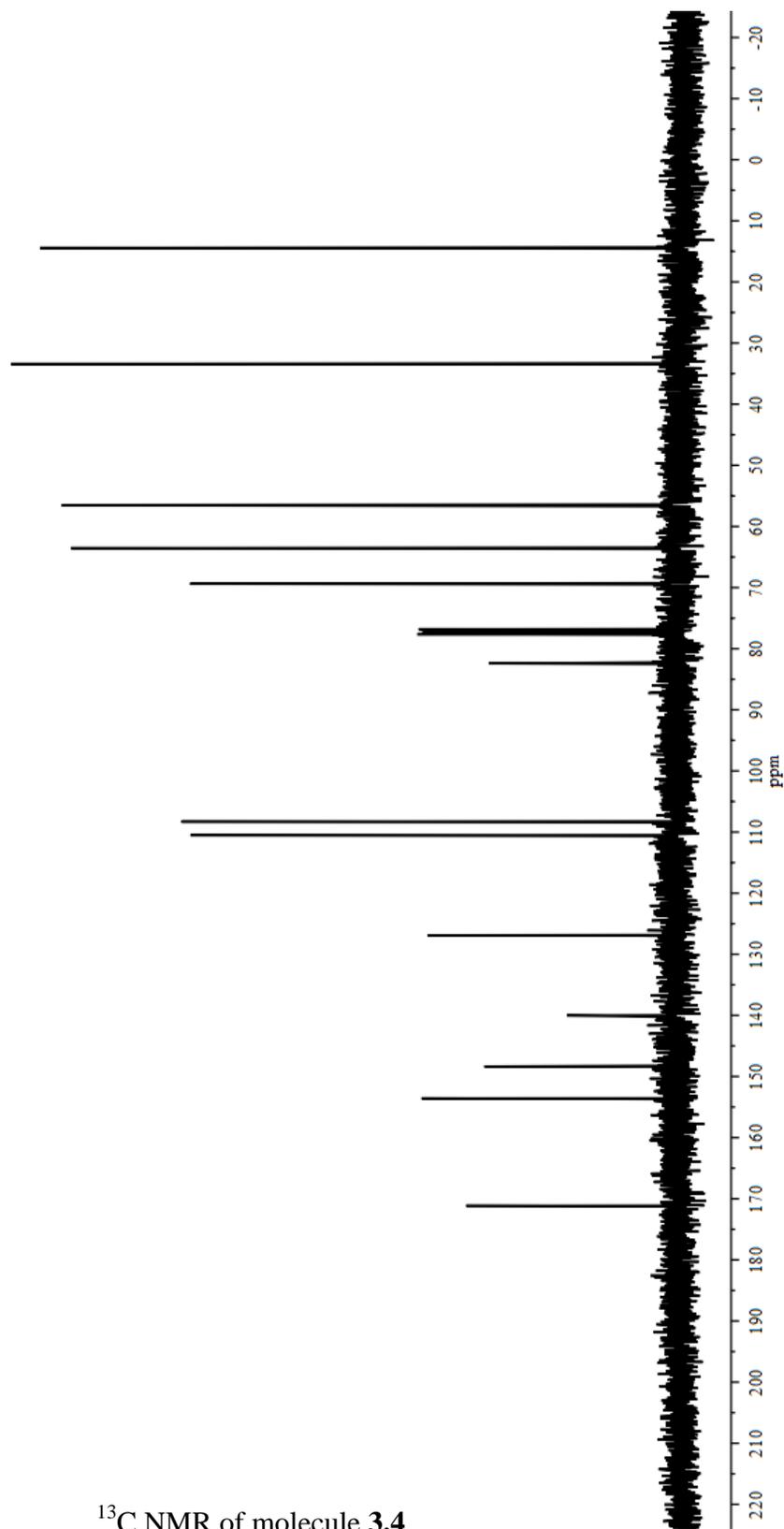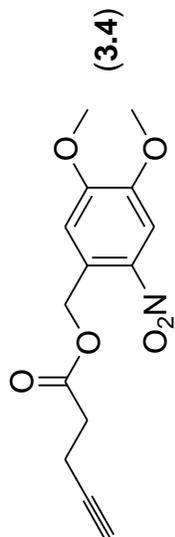
^{13}C NMR of molecule **3.4**
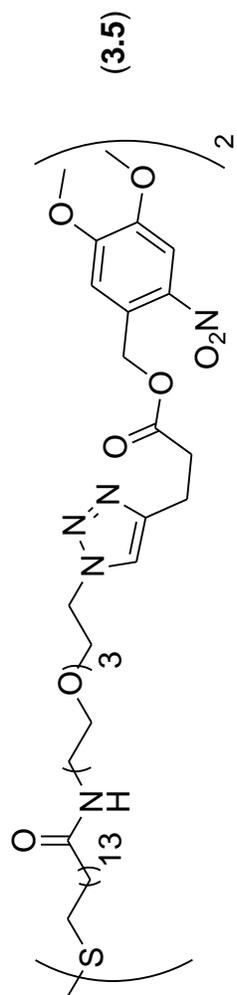
^{1}H NMR of molecule **3.5**

(3.5)

^{13}C NMR of molecule **3.5**
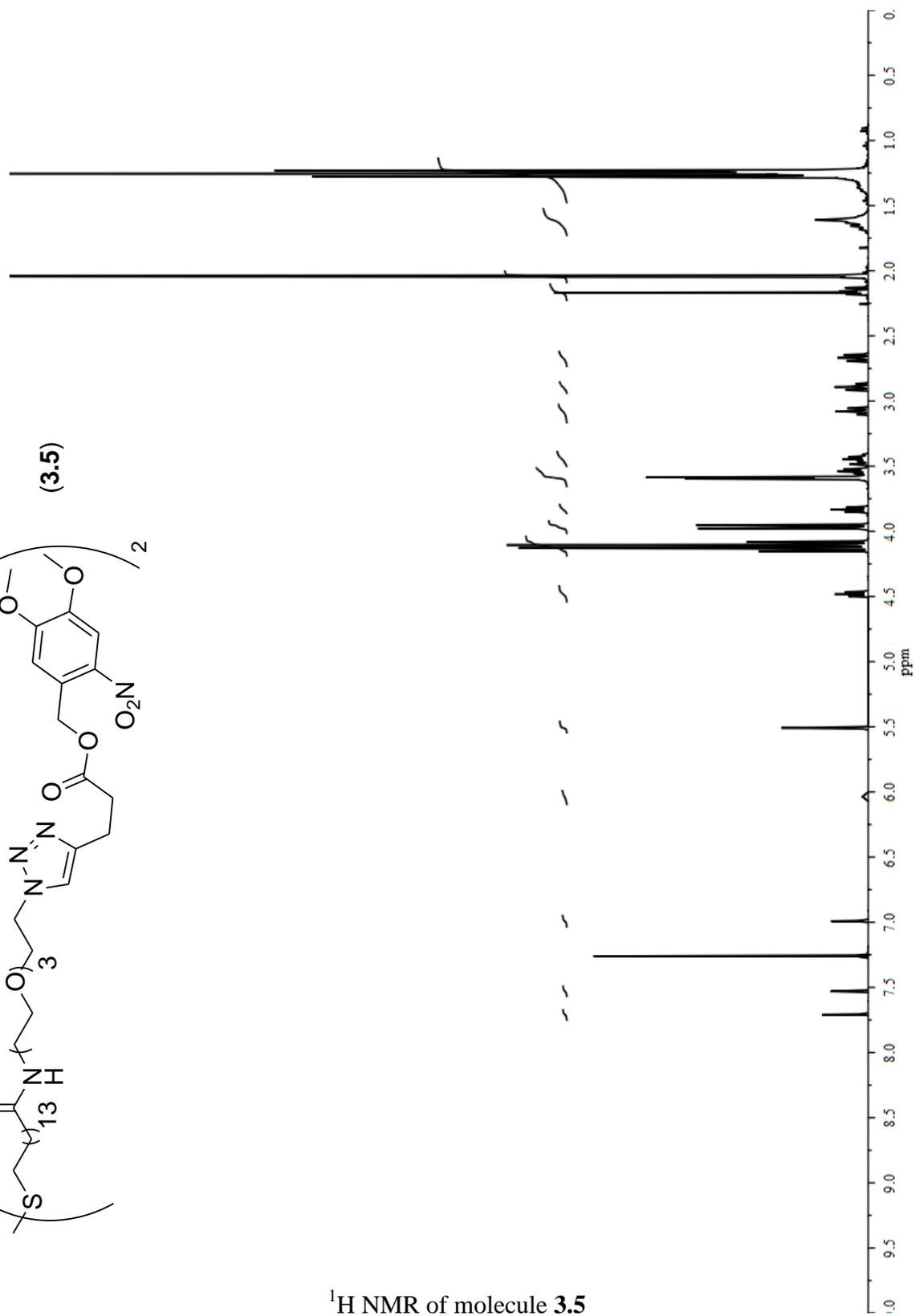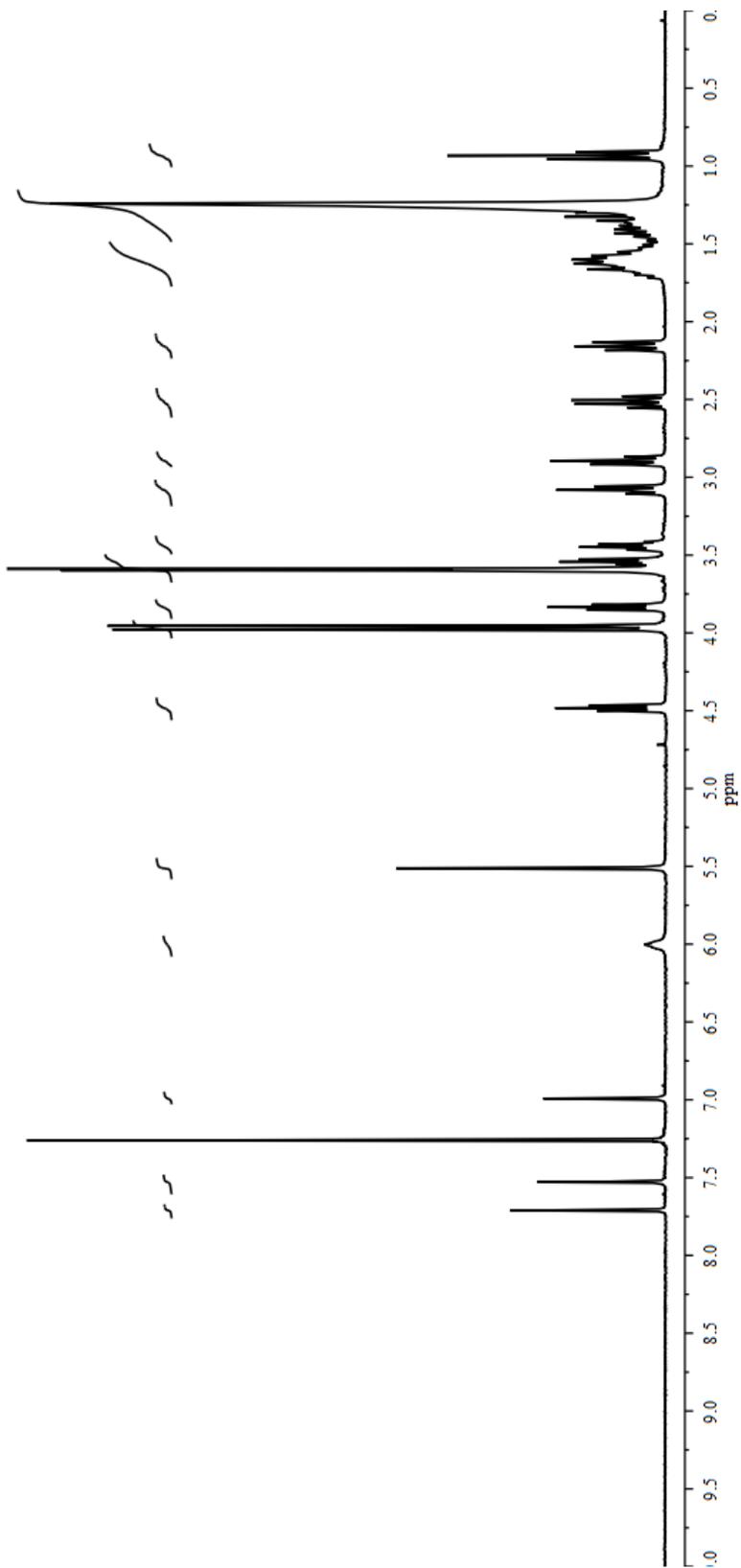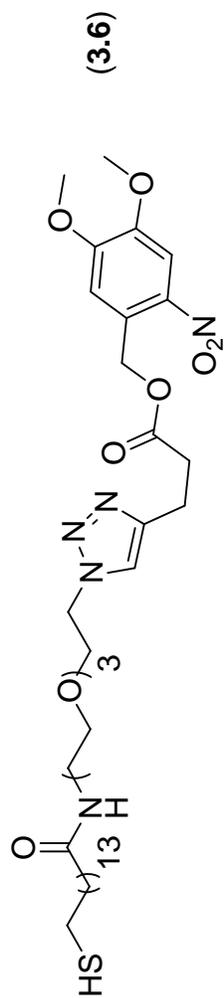
^{1}H NMR of molecule **3.6**

(3.6)
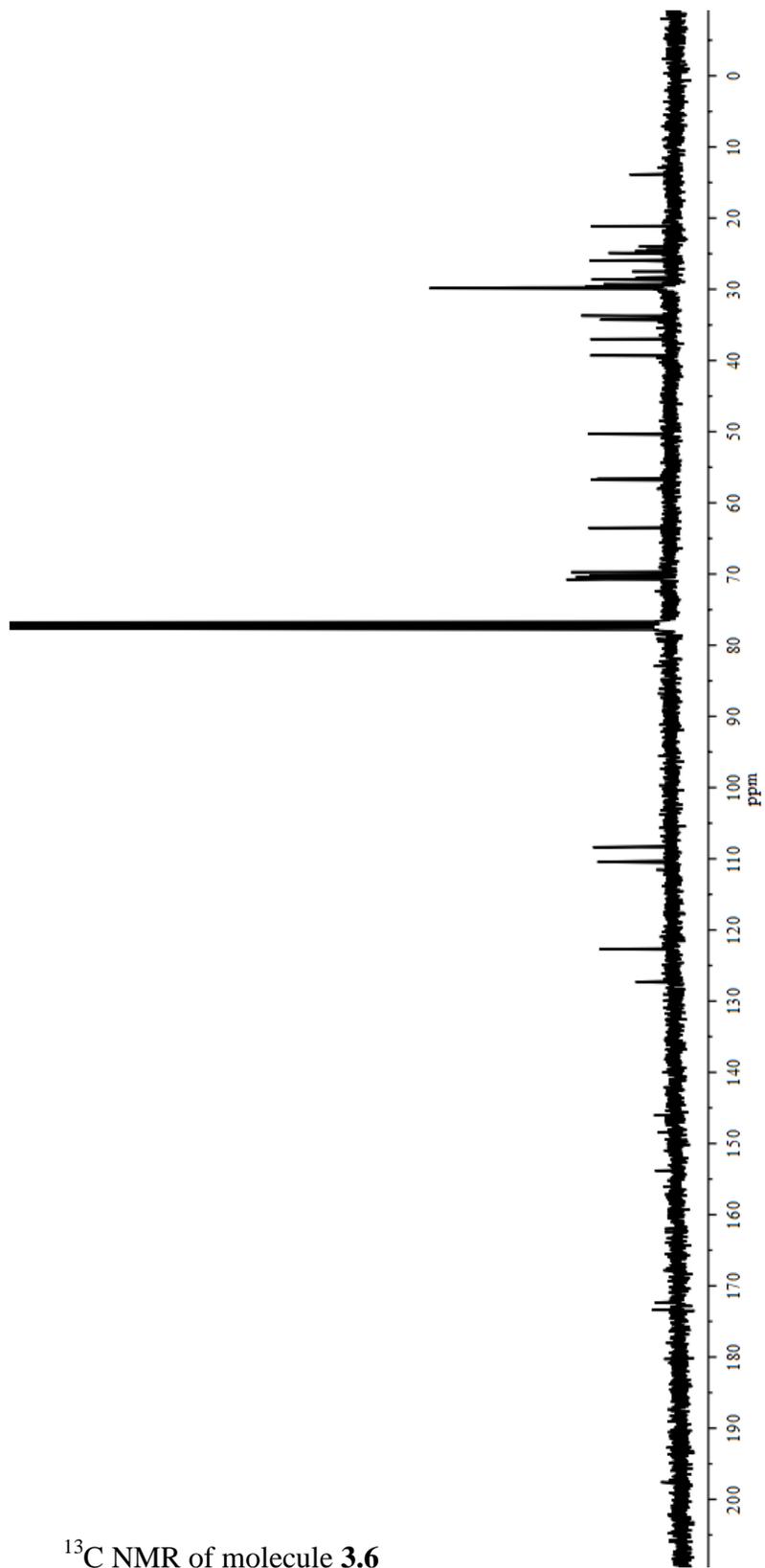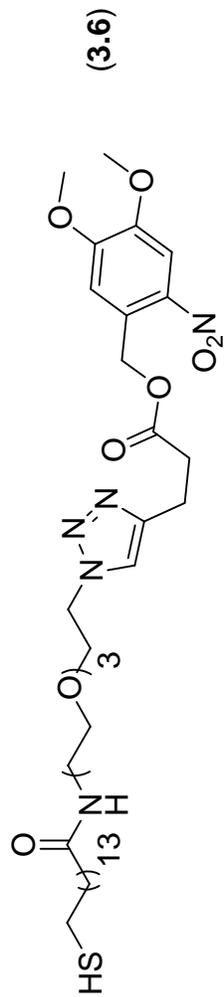
^{13}C NMR of molecule **3.6**
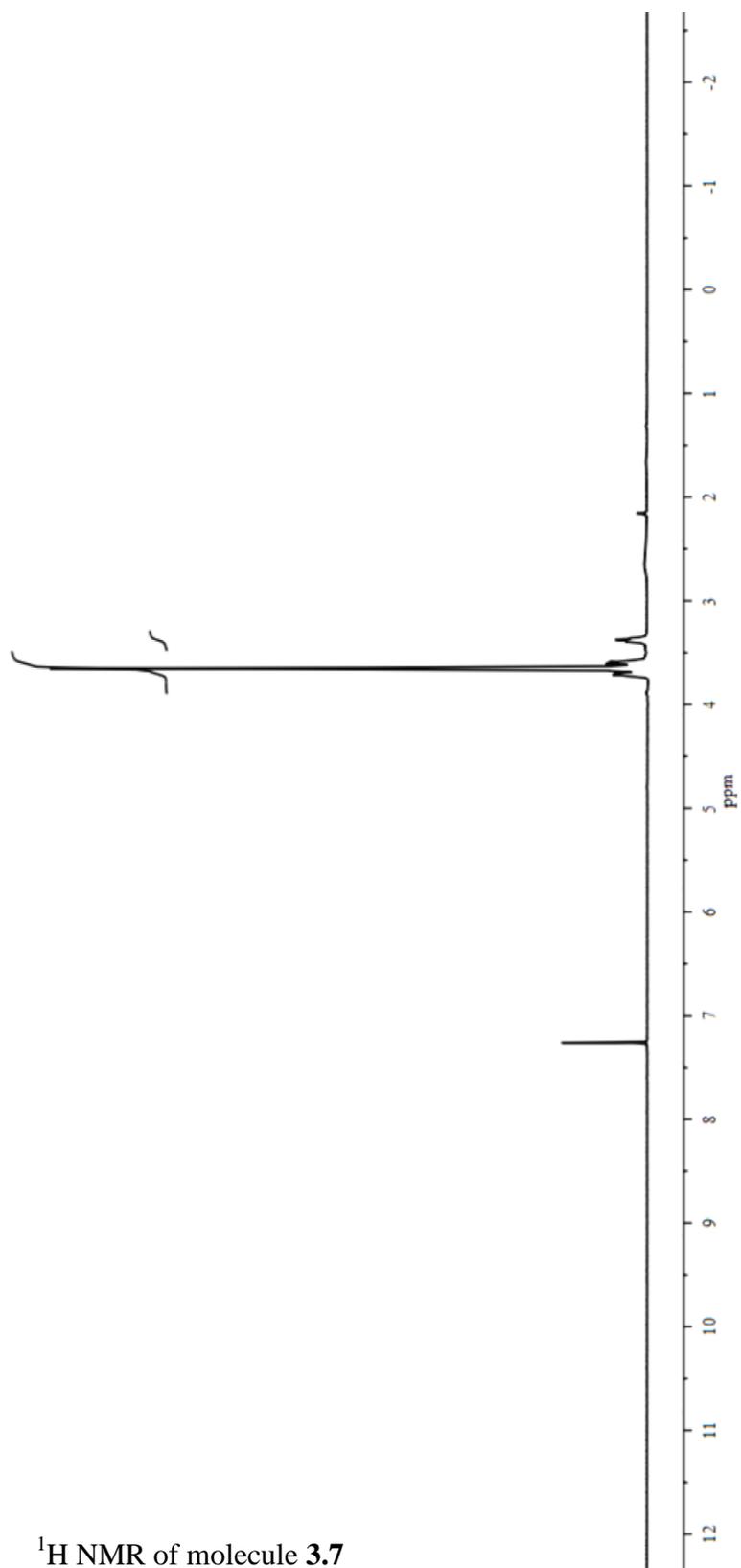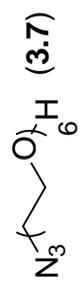
^{1}H NMR of molecule **3.7**

163
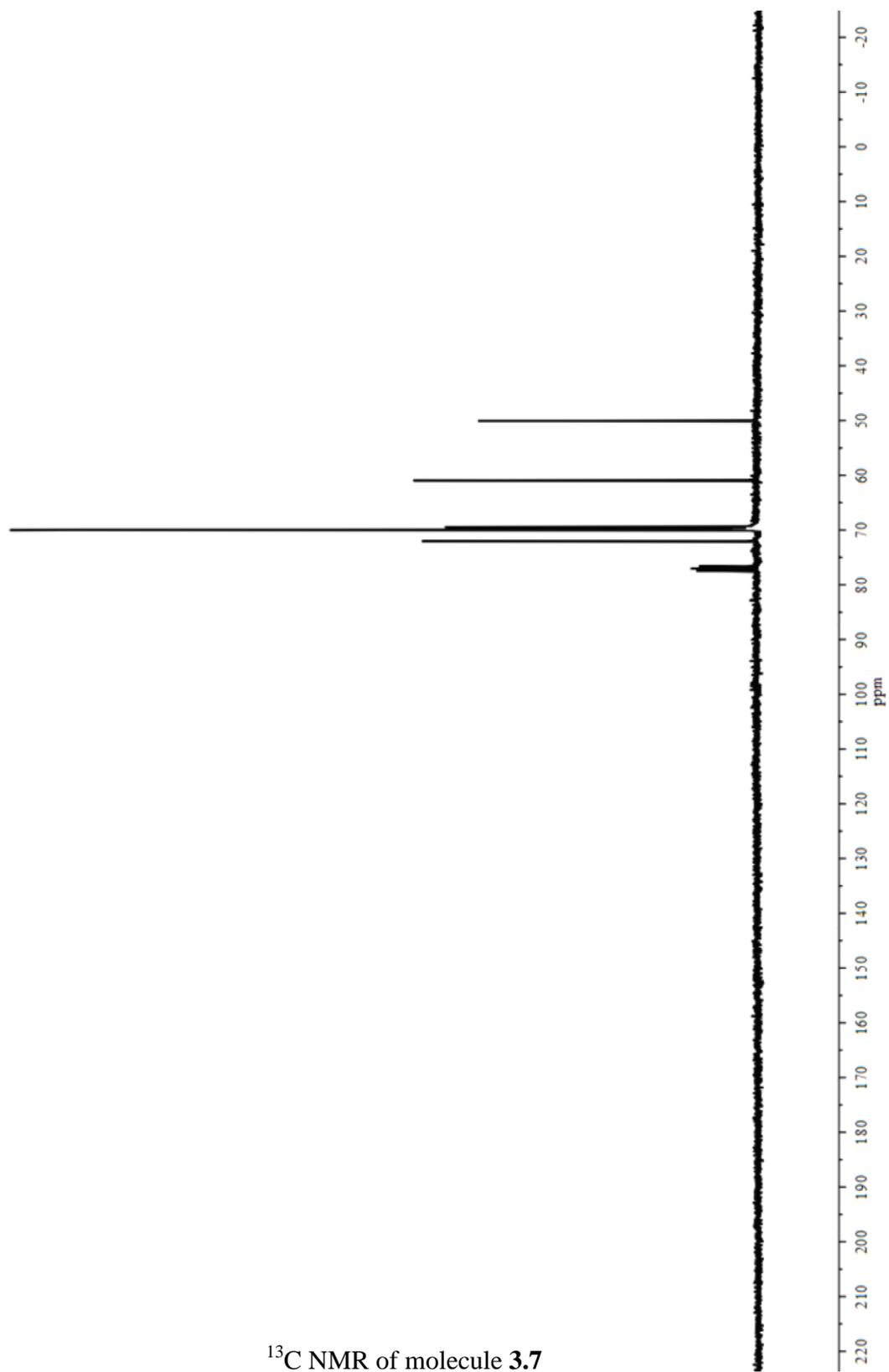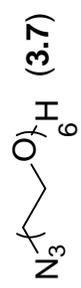
^{13}C NMR of molecule **3.7**
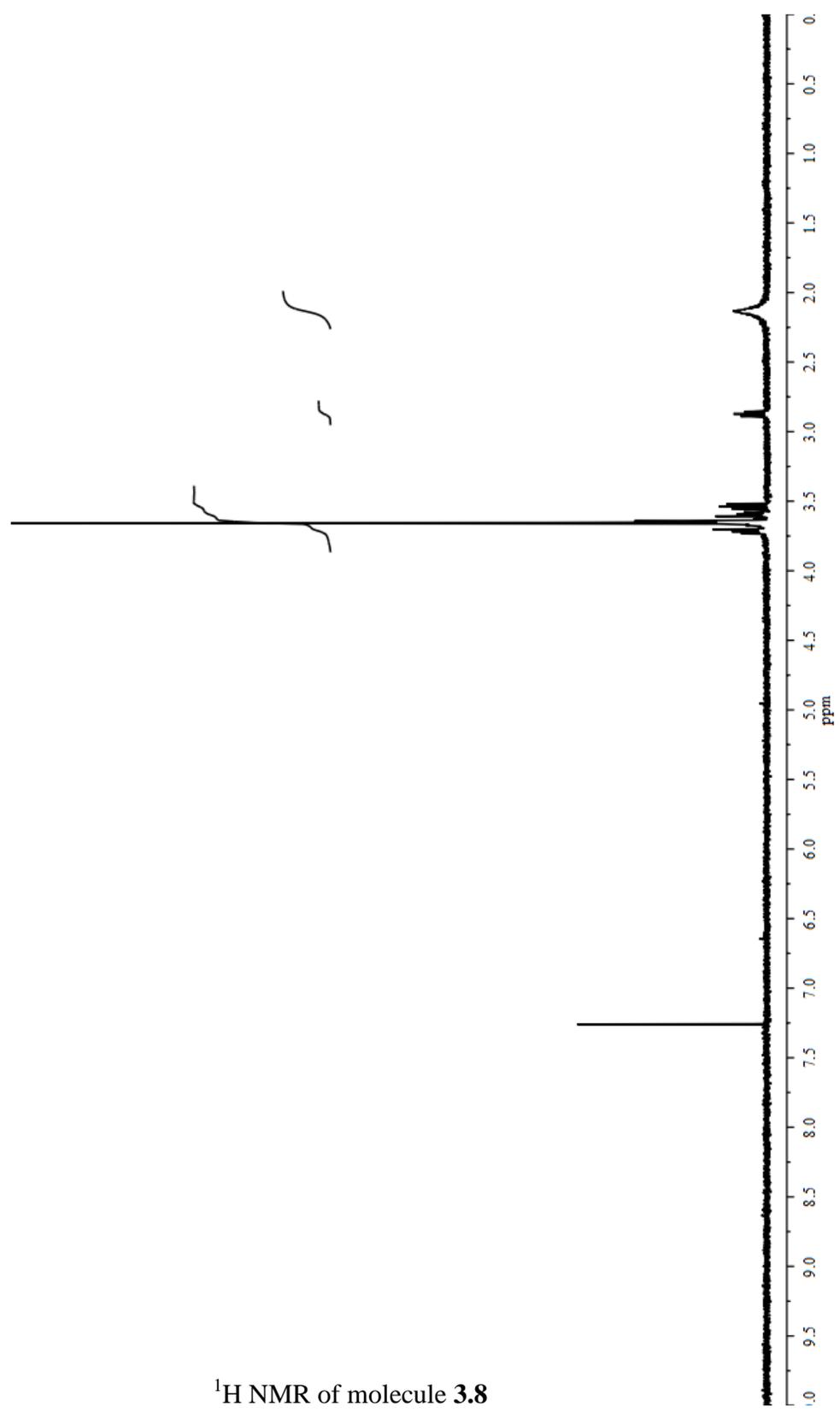
^{1}H NMR of molecule **3.8**

^{13}C NMR of molecule **3.8**

Appendix D

¹H and ¹³C NMR for Chapter 4
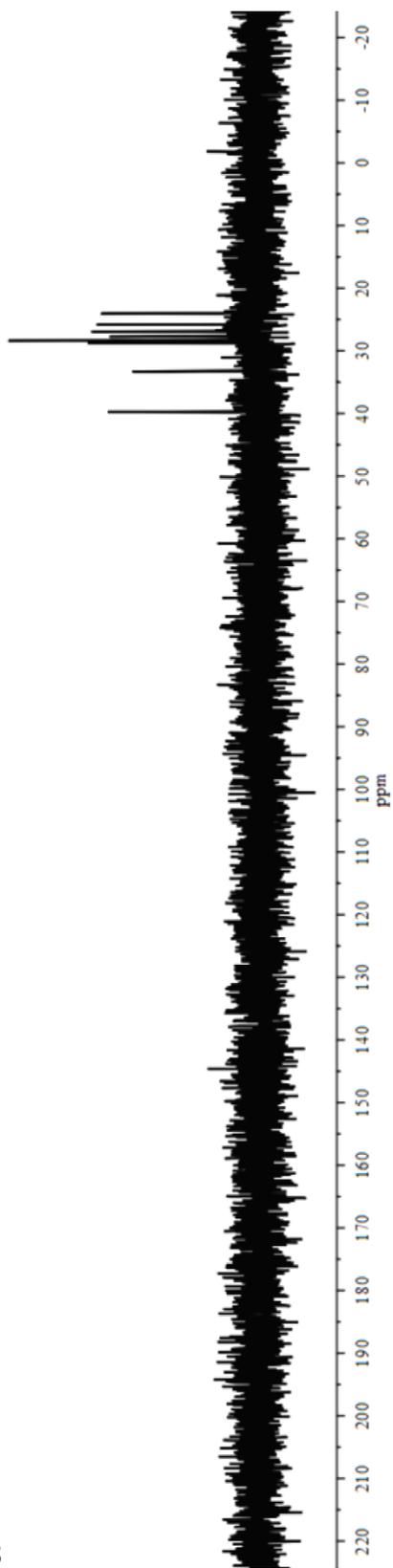
Appendix D

¹H and ¹³C NMR for Chapter 4
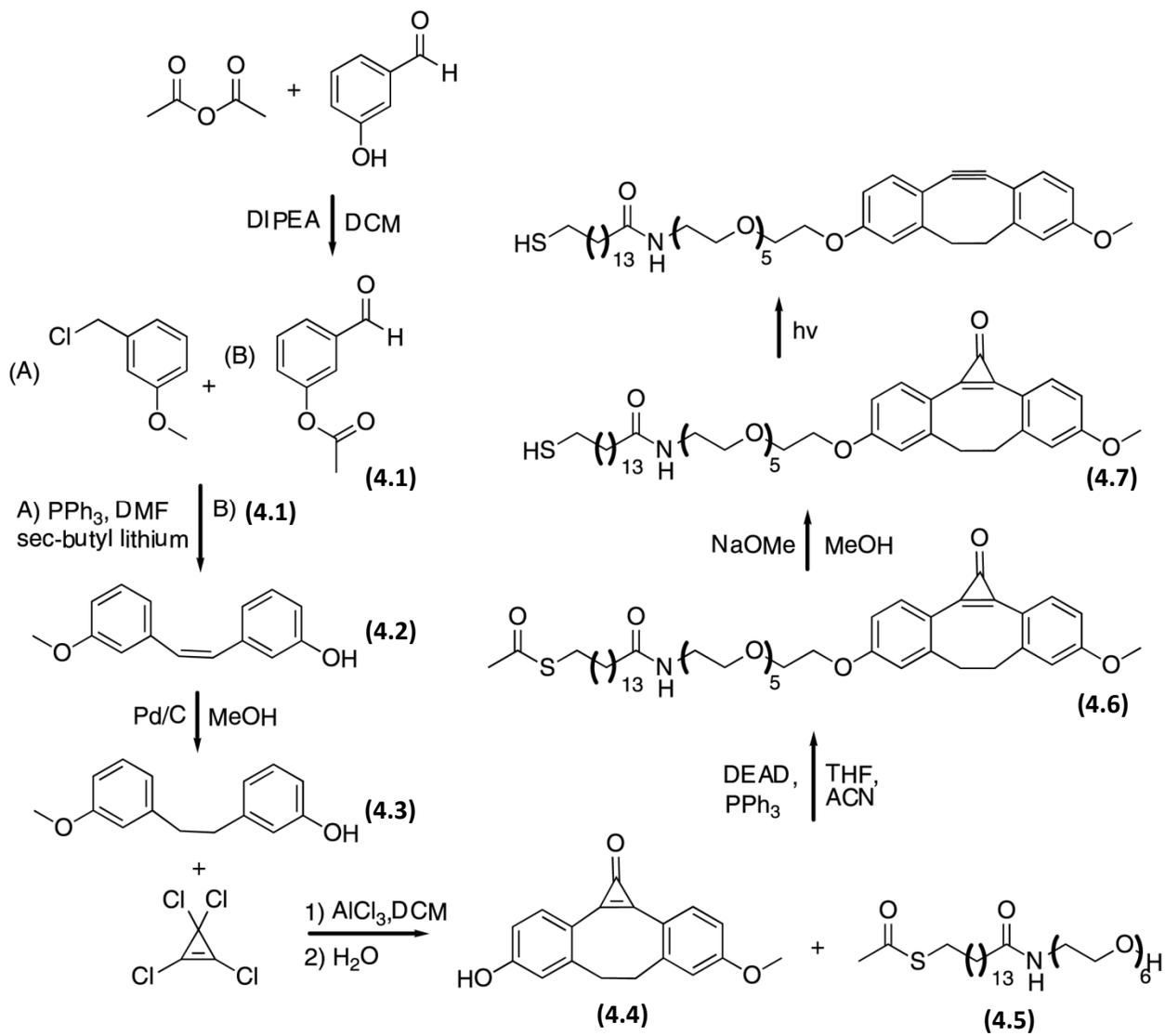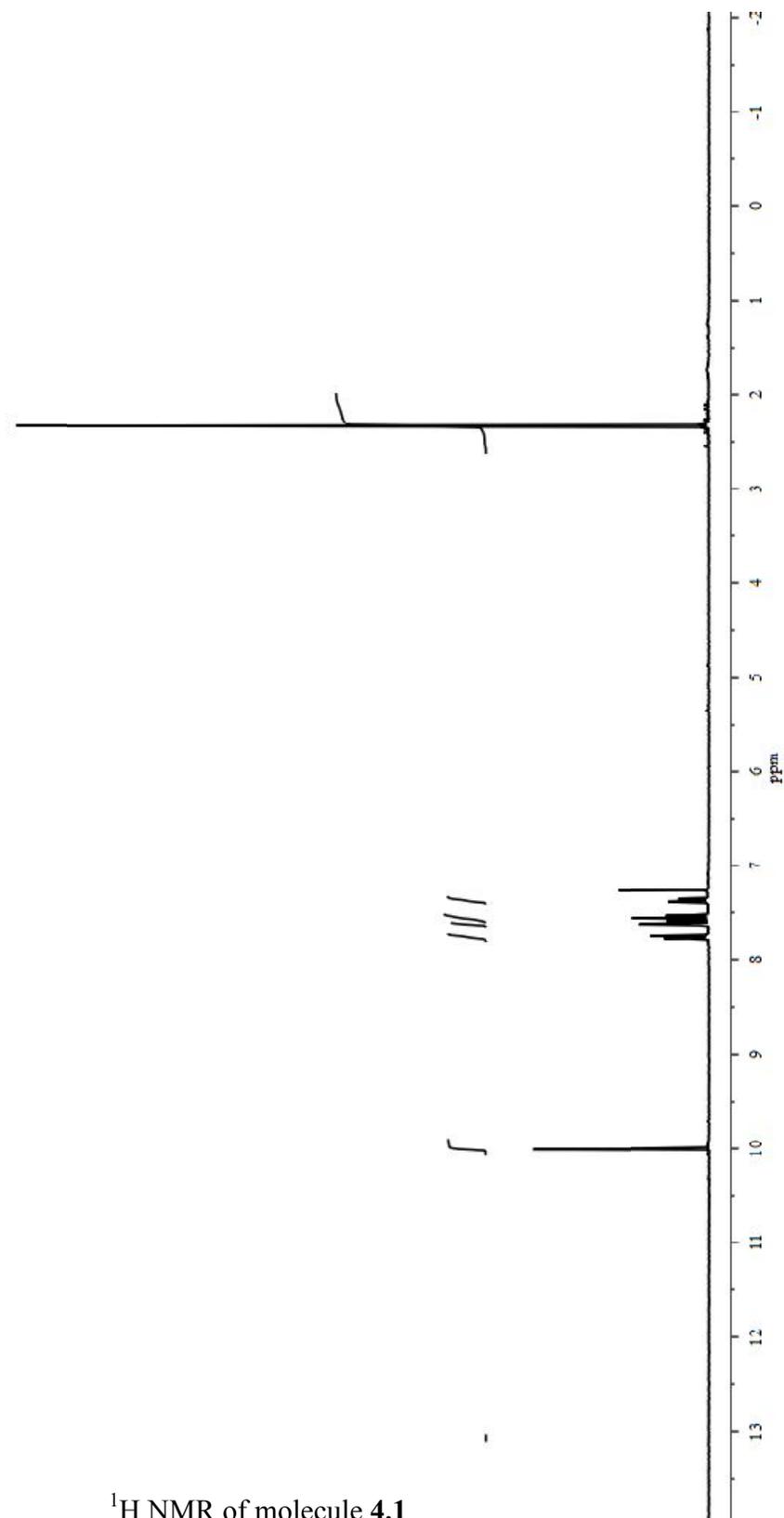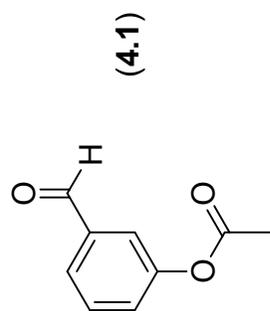
^{1}H NMR of molecule **4.1**
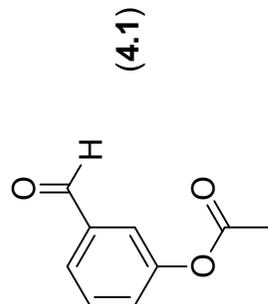
^{13}C NMR of molecule **4.1**

(4.2)
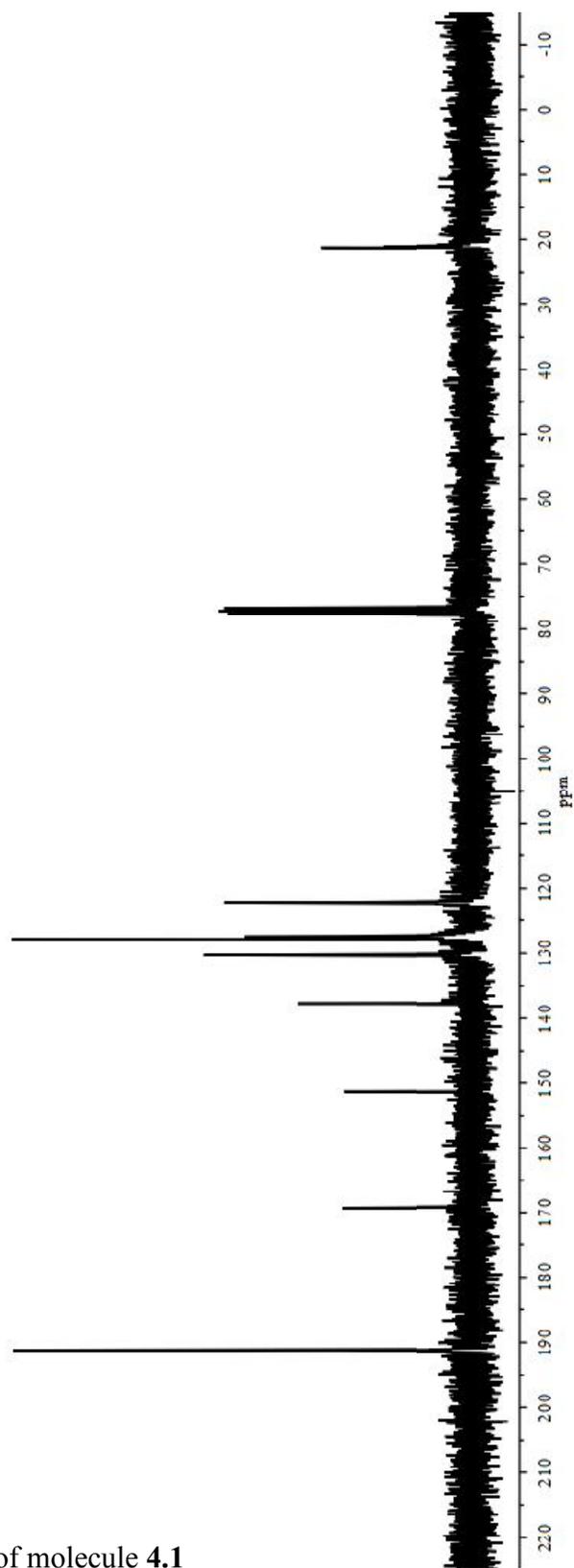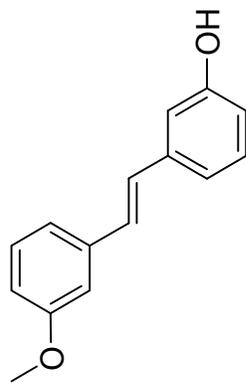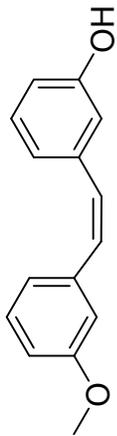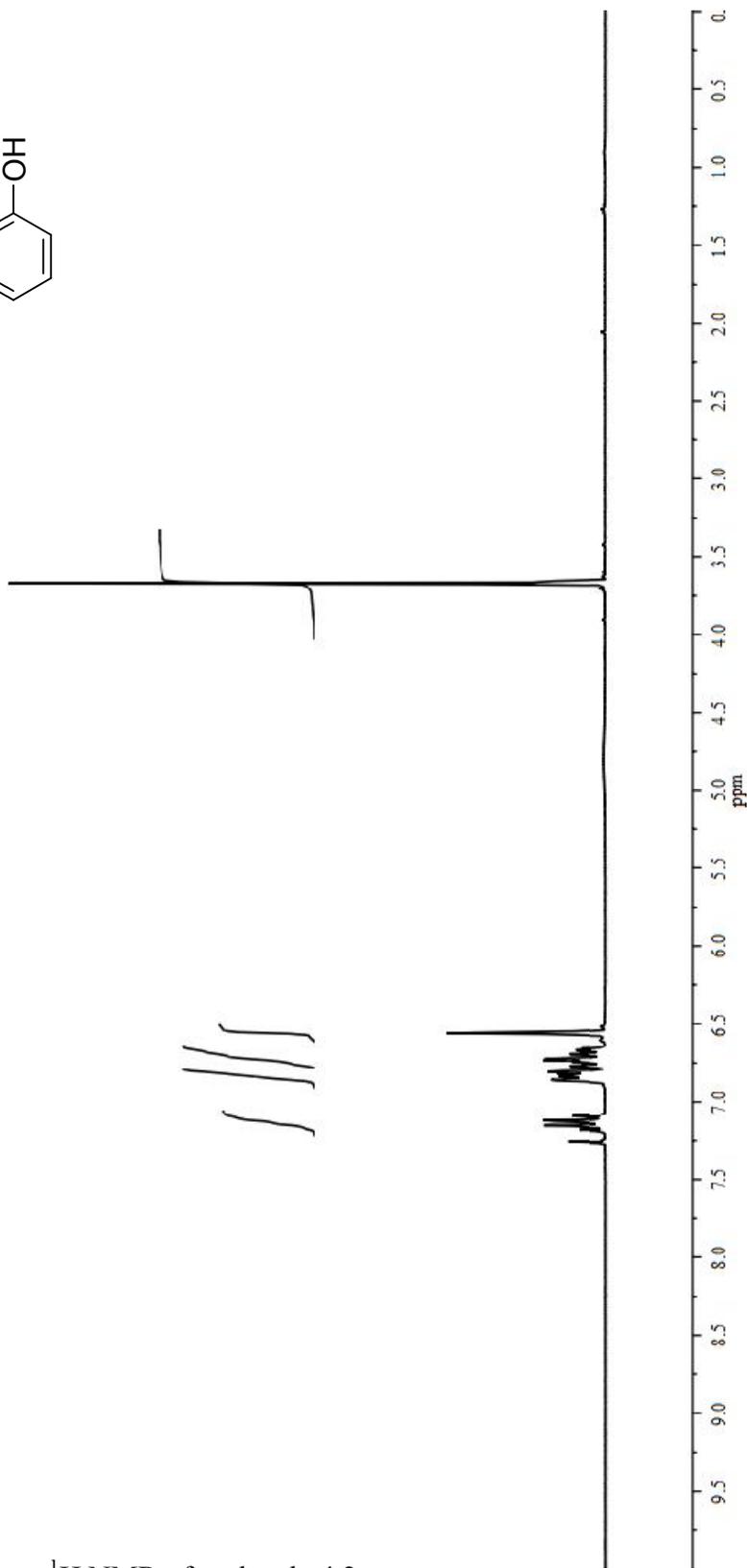
^{1}H NMR of molecule **4.2**
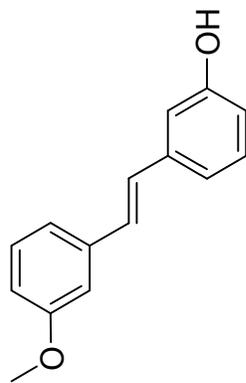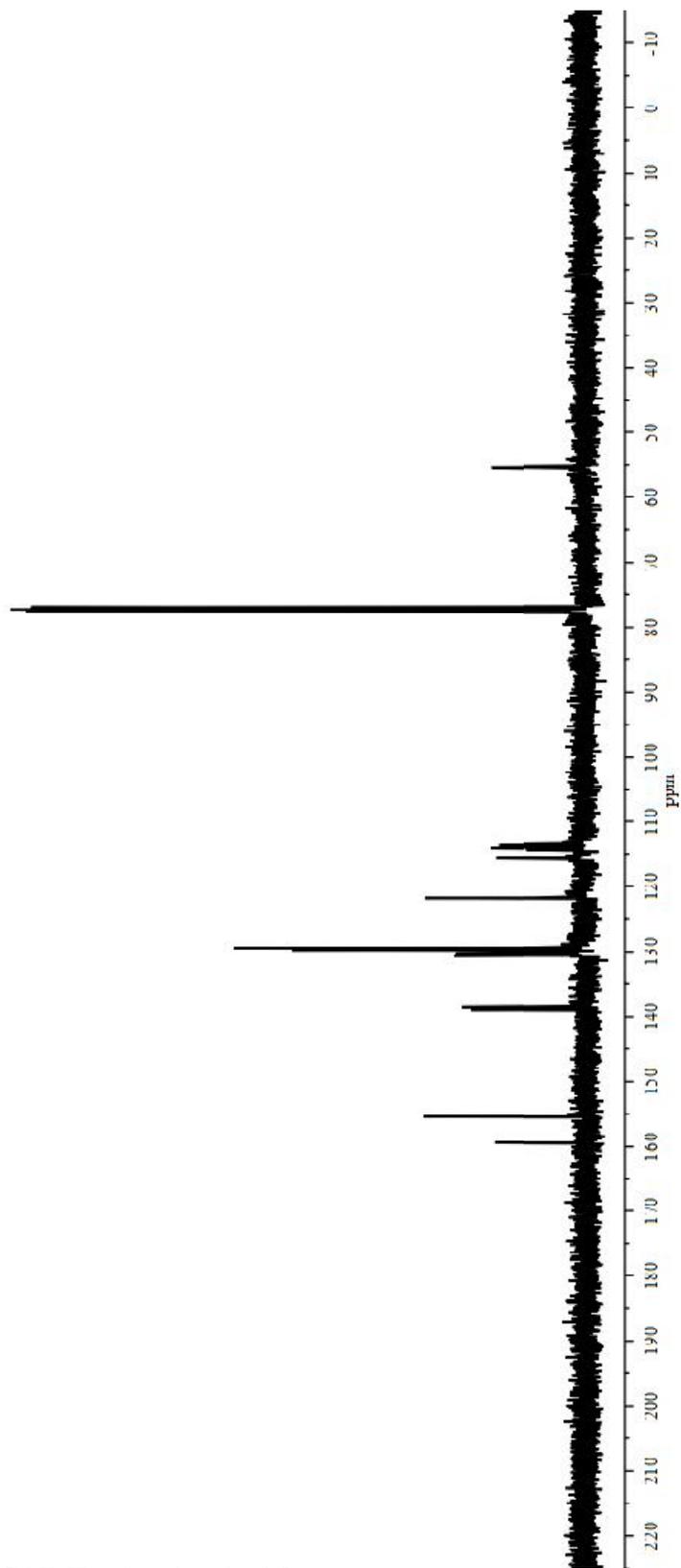
^{13}C NMR of molecule **4.2**
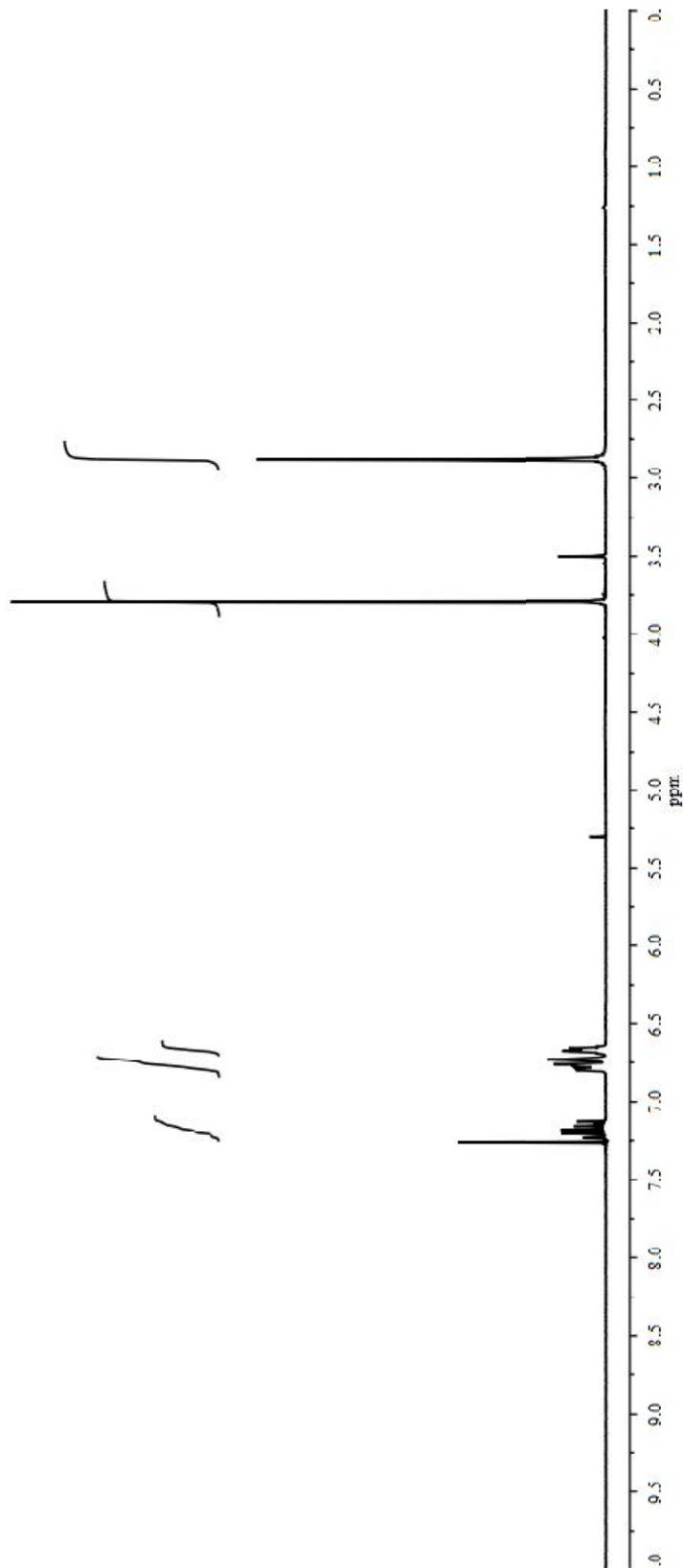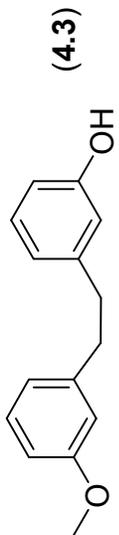
^{1}H NMR of molecule **4.3**

(4.3)

^{13}C NMR of molecule **4.3**

173
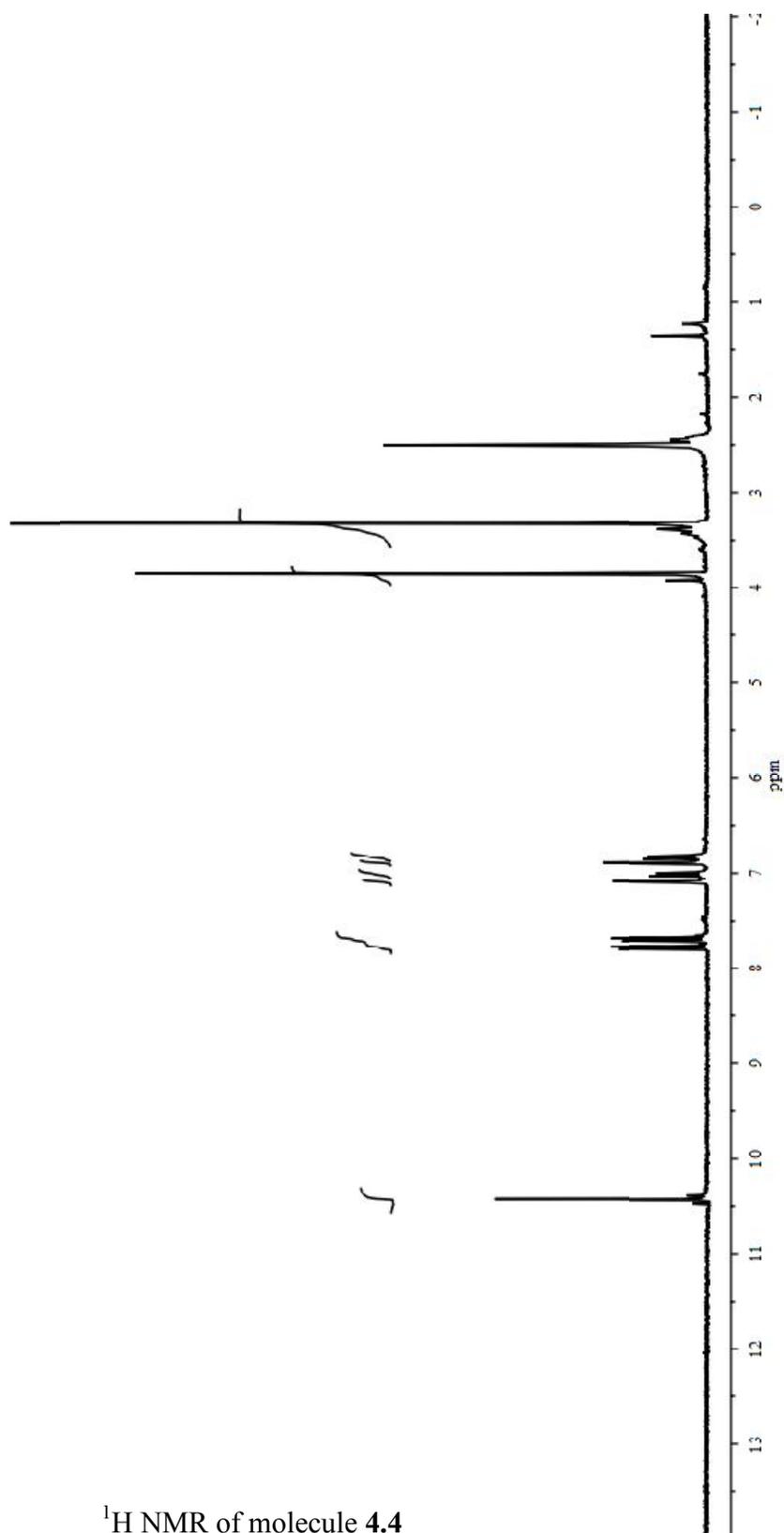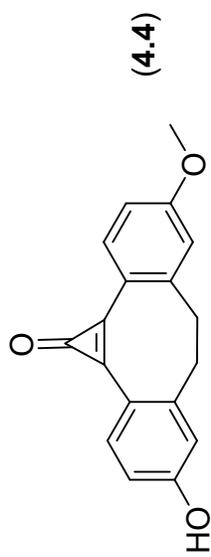
^{1}H NMR of molecule **4.4**

(4.4)
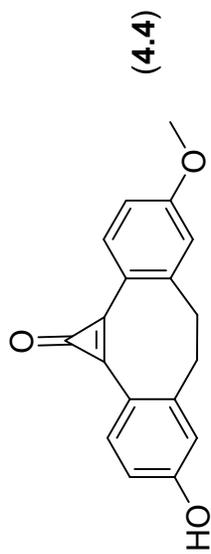
^{13}C NMR of molecule **4.4**

175
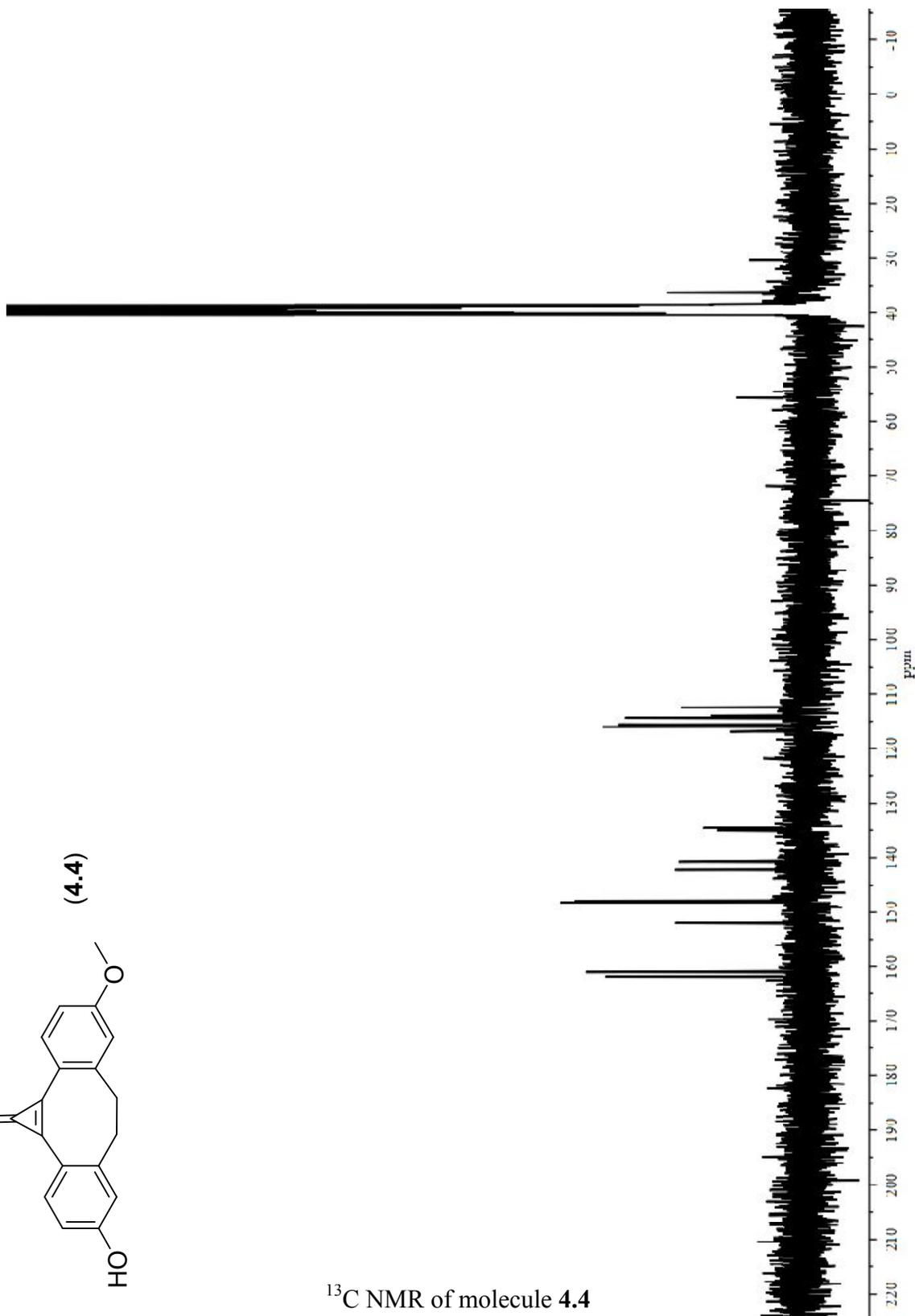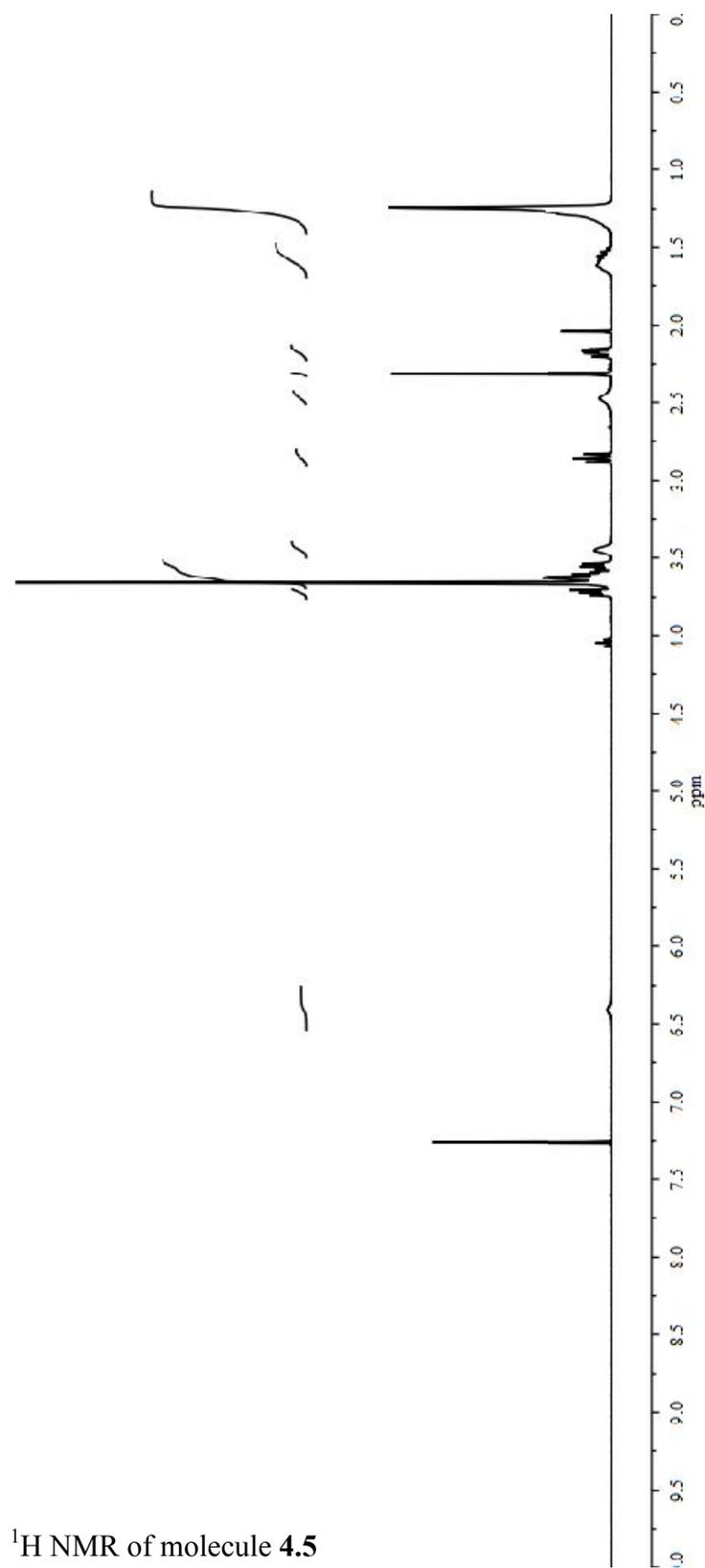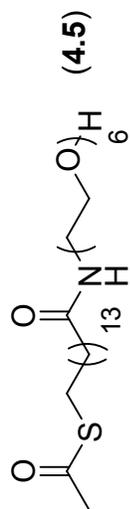
^{1}H NMR of molecule **4.5**
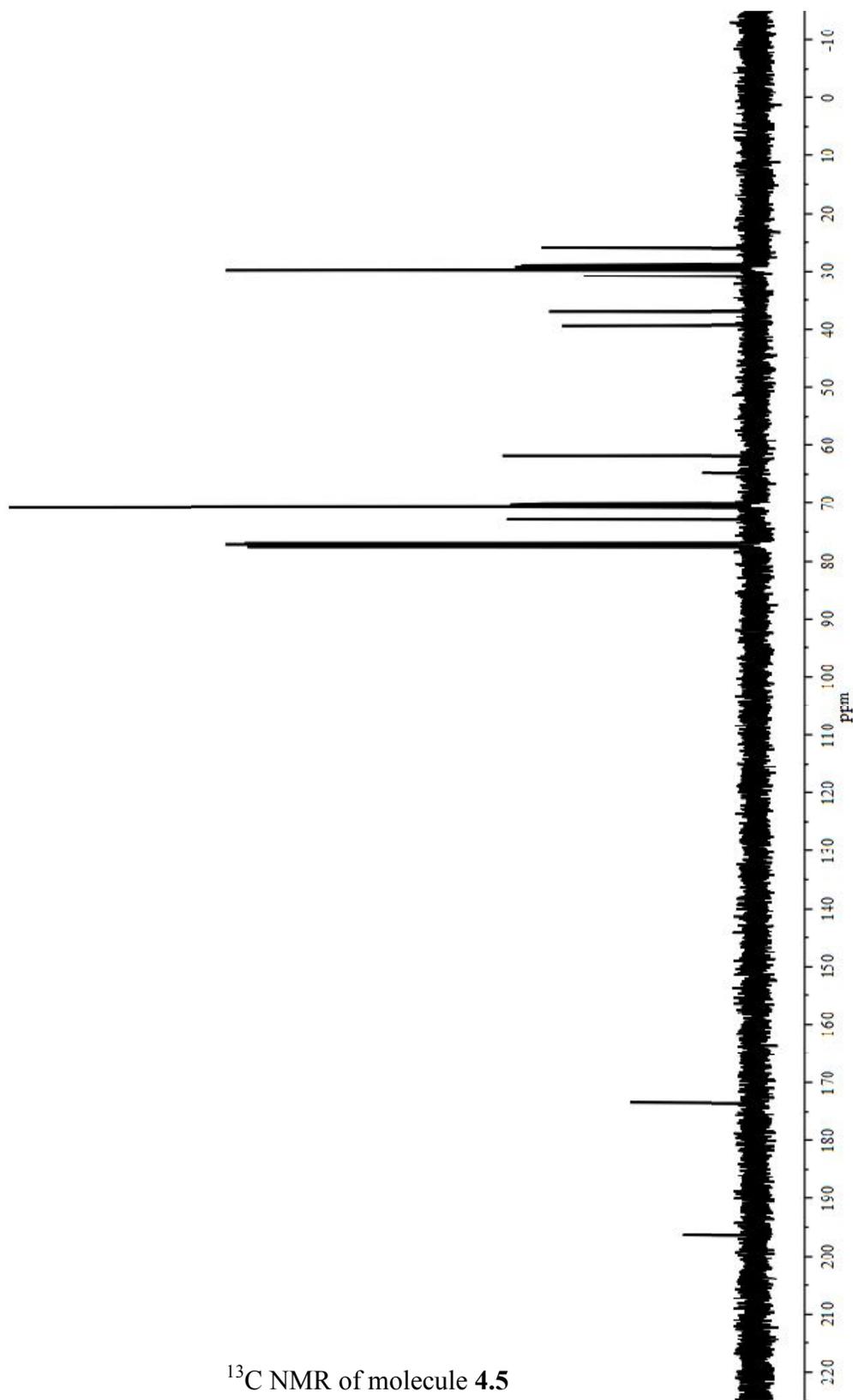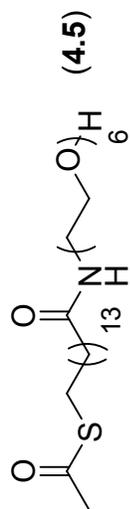
^{13}C NMR of molecule **4.5**

177

(4.6)
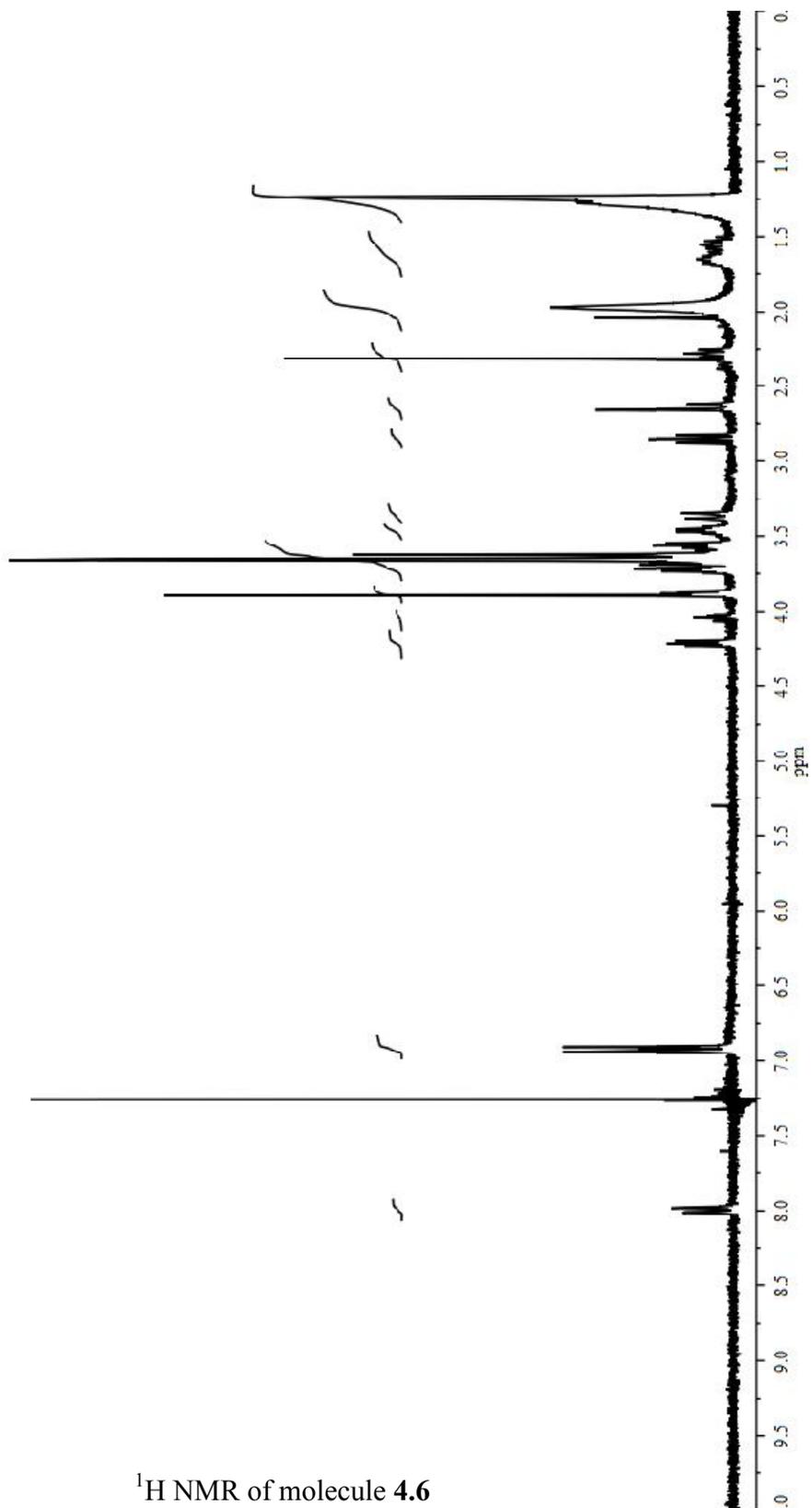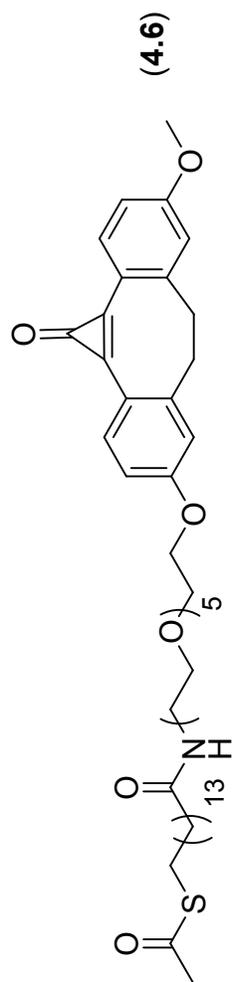
^{1}H NMR of molecule **4.6**

178

(4.6)
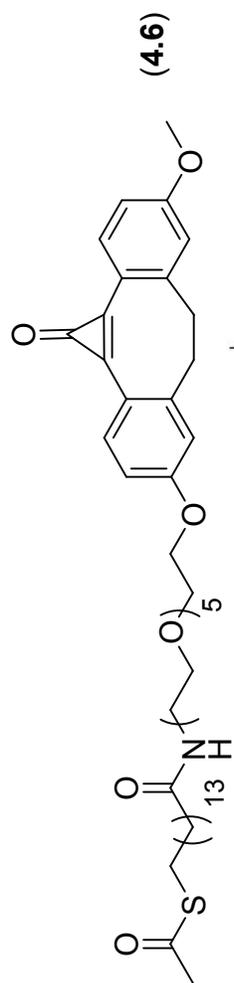
^{13}C NMR of molecule **4.6**
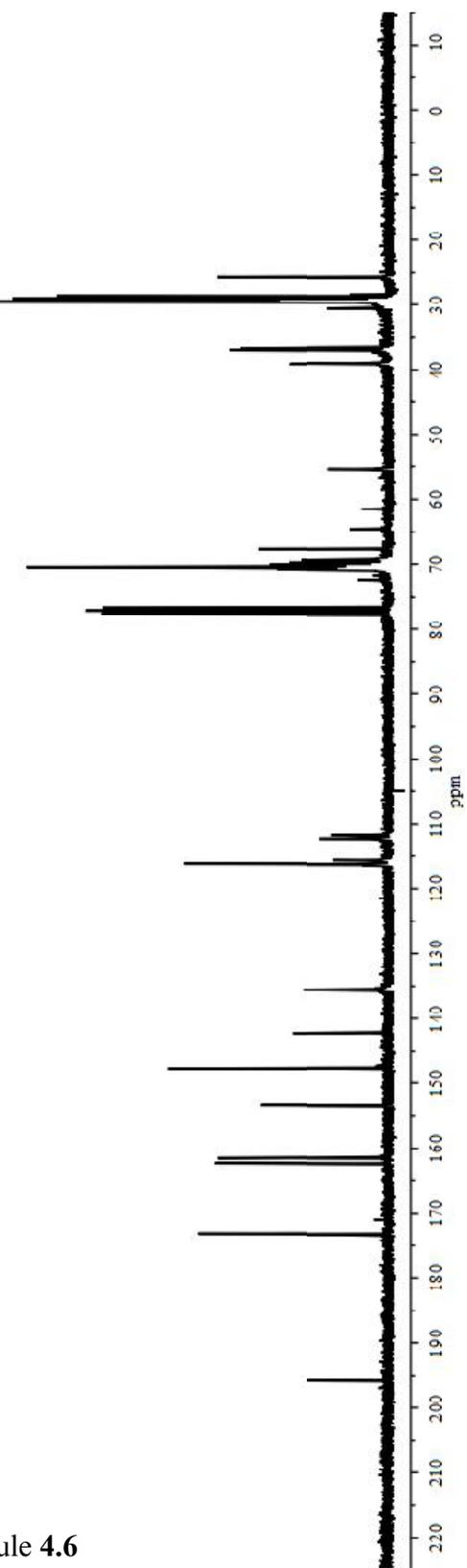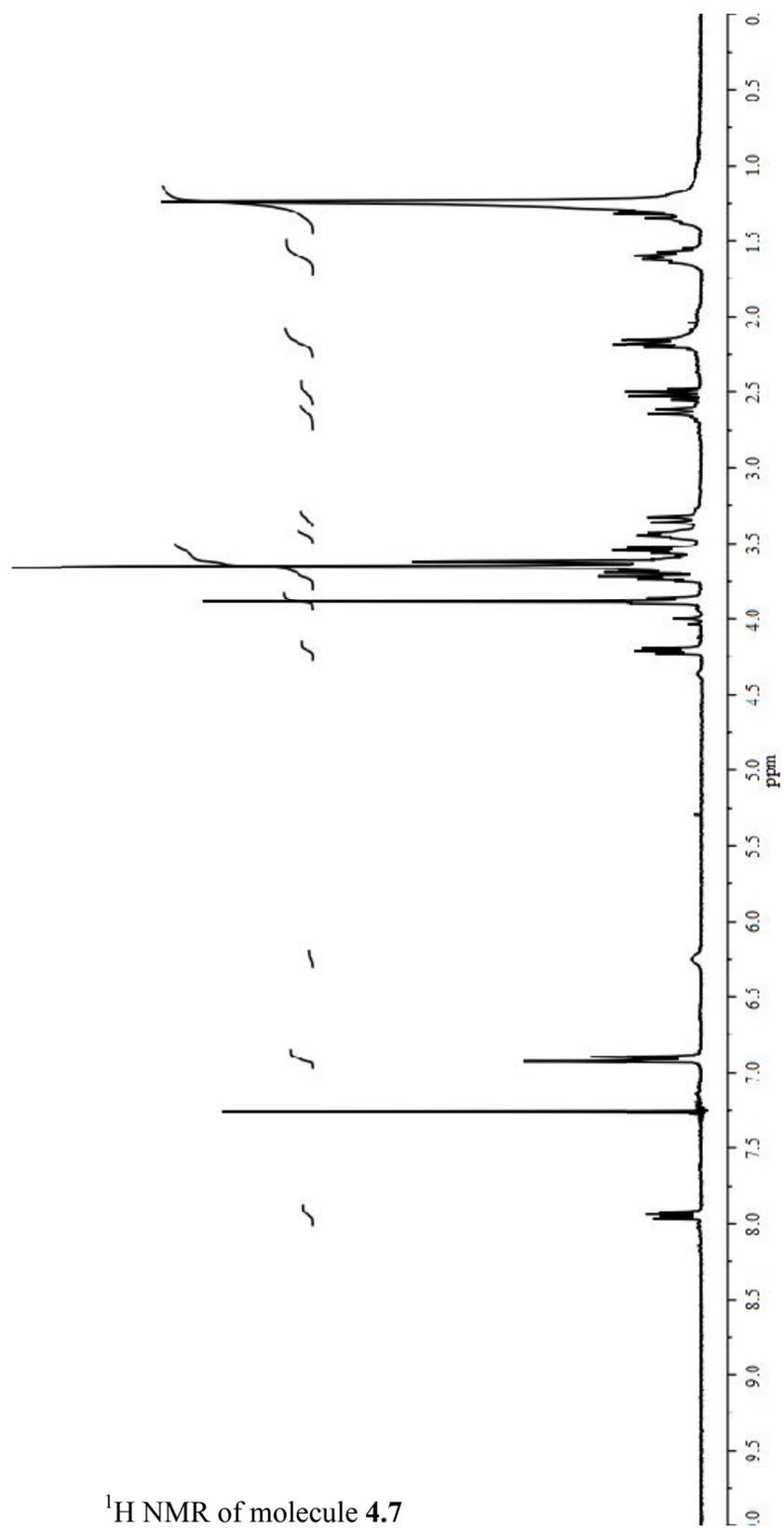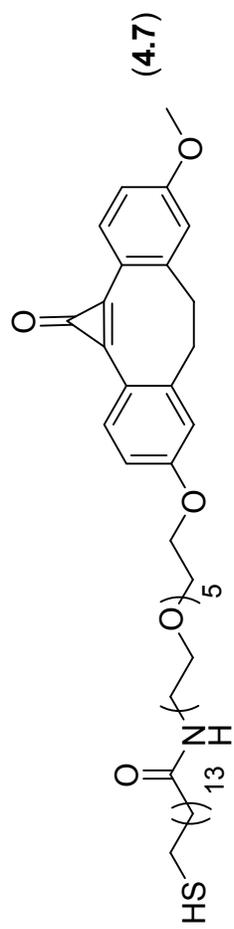
^{1}H NMR of molecule **4.7**

^{13}C NMR of molecule **4.7**